Bio-Design and Manufacturing
https://doi.org/10.1631/bdm.2600246

REVIEW

Biofabrication and biomedical manufacturing research frontiers in the United States

Yunxia Chen[1] · Kyle R. Phillips[2] · Eben Alsberg[3,4,5] · Thomas E. Angelini[1,2,6,7] · Nasim Annabi[8,9] · Anthony Atala[10] · Amit Bandyopadhyay[11] · Leon M. Bellan[12,13] · Luiz E. Bertassoni[14,15,16,17,18] · Adriana Blazeski[19] · Thomas Boland[20] · Susmita Bose[11] · Jason A. Burdick[21,22] · Robert C. Chang[23] · Christopher S. Chen[24,25] · Roland K. Chen[11] · Douglas B. Chrisey[26,27] · Elizabeth Cosgriff-Hernandez[28] · Paul D. Dalton[29] · David Dean[30] · Aixiang Ding[3] · Bin Duan[31] · Marc Ferrer[32] · John P. Fisher[33,34] · Gabor Forgacs[35,36] · Debolina Ghosh[37] · Warren L. Grayson[38,39,40,41,42] · Murat Guvendiren[43,44] · MD Ahasan Habib[45] · Sarah C. Heilshorn[46] · Ashley Hicks[28] · Scott J. Hollister[47] · Congrui Jin[48] · Yifei Jin[49] · Roger D. Kamm[19,50] · Bashir Khoda[51] · Robert Langer[52,53] · Cato T. Laurencin[37,54,55,56,57] · Sang Jin Lee[10] · Kam W. Leong[58,59] · Ming C. Leu[60] · Wei Li[61] · Michael Mak[62] · Amir K. Miri[44] · Roger J. Narayan[63,64] · Liqun Ning[65] · Brenda M. Ogle[66,67] · Ibrahim T. Ozbolat[68,69,70,71,72,73] · Zhijian Pei[74] · Peihua Qiu[75] · Krishanu Saha[30,76] · Jayant Saksena[26,27] · Vahid Serpooshan[77,78] · Albert Shih[79] · Rohan A. Shirwaiker[80,81,82] · Pranav Soman[83] · Ali Tamayol[84] · Mark W. Tibbitt[85] · Changxue Xu[86] · Yunzhi Peter Yang[46,87,88] · Lijie Grace Zhang[89] · James J. Yoo[10] · Shaochen Chen[90,91] · Yu Shrike Zhang[92,93,94] · Yong Huang[1,2,7]

Received: 1 May 2026 / Accepted: 11 June 2026

Abstract

Biofabrication and biomedical manufacturing are inherently multidisciplinary, integrating living systems with advanced manufacturing to create functional products for applications spanning regenerative engineering and medicine, in vitro disease modeling, drug discovery, and medical devices. As these technologies develop, they are emerging as core enablers of next-generation healthcare and life-science innovation. In the United States (U.S.), rapid progress across fabrication processes, material systems, physics-based modeling, and translation-oriented strategies is expanding the achievable design space and accelerating movement from laboratory demonstrations toward clinical and commercial deployment. We introduce major U.S. research frontiers and highlight representative advances in this field that support applications including organoids and other microphysiological systems for in vitro testing, engineered tissue constructs for in vivo use, and medical devices and biohybrid platforms. We further provide an outlook on advancing robust, ethical biofabrication and biomedical manufacturing in the U.S. research ecosystem.

Graphical abstract

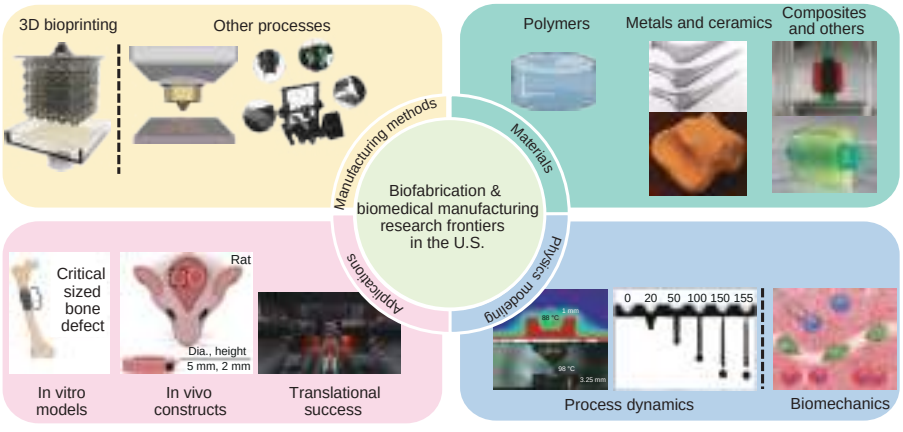

Keywords Biofabrication · Biomedical manufacturing · United States · Biomaterials · Physics modeling · Biomechanics

Extended author information available on the last three pages of the article

Table of Contents

1 Introduction

1.1 Motivation

Technological advances have delivered substantial economic and public health benefits across the life science and biomedical sectors. In particular, biofabrication and biomedical manufacturing are rapidly advancing as enabling foundations for human-based research and next-generation biomedical products. Progress is increasingly driven by the convergence of manufacturing-process innovation, materials development, and physics-informed model design, which together support controlled construction of biologically relevant living and biohybrid systems with suitable geometrical structure, material composition, and microenvironmental cues. These capabilities are reshaping what can be fabricated (e.g., functional constructs, living tissues, organoids, medical implants, and surgical devices), how they can be fabricated (multiprocess, multimaterial, and multiscale manufacturing), and how performance can be validated (quantitative quality and model-informed process).

While sporadic research on biofabrication and biomedical manufacturing existed in the United States (U.S.), systematic research efforts and dissemination did not materialize until the early 2000s. These efforts were contributed by various researchers, including Dr. Thomas Boland (Clemson University/University of Texas at El Paso), Dr. Vladimir Mironov (Medical University of South Carolina), Dr. Wei Sun (Drexel University), and Dr. Gabor Forgacs (University of Missouri), to name a few, as well as by Dr. Anthony Atala at the Wake Forest Institute for Regenerative Medicine, who led significant translational work. It is noted that traditional manufacturing also has a good contribution in biomedical manufacturing, which was led by Dr. Stephen Malkin at the University of Massachusetts at Amherst in the 1990s and by Dr. Albert Shih at the University of Michigan at Ann Arbor from the 2000s. Throughout the history of biofabrication and biomedical manufacturing, researchers based in the U.S., along with many others globally, have been at the forefront of the field, from some of the earliest developments in bioprinting [11–13] and tissue-engineered organ implantation [14] to more recent advances in biofabrication and biomedical manufacturing approaches. The U.S. National Science Foundation specifically dedicated an Additive Manufacturing (AM) for Health workshop to examining the current state, gaps, and research needs, and formulating recommendations related to AM for health, in particular, hard structure and medical product printing and soft construct bioprinting, in 2016 [15]. Ten years later, this review serves as a snapshot of current work and innovation being conducted in the U.S., focusing on frontiers in biofabrication and biomedical manufacturing research relating to manufacturing processes, materials, modeling, and applications, both for in vitro and in vivo applications.

1.2 Background

While the terms biofabrication and biomedical manufacturing are used interchangeably in many research papers, their definitions have evolved over time, and researchers from disparate disciplines may prefer one term over the other. Generally, biofabrication broadly describes a fabrication field using the combination of cells and/or biomaterials to create complex biological or biomedical products [15–18]. It bears particular relevance to biomedical engineering, where biofabrication technologies have emerged as promising tools for tissue and organ recreation. Within the areas of tissue engineering and regenerative medicine (TERM), biofabrication can be described as an approach to tissue engineering, allowing for the creation of cellular constructs with precise spatial organization [19, 20]. In the context of TERM, biofabrication is defined as the generation of structurally organized, biologically functional products from living cells, bioactive molecules, biomaterials, cell aggregates such as microtissues, and/or hybrid cell–biomaterial constructs through bioprinting or bioassembly and subsequent tissue maturation processes [20]. This review mainly focuses on biofabrication research that has been applied to TERM applications.

Similarly, biomedical manufacturing focuses on improving health outcomes through an engineering approach but is often defined as having a wider purview, particularly by physicists and mechanical engineers. Originally described more narrowly as primarily concerning biomedical device manufacturing, the field has since seen its definitions expanded to include the applications of manufacturing technology to advance the safety, quality, cost, efficiency, and speed of healthcare service and research [21]. As a result, the scope includes not only medical devices, but also the production of engineered tissues and organs, microphysiological systems, cell- and protein-based therapeutics, and

Copyright information for the graphical abstract: "Manufacturing methods"—3D bioprinting (reproduced from [1], with permission from the American Chemical Society), other processes (reproduced from [2], licensed under CC BY); "Materials"—metals and ceramics (reproduced from [3], with permission from Acta Materialia Inc.; reproduced from [4], with permission from the American Ceramic Society), composites and others (reproduced from [5], with permission from Wiley-VCH GmbH); "Physics modeling"—process dynamics (reproduced from [6], with permission from Wiley-VCH GmbH; reproduced from [7], with permission from the American Chemical Society); "Applications"—in vitro models (reproduced from [8], licensed under CC BY-NC-ND), in vivo constructs (reproduced from [9], licensed under CC BY), translational success (reproduced from [10]).

biomaterials, as well as the application of manufacturing technology in surgical operations and hospital scheduling [22]. By this definition, TERM is also strongly related to biomedical manufacturing, as is TERM-related biofabrication. Although still largely focusing on biomedical manufacturing developments that overlap with TERM applications, this review also explores a few select developments in biomedical device manufacturing research.

While defining biofabrication and biomedical manufacturing, it is also beneficial to establish definitions for a few terms central to these fields: bioprinting, printing, bioink, and biomaterial ink. While exact definitions of these terms may vary within the field, a common understanding is established for the purposes of this review article. Printing in this context refers to three-dimensional (3D) printing, the use of AM technologies to create 3D structures, traditionally in a layer-by-layer manner. In regard to biofabrication, bioprinting and printing are sometimes used interchangeably, but a distinction is often used to differentiate the two: bioprinting is a subcategory of printing, usually defined as the use of computer-aided transfer processes for patterning and assembling living and nonliving materials with a prescribed organization to produce bioengineered structures [17, 23], or as layer-by-layer precise positioning of biological materials, biochemicals, and living cells with spatial control over the placement of functional components [24]. Under these circumstances, bioprinting is also sometimes termed cell printing, cell direct writing, or organ printing. A similar distinction is often drawn between bioink and biomaterial ink: a bioink is a formulation suitable for processing by a biofabrication technology that includes cells as a component of the ink, while a biomaterial ink does not include cells during the fabrication process, although they can be seeded at a later point [18]. While these definitions are commonly held, some ambiguity still exists, particularly in terms of the direct inclusion of living cells/materials during printing. As such, in this review, these terms have been standardized where possible for clarity and consistency throughout the broader discussions, while preserving the terminology chosen by the respective contributing research groups; therefore, some terms may still be used interchangeably in certain cases.

This review synthesizes advances across four tightly coupled dimensions: (i) biofabrication and biomedical manufacturing processes, (ii) enabling material systems, (iii) physics-based modeling, and (iv) translation-oriented strategies toward clinical and commercial deployment. Manufacturing processes are the cornerstone of biofabrication and biomedical manufacturing, serving as the mechanism by which the desired constructs are realized. Processes have progressed significantly in recent years, building upon and innovating existing manufacturing technologies, as well as introducing novel ones. Particularly, researchers in the U.S. have modified and expanded existing 3D printing modalities, such as extrusion bioprinting, vat polymerization, and inkjetting, working to enable them to make complex biomimetic and biological systems [15, 25–27]. Outside of conventional bioprinting, alternative fabrication technologies, such as four-dimensional (4D) bioprinting [28], melt electrowriting (MEW) [29–31], cell spheroid/organoid biofabrication [32, 33], cryobioprinting [34], and ultrasound-assisted biofabrication [35], have also been developed and modified to push further what is possible for biofabrication and biomedical manufacturing.

Materials represent both a primary limiting factor and a leading frontier for innovation in biofabrication and biomedical engineering. U.S. researchers have been consistently advancing this aspect, expanding the field's focus from foundational goals of high structural fidelity, printing resolution, and in vivo biocompatibility [1, 36] toward the development of highly dynamic, functionalized matrices and constructs. Furthermore, current research emphasizes materials engineered to actively support cell migration [37, 38], seamless scaffold integration [39, 40], and effective fabrication [1, 41]. The focus is shifting toward fabricating bioactive microenvironments that not only maintain cell viability during the mechanical stresses of printing but also consider physical, chemical, and biological interactions to direct cell behaviors, tissue maturation, and multiscale functionalities post-fabrication. These material innovations effectively bridge the gap between printed structures/constructs and living, active tissue models/replacements.

Physics modeling in biofabrication and biomedical manufacturing helps transition research from empirical, trial-and-error fabrication to repeatable and predictable modeling processes. The complexity of biofabrication, which involves multiphase composites, complex fluid dynamics, and sensitive living cells, demands sophisticated computational models to ensure reproducibility and physics-based predictability. With the multitude of parameters that must be specified for any biofabrication process, physics-based modeling offers the opportunity to efficiently realize optimized print fidelity without time-intensive trial-and-error experimentation [42, 43]. Leading research groups have been developing multiphysics modeling to optimize not only the intricate fabrication process and fabricated parts' geometrical/mechanical/rheological properties and performance, but also biological interactions [44]. They have also investigated the connection between material properties and bioprinting outcomes [45] and printing process characterization [7, 46]. Another research focus of U.S. researchers is the investigation and modeling of cells' complex responses to their physical microenvironment as well as to biofabrication processes, which includes the study of cell behavior in embedded printing materials [47], as well as process-induced cell death [48] and mechanotransduction changes [49].

Building upon the manufacturing processes, materials, and modeling-related efforts, U.S.-based researchers have been able to apply them to a wide variety of purposes, both in vitro and in vivo. For in vitro applications, researchers have been able to fabricate complex heart [50–52], bone [53], neural [54, 55], vascular [56–58], and breast cancer [59] models, among others, serving as testing platforms, tissue simulants, and more. For in vivo applications, bone constructs for regeneration [60–62], intraoperative bioprinting [9], skin constructs [63], and other complex tissues for implantation [64] have been developed to improve health conditions. There has also been significant success in the development and commercialization of biomedical manufacturing products, with interventional neurocardiovascular devices [65], advanced resorbable implants [66], and even biofabricated leather and food. A recent translational success further illustrates the healthcare impact of U.S. biomedical manufacturing innovation. For example, Amplitude Vascular Systems (AVS) was acquired by Stryker in 2026 [67], and its intravascular lithotripsy platform has already advanced into a first-in-human coronary clinical study, demonstrating a clear path from academic innovation to commercial and clinical deployment [68]. As part of the "BDM at the Frontiers: Geography and Science" series, and consistent with previously published regional frontier articles, this U.S.-based review is not intended to provide an exhaustive review of all U.S. biofabrication and biomedical manufacturing research. Rather, with the aim of being as inclusive as possible within the scope of a single review, it offers a structured snapshot of recent, representative, and high-impact directions being pursued by active U.S. research groups, highlighting themes that collectively define current research frontiers. The overall framework of this review is shown in Fig. 1.

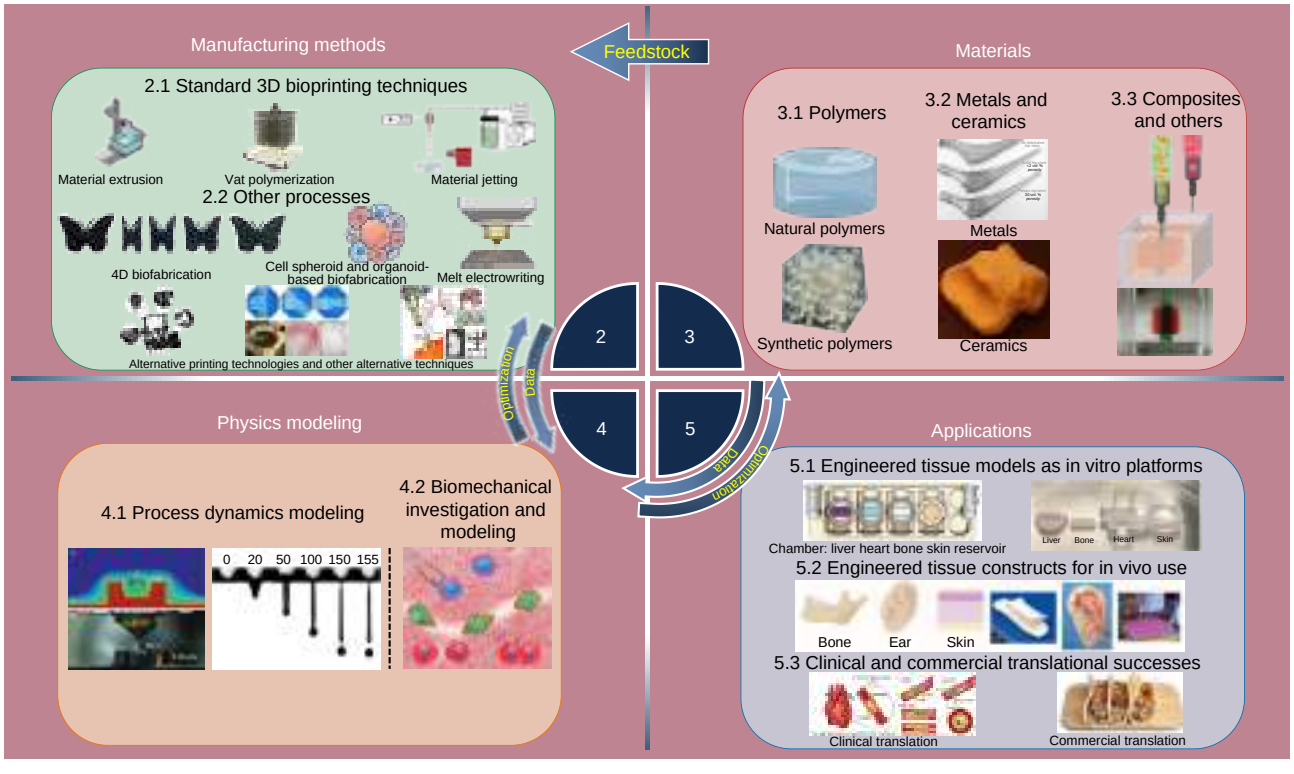

Fig. 1 Overall framework of this review paper, showing the organization of sections and key themes discussed. Copyright information: 2.1 "Material extrusion" (reproduced from [69], licensed under CC BY), "Vat polymerization" (reproduced from [1], with permission from the American Chemical Society), "Material jetting" (reproduced from [70], with permission from IOP Publishing Ltd.); 2.2 "4D biofabrication" (reproduced from [71], licensed under CC BY-NC 4.0), "Alternative printing technologies and other alternative techniques" (reproduced from [2], licensed under CC BY; reproduced from [35], with permission from IOP Publishing Ltd.; reproduced from [72], licensed under CC BY 4.0); 3.1 "Synthetic polymers" (reproduced from [1], with permission from the American Chemical Society); 3.2 "Metals" (reproduced from [3], with permission from Acta Materialia Inc.), "Ceramics" (reproduced from [4], with permission from the American Ceramic Society); 3.3 "Composites and others" (reproduced from [5], with permission from Wiley-VCH GmbH); 4.1 "Process dynamics modeling" (reproduced from [6], with permission from Wiley-VCH GmbH; reproduced from [7], with permission from the American Chemical Society); 5.1 "Engineered tissue models as in vitro platforms" (reproduced from [73], under exclusive licence to Springer Nature Limited); 5.2 "Engineered tissue constructs for in vivo use" (reproduced from [74], with permission from Wiley-VCH GmbH; reproduced from [75], with permission from Springer Nature America, Inc.; reproduced from [76], under exclusive licence to the American Association for the Advancement of Science); 5.3 "Clinical and commercial translational successes" (reproduced from [65], licensed under CC BY 4.0; reproduced from [77])

2 Biofabrication and biomedical manufacturing methods

In order to create functional, biologically active constructs and devices, ways to specifically and accurately organize materials and cells are needed. This section introduces some representative cutting-edge biofabrication and biomedical manufacturing research being conducted in the U.S. (Fig. 2), including standard 3D bioprinting techniques as well as alternative processes, such as MEW, organoid assembly/biofabrication, and other biofabrication and biomedical manufacturing innovations, such as 4D biofabrication and some newly developed biomedical manufacturing techniques.

2.1 Standard 3D bioprinting techniques

Traditional 3D printing is a family of AM processes that historically involve the deposition of a chosen material, layer by layer, to create customized parts [78, 79]. These processes all allow for the controlled deposition of materials, but the mechanisms behind the techniques in this family are highly diverse, as are the requirements for the materials used. These technologies are generally placed into seven standard categories [25, 80, 81]: material extrusion, powder bed fusion, vat polymerization, material jetting, binder jetting, sheet lamination, and directed energy deposition. Initially, often used for rapid prototyping and specialized part creation of engineering parts [78], many of these technologies were later adapted and applied toward the fabrication of biological constructs and products [15]. In particular, material extrusion, vat polymerization, and material jetting, often used in bioprinting, have emerged as burgeoning areas of biofabrication and biomedical manufacturing research and innovation. This section highlights some key U.S.-based bioprinting innovations, and the overall structure is shown in Fig. 3.

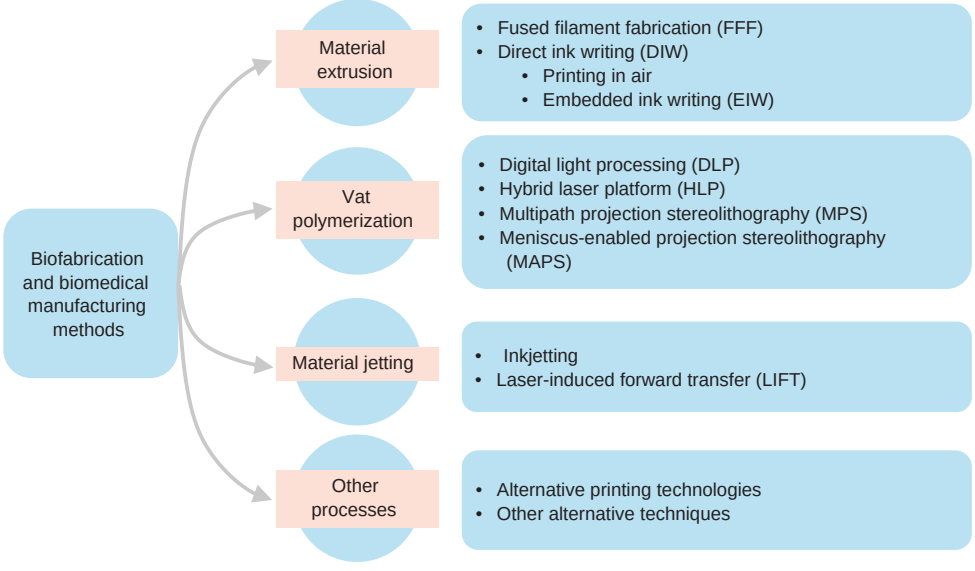

Fig. 2 Biofabrication and biomedical manufacturing methods

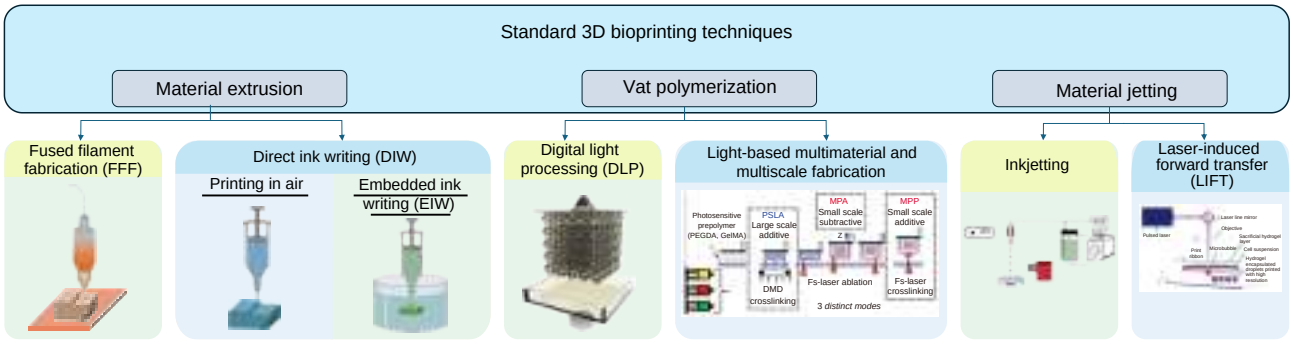

Fig. 3 Standard 3D bioprinting techniques. Copyright information: "Vat polymerization"—DLP (reproduced from [1], with permission from the American Chemical Society), light-based multimaterial and multiscale fabrication (reproduced from [82], with permission from WILEY-VCH Verlag GmbH & Co. KGaA, Weinheim); "Material jetting" (reproduced from [70], with permission from IOP Publishing Ltd.; reproduced from [83])

2.1.1 Material extrusion

Material extrusion bioprinting involves the controlled deposition of the chosen material as a continuous filament through extrusion and is one of the most commonly used bioprinting modalities due to its relative ease and cost-effectiveness [84]. Material extrusion mainly includes fused filament fabrication (FFF) and direct ink writing (DIW). FFF involves the melting or plasticization of a thermoplastic polymer to deposit it in layers, and has been broadly adopted for the printing of polymer-based scaffolds. Complementarily, DIW extrudes viscoelastic and viscoplastic inks for layer-by-layer deposition, usually at or near room temperature, and is therefore more compatible with biofabrication. DIW typically favors materials with shear-thinning properties that enable flow under pneumatic or mechanical pressure while maintaining shape with an in situ rapid solidification mechanism after deposition. Within DIW, subcategories exist, where much research is being conducted. Most commonly, material extrusion occurs on a build plate, where the filaments are deposited layer by layer to create the desired structure, which is referred to as printing in air. An alternative approach, known as embedded extrusion printing or embedded ink writing, involves the extrusion of a bioink within a support bath, usually a yield-stress bath [85], allowing for freeform deposition that does not necessarily rely on in situ rapid solidification and support structures [69, 86].

This section highlights snapshots of work done by researchers from Carnegie Mellon University, the University of Nevada Reno, and the New Jersey Institute of Technology, focusing on developing technology for embedded printing. Aside from the work featured in this section, many U.S.-based researchers have made strides in extrusion bioprinting. For example, the Lewis laboratory at Harvard University has developed a wide variety of extrusion approaches, from high-density embedded printing [58] to adaptive multinozzle extrusion [87]; the Burdick laboratory at the University of Colorado Boulder has explored many embedded printing approaches [88], including guest-host-enabled embedded spheroid printing [89]; the Skylar-Scott laboratory at Stanford University has made strides in multinozzle gradient bioprinting approaches [90, 91]; and the McAlpine laboratory at the University of Minnesota has developed technologies to enable soft, integrated biosensor fabrication [92] and complex extrusion toolpathing [93]. Many others, both in the U.S. and beyond, have made further significant contributions to the development of these technologies.

2.1.1.1 Fused filament fabrication

FFF, also referred to as fused deposition modeling (FDM), has been used as a practical and highly accessible method for producing patient-specific porous ceramic bone grafts for bone tissue engineering. The Bandyopadhyay and Bose groups at Washington State University have applied the FFF process to fabricate controlled-porosity alumina bone grafts as well as polymer-ceramic composite scaffolds and bone grafts [4, 94–96]. These studies have further evaluated biocompatibility through cytotoxicity and cell proliferation using different cell types, and examined the effect of porosity on structural performance. By engineering both uniform and spatial gradient porosity, their work has demonstrated the utility of FFF for the fabrication of customized orthopedic implants.

2.1.1.2 Embedded printing

2.1.1.2.1 Freeform reversible embedding of suspended hydrogels (FRESH)

The Feinberg laboratory at Carnegie Mellon University has focused on the development of embedded printing technologies, both with a particular emphasis on the creation of fabrication approaches and the equipment required to use them. They developed a microgel-based printing technique dubbed FRESH, which was one of the first examples of using a granular support bath to allow for freeform hydrogel fabrication [97]. While initially using a mechanically blended gelatin slurry as the support matrix, the process was later improved by replacing the slurry with granular gelatin particles generated through coacervation, which significantly enhanced printing resolution [98]. The Feinberg group has also developed a number of open-source, accessible machines to help enable FRESH printing [99–101].

FRESH technology has since been utilized to fabricate complex biological geometries, notably cardiac tissues [98, 102] and biomimetic hydrogel actuators [103]. Further adaptations have resulted in the inclusion of porogens for enhancing transport [104] and the fabrication of microfluidic devices that can support high cell density and a pancreas-like glucose-sensitive, insulin-producing environment [105].

2.1.1.2.2 Advanced embedded ink writing of full-scale human tissue and organ analogs

Embedded ink writing (EIW) has drawn significant attention due to its exceptional capability of constructing complex architectures as well as strong compatibility with various printable biomaterials and cell types. In EIW, a cellular bioink is extruded through a nozzle within a support bath to print 3D constructs layer by layer [106]. Despite its advantages, current EIW methods still struggle with two major engineering challenges. The first challenge is the difficulty of creating large-scale human tissue and organ constructs with high cell viability. This is because the printing process needs a long nozzle, which increases shear stress and extends shear time in the bioink extrusion, thus causing inevitable

and fatal cell damage. To address this challenge, the Jin group at the University of Nevada Reno recently developed a multiscale embedded printing (MSEP) method [107]. The support bath material used in this method is a stimuli-responsive yield-stress fluid (YSF) consisting of two components: the thermosensitive Pluronic F127 hydrogel and the yield-stress nanoclay additive [108]. The former enables the fluid to transition between sol and gel states by regulating the ambient temperatures, while the latter allows the fluid to exhibit given rheological properties at higher temperatures for embedded printing. Based on this fluid, the MSEP method was established, in which a large-scale human organ construct was segmented into multiple sections. A short nozzle was leveraged to print each section within the support bath at 37 °C to ensure cell viability. Between sections, 4 °C support bath material was perfused into a stackable container and kept until its temperature increased to 37 °C (Fig. 4a). To explore the fundamental physics, the Jin group used small-angle neutron scattering (SANS) to identify the microstructure evolution upon temperature change (Fig. 4b). Additionally, four representative human tissue and organ analogs (cornea, eyeball, aortic heart valve, and full-scale human heart) were printed by MSEP to demonstrate its excellent printing capability (Fig. 4c).

The second challenge is the speed barrier (on the order of 10 mm/s) in current EIW methods, which causes one severe biological issue: cell damage due to prolonged printing time. The limited printing speed of EIW is primarily due to the inability of current support baths to provide the desired rheological properties for high-speed printing. The existing support bath materials are commonly formulated using a particulate-dominated method, in which particle additives are dispersed in an aqueous solvent to prepare YSFs. Filament defects are observed when printing at high speeds [109]. To address this challenge, the Jin group recently proposed a particle-hydrogel interactive system to design YSFs, wherein the interactions between particle additives and hydrogel solvents were utilized to enhance the yield-stress level and extend the thixotropic response

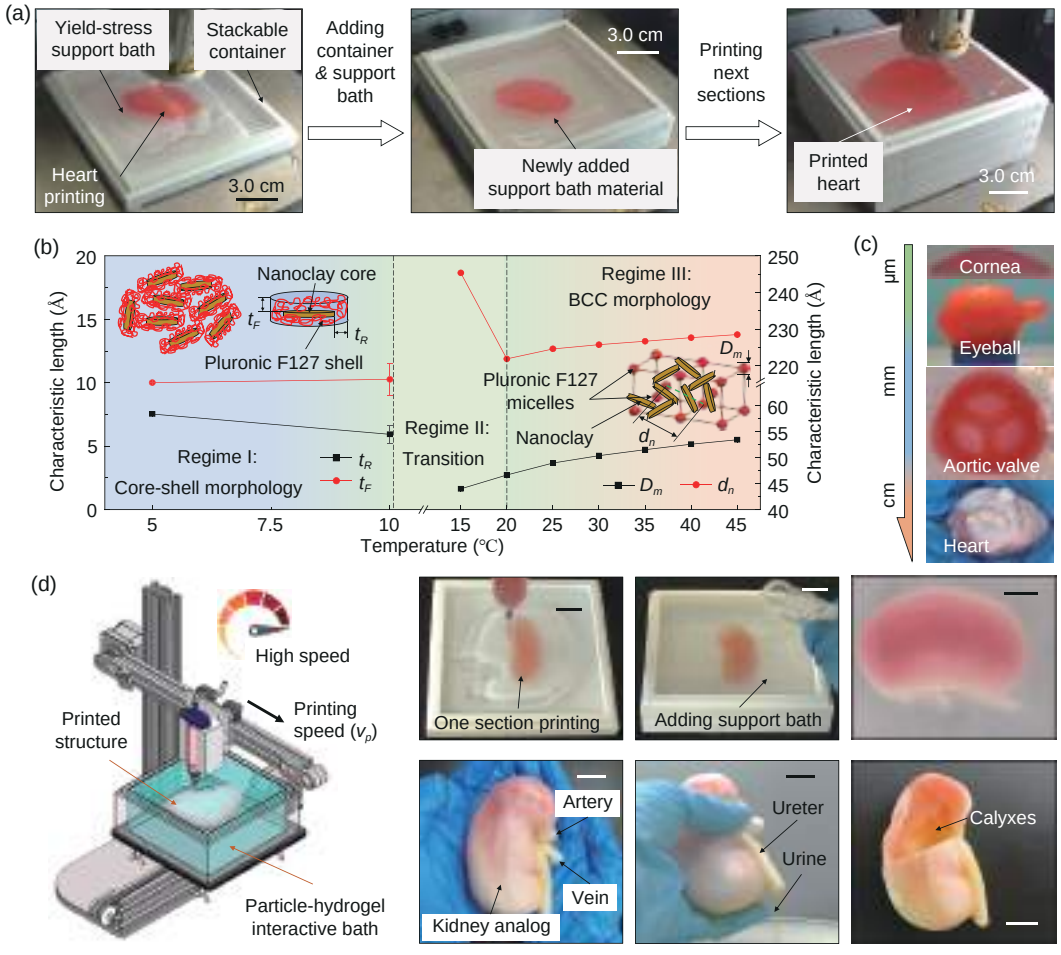

Fig. 4 Advanced EIW methods. (a) MSEP of multiscale human tissue and organ constructs in a section-by-section manner. (b) Microstructure evolution in the stimuli-responsive YSF through SANS. (c) Multiscale human tissue and organ analogs printed by MSEP. Reproduced from [107], licensed under CC BY-NC-ND. (d) High-speed EIW of human kidney analog (reproduced from [69], licensed under CC BY)

time [110]. Different interaction mechanisms between nanoclay and diverse hydrogels were systematically studied through SANS [111] and filament printing experiments [112, 113]. A high-speed EIW method was consequently developed to print an anatomic-size human kidney analog in only 4.2 h, which demonstrated a well-defined outer structure and detailed inner structures (Fig. 4d) [69].

2.1.1.2.3 Embedded bioprinting with photocuring for heterogeneous environment creation

Embedded bioprinting provides a powerful route for depositing cell-only or cell-laden inks within supportive hydrogel matrices; however, most existing support baths behave as temporary scaffolds or offer only uniform mechanical and biochemical properties, limiting their ability to recapitulate the spatial heterogeneity, dynamic reciprocity, and functional gradients characteristic of native tissues [114]. Overcoming these limitations is particularly important for engineering complex tissue interfaces, where local variations in extracellular matrix (ECM) composition, stiffness, degradation, and bioactivity play essential roles in guiding cellular organization and lineage specification. To address these challenges, the Guvendiren group at the New Jersey Institute of Technology has reported a versatile embedded bioprinting platform centered on a photocurable viscous support layer into which dense multicellular aggregates, cell-laden bioinks, or sacrificial inks can be printed and subsequently stabilized through brief light exposure (Fig. 5a) [86, 115, 116]. This photocurable support concept eliminates the traditional requirement for shear-thinning and shear-recovery behavior, substantially broadening the range of materials that can serve as support matrices, including both temporally stable and permanently crosslinkable hydrogels [117, 118].

This platform has enabled a suite of advanced biofabrication capabilities, including printing of complex perfusable 3D channels within cell-laden matrices for nutrient transport and vascularization studies, spatial modulation of support-bath heterogeneity by locally tuning polymer concentration or crosslinking density, incorporation and patterned presentation of biochemical signals such as adhesion peptides or growth factors, and precise patterning of dense multicellular structures that mimic developmentally relevant cell–cell interactions (Fig. 5b). These capabilities collectively allow the construction of heterogeneous hydrogel environments with unprecedented control over local ECM-mimetic cues.

Using methacrylated hyaluronic acid (MeHA) as a representative photocurable support, the Guvendiren group has demonstrated fine spatial control over human mesenchymal stem cell (hMSC) behavior by printing dense cellular aggregates into regions that differed in polymer concentration, Arg-Gly-Asp (RGD) functionalization, or inclusion of osteogenic cues such as tricalcium phosphate (TCP) particles and bone morphogenetic protein-2 (BMP-2). hMSC strands embedded in less dense (5%) MeHA regions exhibit significantly higher cell spreading, elongation, and osteogenic upregulation than strands in denser 10%–15% regions, illustrating how microscale mechanical heterogeneity can be leveraged to direct site-specific differentiation. Similarly, TCP-rich domains or BMP-2-releasing regions further enhance local osteogenesis, confirming the platform's ability to engineer biochemical gradients that modulate cell fate with high spatial precision (Fig. 5b) [115]. Extending this

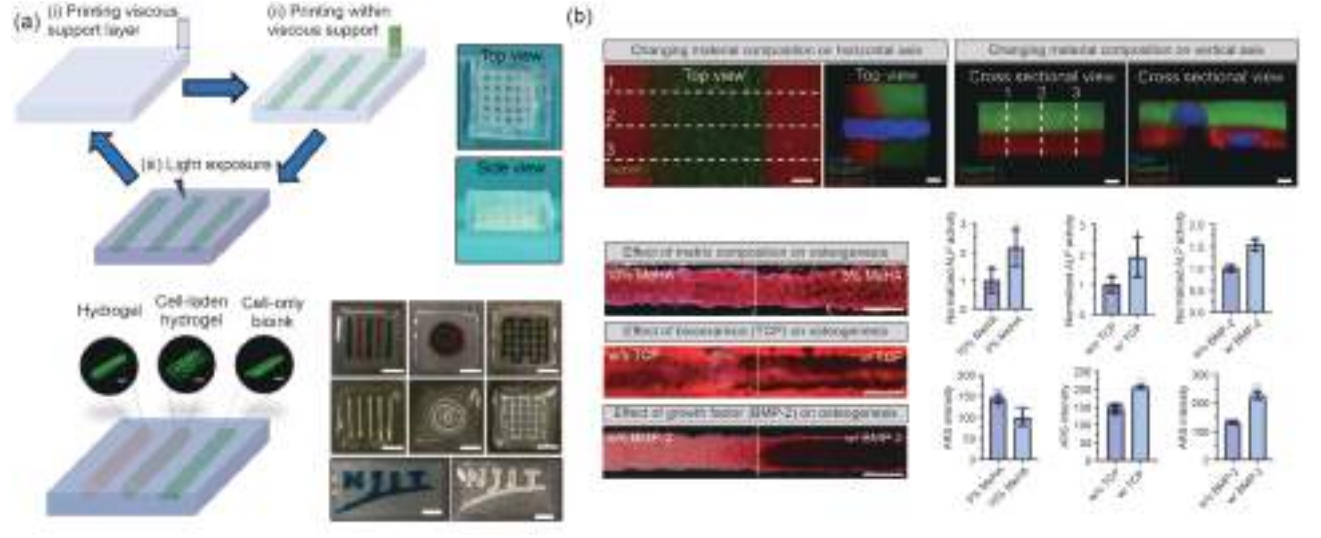

Fig. 5 Embedded bioprinting supports dense cellular fabrication and microenvironmental control. (a) Schematic and representative images of an embedded bioprinting approach for fabricating dense cell-laden and cell-only structures within functional hydrogels. (b) Controlling support matrix heterogeneity spatiotemporally modulates stem cell osteogenesis as demonstrated by calcium deposition after 14 d of culture in osteogenic induction medium within biphasic MeHA hydrogel supports. Reproduced from [115], with permission from IOP Publishing Ltd.

framework, the Guvendiren group also demonstrated that hydrogels embedded with human bone allograft particles provide intrinsically osteoinductive microenvironments capable of driving osteogenesis of hMSC strands even under basal culture conditions, with the magnitude of osteogenic response strongly dependent on particle concentration [116]. This finding highlights the potential of integrating clinically relevant biomaterials into printed constructs to better recapitulate native bone matrix cues and accelerate translational applications.

Collectively, these studies have established a robust and broadly applicable embedded bioprinting strategy for fabricating densely packed, developmentally inspired multicellular architectures within cell-instructive, spatially patterned hydrogel matrices. By enabling precise control over microenvironmental properties, cellular arrangement, and perfusable features, this platform represents a critical step toward engineering highly heterogeneous tissues, such as osteochondral units, vascularized bone, and complex stromal interfaces, with the structural and functional fidelity required for next-generation regenerative medicine and disease modeling.

2.1.2 Vat polymerization

Although one of the first 3D printing methods to be developed, vat polymerization was not applied to biomedical applications until the early 2000s [119, 120]. Since then, however, it has emerged as a manufacturing approach with incredible promise in biofabrication due to the relative speed and feature sizes attainable with these technologies. In general, vat polymerization refers to 3D printing techniques that selectively crosslink a vat of material, often referred to as a resin. Almost always, light is used as the mechanism of crosslinking, polymerizing components within the vat, traditionally layer by layer, to create a 3D structure. In the context of biofabrication and biomedical manufacturing, the materials used for this printing approach are often biocompatible and can form ultraviolet (UV)-crosslinked hydrogels upon polymerization. Within this category, there are subcategories that use variations of this approach, such as stereolithography (SLA), two-photon lithography (TPL), and digital light processing (DLP) [119]. Although many innovations related to vat polymerization have focused on material modification and optimization, some of the most significant breakthroughs have occurred as a result of hardware, software, and process developments [121, 122].

In the U.S., vat polymerization-based biofabrication has evolved from rapid photopatterning of scaffolds to increasingly sophisticated platforms for heterogeneous, high-resolution, and functionally organized living constructs. The Chen group at the University of California San Diego has established this direction by developing projection SLA approaches for tissue-engineering scaffolds with microscale architectural control [123]. Later, the Miri lab, now at the New Jersey Institute of Technology, along with the Khademhosseini group, Zhang group, Chen group, and other colleagues, extended the technology to microfluidics-enabled multimaterial maskless stereolithographic bioprinting, enabling rapid switching among bioresins for heterogeneous hydrogel constructs [124]. The Soman group at Syracuse University has further contributed to process innovation by developing a vat-free droplet DLP bioprinting strategy that reduces bioink waste and cell-settling artifacts while maintaining high-resolution printing of cell-laden constructs [125]. More recently, the Burdick group at the University of Colorado has expanded vat photopolymerization to microgel-reinforced hydrogels, illustrating how resin design can broaden the mechanical and processing window of light-based biofabrication [126]. These efforts illustrate how U.S. groups have pushed vat polymerization from a high-resolution shaping method toward a more versatile platform for multimaterial, microarchitecturally controlled, and functionally programmed biofabrication. This section provides some snapshots of the developments in vat polymerization for biofabrication in the U.S.

2.1.2.1 Digital light processing

The Chen group at the University of California San Diego has focused on developing 3D bioprinting technologies aimed at tackling many key manufacturing challenges, including materials synthesis, printer design, light-matter interactions, mechanics of the tissue construct, printing throughput, reproducibility, and scalability. In their early work, the Chen group developed a microscale 3D printing platform for hydrogel biomaterials [127, 128]. In 2006, they developed a rapid, projection 3D printing method to produce highly precise, 3D microstructures from a broad selection of functional materials—a first in the field for projection 3D printing of hydrogel biomaterials for tissue engineering [123]. In contrast to a traditional 3D printing process (e.g., SLA or extrusion-based printing) where a 3D device is fabricated point-by-point or line-by-line using DLP, this light-projection printing method enables an entire layer of biomaterial to be fabricated simultaneously, resulting in a much faster printing speed and better device integrity.

Building upon this DLP-based 3D printing technique, the Chen group invented a dynamic optical projection stereolithography method (DOPsL) [129]. This is another first in the field of dynamic and continuous 3D printing of hydrogel biomaterials. DOPsL enables rapid 3D bioprinting that is 1000 times faster in printing speed and 100 times higher in printing resolution compared to traditional extrusion-based 3D printing. This continuous printing approach significantly improves the structural integrity of the 3D-printed

parts since the process does not create artificial interfaces within the part. More recently, the Chen laboratory invented a high-throughput, direct in-well bioprinting method for 3D microtissues in a standard multiwell plate (Fig. 6) [130]. This technique has enabled pharmaceutical companies to conduct high-throughput drug screening using bioprinted microtissues with much-needed speed, throughput, resolution, and well-plate compatibility.

One of the major bottlenecks for future organ manufacturing is the ability to print organs with a high cell density for critical cell–cell interactions to recapitulate physiological conditions. The Chen group invented a high cell density bioprinting method for future organ printing (Fig. 7) [121]. They designed a novel bioink material containing an optical tuning agent that can minimize light scattering by the cells and enable printing living materials at high resolution and high cell viability. This work represents the first DLP-based bioprinting for high-cell-density vascularized tissues in the field.

2.1.2.2 Light-based multimaterial and multiscale fabrication

Nature's manufacturing capabilities outperform human engineering through hierarchical structuring, resource efficiency, and versatile self-assembly. Man-made methods, in contrast, are often energy-intensive and create less complex, single-function materials. To overcome these limitations, the Soman laboratory at Syracuse University seeks to create functional structures from soft biomaterials that resemble the complex, multifunctional designs found in native tissues. Over the years, the Soman group has utilized a mutually reinforcing positive feedback loop between technology, scientific discovery, and application to drive sustained scientific impact in the fields of bioprinting [125, 131, 132], organ-on-chip [133–136], tissue engineering [137–139], and microfabrication [140–142].

To shape hydrogel-based bioinks into multiscale and multimaterial 3D constructs, the Soman group developed several 3D bioprinting platforms. (1) Hybrid laser platform (HLP) [82, 143] (Fig. 8a)—HLP can be switched between three modes of operation, namely (i) additive projection stereolithography mode (PSLA) capable of printing inch-sized 3D constructs with a resolution of approximately 50 μm, (ii) subtractive multiphoton ablation (MPA) mode, and (iii) additive two-photon polymerization (MPP) mode. MPA/MPP can achieve a resolution of approximately 1 μm. By combining these modes of hydrogel processing into one versatile machine, HLP can print 3D structures that are not possible with current technologies. (2) Multipath projection stereolithography (MPS) [144] (Fig. 8b) —inspired by conventional microscopes that can switch objectives to achieve multiscale imaging, MPS can switch between high- and low-resolution optical paths, and address the inherent tradeoffs between print resolution, design complexity, and build sizes. This required the design of two illumination and projection systems, slicing software, and hardware that seamlessly work as a single integrated unit. Using microfluidic devices with embedded micromixers as a test case, MPS can print centimeter-sized chips (3 cm×6 cm) with a feature resolution of approximately 10 μm, which opens doors to multiscale hydrogel printing. (3) Meniscus-enabled projection stereolithography (MAPS) [122] (Fig. 8c)—MAPS is a vat-free method that relies on generating and maintaining a hydrogel meniscus between a crosslinked structure and a bottom window to print lateral, vertical, discrete, or gradient multimaterial 3D structures with no waste and user-defined mixing between layers. MAPS's ability to print

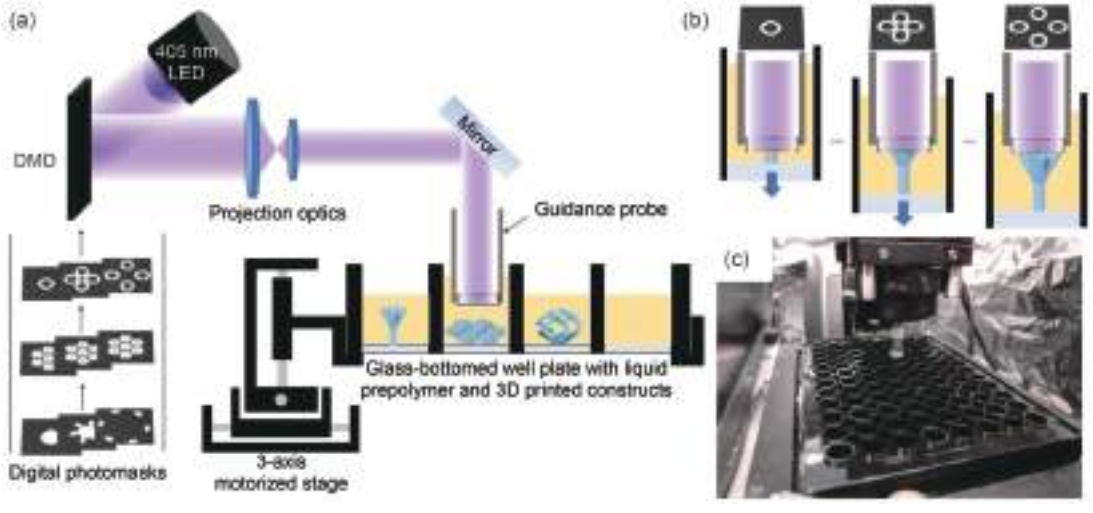

Fig. 6 High-throughput bioprinter system. (a) Schematic of the high-throughput bioprinter, in which digital photomasks projected through a digital micromirror device photopolymerize prepolymer solutions in a well plate on a motorized stage. (b) Time-lapse schematic depicting synchronized mask projection and stage motion for rapid continuous printing of a single 3D construct. (c) Photograph of high-throughput bioprinter setup printing in a standard 96-well plate. Reproduced from [130], with permission from IOP Publishing Ltd.

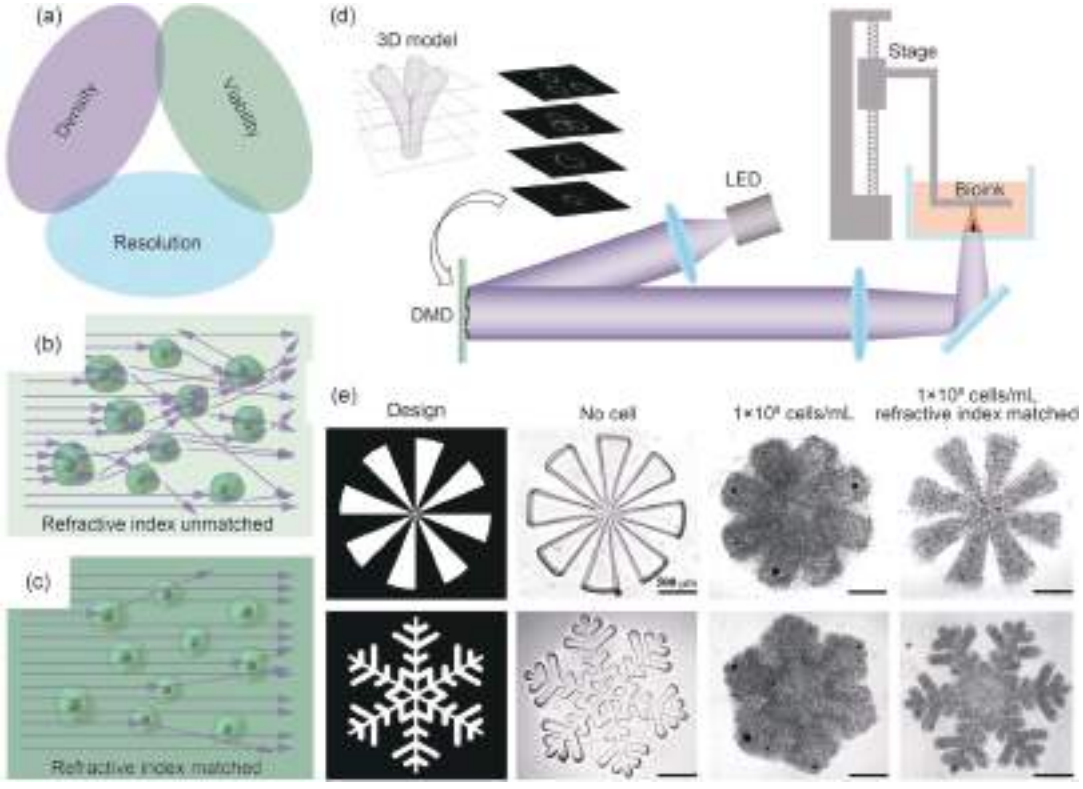

Fig. 7 Achieving high fabrication resolution in high-cell-density bioinks. (a) The "impossible trinity" in bioprinting: high cell density, high cell viability, and high fabrication resolution. Schematics showing light propagation in refractive-index-unmatched (b) and refractive-index-matched (c) bioinks, showing reduced light scattering in the matched system. (d) Working principle of the DLP-based bioprinter. (e) Printing resolution comparison among three different bioink compositions: bioink without cells, bioink with 1×10^8 cells/mL, and refractive-index-matched bioink with 1×10^8 cells/mL (scale bars: 500 μm). Reproduced from [121], licensed under CC BY 4.0

hydrogel structures with microscale variations in mechanical stiffness, opacity, surface energy, cell densities, and magnetic properties without requiring specialized hardware, software, or complex washing protocols provides a generic method to make advanced materials for a broad range of applications. In science, new technologies often trigger new unforeseen lines of scientific inquiry. For instance, the Soman group discovered that femtosecond (fs) laser 'densification' can be used to align single cells in user-defined patterns within a 3D hydrogel matrix [145]. The Soman group also discovered that laser-assisted cavitation can be used to generate 3D single-cell circuits (Cellnets) in custom architectures within natural collagen, and its response to stimuli can be studied in a reproducible manner [146] (Fig. 8d). The Soman group envisions that Cellnet technology, which is agnostic of cell types, ECM formulations, 3D cell connectivity designs, and the location/timing of network disruptions, will enable broad adoption in the field to elucidate higher-level emergent properties.

2.1.3 Material jetting

Material jetting, often implemented using inkjetting and laser-induced forward transfer (LIFT), uses a similar approach to two-dimensional (2D) inkjetting, where ink droplets are ejected from a head onto a substrate, either continuously or on demand [147]. In particular, inkjetting was one of the first 3D printing technologies used for tissue engineering [148]. When applied to biofabrication, the selected inks are often biocompatible materials with encapsulated cells, which are precisely arranged to create layers of a 3D structure. While all material jetting biofabrication approaches involve the creation of bioink droplets, the mechanisms used to accomplish this can vary widely and depend on the material systems being used. Droplets can be produced via piezoelectric actuators, thermal interactions, and electrostatic interactions, to name a few [147], as well as a pulsed laser [149]. The strength of material jetting for biofabrication comes from the ability to rapidly and precisely pattern droplet deposition on the substrate with a large direct-write height, allowing for spatial control of cells and materials [150]. Many recent material jetting process innovations relate to optimizing cell distribution and the fabrication of 3D structures [151, 152].

Material jetting has been shaped by influential U.S. contributions that established droplet-based cell deposition as a viable biofabrication strategy. In terms of inkjetting, the Boland group, now at the University of Texas at El Paso,

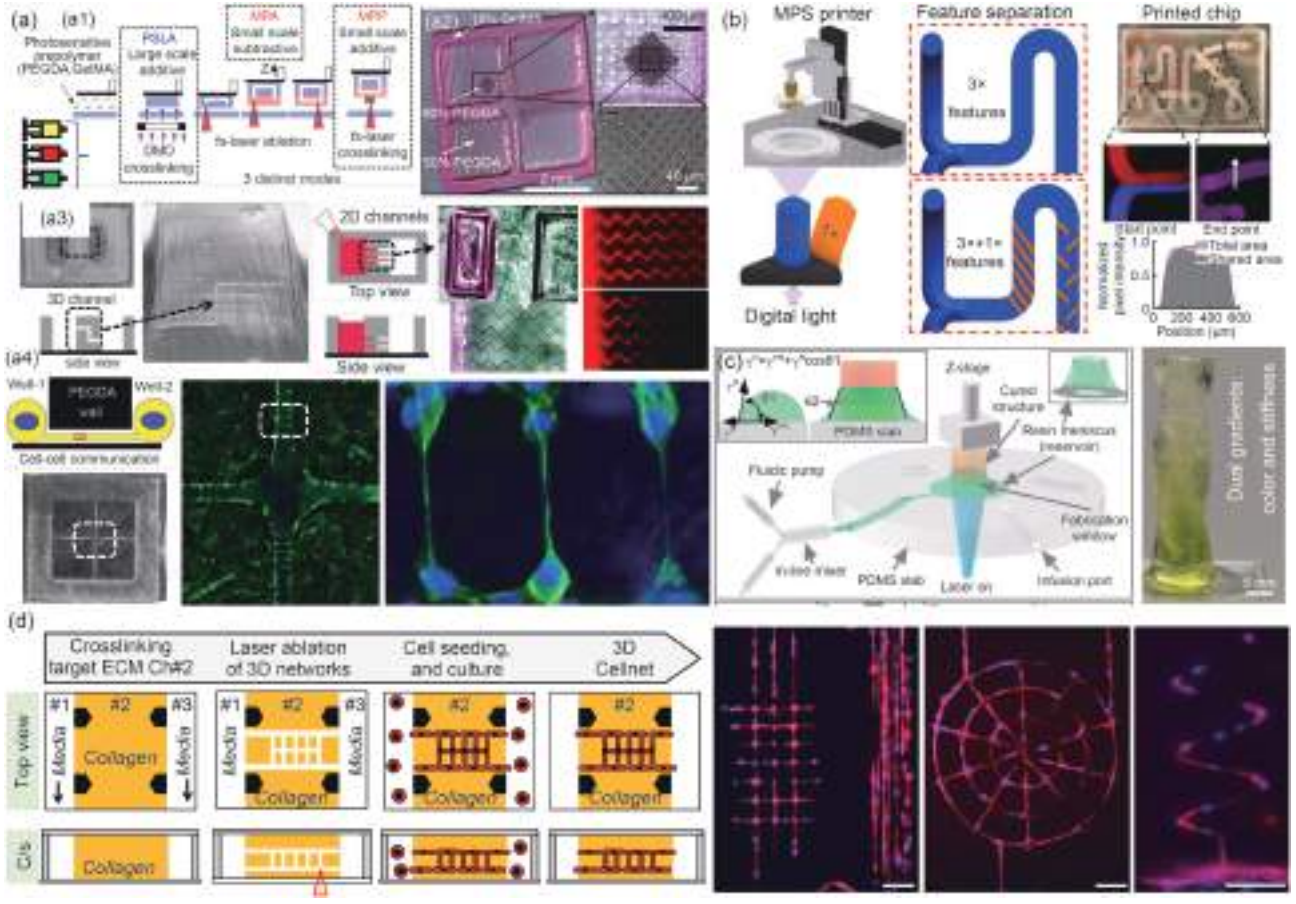

Fig. 8 Representative advances in light-based multimaterial and multiscale fabrication. (a) HLP platform: (a1) HLP in sequential additive-subtractive mode; (a2) bright-field image of a four-well polyethylene glycol diacrylate (PEGDA) chip with interwell microchannels (fluorescence images show actin (green) and nuclei (blue); MLO-Y4 cells seeded in neighboring wells communicate with each other by extending cell processes within the ablated channels; white arrows point to communication channels with a diameter of 5 μm); (a3) printing user-defined two-well PEGDA chips with interconnecting out-of-plane microchannels (side, isometric, and top views of 3D channels spanning multiple crosslinked layers are depicted); (a4) HLP in sequential macro-additive and micro-additive mode to print three woodpile structures at different depths. Reproduced from [82], with permission from WILEY-VCH Verlag GmbH & Co. KGaA, Weinheim. (b) MPS printer with two additive printing modes similar to those of conventional microscopy. MPS uses flip-mounted mirrors to switch between objectives to print a 3D microfluidic device with embedded micromixers of various types. Reproduced from [144], licensed under CC BY 4.0. (c) Schematic setup illustrating the MAPS 3D printing by a continuous flow of resin solution using syringe pumps and an inline micromixer. The programmed updown motion of the z-stage draws the liquid into the fabrication area, while the projected light crosslinks the resin solution. Gradient property printing of the twisted tower shows dual-color and compressive modulus gradients with PEGDA resins. Reproduced from [122], licensed under CC BY. (d) Schematic showing the workflow to generate Cellnets. Representative images show single cells organized within user-defined architectures (scale bars: 100 μm; actin: red; nucleus: blue). Reproduced from [146], licensed under CC BY 4.0

has expanded thermal inkjet bioprinting by demonstrating that viable mammalian cells could be dispensed from a modified commercial printer while retaining short-term function, laying the foundation for low-cost, computer-aided cell patterning [153]. The Huang group, now at the University of Florida, developed scaffold-free and reactive-material jetting strategies that expanded the process beyond simple droplet deposition, demonstrating platform-assisted inkjet printing of 3D zigzag cellular tubes [154]. The Huang group further developed an intersecting jet-based inkjet bioprinting method for in situ printing-then-mixing of reactive and heterogeneous materials [155]. More recently, the Xu group at Texas Tech University developed circulation-assisted inkjet bioprinting to mitigate cell sedimentation and aggregation, improving printing reliability for cell-laden bioinks [70]. Regarding LIFT, the Chrisey group, now at Tulane University, has advanced laser direct-write/matrix-assisted pulsed laser evaporation direct writing (MAPLE DW) methods, now also known as LIFT, for the spatially precise transfer of cells and biomaterials [149]. The Huang group further implemented LIFT for 3D construct printing in a support bath by controlling the gelation rate of deposited cellular droplets [156]. These representative efforts demonstrate U. S. research progress in material

jetting-based biofabrication, which enables noncontact deposition, high spatial precision, and process innovations that improve structural complexity and bioink handling. Some of these recent innovations are highlighted in this section.

2.1.3.1 3D inkjet bioprinting of cell-laden tissue and tumor microenvironment model

Bioprinting has rapidly evolved as a transformative AM technology toward the fabrication of functional tissues and organs. However, cell sedimentation and aggregation have been widely recognized as significant challenges during the printing process, which significantly affect cell distribution as well as corresponding tissue growth and the final functionality of the fabricated tissues and organs.

To address these challenges, the Xu group at Texas Tech University systematically investigated cell sedimentation and aggregation mechanisms and their effects on printing performance during bioprinting of vascular structures [70, 151, 152, 157–162]. First, the mechanisms of cell sedimentation and aggregation have been studied by analyzing the forces on individual cells during inkjet-based bioprinting, including gravitational force, drag force, buoyant force, and force due to cell–cell interaction based on the bond model [151, 158]. The sedimentation velocity is almost constant at different printing times of 0–60 min with an interval of 15 min. In the bioink with 0.5% and 1% sodium alginate, the fibroblast sedimentation velocities are 1.45 μm/s and 0.65 μm/s, respectively [158]. Second, cell sedimentation and aggregation have been investigated within the bioink reservoir and the nozzle during bioprinting and within microspheres after bioprinting (Fig. 9a) [152]. Within the bioink reservoir, the percentage of cells forming cell aggregates increased significantly from 3.6% to 54.5% for the bioink with 0.5% sodium alginate and 1.5×10^6 cells/mL fibroblasts. Inside the nozzle, more than 80% of cells have formed cell aggregates at a printing time of 15 min, and the cell aggregates migrated to the nozzle centerline region due to the weak shear-thinning properties of the bioink. After bioprinting, approximately 30% of microspheres contain

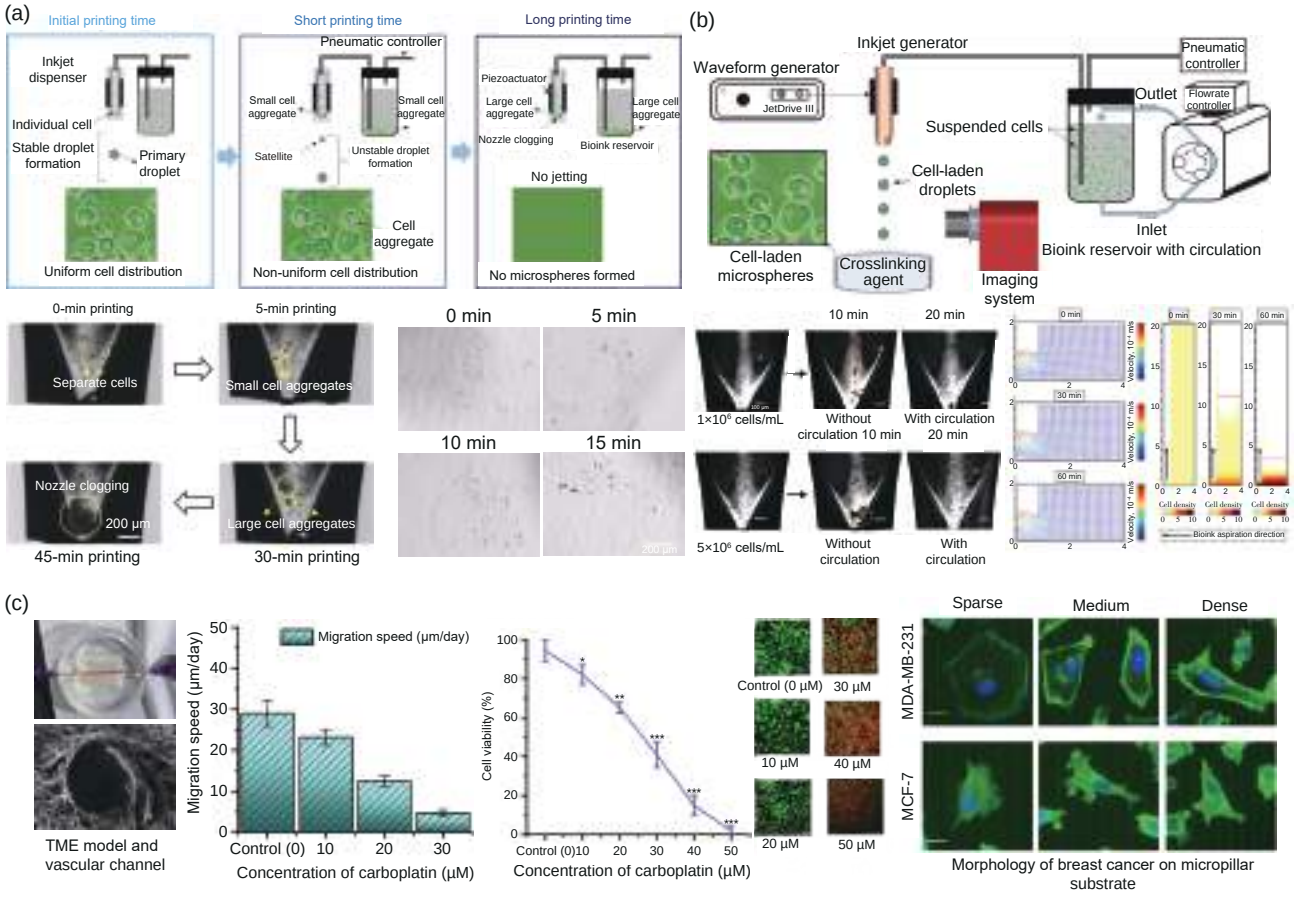

Fig. 9 Bioink handling and perfusable tumor models enabled by material jetting. (a) Cell sedimentation and aggregation within the bioink reservoir, the nozzle, and microspheres (reproduced from [152], with permission from the American Chemical Society). (b) Active bioink circulation to reduce cell sedimentation and aggregation (reproduced from [70], with permission from IOP Publishing Ltd.; reproduced from [159], with permission from the Society of Manufacturing Engineers). (c) 3D-printed perfusable ovarian tumor microenvironment model to study the behavior of chemo-naïve and chemo-resistant ovarian cancer cells under dynamic drug delivery and the morphology of low- and high-metastatic potential breast cancer cells (reproduced from [166], licensed under CC BY 4.0; reproduced from [167], with permission from Elsevier B.V.)

cell aggregates at a printing time of 15 min [157]. Finally, a novel active bioink circulation-assisted inkjet-based bioprinting has been proposed to mitigate cell sedimentation and aggregation. At both low (1×10^6 cells/mL) and high (5×10^6 cells/mL) cell concentrations, the active circulation system significantly improves cell distribution uniformity, reducing large cell aggregates by approximately 50% (Fig. 9b) [70, 163]. A computational model has been developed to predict the dynamic performance of cell distribution, considering the influence of cell sedimentation and active bioink circulation [164]. The post-printing cell viability is 60% without active circulation and 92%–94% with active circulation [165].

The tumor microenvironment (TME) plays a critical role in cancer metastasis. Traditional 2D models and 3D spheroid/organoid models are limited in capturing cancer migration and invasive phenotypes due to their limited capacity to reproduce the native TME. The Xu laboratory developed a perfusable 3D gelatin methacryloyl (GelMA)-based TME model to investigate the behavior of chemo-naïve and chemo-resistant ovarian cancer cells under dynamic drug delivery (Fig. 9c) [166]. Under continuous carboplatin perfusion, cell migration significantly declines from 29 to 5 μm/day with predominantly random trajectories, and viability drops to 5% at 50 μmol/L carboplatin. In addition, graded micropillar substrates have been utilized to study how mechanical and topographical cues regulate the morphology of breast cancer cells with low and high metastatic potential [167]. MDA-MB-231 cells become progressively elongated, while MCF-7 cells show minimal morphological changes, demonstrating that the highly metastatic cells strongly remodel their morphology in response to ECM topography.

2.1.3.2 Laser direct-write (LDW) bioprinting

Laser direct-write bioprinting (LDW-B), or LIFT, utilizes a nanosecond pulsed excimer UV-C laser beam focused on a transparent print ribbon coated with the cells suspended on a sacrificial matrix hydrogel layer (most commonly gelatin), resulting in rapid forward transfer of cells while protecting them from adverse effects of laser radiation (Fig. 10a).

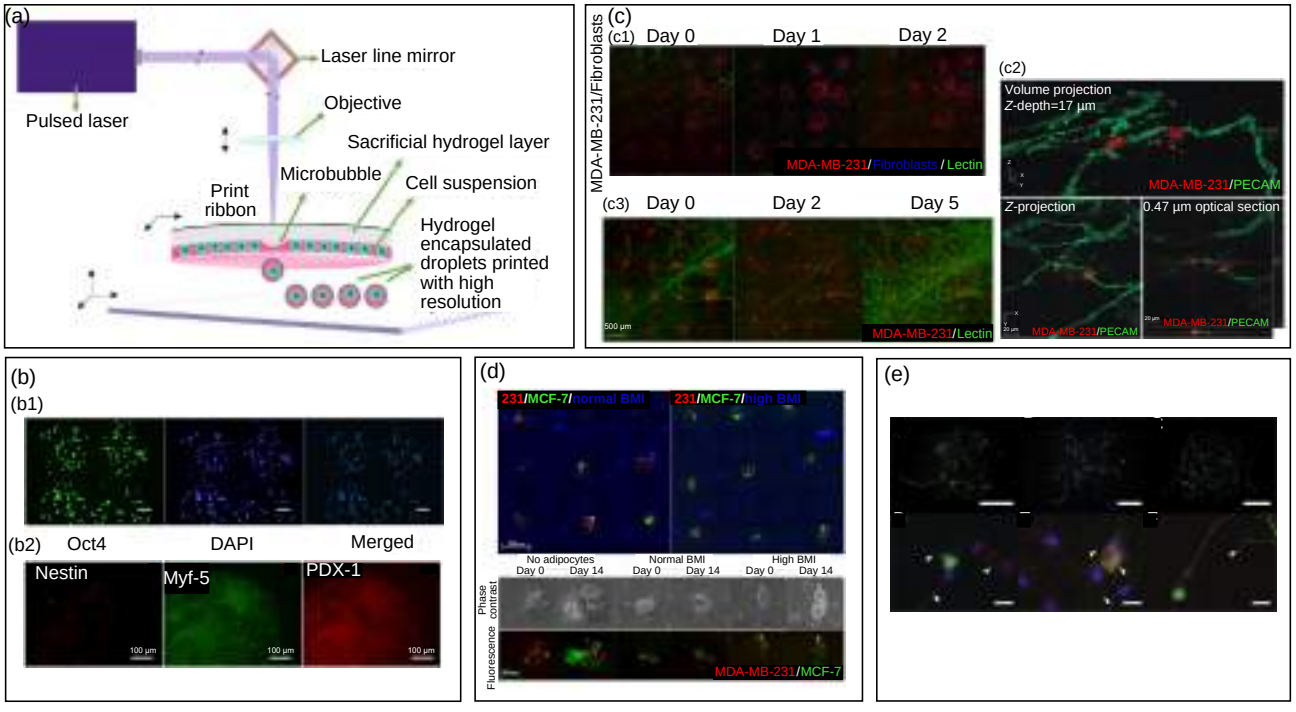

Fig. 10 Laser direct-write (LDW) bioprinting supports high-resolution cell patterning and disease modeling. (a) LDW bioprinting process (reproduced from [83]). (b) LDW bioprinted embryonic stem cells maintain pluripotency and differentiation potential: (b1) over 99% of embryonic stem cells express Oct4 post-printing; (b2) printed stem cells retain the ability to differentiate into cell types expressing markers for ectoderm, mesoderm, and endoderm. Scale bars: 100 μm. Reproduced from [173], with permission from Elsevier Ltd. (c) LDW bioprinted human breast cancer cells onto vascular networks recapitulate metastatic processes: (c1) fibroblast-directed migration of printed breast cancer cells toward areas of high vascular density; (c2) single-cell resolution LDW bioprinting and invasion of breast cancer cells into vasculature (scale bar: 20 μm); (c3) printed breast cancer cells inducing neoangiogenesis in mesenteric tissue (scale bar: 500 μm). Reproduced from [176], with permission from The Royal Society of Chemistry. (d) Microbead-encapsulated human breast cancer cells bioprinted on adipose matrix derived from high body mass index (BMI) patients show invasion (cancer cell outgrowth from microbeads) while those printed on matrix derived from normal BMI patients or no adipose matrix do not. Top panel scale bar: 500 μm; bottom panel scale bar: 200 μm. Reproduced from [178], with permission from IOP Publishing Ltd. (e) Immunofluorescence images of developing networks formed by LDW bioprinted primary dorsal root ganglia (reproduced from [180], with permission from IOP Publishing Ltd.)

During printing, cell-laden droplets are encapsulated in the hydrogel, cushioning them from shear stress when the droplet lands on the harder receiving substrate. This makes LDW-B gentle on the cells and leads to high post-printing viability. Due to the high precision enabled by computer-aided design and computer-aided manufacturing integration and in situ, real-time optical imaging of the ribbon and substrate, LDW-B has the capability to better mimic the complexity of native human tissue at the cellular scale, reproducibly pattern multiple cell types with high resolution and fidelity, and control cell–cell and cell–microenvironment interactions, which could ultimately enable the construction of tissues in hierarchical units rather than simply growing them. Additionally, as an automated, noncontact, scaffold- and nozzle-free bioprinting technique, LDW-B can offer unique advantages for biomedical manufacturing in terms of enhancing throughput, sterility, and customization [83, 149, 168–171].

The Chrisey group at Tulane University has adapted direct-write rapid prototyping technologies to develop gentle and versatile laser-assisted bioprinting techniques, with the aim of expanding upon traditional tissue engineering methods to take the next step toward the eventual goal of printing functional tissues. They have demonstrated the applicability of gelatin-based LDW-B to engineer disparate physiologically relevant tissue constructs in vitro, ranging from the stem cell niche to the breast cancer microenvironment to neuronal networks.

The ability to precisely pattern stem cells into predefined geometries is an important step for engineering the stem cell niche to facilitate functional tissue regeneration [172]. The Chrisey group has demonstrated the ability to viably print mammalian embryonic stem cells in precise spots using LDW-B. The printed stem cells maintained their pluripotency as well as the ability to differentiate into ectodermal, mesodermal, and endodermal lineages (Fig. 10b) [173]. Similarly, cancer cell invasion and metastasis are highly dependent on interactions of cancer cells with the stroma and vasculature [174, 175]. The Chrisey group has demonstrated viable LDW-B of human breast cancer cells with up to single-cell resolution into microvascular networks, enabling time-lapse evaluation of cancer cell dynamics. Printed breast cancer cells exhibited stromal-directed migration toward denser vasculature, stromal-mediated invasion into vasculature, and propensity to induce neoangiogenesis—recapitulating metastatic phenomena observed in vivo and potentially serving as a novel model to test targeted therapies (Fig. 10c) [169, 171, 174–176]. The research group has also demonstrated the capability of the LDW-B system to reproducibly fabricate and pattern cell-laden microbeads [177]. Human breast cancer cells encapsulated within microbeads showed increased invasiveness when printed onto adipose matrices derived from obese patients, compared with adipose matrices derived from lean patients (Fig. 10d) [178]. Finally, viable and functional printing of highly sensitive cells, such as neurons, is extremely challenging with conventional bioprinting techniques [179]. The Chrisey group has demonstrated viable, accurate, and reproducible patterning of mammalian dorsal root ganglion neurons and glial cells with LDW-B. The printed neurons displayed neurite outgrowth, network formation, and neurotransmitter transporter expression, indicating the potential to model healthy and diseased states for neurodegenerative disorders in vitro (Fig. 10e) [180].

In addition, the Huang group at the University of Florida has explored drop-on-demand approaches for biofabrication, researching both inkjetting for its good jetting and droplet formation controllability [181, 182] and LIFT for its orifice-free printing nature in depositing highly viscous bioinks. Figure 11a shows some inkjet-printed structures with both horizontal and vertical branching features [181], without (Fig. 11a1) and with (Fig. 11a2) cell-laden bioinks, and Fig. 11b depicts a LIFT-printed Y-shaped cellular tube [156]. Both have utilized a buoyancy support-assisted approach.

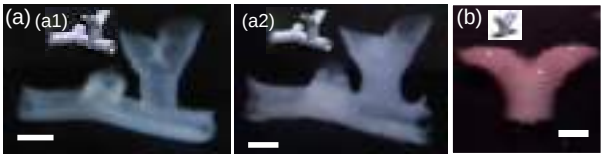

Fig. 11 Representative images of structures printed with drop-on-demand (DOD) approaches. (a) Inkjet-printed bifurcated structures, with (a1) alginate-only ink, allowing for higher geometric fidelity, and (a2) cell-laden inks. Scale bars: 3 mm. Reproduced from [181], with permission from Wiley Periodicals, Inc. (b) Y-shaped cell-laden alginate tubes printed using LIFT. Scale bar: 5 mm. Reproduced from [156], with permission from IOP Publishing Ltd.

2.2 Other biofabrication and biomedical manufacturing processes

Aside from standard 3D printing technologies that have been applied to biofabrication and biomedical manufacturing, a number of approaches that fall outside these techniques have emerged as effective methods for creating tissue-engineered constructs. Although they bear distinctions from standard bioprinting modalities, the techniques in this section are also capable of producing structurally organized, biologically functional products. Commonly implemented processes within this category include 4D biofabrication and programmable functions [183], cell-spheroid and organoid-based biofabrication [184], electrodynamic-based processes, and other printing and alternative manufacturing processes, such as platforms that address long-standing bottlenecks in translation, such as cryobioprinting for preservation and logistics [185, 186], advanced bioink formulations for

structural stability [187], and precision methods for patient-specific scaffold fidelity and physiological-material printing [72]. These innovations (Fig. 12) demonstrate how U.S. groups are pushing biofabrication forward toward engineering smart, biomimetic, and clinically relevant constructs using innovative techniques.

2.2.1 4D biofabrication

Despite various advances, conventional 3D bioprinted constructs remain geometrically static after fabrication, overlooking the dynamic morphogenetic processes that drive tissue development in vivo [188, 189]. 4D biofabrication, a cutting-edge biofabrication technology that incorporates the temporal dimension, has demonstrated the ability to create tissue constructs capable of preprogrammed, stimuli-responsive transformations using cytocompatible and biodegradable biomaterials. As an emerging advanced biofabrication technique, 4D bioprinting shows great promise for creating "smart" structures with dynamic and programmable behaviors [183, 190]. By responding to specific external stimuli, 4D-printed scaffolds can undergo controlled shape or functional changes, enabling better adaptation to the dynamic nature of native tissues.

2.2.1.1 4D printing multiresponsive nano/smart structures

The Zhang group at George Washington University developed 4D printing multiresponsive nano/smart structures and explored applications in complex tissue regeneration and soft biorobotics [28, 71, 190–195]. In this effort, they systematically investigated the kinetics of shape transformation [28], refined a series of shape memory polymer (SMP) formulations [28, 71], and integrated these materials across extrusion [71, 191], SLA [28, 194, 196], and DLP [197] printing platforms. Notably, the Zhang group synthesized natural SMPs derived from soybean oil for 4D bioprinting for the first time [28]. Using an SLA-based printing technique, novel multiresponsive 4D structures were created (Fig. 13a), which exhibited both reversible solvent-induced 4D shape transformation and a thermoresponsive shape memory effect [28]. To achieve highly precise and remotely controlled 4D shape transformations, nanomaterials were integrated with thermal-responsive SMPs to enable reliable near-infrared (NIR) light-triggered actuation [71, 191]. In a recent study, the Zhang group developed a dual NIR- and magnetically responsive nanocomposite for 4D printing by doping polypyrrole (PPy)-coated magnetic iron oxide (Fe_2O_3) nanoparticles into an SMP matrix [71]. The nanocomposite enabled the fabrication of three smart biorobots with cargo-delivery capabilities (Fig. 13b), which can be remotely actuated by NIR illumination and an external magnetic field.

Importantly, their 4D bioprinting strategy has advanced into neural and cardiovascular regeneration. A proof-of-concept, reprogrammable nerve guidance conduit that promoted neurogenic differentiation of hMSCs highlights its potential for nerve repair [28]. In another study, the Zhang group fabricated a 4D self-morphing substrate to evaluate its feasibility for enhancing the dynamic growth and differentiation of neural stem cells for the first time (Fig. 13c) [192]. The 4D culture system exhibited a time-dependent morphing process that played a critical role in regulating neural stem cell behaviors in a spatiotemporal manner, resulting in enhanced neural differentiation and significant axonal alignment.

Beyond nerve regeneration, the Zhang group has explored myocardial regeneration by developing a biomimetic, hydrogel-based 4D anisotropic cardiac patch capable of achieving superior dynamic integration with the beating heart in a murine myocardial infarction model (Fig. 13d) [194]. The 4D cardiac patch demonstrated robust epicardial engraftment, structural durability, and heart-to-patch blood perfusion for a 4-month implantation. In addition, the printed cardiac patch showed the formation of capillary-like endothelial networks, and the vascularized structure greatly improved the viability and functionality of human induced pluripotent stem cell-derived cardiomyocytes (hiPSC-CMs) [194].

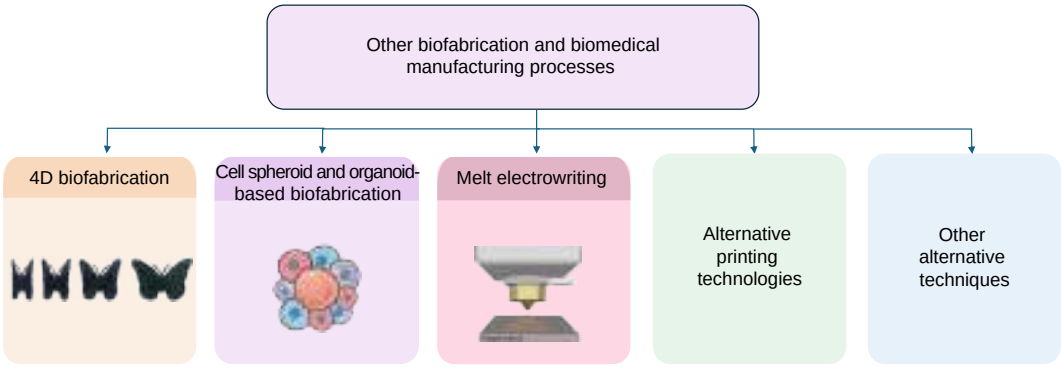

Fig. 12 Alternative biofabrication and biomedical manufacturing processes. Copyright information: "4D biofabrication" (reproduced from [71], licensed under CC BY-NC)

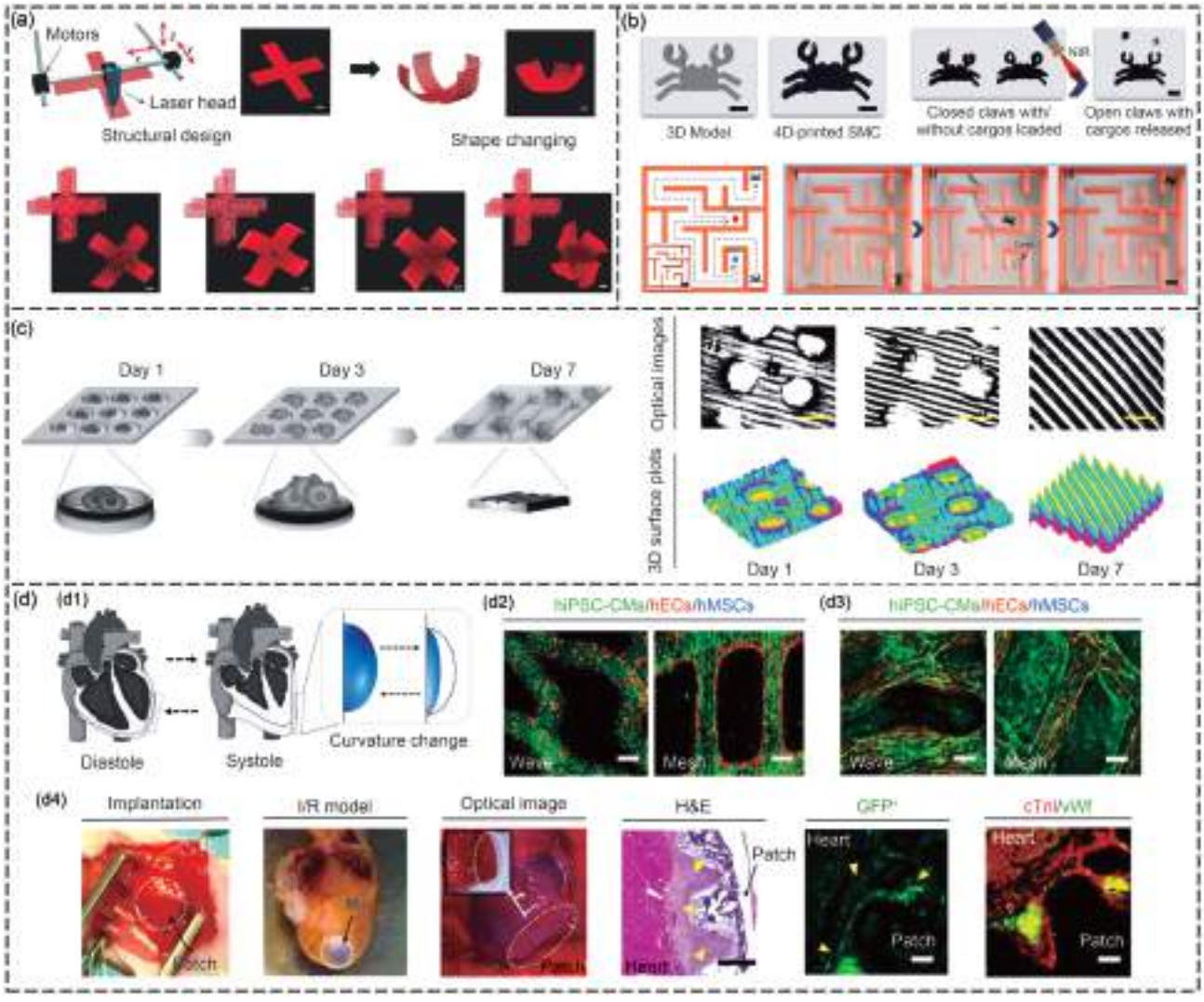

Fig. 13 4D bioprinting for biomedical applications. (a) 4D pattern design and shape transformation achieved using multiresponsive SMP and SLA printing. Scale bars: 2 mm. Reproduced from [28], with permission from WILEY-VCH Verlag GmbH & Co. KGaA, Weinheim. (b) Smart crab robot printed with NIR- and magnetically responsive nanocomposite (scale bars: 2 mm). The 4D-printed smart crab can perform cargo delivery tasks in a maze. Reproduced from [71], licensed under CC BY-NC. (c) Dynamic 4D self-morphing culture substrate for promoting neural stem cell function over 1, 3, and 7 d. Scale bars: 800 μm. Reproduced from [192], licensed under CC BY. (d) Bioprinted 4D vascularized cardiac patches with adaptable curvatures for improved tissue engraftment: (d1) schematic showing curvature changes in the human heart; (d2, d3) fluorescence microscopy images of hiPSC-CMs (green), human endothelial cells (hECs, red), and hMSCs (blue) on the cellularized cardiac patches after 1 d (d2) and 7 d (d3); (d4) in vivo analysis of the bioprinted cardiac patches. The optical images show firm adhesion following implantation, the H&E image shows densely packed cell clusters, and the fluorescence images show a high engraftment rate (scale bars: 100 μm). Reproduced from [194], licensed under CC BY-NC

Collectively, these studies have underscored the unique capability of 4D bioprinting to create dynamic and programmable microenvironments that regulate cellular behaviors and promote tissue-specific differentiation. These advances offer promising avenues for complex tissue/organ regeneration and various biomedical applications.

2.2.1.2 4D bioprinting for tissue engineering

Native tissues continuously remodel and evolve in shape, adapting to their microenvironment and providing specialized functions, such as alveolar branching of the lung for efficient gas exchange [188, 189]. The Alsberg laboratory from the University of Illinois Chicago and colleagues have multiple illustrations of advanced 4D biofabrication. For instance, multilayered hydrogels with distinct swelling and/or degradation profiles have demonstrated the first ultrahigh-cell-density 4D system (1×10^8 cells/mL bioink) [198] and achieved up to five-stage shape transformations that effectively mimicked lung branching morphogenesis (Fig. 14a) [199]. Similarly, gradient hydrogel networks have enabled programmed shape morphing in a one-layer,

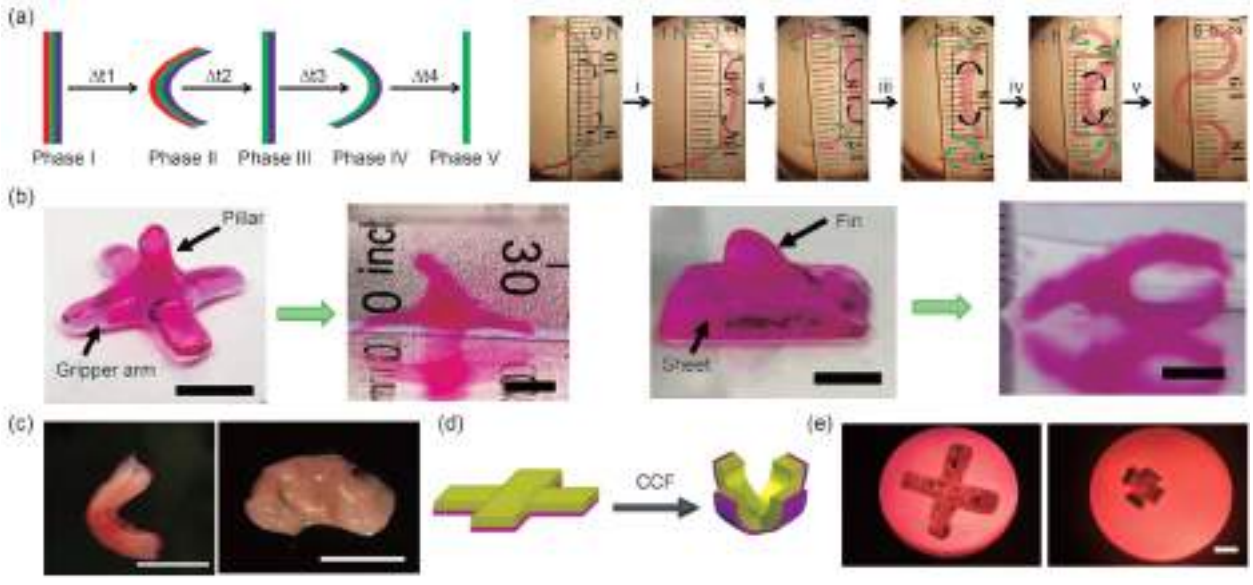

Fig. 14 Representative 4D biofabrication strategies for programmed shape transformation. (a) Five-stage shape transition of a trilayered hydrogel construct with distinct degradation and swelling profiles in each layer, demonstrating biomimicry of lung branching morphogenesis (reproduced from [199], licensed under CC BY). (b) 3D-to-3D shape transformations in printed constructs with spatially defined gradients in polymer network density. Scale bars: 5 mm. Reproduced from [202], with permission from Wiley-VCH GmbH. (c) Cell condensation-based 4D engineered cartilage-like tissues with letter "C"-shaped and helix-shaped morphologies. Scale bars: 10 mm (C shape) or 5 mm (helix shape). Reproduced from [203], licensed under CC BY-NC-ND. (d) Cell contractile force (CCF)-induced shape morphing in a cross-shaped cell-laden (yellow)/cell-free (magenta) bilayer hydrogel and (e) corresponding photomicrographs showing the original (left) and deformed (right) structures. Scale bar: 5 mm. Reproduced from [205], with permission from Elsevier Inc.

one-step fabrication process using photolithography [200] or ion transfer printing technology [201], while bioprinting of jammed microflake bioinks integrated with gradient networks has supported unique 3D to 3D transformations that have not been achieved in other cytocompatible cell-laden systems (Fig. 14b) [202]. The convergence of cell-only printing, jammed microgels, and gradient network design has ultimately enabled the first 4D cell-condensate bioprinting technology, advancing the engineering of biomaterial-free tissue with well-defined architectures (Fig. 14c) [203]. To further enhance morphing freedom by decoupling deformation regions from neighboring units, the team recently developed the first 4D bio-kirigami system, which allowed precisely controlled local morphing and enabled the engineering of highly curved tissues with complex architectures [204].

However, these systems, which rely on external stimuli such as hydrogel swelling, overlook the intrinsic roles of cells in driving tissue remodeling and morphogenesis in vivo. To address this limitation, the team harnessed contractile forces generated by embedded cells within self-softening hydrogels to establish cell-instructed, self-powering 4D bioprinting (Figs. 14d and 14e) [205, 206]. This approach eliminates the need for external triggers and enables morphogenetic engineering of multiscale tissues with enhanced adaptability and functionality. This advancement represents significant progress in 4D bioprinting by harnessing internally derived stimuli, thereby ensuring excellent cytocompatibility and enhancing accessibility for in vivo applications.

2.2.2 Cell spheroid and organoid-based biofabrication

2.2.2.1 Aspiration-assisted bioprinting (AAB)

Most efforts in 3D bioprinting involve the use of hydrogel-based bioinks, which have fundamental limitations. Specifically, it is challenging to achieve a physiologically relevant cell density (1×10^8–5×10^8 cells/mL) similar to that seen in native tissues [207, 208]. Indeed, most hydrogel bioinks are a compromise between cell density and polymer density to achieve printability, and often neither is ideal for the intended application. In this regard, spheroids with high cell density (i.e., up to 10^4 cells/spheroid) are considered promising candidates. However, spheroid bioprinting has rarely been applied due to the lack of robust, practical, precise, and scalable techniques [209, 210]. In 2020, the Ozbolat laboratory at Penn State University introduced a technique called "aspiration-assisted bioprinting" [211], which has enabled the bioprinting of spheroids with an order of magnitude size range (80–800 μm diameter) with minimal cellular damage (>90% viability) at an unprecedented precision (approximately 11% with respect to spheroid size) (Fig. 15a). ABB has also been reconfigured for freeform

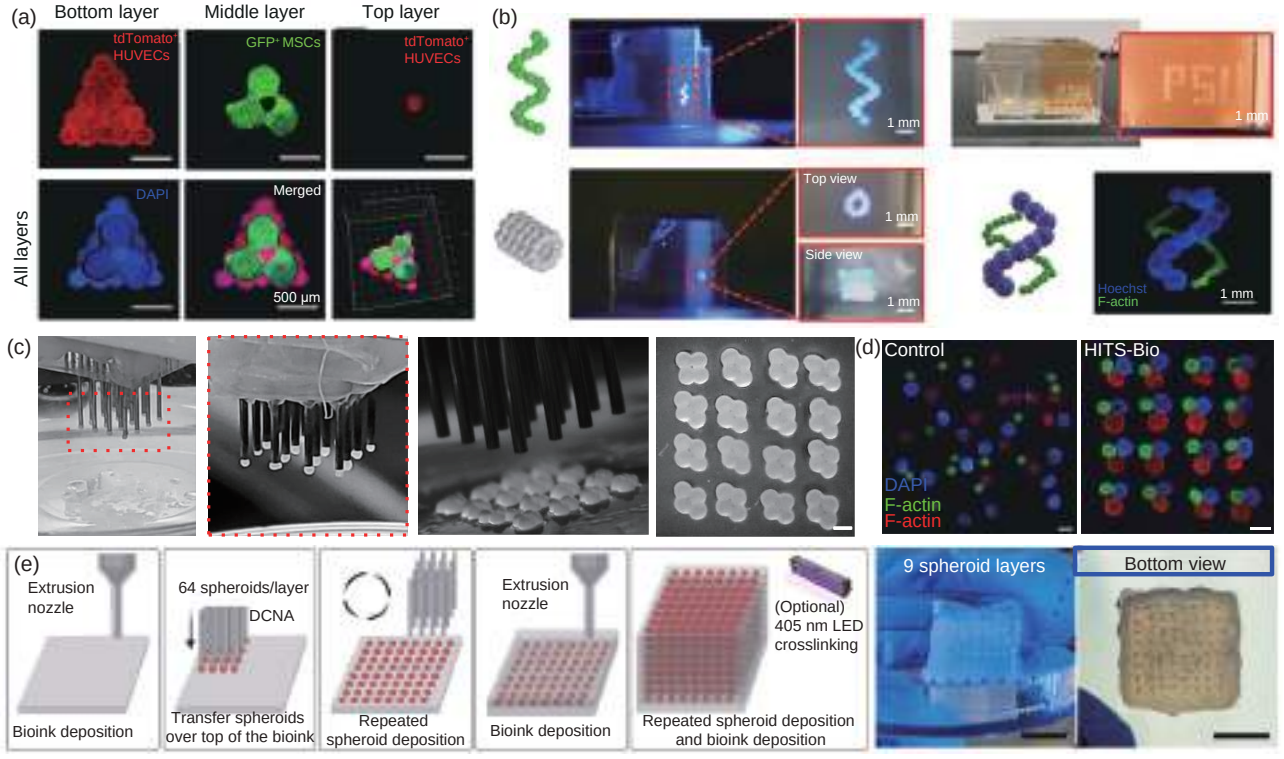

Fig. 15 Aspiration-assisted bioprinting (AAB). (a) Pyramid-shaped AAB-built heterotypic structures using spheroids of different sizes and types (reproduced from [224], licensed under CC BY-NC). (b) Freeform AAB-generated configurations (reproduced from [211], licensed under CC BY 4.0). (c) High-throughput AAB for the spheroid lifting and placement process on a hydrogel substrate. Scale bar: 300 μm. (d) Comparison between bioprinted (right) and manually mixed (left) spheroids of varying size, demonstrating the capability of high-throughput bioprinting. Scale bars: 500 μm. (e) Schematic of the scalable tissue fabrication via high-throughput bioprinting. Reproduced from [223], licensed under CC BY-NC-ND

bioprinting [211, 212] (Fig. 15b) and applied in biofabrication of various tissues, such as cartilage [213], bone [214, 215], osteochondral [216, 217] and bone/vascular tissue [218] interfaces, and tumor models [219–222]; however, the process was slow (approximately 30 s/spheroid). In recent studies [33, 223], the Ozbolat laboratory has advanced the technology further to facilitate high-throughput spheroid bioprinting, which enables the fabrication of scalable tissues (i.e., <3 s/spheroid with a total of <40 min to build cm^3 tissue) (Figs. 15c–15e).

2.2.2.2 Assembloid biofabrication

While many biofabrication technologies have advanced to achieve feature sizes on the micrometer scale, direct manipulation of cells when creating larger structures remains difficult. One strategy that has emerged to accomplish this involves utilizing cells themselves as the fabrication technique, placing cell aggregates, and allowing for self-assembly. This section highlights a key development in this area, "pick-and-place" biofabrication, using a combination of self-assembly and AM.

The development of organoids, which are 3D cultures of multiple cell types that self-pattern into engineered tissues with emergent, organ-like properties, has immense promise for the modeling and replacement of human tissues. To integrate the advantages of emergent, organoid biology with top-down biofabrication strategies, both new ink materials and new bioprinting processes need to be developed [225]. Typically, organoids are grown in an animal-derived, decellularized basement membrane that is not suitable for bioprinting. In response, multiple groups are developing engineered, printable biomaterials with tunable mechanical and biochemical properties for reproducible organoid development [59, 226, 227]. These biomaterials can be designed to mimic specific biological states, such as healthy and cancerous pancreatic tissue states [228]. More recently, new strategies to modulate biomaterial stiffness have been developed to investigate the mechanics of matrix stiffness regulating lipid droplet accumulation in organoid models for nonalcoholic fatty liver disease [229].

Furthermore, as cell–cell interactions are indispensable for guiding stem cell morphogenesis, new biomaterials to mimic cell–cell signaling have been developed [230]. Currently, an open challenge is the merging of bottom-up emergent tissue structures with top-down biofabricated structures. To begin to address this need, an emerging concept

for organoid bioprinting is "pick-and-place" biofabrication of preformed organoids to form so-called assembloids [225]. While vacuum-assisted movement is quite successful for cell spheroids, the required pressures can be damaging to human organoids [32]. The Heilshorn laboratory at Stanford University has developed magnet-assisted movement of organoids using temporary magnetic inks, which have been used to fabricate neural assembloids with specified 3D geometries (Fig. 16a) [32].

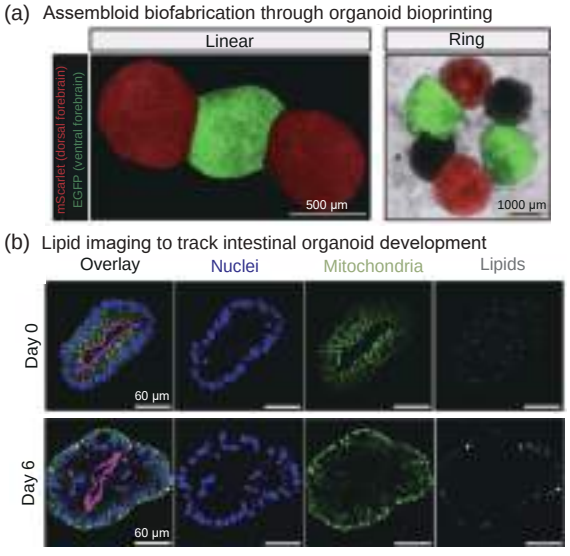

Fig. 16 Organoid-based biofabrication and analysis strategies. (a) Assembloids can be fabricated into specific geometries using magnet-assisted "pick-and-place" bioprinting of organoids pre-patterned into dorsal (red) and ventral (green) forebrain neural tissue (reproduced from [32], licensed under CC BY 4.0). (b) Organoid development of human intestinal enteroids can be noninvasively followed by label-free imaging of lipids using coherent anti-Stokes Raman scattering (CARS) microscopy, which correlates with mitochondrial polarization. Confocal microscopy shows actin in magenta, nuclei in blue, mitochondria in green, and lipid CARS signal in white. Reproduced from [231], with permission from the American Chemical Society

As organoid production continues to improve in reproducibility and scalability (Fig. 16b) [231], the use of organoids as building blocks for biofabrication will continue to grow. Future opportunities include integration with real-time analysis techniques that are nondestructive to track organoid phenotype over time [232], which will enable eventual automation for high-throughput studies.

2.2.3 Melt electrowriting

Although in some ways bearing resemblance to standard 3D printing techniques, electrodynamic processes, such as electrospinning and MEW, involve material deposition enabled by the application of an electric field. MEW in particular, sometimes described as the missing link between FFF and electrospinning [233], has emerged as a method of micron-scale fabrication with tissue engineering applications. Involving the heating of a thermopolymer and precise deposition on a collector as a result of an applied voltage [234], MEW has shown promise for a variety of tissue engineering applications, although due to the relative newness of the technique, there remains much research and exploration to be done on MEW process dynamics and applications. Explored in this section are developments in creating an accessible MEW device for fabricating highly porous scaffolds, as well as the development of a charge-aware, data-guided MEW system.

2.2.3.1 Melt electrowriting of highly porous scaffolds

MEW is an electrohydrodynamic-based AM paradigm that directly writes microscale polymer fibers under a high electric field. MEW equipment employs a configuration similar to FFF but exploits electrohydrodynamic stabilization to prevent jet breakup, enabling continuous molten polymer jets at low flow rates. Fiber diameters range from 0.35 μm to 50 μm, depending on the processing conditions [235, 236]. This represents a resolution more than two orders of magnitude smaller than conventional FFF, necessitating significantly reduced throughput (2–20 μL/h) to the nozzle.

MEW distinguishes itself through small-diameter microfibers that yield high-porosity scaffolds, typically exceeding 85%. The fiber diameter scales proportionally with the flow rate [235], allowing the fabrication of multiphasic scaffolds. These microporous materials, or scaffolds, provide 3D substrates first proposed for tissue engineering [237, 238] but now applied across cancer research [239], biofabrication [240], and drug discovery [241]. Unlike matrices, scaffolds possess open-pore morphologies that permit cell and tissue penetration. AM improved reproducibility and expanded the range of achievable scaffold properties, yet most technologies cannot achieve micron-scale resolution. Additionally, conventional scaffolds exhibit porosities between 50% and 80%. At these elevated porosities, MEW scaffolds function as reinforcement structures, imparting programmable mechanical properties into otherwise uniform materials such as silicones [242] or matrices [243, 244].

Given MEW's configurational similarity to FFF printers, the Dalton group at the University of Oregon released an open-source MEW 3D printer (the "MEWron") in 2023 to democratize access to this technology (Figs. 17a–17c) [29]. Built upon the existing open-source Voron 0.1 FFF printer, the MEWron employs geared-down motors and half-stepping to produce microfibers down to 1.5 μm diameter (Fig. 17d). This modification enabled MEW processing of polycaprolactone (PCL) and high-density polyethylene into scaffolds [245] and deposition of nylon-12 onto heated, cylindrical collectors [6]. The Dalton group further modified

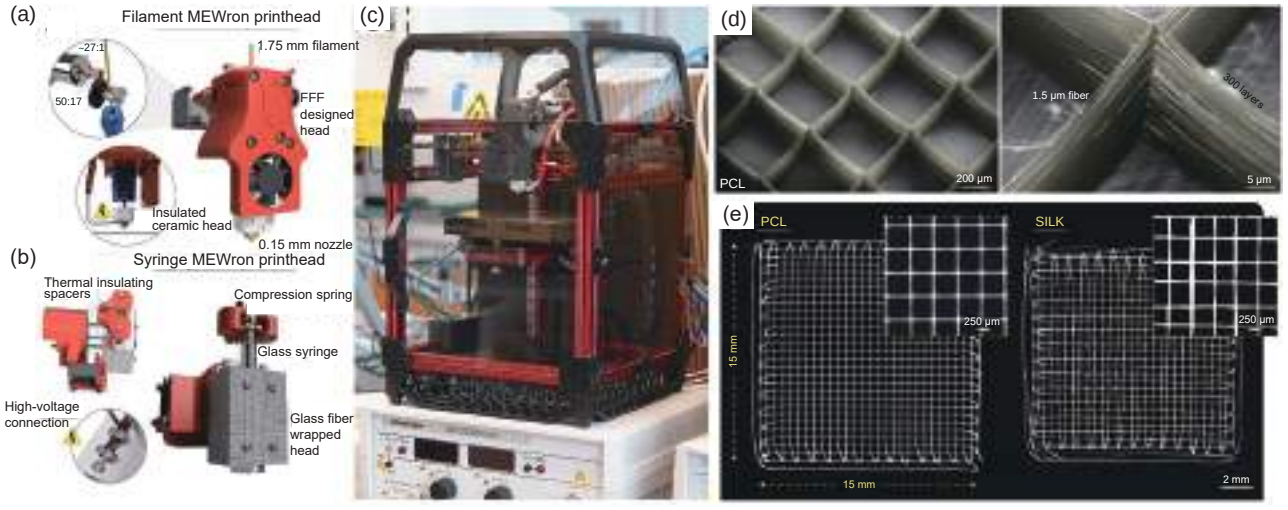

Fig. 17 The MEWron open-source hardware ecosystem, which is built upon a Voron Design FFF 3D printer. Either filament (a) or syringe (b) delivery systems are available, and the compact system (c) sits upon a low-current high-voltage supply. It produces small-diameter MEW fibers, shown in (d) with a 1.5 µm diameter fiber layered upon each other 300 times. (e) A PCL and a silk scaffold, with the latter made using a modified Voron 0.1 with a − 30 °C collector plate. (a, b, d) are reproduced from [29], licensed under CC BY 4.0; (e) is reproduced from [30], licensed under CC BY 4.0

the Voron platform to jet silk solutions onto a − 30 °C collector plate for cryogenic preservation of the fiber structure [30]. Following lyophilization, the dehydrated silk scaffold was immersed in ethanol to induce beta-sheet formation, conferring aqueous stability. Silk microfiber scaffolds (Fig. 17e) demonstrated significantly enhanced cell proliferation compared to dimensionally matched PCL microfiber scaffolds [30].

MEWron's rapid build time and low cost ($1200 compared to $50,000+ for commercial systems) facilitate polymer-specific modifications. For example, polydioxanone (PDX)—a clinically relevant yet academically underinvestigated polymer with 3–6-month degradation kinetics as a suture material—could be processed into microfiber scaffolds using a MEWron equipped with a filament drying line. In another iteration, the Dalton group developed a coaxial nozzle configuration enabling core–shell fiber production and dynamic polymer switching by selective extrusion from either the inner or outer nozzle channel.

These open-source developments demonstrate that microfiber 3D printing will enable the production of biomedical constructs at resolutions replicating natural tissue ultrastructure, while maintaining accessibility through democratized technology platforms.

2.2.3.2 Charge-aware, data-guided melt electrowriting for microscale 3D structured engineered tissues

Biofabrication is increasingly constrained not by whether we can print but rather by whether we can manufacture biologically instructive microarchitectures reproducibly, at scale, with quantitative quality assurance. The Chang group at the Stevens Institute of Technology has focused on advancing MEW. Because MEW is solvent-free and highly tunable, it enables high-resolution fibrous 3D structured materials for engineered tissues, where fiber diameter, spacing, anisotropy, and stacking define cellular operating length scales, transport pathways, and mechanical cues.

To move MEW beyond trial-and-error parameter tuning toward quality-by-design, the Chang group has paired process-physics frameworks with in situ metrology. First, they advanced a dimensionless "Printability Number" (via dimensional analysis) to reduce a large, coupled parameter space (melt flow, electric field, temperature, and stage kinematics) into governing groups [246]. This framework has enabled principled selection of stable free-flow conditions and translation-speed regimes that improve mesh fidelity while mitigating instabilities such as coiling, waviness, and systematic fiber deviation [247]. Second, the Chang group has developed a real-time, image-based jet-lag tracking methodology to quantify dynamic jet behavior and connect jet signatures to fiber-quality outcomes [248]. By measuring deposition lag and transient jet dynamics during printing, this approach has provided a systematic pathway for rapid parameter optimization, repeatable printing, and on-ramp to closed-loop control.

A core biomedical manufacturing frontier for MEW is understanding and controlling electrostatics in multilayer microstructures. Polymer melts are semiconductive, wherein printed fibers can retain net residual charge while also polarizing in the applied electric field. These coupled effects generate competing jet–fiber attraction and repulsion that degrade lateral placement accuracy and complicate vertical stacking in 3D builds [249]. To address this, the Chang group has established charge-aware measurement and

modeling tools spanning (i) conductivity-dependent fiber overlap versus divergence behaviors and the resulting attraction/repulsion signatures, (ii) residual-charge quantification (nanocoulomb-scale) and parametric studies that reveal how process choices influence charge entrainment and dissipation, and (iii) analytical, residual-charge-based models that explain accuracy loss in multilayer scaffolds through evolving "energy landscapes" incorporating global fields, local interactions, and polarization effects [250–252]. Together, these tools have converted electrostatics from an uncontrolled disturbance into a design variable with actionable manufacturing rules.

These manufacturing advances have enabled healthcare-relevant biofabrication platforms. The Chang group has established the convergence of MEW-produced 3D substrates designed at approximately 10–100 μm cellular operating lengths with automated confocal imaging and computational (including machine learning-enabled) metrology to extract whole-cell morphology and focal-adhesion features, enabling classification of confinement-driven phenotypes. This workflow supports biologically qualified scaffold design, where manufacturing decisions are guided by measured cell responses rather than geometry-only targets [246, 253]. In parallel, the Chang group has leveraged controlled fiber sagging and charge-mediated effects to fabricate fibrous spindle-like constructs, illustrating how manufacturing physics can be harnessed to create specialized, tissue-inspired microstructures [252, 254]. Looking forward, the Chang group envisions a near-term U.S. opportunity in closed-loop, charge-aware scaffold manufacturing that integrates real-time jet sensing, predictive residual-charge models, and single-cell biological metrology into a unified digital thread for scalable, design-qualified tissue constructs with traceable process–structure–function relationships (Fig. 18).

2.2.4 Alternative printing technologies

2.2.4.1 Cryobioprinting

In conventional bioprinting workflows, biological constructs typically must be used immediately after fabrication, which limits opportunities for long-term storage and transportation to off-site locations. To address this challenge, the Zhang group at Harvard Medical School has recently developed a cryobioprinting strategy that integrates standard extrusion-based bioprinting with a meticulously engineered cryogenic substrate [185, 186]. In this approach, bioinks deposited onto the subzero substrate undergo rapid cooling, enabling simultaneous bioprinting and freezing of 3D tissue architectures that are directly shelf-ready (Fig. 19a) [34, 255]. Importantly, the in situ freezing process also mechanically reinforces the otherwise soft hydrogel-based filaments, enabling the fabrication of stable 2D and 3D patterns using single- or multimaterial formulations. This added mechanical stability allows for the direct printing of free-standing architectures in open air (Fig. 19b), which would otherwise be difficult to achieve using conventional extrusion bioprinting without embedded support due to gravitational deformation.

To enable the incorporation of living cells into the cryobioprinting process, bioink formulations have been optimized to provide cryoprotective effects and minimize ice crystal formation during freezing. A combination of permeable cryoprotectants, such as dimethyl sulfoxide, together with nonpermeable cryoprotectants, including disaccharides or trisaccharides, has demonstrated strong protective efficacy. Using these optimized bioinks, both cell lines and primary cells have been successfully cryobioprinted and stored in liquid nitrogen for up to three months. Upon thawing and subsequent culture, cell viabilities exceeding 80% have been consistently observed (Fig. 19c) [34, 255]. Furthermore, when hMSCs have been cryobioprinted and induced to undergo osteogenic, chondrogenic, or adipogenic differentiation, no noticeable differences have been observed compared to nonfrozen control constructs, indicating preserved stem cell functionality (Fig. 19d) [34, 255].

Beyond conventional extrusion-based approaches, cryobioprinting can be readily adapted to other bioprinting modalities. For example, a key limitation of traditional droplet-based bioprinting is the requirement for very low-viscosity bioinks, which complicates the construction of volumetric structures unless a support bath is used. In contrast, in cryobioprinting, droplets freeze immediately upon contact with the cold substrate, providing sufficient mechanical integrity to enable direct, in-air deposition of complex 3D architectures (Fig. 19e) [2]. Cryobioprinting is also compatible with coaxial bioprinting, in which multilayer nozzles enable vertical bioprinting of hollow or compositionally distinct filaments depending on programmed bioink delivery (Fig. 19f) [256]. Using the alternating vertical cryobioprinting strategy, multiple interfacial tissue types can be engineered, including musculovascular junctions (Fig. 19g) [256], musculotendinous junctions (Fig. 19h) [256], and neuromuscular junctions (Fig. 19i) [257].

2.2.4.2 Ultrasound-assisted 3D biofabrication of biomimetically organized soft tissue constructs

Recapitulating the hierarchical organization of cells and ECM that underlies the structure and function of soft tissues (e.g., musculoskeletal, cardiovascular) remains a central challenge in biofabrication and biomedical manufacturing. Typical bioprinting approaches yield constructs where cells are randomly distributed within micro/meso-scale fibers (e.g., extrusion bioprinting) or across the bulk structure (e.g., vat photopolymerization), but they fail to impart controlled organization of cells and ECM essential for biomimicry. To overcome these limitations, the Shirwaiker group at North

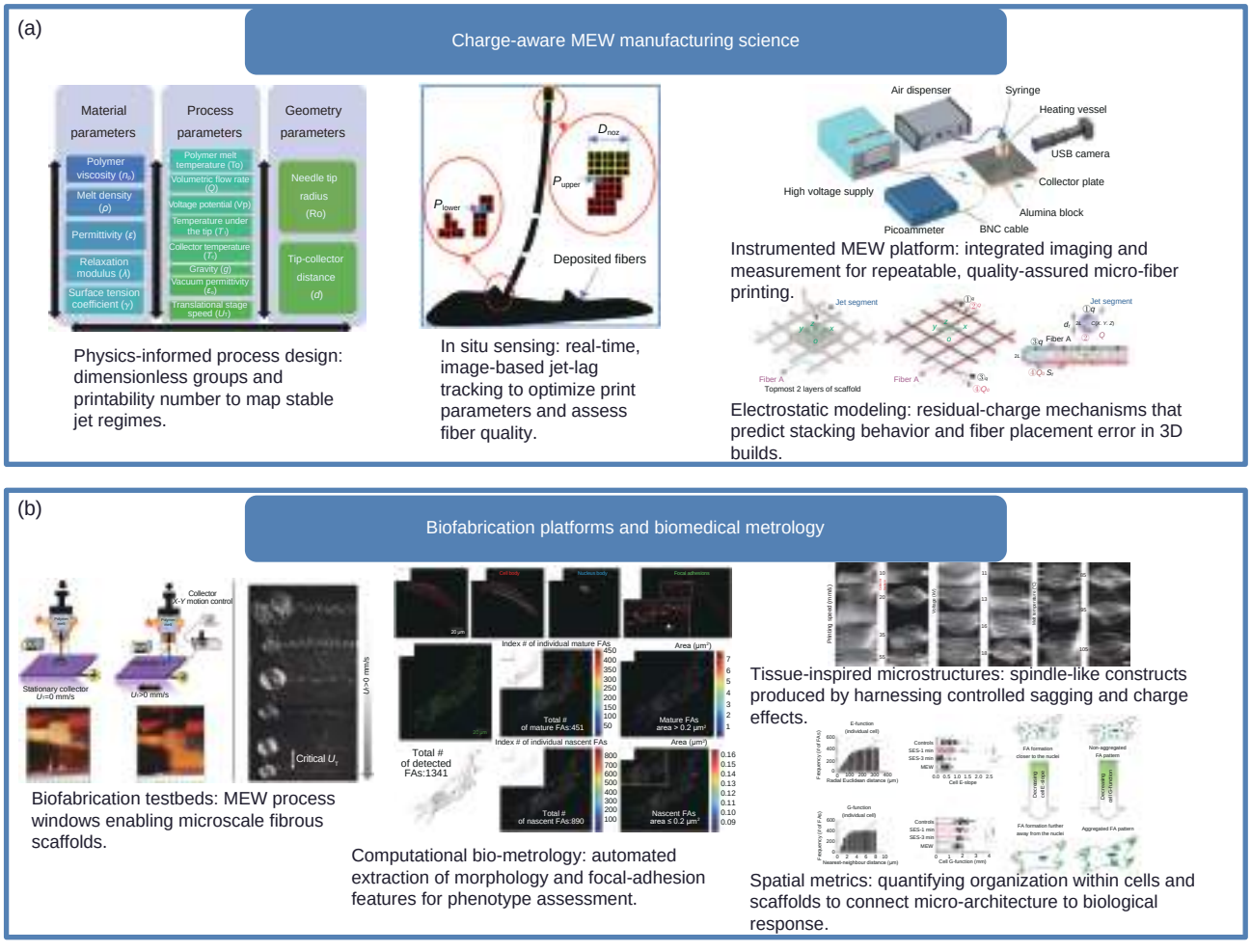

Fig. 18 Advances in melt electrowriting (MEW) for process control, modeling, and biomedical scaffold fabrication. (a) Charge-aware MEW manufacturing science spanning physics-informed process design, instrumented MEW platforms for quantitative quality assurance, real-time image-based jet-lag tracking for parameter optimization, and residual charge-based electrostatic modeling to predict multilayer stacking and fiber placement error. (b) Biofabrication platforms and biomedical metrology connecting MEW process windows to healthcare-relevant fibrous scaffolds, fabrication of tissue-inspired spindle-like microstructures, and computational biometrology. Part (a, left) is reproduced from [246], with permission from the American Society of Mechanical Engineers; Part (a, middle) and Part (a, right top) are reproduced from [248], with permission from Elsevier B.V.; Part (a, bottom right) is reproduced from [252], licensed under CC BY; Part (b, left), Part (b, middle), and Part (b, bottom right) are reproduced from [253], licensed under CC BY 4.0; Part (b, right top) is reproduced from [254], licensed under CC BY 4.0

Carolina State University has developed ultrasound-assisted biofabrication (UAB) strategies that leverage standing bulk acoustic waves (SBAWs) to rapidly and noninvasively pattern cells and extracellular constituents within 3D hydrogel matrices with synergistic crosslinking (Fig. 20). This patented technology [258] is underpinned by a theoretical framework coupling process physics with material crosslinking chemistry, experimentally characterized material–process–structure–function interrelationships, and translational workflows that integrate real-time acoustic manipulation with 3D bioprinting to fabricate biomimetic tissue constructs [35, 258–265].

At the core of the UAB is the generation of an SBAW within a bioink matrix by actuating piezoelectric transducer(s) paired with reflector(s) (Fig. 20a). The interference of the emanating and reflected waves creates pressure nodes (planes in 3D), and the resulting acoustic radiation forces (ARFs) drive suspended cells and additives (e.g., microfibers) toward nodal planes, organizing them into highly ordered arrays [35, 258–265]. These arrays are stabilized through synergistic crosslinking modalities (e.g., thermoreversible gelation, ionic crosslinking, and UV photocrosslinking) that provide temporal control over matrix viscosity and enable precise entrapment during gelation. With appropriate optimization, anisotropic organization can be achieved within seconds, even in viscous hydrogels, while maintaining high cell viability. Array orientation can be varied layer-wise by selectively actuating different transducer–reflector pairs. This mechanism is broadly compatible with vat photopolymerization and extrusion bioprinting, enabling

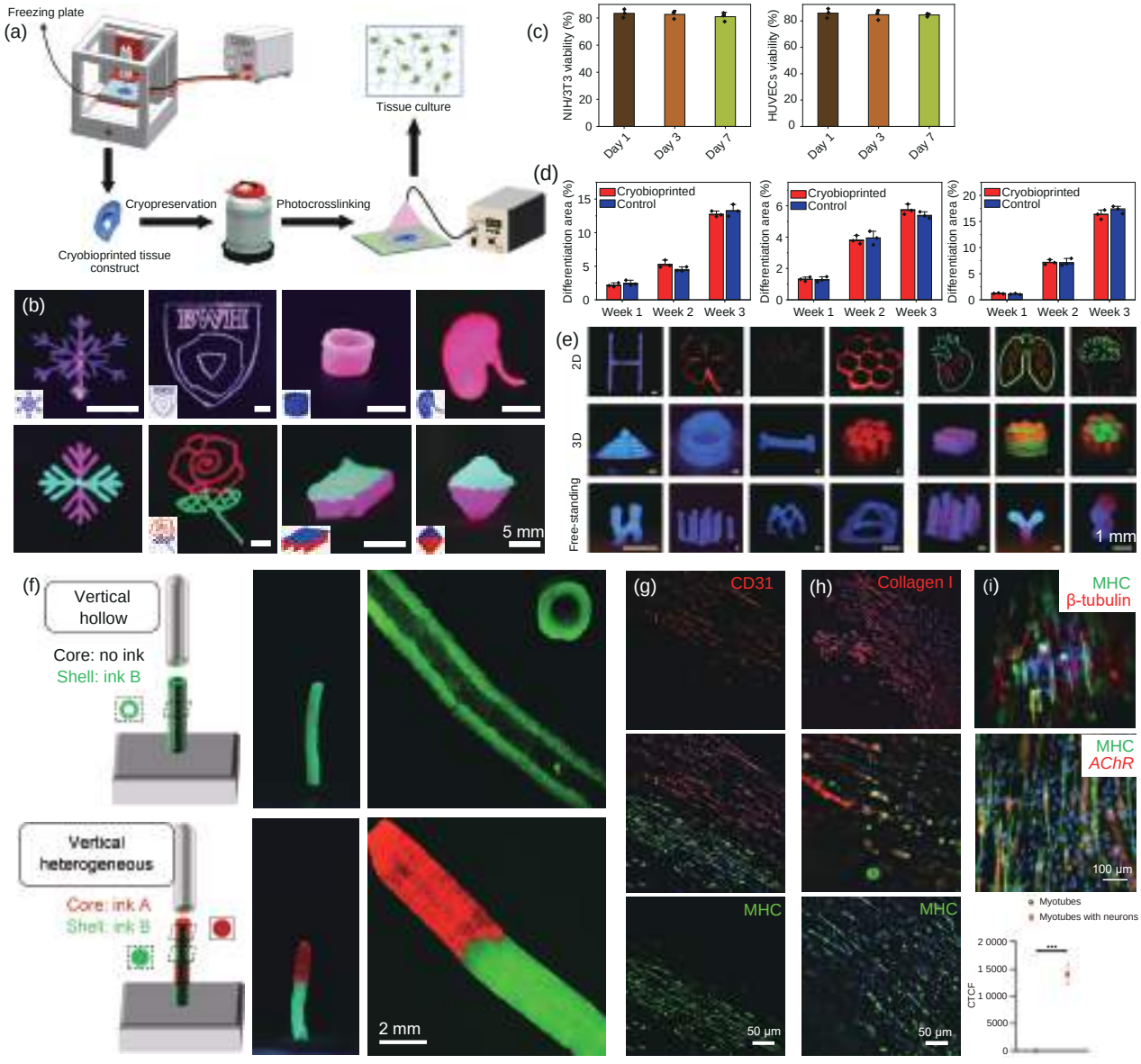

Fig. 19 Representative cryobioprinting strategies for simultaneous fabrication and preservation of cell-laden constructs. (a) Schematic illustration of cryobioprinting of tissue constructs for simultaneous cryopreservation. (b) Cryobioprinted gelatin and GelMA structures. (c) Quantified viabilities of NIH/3T3 fibroblasts and human umbilical vein endothelial cells (HUVECs) cryobioprinted and stored in liquid nitrogen for 3 months. (d) Quantified osteogenic (left), chondrogenic (middle), and adipogenic (right) differentiation levels of hMSCs for cryobioprinted and control constructs. Reproduced from [34], with permission from Elsevier Inc. (e) Droplet cryobioprinting for building free-standing structures (reproduced from [2], licensed under CC BY). (f) Coaxial vertical cryobioprinting to create frozen hollow and alternating freestanding filaments. (g–i) Vertically cryobioprinted musculovascular junction (g), musculotendinous junction (h), and neuromuscular junction (i) tissues with quantified corrected total cell fluorescence values. (f–h) are reproduced from [256], with permission from Wiley-VCH GmbH; (i) is reproduced from [257], licensed under CC BY 4.0

microscale acoustic patterning within tissue-specific geometries without compromising throughput or resolution.

The process physics have been elucidated through analytical and multiphysics models describing the effects of ultrasound frequency, wavelength (λ), bioink viscosity, and boundary conditions on nodal spacing and ARF magnitude [35, 259–261]. These models accurately predict $\lambda/2$ interarray spacing and nonlinear frequency–pressure relationships observed experimentally, informing the balance between ARFs and viscous drag forces that governs patterning kinetics (Fig. 20b). Such mechanistic insights inform the systematic design of ultrasound-enabled bioprinting platforms and actuation schemes for reproducible patterning across biologically relevant geometries.

UAB has been demonstrated across hydrogel systems (e.g., alginate, GelMA) and with diverse cell types (e.g.,

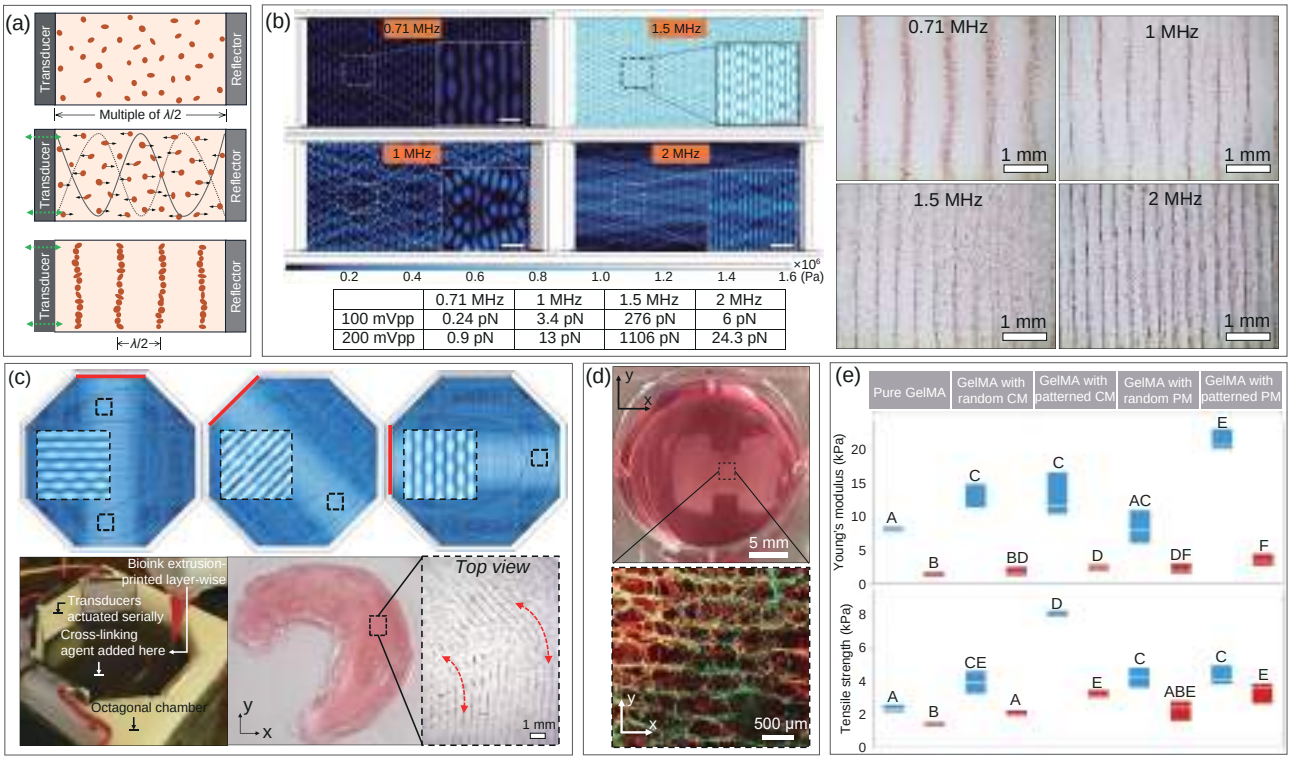

Fig. 20 Highlights of ultrasound-assisted 3D biofabrication. (a) Schematic illustrating process physics where actuation generates an SBAW in the bioink and ARFs that drive cells and additives toward their nearest pressure nodal planes. (b) Computational modeling of acoustic pressure fields and ARF magnitudes at different ultrasound frequencies and (transducer) input voltages (reproduced from [35], with permission from IOP Publishing Ltd.; reproduced from [261], with permission from Elsevier B.V.). (c) Simulated SBAW nodal patterns under sequential transducer actuation and experimental demonstration of a biomimetic knee meniscus construct (reproduced from [35], with permission from IOP Publishing Ltd.). (d) Biological functionality illustrated by a highly organized network of cells (actin, green) and deposited ECM (collagen II, red). (e) Structure–function relationships highlighted through tunable GelMA stiffness and tensile property improvements with patterned collagen microaggregates and PCL microfibers. Reproduced from [263], licensed under CC BY-NC-ND

adipose-derived stem cells, chondrocytes, fibroblasts, MG63 cells) [35, 258–265]. The ability to generate linear and circular patterns with uniform orientation or layerwise variations (e.g., 0°–90°, 0°–45°–90°) supports applications to anisotropic tissues, including the meniscus, tendon, ligament, annulus fibrosus, skeletal muscle, and cardiac muscle (Fig. 20c) [35, 259–263]. The interplay between bioink composition, UAB parameters, and crosslinking modality governs emergent structure–function relationships. For example, in GelMA (80% degree of substitution, 0.05 g/mL), modulation of the pre-photocrosslinking temperature and UV exposure regulates the equilibrium between thermoreversible and covalent crosslinking, yielding matrices with tunable stiffness (0.25–17 kPa), pore architecture, and degradation profiles [262]. Moderately stiff matrices support cellular elongation, alignment, and ECM deposition (Fig. 20d), whereas dense networks restrict remodeling. Hybrid GelMA bioinks further enhance functionality in that patterned collagen microaggregates improve the tensile modulus and aligned collagen II deposition during chondrogenic culture, while patterned PCL microfibers provide uniaxial cues guiding cellular and ECM alignment (Fig. 20e) [263].

Collectively, UAB has emerged as a versatile strategy for engineering anisotropic tissue constructs with structural and functional biomimicry. Beyond biomedicine, the UAB process will also be relevant to cultivated meat applications in which muscle fiber alignment and structural anisotropy are essential for texture and the overall sensory experience [266]. Future directions include improving acoustic coupling in thicker constructs, leveraging dynamic ultrasound stimulation to enhance ECM formation, expanding to diverse hydrogel/composite systems for biomedical and food applications, and developing automated platforms for real-time, high-throughput manufacturing.

2.2.4.3 Volumetric (bio)printing

Relatedly, the Zhang group at Harvard Medical School and the Yao group at Duke University have co-developed deep-penetration acoustic volumetric printing (DAVP), a light-free volumetric bioprinting strategy that uses focused ultrasound to pattern engineered sonoinks through optically opaque or scattering biological tissues [267, 268]. In contrast to conventional optical bioprinting approaches, whose

penetration depth and spatial precision can be compromised by material absorption and scattering, DAVP harnesses the substantially greater tissue penetrability of acoustic energy to induce localized sono-thermal effects and trigger gelation only at targeted focal regions. This mechanism enables the formation of complex 3D hydrogel architectures not only within transparent constructs but also across thick tissue barriers and at buried anatomical sites, thereby expanding printing from open, surface-accessible fabrication toward minimally invasive and potentially in situ biofabrication. By integrating acoustic energy delivery with self-enhancing sonoinks, DAVP provides a general framework for constructing tissue-like structures in environments that are otherwise inaccessible to light-based printing methods.

On the other hand, volumetric bioprinting (VBP) has emerged as a powerful light-based manufacturing approach that creates entire 3D structures by selectively solidifying photosensitive bioinks throughout a volume, eliminating the need for conventional layer-by-layer deposition. This enables the rapid fabrication of complex, cell-laden constructs while reducing printing times from hours to seconds or minutes. Recent advances have expanded VBP beyond synthetic hydrogels to include pristine protein-based bioinks [269], such as silk fibroin [270] and decellularized ECM [271] materials, allowing the fabrication of biologically relevant constructs with improved biomimicry and cellular compatibility.

These developments have demonstrated the potential of volumetric (bio)printing for tissue engineering and regenerative medicine while also revealing a key limitation of light-based approaches: their dependence on optical access and transparency [272]. This limitation motivates the exploration of alternative energy sources, such as ultrasound, to extend volumetric fabrication into optically opaque environments and biological tissues. Collectively, these studies reflect a broader shift from rapid 3D printing of synthetic materials toward cell-compatible and clinically relevant bioprinting platforms. The presentation will frame volumetric (bio) printing as a next step in this evolution, with potential applications in tissue engineering, regenerative medicine, and minimally invasive biofabrication.

2.2.4.4 Robot-assisted precision biofabrication for patient-specific scaffolds

To recreate complex organ architectures, the Habib group from the Rochester Institute of Technology and colleagues have integrated robotics into bioprinting for anatomically faithful lung model fabrication. The lung's branching airways and curved surfaces pose a challenge for traditional three-axis printers, often causing sagging or geometric inaccuracies [273, 274]. They have overcome this by implementing a six-axis robot-assisted bioprinter that dynamically orients the print nozzle, enabling accurate deposition on complex 3D contours. Using an optimized alginate–carboxymethyl cellulose (CMC) hydrogel formulation, the system has successfully printed tubular and bifurcating airway constructs that closely replicate patient-specific airway geometries (Fig. 21a) [72]. The printed second-generation lung lobe has maintained open lumen structures across multiple branches without collapse and has withstood compression forces comparable to native lung tissue. Quantitative printability analysis (Pr≈1.0) has confirmed high pore fidelity across the constructs, and mechanical tests have demonstrated

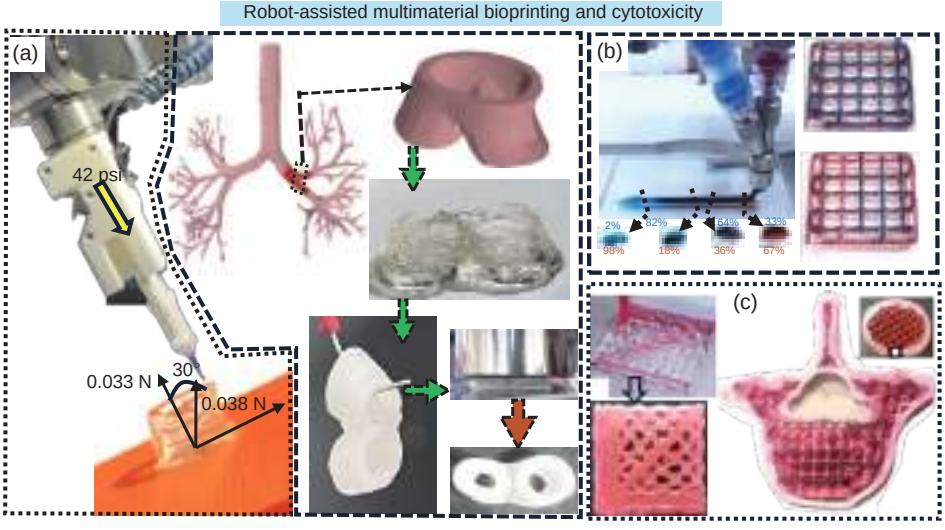

Fig. 21 Multimaterial and robot-assisted biofabrication strategies. (a) Robot-assisted bioprinting of anatomically inspired constructs, such as an airway model, alongside mechanical testing (reproduced from [72], licensed under CC BY 4.0). (b, c) Multimaterial deposition with gradient (reproduced from [275], with permission from the American Society of Mechanical Engineers; reproduced from [276], with permission from the American Society of Mechanical Engineers)

elastic recovery of the hydrogel airways under repeated loading [72]. This robotic platform's precise deposition has markedly improved geometric fidelity over gantry-based methods, reducing support needs and maintaining uniform wall thickness in curved airways. It has also enabled realistic lung scaffolds suitable for preliminary in vitro aerosol deposition studies, demonstrating their potential for inhaled drug delivery research. Together, the robot-assisted approach has advanced next-generation organ models by integrating precise kinematic control with biofabrication, enabling high-fidelity, patient-specific respiratory scaffolds.

2.2.4.5 Tunable rapid assembly of collagenous elements (TRACE)

The development of biofabrication strategies that utilize natural, unmodified ECM components is critical for advancing tissue engineering toward physiologically relevant models. One notable innovation in this space is the TRACE platform (Fig. 22a) [277] developed by the Mak group at Stony Brook University. TRACE enables the rapid transition of collagen I from solution to gel, addressing a longstanding limitation in the field: the inherently slow gelation kinetics of collagen under cell-compatible conditions. Typically, neutralized collagen solutions at concentrations of 1–4 mg/mL—commonly used in live cell applications—require extended incubation times to form stable gels, which limits compatibility with bioprinting and biofabrication. TRACE circumvents this challenge by providing a rapid assembly mechanism, based on macromolecular crowding, that works across acidic and neutralized, high- and low-concentration collagen formulations. Importantly, TRACE eliminates the requirement of using high-concentration collagen, which needs to be maintained in acidic buffers for solubility, for extrusion-based collagen printing [98, 278], thereby enhancing biocompatibility and expanding the range of usable conditions. Beyond collagen I, TRACE has demonstrated versatility with other ECM sources, including decellularized matrices derived from specific organs such as the heart, muscle, liver, and intestine [279]. This adaptability allows the platform to capture tissue-specific biochemical cues, which are essential for guiding cell differentiation and maturation.

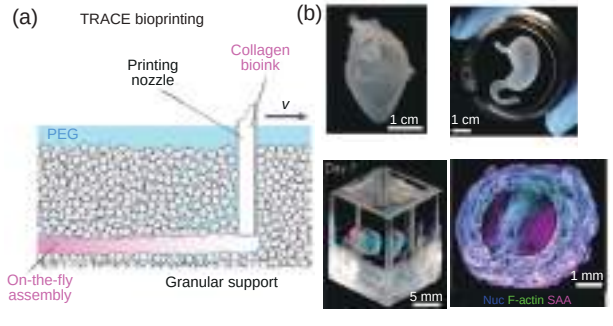

Fig. 22 TRACE biofabrication and bioprinting: (a) TRACE leverages crowding to accelerate collagen and ECM gelation, enabling versatile 3D biopatterning and bioprinting of natural bioinks; (b) Collagen can be printed with and without living cells into complex physiologically relevant geometries. Reproduced from [277], under exclusive licence to Springer Nature Limited

Using native ECM, TRACE has been applied to fabricate a variety of 3D patterned tissues (Fig. 22b). Examples include patterned intestinal strips and tubes and bioprinted cardiovascular vessels, chambers, and rings. These engineered tissues not only replicate physiologically relevant structural complexity but also exhibit functional maturation. Biopatterned intestinal tissues derived from induced pluripotent stem cells (iPSCs) progressed to mature gut-like constructs, expressing appropriate lineage markers. Similarly, bioprinted cardiac tissues achieved coordinated calcium signaling, resulting in synchronous contractions and effective fluid pumping—hallmarks of functional myocardium [277, 280].

These findings underscore the importance of biofabricating tissues from natural physiological components under cell-compatible conditions without reliance on artificial modifications or harsh processing steps. TRACE supports the creation of tissues that more closely recapitulate native biology. Moreover, the platform is inherently scalable: its programmable, rapid 3D printing capabilities allow for reproducible manufacturing of complex tissues at sizes and formats suitable for research and translational applications. This scalability positions TRACE as a powerful tool for drug discovery and development, where human-relevant tissue models are increasingly sought to replace or complement animal testing.

Overall, TRACE represents a significant advance in the biofabrication of natural ECM-based tissues. By combining speed, versatility, and physiological relevance, it facilitates the production of advanced human tissue models that accelerate research and development in non-animal systems. In doing so, TRACE contributes to the broader goal of establishing human-centric platforms for understanding disease mechanisms and developing therapeutic interventions. Its ability to integrate unmodified ECM components into functional constructs highlights a paradigm shift in tissue engineering—moving away from reliance on synthetic scaffolds and toward the direct use of natural materials to achieve maturation, function, and translational impact.

2.2.4.6 Cell-only embedded bioprinting

The Alsberg group at the University of Illinois Chicago has developed a cell-only bioprinting strategy, employing living individual cells or cell aggregates themselves as the bioink (Fig. 23a) [184]. This advance is enabled by photocurable, shear-thinning, and self-healing microgels composed of oxidized, methacrylated alginate, which act as a supporting

bath for freeform deposition of cells. Unique to this approach is that once printing is complete, the microgel bath can be photocrosslinked to further stabilize the construct, maintaining cellular architecture during handling and long-term culture to allow for cell condensation formation. Using this platform, hMSC-based cell-only bioinks were printed into complex tissue geometries and successfully differentiated, enabling the formation of C- and femur-shaped bone-like constructs and ear-shaped cartilage-like constructs (Figs. 23b and 23c). The strategy has since been adapted to engineer coronary artery mimicking constructs with tunable wall thickness using smooth muscle cells and printing needles of varying diameters [281]. A further advancement has introduced tissue-specific bioinks comprised of individual cells or cell aggregates with incorporated growth factor-laden microparticles, thereby eliminating the need for exogenous growth factor supplementation and enabling controlled spatial and temporal presentation of cues during regeneration [282]. This has proved particularly advantageous for engineering multiphase tissues, such as osteochondral constructs composed of integrated bone and cartilage. More recently, patterned printing of specialized cell-only bioinks into preformed, cell-laden microgel constructs has been demonstrated as a powerful strategy for developing complex multiphase tissues, such as bone-like constructs with prevascularized networks that hold strong promise for clinical translation [283].

2.2.4.7 Intelligent bioprinting for in vivo applications

In the past decade, (bio)printing has emerged as a technology that can create highly organized tissue constructs that mimic the complex architecture of various organs [75]. 3D bioprinters are capable of printing both hard and soft polymers or their combinations [24]. In the current (bio)printing paradigm, post-injury or disease, a digital architecture of the defect or the diseased tissue is created using various imaging modalities and image processing tools. Then, scaffolds are bioprinted from hard or soft polymers or their combinations [24]. This traditional paradigm that has been heavily pursued in regenerative medicine has two important limitations, which have limited the translation of these technologies to clinical practice: (1) the response time to the injury is long as bioprinters have been outside of the operating rooms, and the slow printing process does not allow rapid production of scaffolds within the timeline of a surgery. This means that a minimum of two major surgeries are required for the treatment of injuries. (2) Bioinks are typically hydrogel-based, so they can carry cells and biologics [284].

Hydrogels are difficult to suture and, once fabricated, do not adhere properly to host tissue [285, 286]. Therefore, the implantation and presentation of the dislocation become challenging. An alternative trend that recently has gained traction is to move from "in vitro bioprinting and subsequent implantation" toward direct printing of the bioink inside the defect, usually termed "in vivo bioprinting" or "in situ bioprinting" [287, 288]. The Tamayol laboratory at the University of Connecticut, along with others, has focused research on this area. In this alternative paradigm, a 3D scanner or imaging tool is used to image the defect and then creates a scaffold within the defect site [289]. In this strategy, the ink and crosslinking process should be nontoxic and nonimmunogenic. In addition, if proper chemistries are used, the in situ crosslinked scaffolds can adhere to

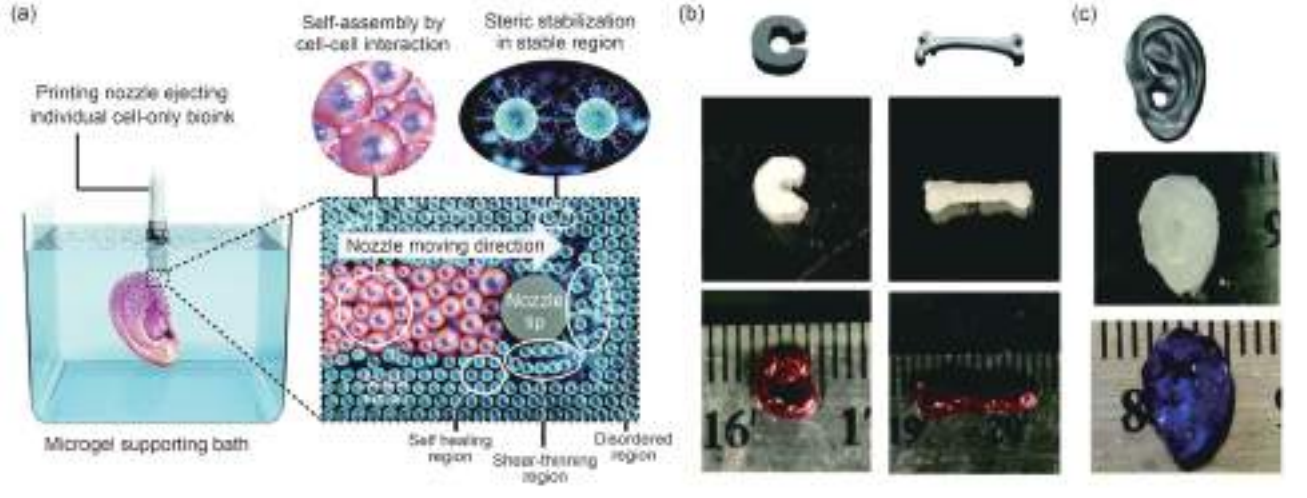

Fig. 23 Cell-only bioprinting within a supportive microgel matrix for tissue-specific construct formation. (a) Schematic illustration of cell-only bioprinting within a photocurable, shear-thinning, and self-healing microgel support bath. Letter "C"-shaped and femur-shaped bone-like tissues (b) and ear-shaped cartilage-like tissues (c) generated through cell-only bioprinting followed by culture in tissue-specific differentiation media. Reproduced from [184], with permission from the Royal Society of Chemistry

surrounding tissues. While extrusion-based bioprinters have been more common for in vivo bioprinting [9, 290], volumetric, two-photon, and SLA-based bioprinters have also been used for in vivo printing of scaffolds [267, 291, 292]. A new alternative to this paradigm is replacing the imaging modality, image processor, and automated printer with the surgeon's eye, brain, and arm. In this way, a handheld device that can extrude material at a controlled rate can be used to seamlessly fill the defect site [293, 294]. Perhaps the resolution of the feature sizes is not comparable to that of automated bioprinters, but this can easily be integrated into the surgical workflow [295].

2.2.4.8 Multimaterial printing

Biofabrication and biomedical manufacturing seek to recreate the structural, mechanical, and biological complexity of native tissues in a scalable and clinically relevant manner. Recent developments in the field—including embedded printing, volumetric printing, and continuous liquid interface printing—have made substantial advances in the complexity and speed of biofabrication and biomedical manufacturing [88, 97, 296, 297]. However, most advanced processes still rely on layer-by-layer or voxel-by-voxel printing and are often constrained to one material class. This limits the ability to fabricate cell-laden biomaterials in complex geometries with mechanical properties that recapitulate features of human organs. Many tissues—particularly musculoskeletal and interfacial tissues—exhibit multimaterial composition, graded mechanics, and spatially regulated biochemical signaling that exceed the capabilities of single-material or single-process bioprinting. These tissues in the body incorporate both soft, cell-laden compartments with more rigid elements that provide structure or mechanical anisotropy [298]. Therefore, biofabrication and biomedical manufacturing processes that combine rigid and soft materials are needed to engineer self-supporting, anisotropic, and biofunctional materials.

Multimaterial printing, which includes embedded printing, offers a solution to manufacture biomaterial implants or tissue scaffolds that combine soft hydrogels with more rigid supports [58, 75, 90]. A complementary approach, developed in the Langer laboratory at the Massachusetts Institute of Technology has exploited the ability to suspend liquid films using porous materials to rapidly integrate soft, cell-laden hydrogels with rigid support materials (Fig. 24) [31]. Surface tension-assisted AM builds on advances in suspended or open microfluidics, wherein liquid films can be suspended by rigid supports [299]. Building on this, the biofabrication approach leverages liquid surface tension to coat fenestrated rigid objects with suspended films. When a suitable scaffold is dipped into a hydrogel precursor solution and withdrawn, surface tension suspends liquid films across each window. These metastable films are then solidified—via photopolymerization, thermal gelation, or ionic crosslinking—forming continuous hydrogel windows that convert the open-frame lattice into a mechanically integrated multicomponent structure. In this manner, traditional 3D printing can be used to prepare arbitrary support structures that can then be combined with

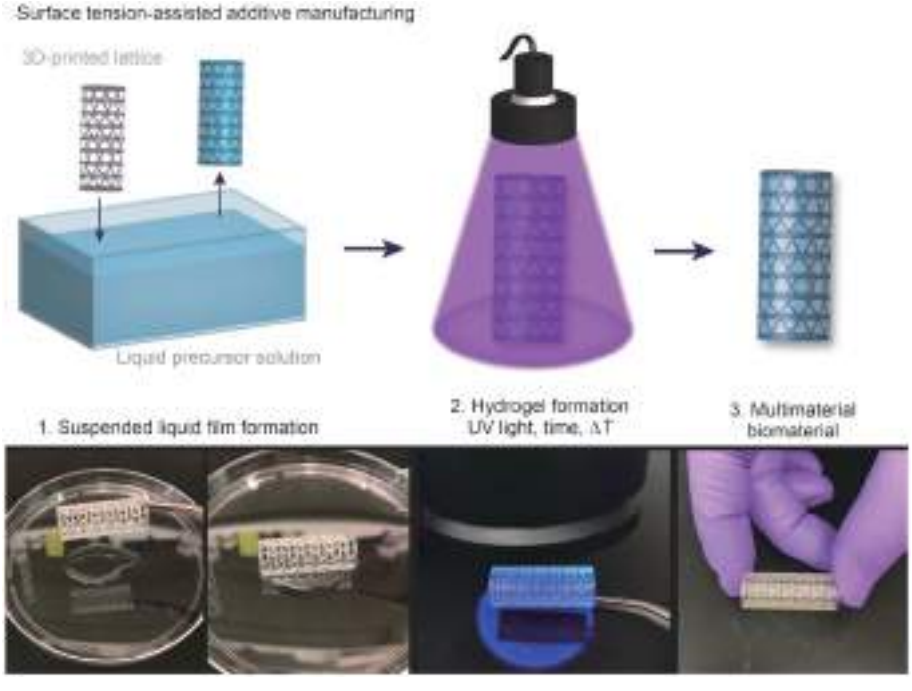

Fig. 24 Surface tension-assisted AM. 3D-printed lattice structures are immersed in a liquid precursor solution to suspend liquid films across the windows that can be transformed into solid hydrogels to fabricate multimaterial biomaterials. Reproduced from [31], licensed under CC BY 4.0

cell-laden hydrogels in a second step to render the final multimaterial construct. In one example, this has been used to biofabricate tubular constructs, inspired by the human trachea, with sufficient mechanical rigidity and anisotropic properties provided by the rigid, 3D-printed support and cell compatibility provided by soft, hydrogel windows. The constructs have supported stromal cells encapsulated within the hydrogel windows and a cell layer on the lumen of the tubular constructs.

The ability to exploit the inherent nature of the surface tension of liquid films to suspend engineered lattices presents many opportunities in the biofabrication of multimaterial constructs. Surface tension-assisted AM has enabled biofabrication of complex structures with tailored properties by engineering both the support scaffold and the hydrogel coating. The accessible and versatile nature of this approach has provided a platform for use in TERM, especially in the design of tubular or complex surfaces. Similar approaches have been extended to the design of multicompartment in vitro tissue models and layer-by-layer fabrication of sophisticated hydrogel scaffolds [300, 301].

2.2.4.9 Hybrid bioprinting for tissue engineering and regenerative medicine

The Yang group's research at Stanford University has focused on the development of hybrid bioprinting strategies that integrate multiple fabrication modalities, materials, and biological cues within unified manufacturing platforms. This work establishes hybrid bioprinting as a generalizable approach for engineering mechanically robust, biologically functional, and spatially complex tissue constructs [302–304].

The Yang group has developed hybrid bioprinter systems that combine complementary AM techniques within a single coordinated workflow. Early work introduced the concept of integrating molten material extrusion with light-based bioprinting to enable seamless fabrication of rigid scaffolds and cell-laden hydrogels in a layer-by-layer process [302]. Building on this foundation, the Yang group later developed modular hybrid platforms that integrate syringe extrusion, molten material extrusion, and droplet-based patterning to enable precise control of both structure and biological signaling [304]. These systems decouple mechanical reinforcement from biological function, allowing each to be independently optimized while remaining fully integrated during manufacturing.

Their hybrid biofabrication approach leverages composite material systems, pairing load-bearing thermoplastics or rigid scaffolds with viscoelastic, cell-laden hydrogels [304–308]. The rigid phase provides immediate structural integrity and surgical handleability, while the hydrogel phase supports cell viability, matrix remodeling, and biofactor delivery [308–311]. Importantly, spatial control over crosslinking density and biofactor localization enables the generation of continuous mechanical and biochemical gradients within a single construct. These design considerations transform hybrid bioprinting from a material-combination strategy into a predictable and scalable manufacturing paradigm [304]. Across their work, the Yang group has demonstrated that interpenetrating or mechanically interlocked scaffold–hydrogel architectures enhance construct robustness while preserving biological performance. This material strategy enables coverage of tissue-relevant mechanical properties spanning multiple orders of magnitude, a key requirement for engineering heterogeneous tissues and interfaces [304].

Hybrid bioprinting has been applied to a range of tissue engineering challenges, including bone, tendon, muscle, and graded tissue interfaces [302–311]. By enabling simultaneous control of mechanics and biology, hybrid constructs are particularly well suited for regenerative applications that demand early load bearing alongside long-term tissue remodeling. Beyond implantation, these platforms also serve as advanced in vitro models for studying mechanobiology, tissue development, and combinatorial biological signaling. Collectively, their work has demonstrated that hybrid biofabrication represents a unifying framework for biomedical manufacturing, capable of overcoming key limitations of conventional bioprinting. Future directions include increased automation, integration of real-time feedback and modeling, and expansion toward multitissue and organ-scale systems. As hybrid bioprinters mature, they are poised to play a central role in translating biofabrication technologies from laboratory innovation to clinical and industrial impact [303].

2.2.4.10 Multimaterial gradient printing

The Habib group at Rochester Institute of Technology and their collaborators have developed multimaterial gradient scaffold techniques to better tailor constructs to patient needs. Their custom bioprinting system uses an interchangeable nozzle to switch bioinks seamlessly during a single print, enabling continuous material gradients within one scaffold [275, 312]. This on-demand deposition of multiple biomaterials with minimal transition distance creates smooth compositional gradients that are difficult to achieve with conventional fixed-nozzle setups. In parallel, they leveraged advanced toolpath strategies to vary pore architecture throughout a structure [276, 313]. By varying layer orientations and patterns, they can create scaffolds with region-specific pore sizes, such as a vertebral construct featuring larger pores in one area and smaller pores in another, to mirror the heterogeneous architecture of natural bone. Such graded scaffolds can be customized to match a patient's anatomical defect or the transition between tissue types, potentially enhancing biological integration and functional performance post-implantation [314]. By combining precise

material placement with controlled porosity, this approach has yielded hierarchical scaffolds that deliver targeted structural and biological cues, embodying the core principle of patient-specific design [315, 316]. The Habib laboratory and their colleagues' integrated contributions have demonstrated how materials science, advanced manufacturing, and design innovation can yield patient-specific constructs.

2.2.5 Other alternative techniques

Some manufacturing processes on the frontier of research do not fall into the previously described categories. While different established methods fit into this category, this section covers representative alternative processes, with a specific focus on developments in microchannel generation using sacrificial meshes, surface tension-assisted multimaterial printing, hybrid printing, flash assembly, and nonviral cell and gene therapy engineering. Beyond the techniques highlighted in this section, several other researchers have also made important contributions to the field. For example, the Shin group and Khademhosseini group at Harvard Medical School have advanced microfluidic bioprinting by using coaxial microfluidic printheads to fabricate heterogeneous, cell-laden hydrogel fibers and tissue constructs with controlled composition and architecture, helping bridge microfluidics and scalable 3D biofabrication [317].

2.2.5.1 Sacrificial microfiber patterning for engineered capillary-like vessels

The vascular tree contains a diverse range of vessel types, with each vessel type exhibiting architecture uniquely suited to its function. For example, larger arteries close to the heart are highly elastic and help dampen upstream pulsatility to achieve smoother downstream blood flow, while capillaries exhibit high density, large overall surface area, and permeable thin walls to support their role as exchange vessels. Given the critical functions of the circulatory system, it is unsurprising that there has been substantial effort to engineer vascular structures at multiple scales [318]. While larger tissue-engineered vascular grafts have been explored since the 1980s [319], efforts to engineer microscale capillary-like vessels (to support the viability of cells within thick engineered tissue constructs) began in the early 2000s [320–323].

Approaches to engineer capillary-like vessels generally fall into one of two categories: "bottom-up" approaches that rely on vasculogenesis or angiogenesis, or "top-down" approaches that rely on pre-patterned channels. While bottom-up approaches can yield architecture that closely mimics that of natural capillary beds, they are often too slow to form a perfusable network in time to support the immediate metabolic needs of cells within a thick hydrogel construct. Top-down patterning techniques, however, are often incapable of producing channel networks that exhibit architecture mimicking that of natural capillary beds.

The Bellan laboratory at Vanderbilt University has developed a top-down patterning approach that employs sacrificial microfibrous meshes as templates to form complex microchannel networks with architectures similar to those of natural capillary beds. Microfibers are spun using a rotary spinning system not unlike a "cotton candy" machine, collected as a 3D mesh, and used as sacrificial templates (Fig. 25a). Early work employed microfibers formed from sugar [324, 325] or shellac [326] to produce microchannels throughout polydimethylsiloxane (PDMS) or gelatin hydrogels, respectively. More recently, microfibers formed from thermoresponsive polymers exhibiting a lower critical solution temperature were used [327, 328]; this has enabled noncytotoxic liquification of the template by cooling from 37 °C to 25 °C so that channels could be formed in the presence of live cells embedded within a hydrogel (Fig. 25b). Characterization of the resulting microchannel network architecture has revealed notable similarity to network parameters (diameter range, branch length, tortuosity, etc.) describing natural capillary beds. When perfused with media, these capillary-like networks significantly enhanced the viability of cells embedded within thick tissue constructs (Fig. 25c). Additionally, these microchannels could be coated with a confluent layer of endothelial cells (ECs; Figs. 25d–25i). While the sacrificial microfiber patterning approach forfeits some control over parameters such as individual channel location and exact specification of individual channel diameters, it exhibits a level of scalability, three-dimensionality, and mimicry of natural capillary architecture that is difficult to achieve with other patterning approaches. The integration of this exchange vessel patterning technique with approaches for producing larger vessel types has the potential to yield a rapid, robust biomanufacturing platform that forms immediately perfusable and functional multiscale vasculature throughout thick engineered tissues.

2.2.5.2 Flash assembly for scalable nanotherapeutics

Biofabrication has traditionally emphasized the macroscopic construction of tissues and microphysiological systems enabled by 3D bioprinting, but comparable innovation is needed at the nanoscale to manufacture nanotherapeutics. Engineered carriers can improve biodistribution, protect labile cargos, and enable tissue- and cell-selective delivery. For translation, however, these materials must be produced reproducibly at scale with tightly controlled critical quality attributes, including size, dispersity, composition, and surface chemistry. Bench methods such as dropwise mixing, vortexing, and sonication often yield heterogeneous products and substantial batch-to-batch variation. While lipid nanoparticle manufacturing for mRNA vaccines benefits

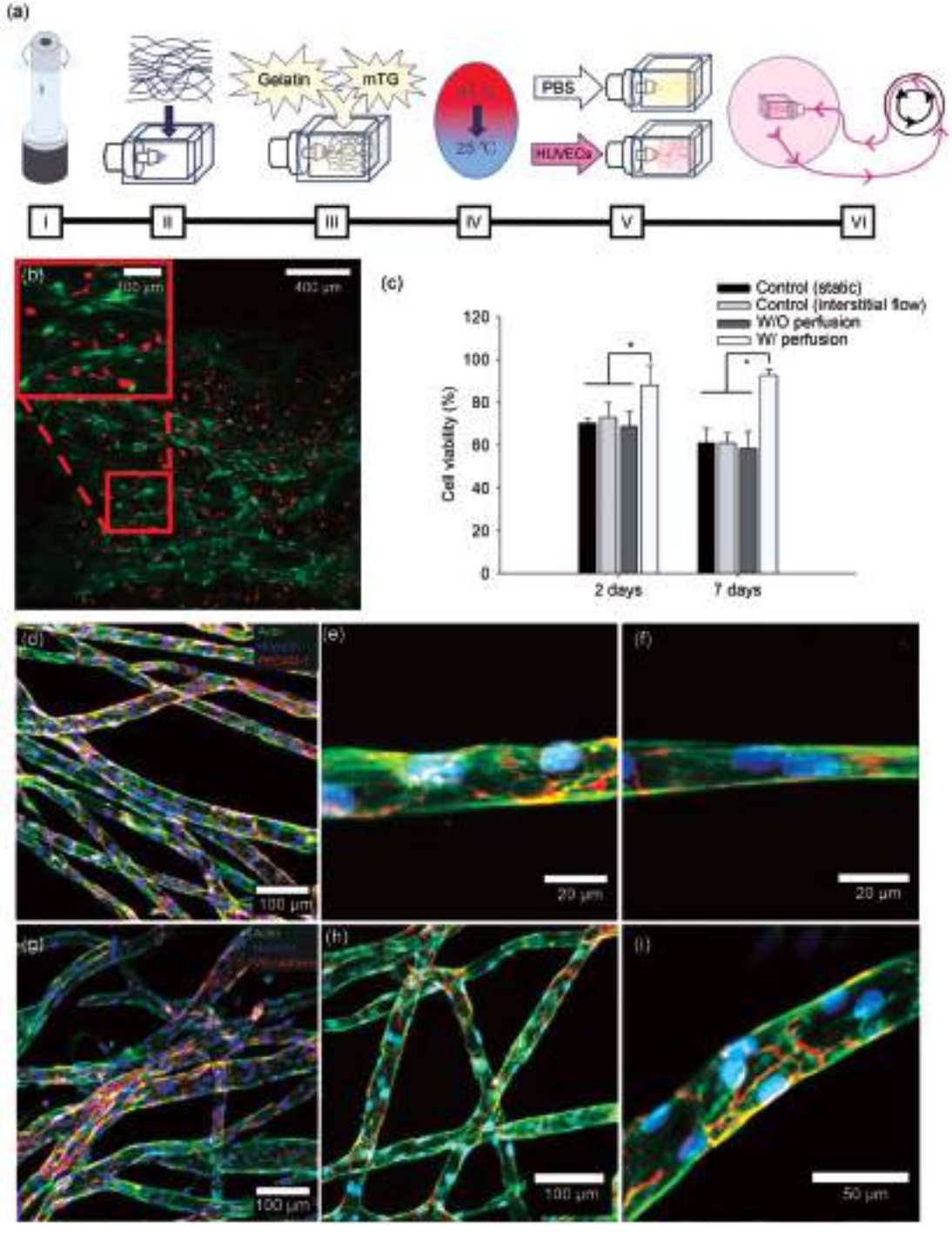

Fig. 25 Sacrificial microfiber templating for perfusable microvascular networks in thick hydrogels. (a) Schematic illustrating the sacrificial thermoresponsive polymer microfiber mesh fabrication process: microfibers are (I) spun into a mesh, (II) placed into a PDMS mold, and (III) embedded within warm gelatin hydrogel precursor solution and placed in an incubator. When the hydrogel has set, the device is (IV) removed from the incubator and allowed to cool to room temperature, causing the fibers to liquify. (V) At this point, the sacrificial polymer is removed by flushing the device, after which ECs (e.g., HUVECs) are seeded into the channels. Once cells have adhered, (VI) the device is attached to an external pump to perfuse the channel network with cell culture media. (b) Red fluorescent protein-expressing human neonatal dermal fibroblasts (RFP-HNDFs) were mixed into the hydrogel precursor prior to casting, resulting in these cells being embedded in gelatin surrounding green fluorescent protein (GFP)-HUVEC-lined channel networks. (c) Perfusion of the capillary-like microchannel networks dramatically enhances the viability of fibroblasts embedded within the thick gelatin hydrogel. (d–i) HUVECs lining the walls of the microchannels stained for actin and PECAM-1 (d–f) or VE-cadherin (g–i). Endothelialized channels smaller than 20 μm can be manufactured via this approach as shown in (f). Reproduced from [327], with permission from WILEY-VCH Verlag GmbH & Co. KGaA, Weinheim; reproduced from [328], licensed under CC BY 4.0

from rapid mixing-driven nanoprecipitation, many nonlipid carriers remain manufacturing-limited, exemplified by polyelectrolyte complexes whose assembly is strongly governed by mixing conditions.

Flash nanoprecipitation is effective for mRNA lipid nanoparticles (LNPs) because solvent exchange drives lipid self-assembly. Lipids in ethanol encounter an aqueous mRNA stream, and millisecond mixing followed by dilution removes solvent and fixes size and dispersity. Polyplexes, in contrast, form through ultrafast electrostatic complexation in fully aqueous media, often on timescales comparable to mixing. This motivates a shift to flash nanocomplexation (FNC), which uses confined mixers and a tuned charge ratio, ionic strength, and pH to keep mixing faster than binding and to minimize aggregation [329]. Under FNC conditions, rapid turbulent mixing establishes homogeneous local environments at the moment of particle formation, enabling kinetic control. Uniformity is achieved when the mixing time (τ_M) remains shorter than the assembly time (τ_A), a criterion rarely met by pipetting or vortexing [329]. The Leong laboratory at Columbia University has focused on developing FNC approaches for nanotherapeutic fabrication.

Across vaccine applications, this kinetic control has translated into improved in vivo performance. In an Enterovirus 71 subunit vaccine model, FNC has produced chitosan–heparin nanovaccines (approximately 90–130 nm, narrow dispersity) that were smaller and more uniform than particles made by manual bulk mixing. These nanovaccines have drained efficiently to proximal and distal lymph nodes, exhibited prolonged nodal retention, and enhanced dendritic cell uptake and maturation, eliciting robust T-helper (Th)1-dominant and strong Th2 responses and protecting mice and gerbils from lethal Enterovirus 71 challenge with efficacy comparable to that of an approved inactivated vaccine [330]. FNC has also enabled scalable fabrication of biomimetic cancer nanovaccines in which cytosine-phosphate-guanosine (CpG)-loaded mesoporous silica nanoparticles were uniformly cloaked with B16-F10 melanoma cell membranes. Compared with bulk sonication, FNC reduced polydispersity and improved colloidal stability, increasing lymph node accumulation and uptake by dendritic cells and macrophages, promoting stronger dendritic cell maturation, higher interleukin (IL)-6/IL-12, and greater antigen gp100-specific T-cell expansion. These immune gains were accompanied by superior prophylactic tumor growth inhibition and longer survival, and by enhanced therapeutic efficacy when combined with anti-cytotoxic T lymphocyte-associated antigen-4 (CTLA-4), consistent with improved antigen presentation in draining lymph nodes [331]. In a related SARS-CoV-2 formulation, genetically engineered membranes displaying the receptor-binding domain (RBD) have been used to cloak CpG-loaded mesoporous silica nanoparticles. FNC-fabricated vaccines outperformed bulk sonication, inducing the highest RBD-specific immunoglobulin G (IgG) titers and elevated serum interferon-γ and tumor necrosis factor-α; sera neutralized SARS-CoV-2 pseudovirus at >80% (vs. approximately 70% for bulk nanovaccines and approximately 30% for membrane vesicles), alongside greater lymph node antigen-presenting cell uptake and stronger T-helper-associated responses, without detectable weight loss or organ toxicity [332].

These and other selected examples have demonstrated FNC as a versatile manufacturing platform for nanomedicine translation by enabling reproducible, scalable control of critical quality attributes [330–335]. By enforcing millisecond turbulent mixing in confined geometries, FNC places nanoparticle formation under kinetic control, improving size uniformity and limiting aggregation in systems where electrostatic complexation competes with mixing. This distinction is central: solvent-exchange nanoprecipitation that is well suited for mRNA LNPs does not directly extend to fully aqueous polyplexes and other assemblies whose outcomes are dominated by mixing-governed kinetics.

2.2.5.3 Nonviral cell and gene therapy engineering

The clinical success of chimeric antigen receptor (CAR)-T cell therapies and clustered regularly interspaced short palindromic repeats (CRISPR)-based treatments for blood disorders has fundamentally altered the oncology and rare disease landscapes [336]. However, the field remains constrained by manual, bespoke manufacturing steps and the limitations of viral vectors, which introduce high costs, safety risks such as insertional mutagenesis, and limited cargo capacity [337]. There is an urgent need for site-specific, nonviral genome editing strategies that can be integrated into automated, closed-system bioprocessing workflows [338, 339].

At the University of Wisconsin-Madison, the Saha laboratory's Cas9-CLIPT (Cleaved, LInearized with Protein Template) technology has addressed these bottlenecks by enabling high-efficiency (up to 60%) site-specific integration of large transgenes (2–6 kb) without the cytotoxicity typically associated with standard double-stranded DNA templates [340]. By using circular nanoplasmid templates linearized in situ by the Cas9-ribonucleoprotein (RNP) (Fig. 26a), this method masks DNA ends from innate immune sensors and promotes an enriched stem cell memory phenotype, which is crucial for therapeutic longevity [341].

Beyond ex vivo cell therapy, the research program has extended to in vivo nonviral gene therapies through the CRISPR Vision Program. This program has focused on treating inherited retinal disorders, such as Best disease and Leber congenital amaurosis (LCA16), using synthetic nanoparticles [342, 343]. As part of the National Institutes

of Health (NIH) Somatic Cell Genome Editing (SCGE) consortium, the program has developed new nanoparticle formulations and tools to measure editing outcomes with high precision for allele-specific editing approaches [344]. These nonviral delivery systems aim to overcome the immunogenicity and packaging limits of adeno-associated viruses (AAVs), facilitating the correction of genetic variants directly within the retinal pigment epithelium (Fig. 26b) [342].

A central frontier is the interface between in vivo and ex vivo modalities. While the rise of in vivo delivery, exemplified by LNP-mediated editing of the liver [345, 346] and recent biopharma investment in in vivo CAR-T approaches [347], has led some to question the long-term utility of ex vivo cell therapies, this view overlooks critical biomedical manufacturing advantages. Ex vivo approaches provide a "gated" control mechanism: they allow for the rigorous selection, expansion, and characterization of edited cells before they reach the patient, effectively eliminating off-target variants or translocations that could be deleterious [337, 348]. Furthermore, complex multigenic "logic gate" engineering in cells remains significantly more feasible ex vivo [349].

The laboratory has accelerated translational programs by using human microphysiological systems and organoids as predictive quality-control platforms [348]. These "on-a-chip" models serve as a surrogate for the in vivo environment and have allowed researchers to monitor the biological consequences of both ex vivo manufactured cells and in vivo delivery vehicles in human-specific genomic contexts [350]. By harmonizing nonviral editing with advanced tissue models, the program aims to broaden access to scalable, high-fidelity genetic medicines.

3 Materials for biofabrication and biomedical manufacturing

Materials lay the foundation of biofabrication and biomedical manufacturing, determining not only printability and structural fidelity, but also cell viability, tissue maturation, and translation-relevant performance [1, 75]. In the U.S., frontier material innovation is increasingly oriented toward the integrated optimization of material properties, process suitability, and biological compatibility and representativeness [245]. Accordingly, rheological behavior, crosslinking kinetics, mechanical properties, and bioactivity are designed to be suitable for specific fabrication processes and targeted functions. This section highlights representative U.S. advances across widely used polymer-based and cellular-based building materials that enable high geometrical fidelity and biomimetic and multifunctional biofabrication. Beyond the

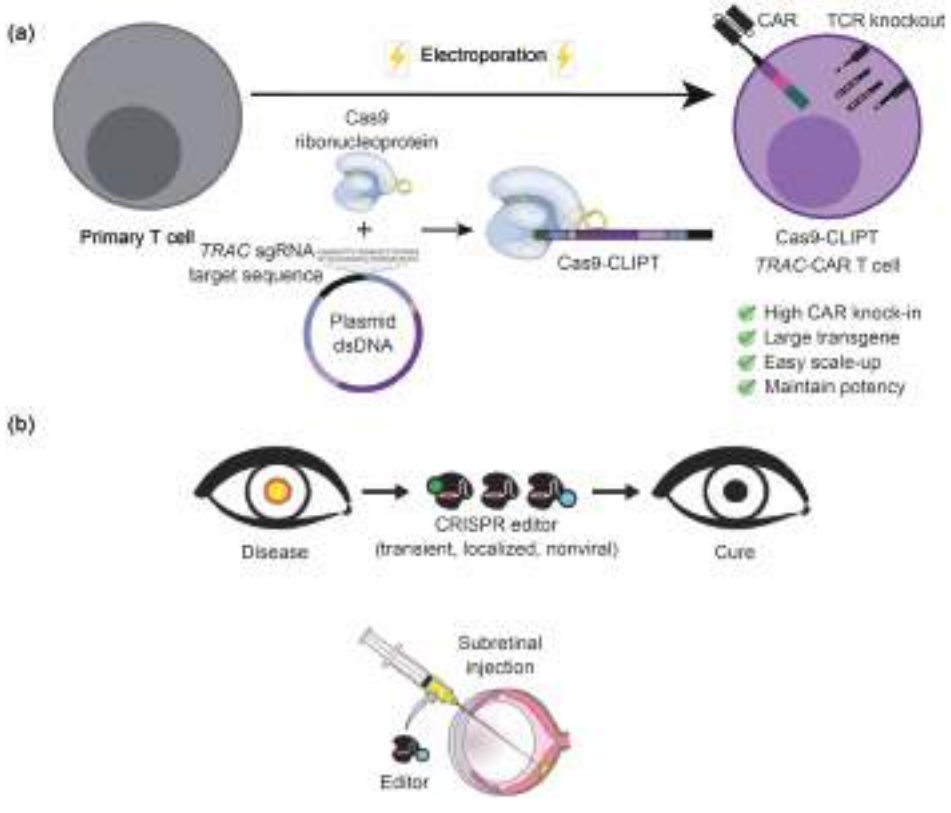

Fig. 26 The spectrum of nonviral genetic medicine. (a) Ex vivo pipeline using Cas9-CLIPT for precise CAR-T biomedical manufacturing (reproduced from [340], licensed under CC BY-NC-ND). (b) In vivo pipeline showing synthetic nanoparticle delivery to the retina. Red RNA components can be tailored to mutant alleles, while green and blue modifications to the delivery vehicle can confer cell type specificity

biomaterials development highlighted in this section, several other researchers have also made important contributions to the field. For example, the Kaplan group at Tufts University established silk fibroin scaffolds as a versatile biomaterial platform for biofabrication by developing porous, mechanically robust silk-based constructs for tissue engineering, including high-strength bone-regenerative scaffolds [351]. The García group at Georgia Institute of Technology showed that integrin-specific synthetic hydrogels can improve transplanted hMSC survival, engraftment, and reparative activity, highlighting how matrix design at the ligand level can direct regenerative outcomes [352]. The Anseth group at the University of Colorado Boulder developed photopolymerized dynamic hydrogels with tunable viscoelasticity, providing a synthetic matrix platform that better captures the evolving mechanics of native tissues and supports more biomimetic cell culture and organoid engineering [353].

3.1 Polymers

3.1.1 Natural polymers

3.1.1.1 Natural and naturally derived hydrogels

Natural hydrogels, such as collagen, gelatin, alginate, and hyaluronic acid (HA), are water-swollen, crosslinked polymer networks that closely resemble key physical and biochemical features of native ECM, making them one of the most important material classes in biofabrication for cell culture, tissue repair, controlled delivery of bioactive cues, and the construction of engineered 3D tissue models and implants.

The Burdick group at the University of Colorado has helped define hydrogels, especially HA-based systems, as a central polymer platform for biofabrication and regenerative medicine [38, 89, 354–365]. Their early work established HA as a highly versatile and biologically relevant backbone that can be chemically modified into "living" hydrogel systems suitable for 3D cell culture, injectable delivery, and tissue repair while preserving the intrinsic advantages of a naturally derived ECM component [364]. Building on this foundation, his group has shown that hydrogel design must move beyond simple bulk stiffness to incorporate cell-mediated remodeling and dynamic mechanics: in covalently crosslinked HA hydrogels, stem cell fate depends on degradation-enabled traction generation rather than stiffness alone [359], and sequentially stiffened HA hydrogels have revealed how time-dependent matrix mechanics regulate mesenchymal stem cell spreading, traction, and lineage commitment [359]. Together, these studies have shifted hydrogel design from passive cell carriers toward dynamically instructive polymer networks that can actively regulate cell behavior.

More recently, the Burdick laboratory's work has expanded the hydrogel toolkit toward materials that are more processable, injectable, and architecturally sophisticated. The group has developed shear-thinning, self-healing, guest–host HA hydrogels and shown that coupling supramolecular assembly with secondary covalent stabilization enables extrusion printing of stable multilayer structures, illustrating how polymer chemistry can be tuned simultaneously for printability and long-term fidelity [358]. In parallel, their work on hydrogel microparticles and granular hydrogels has broadened the concept of hydrogels from continuous bulk networks to modular particulate systems with injectability, microporosity, and tunable cell-instructive properties [361]. These studies have highlighted how hydrogel research has evolved from the molecular design of biologically relevant polymer networks to dynamic control of cell–matrix interactions, and further toward processable hydrogel systems for advanced biofabrication, with a sustained emphasis on making hydrogels more instructive, tunable, and translationally useful for tissue engineering.

Other natural hydrogels, such as GelMA, are another widely used modified natural polymer. GelMA is a semi-natural (or hybrid) hydrogel that combines a natural backbone with synthetic modifications and has been widely used in biofabrication. Using optimized GelMA-based hydrogels and DLP bioprinting, the Serpooshan-Bauser group fabricated perfusable, chamber-like microtissues composed of cardiomyocytes, endocardial, and fibroblast lineages arranged in physiologically relevant patterns [366, 367].

3.1.1.2 GelMA-based macroporous hydrogel foam bioinks

Hydrogels have been the gold standard biomaterials to generate bioinks due to their high water content and similarity to native ECM. Although many of these hydrogels can degrade in vivo over time by enzymatic cleavage [368, 369], cell infiltration from surrounding tissue into the middle of the bulk-implanted scaffold is severely limited. Researchers have noticed that hydrogel scaffolds with large pores better support cell migration and scaffold integration. To this end, two types of inks have been generated and widely used: (1) granular inks, which are formed from tightly packed hydrogel microparticles [109] and (2) multi-material inks with a sacrificial component [370]. Granular hydrogels offer interconnected pores that can expedite vascularization and cell ingrowth. However, the volume occupied by the gel is significant, and the limited contact points between particles reduce elasticity and deformability. Moreover, their printing is challenging and requires surface modification. Multi-material inks are easy to use, but the control over the pore size and pore geometry is limited. The Tamayol group at the University of Connecticut Health Center has developed hydrogel foams using GelMA, which are formed by air-hydrogel precursor emulsions [371]. Hydrogel foams are similar to

whipped cream in pastries and are easy to manipulate and print. They are highly porous with a porosity of approximately 80%, which makes them lightweight and easy to degrade for cells [371]. While all these forms of inks have been used for various tissue engineering applications, hydrogel foams and multi-material inks have been successful in the treatment of highly contractile tissues [37, 371].

3.1.2 Synthetic polymers

3.1.2.1 Modified poloxamer for DLP printing

3D printing/bioprinting continually requires advanced ink/bioink materials with multifunctionality, high performance, and/or excellent cell-supporting capacities. The Duan group from the University of Nebraska Medical Center and their collaborators have developed and implemented a photoreactive poloxamer derivative, Pluronic F-127 diacrylate (Fig. 27a), to achieve DLP 3D-printed micelle-based hydrogels with high structural complexity, resolution, and precision (Fig. 27b) [1]. In addition, the dehydrated hydrogels exhibit a shape-memory effect and are conformally attached to the geometry of the detection point after rehydration, which implies the 4D printing characteristic of the fabrication process (Fig. 27c). The favorable cytocompatibility and in vivo biocompatibility (Fig. 27d) further highlight the potential application of poloxamer micelle-based hydrogels as a platform for multifunctional wearable systems (Fig. 27e) and real-time carbon nanotube sensing [36]. The Duan group has also developed functional bioinks with antioxidative and therapeutic properties by chemically modifying or physically blending functional groups and bioactive components to enhance tissue repair and regeneration [372, 373]. Meanwhile, printing support bath materials have also been developed to improve embedded 3D printing and enhance the structural fidelity and resolution of complex constructs [59, 107].

3.1.2.2 Emulsion inks for 3D printing of medical devices with multiscale porosity

Emulsion inks are a class of printable materials developed for AM to create customizable geometries with multiscale

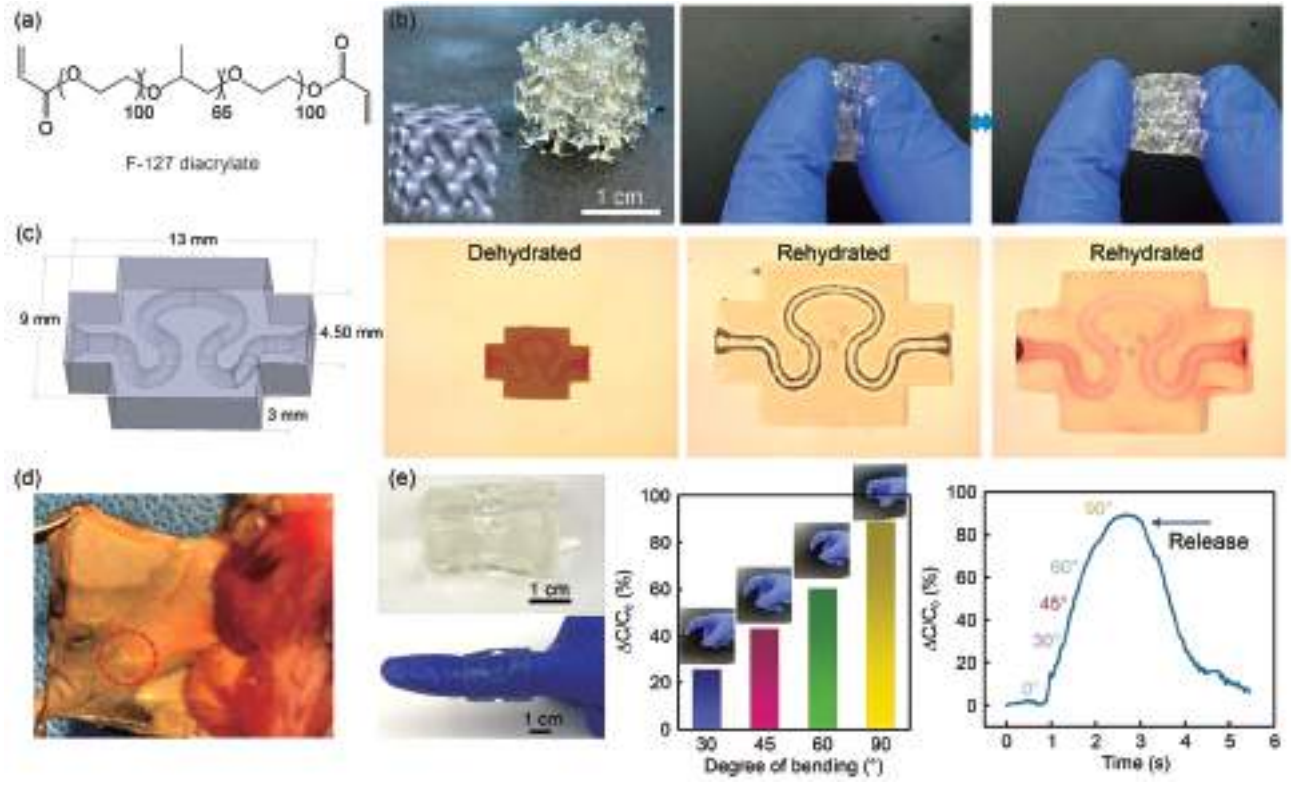

Fig. 27 DLP 4D printing of poloxamer micelles. (a) Chemical structure of Pluronic F-127 diacrylate. (b) 3D-printed gyroid cube, manually compressed gyroid cube, and gyroid cube restored to its original shape. (c) 3D design of a solid object with an open serpentine channel: dehydrated poloxamer hydrogel with the channel, rehydrated poloxamer hydrogel with the channel after dehydration, and rehydrated poloxamer hydrogel with the channel visualized with red dye throughout. (d) Poloxamer hydrogel after a 4-week subcutaneous implantation, showing approximately 50% degradation with a minimal foreign body reaction. (e) From left to right: customized and 4D-printed wearable hydrogel; relative capacitance changes of the wearable capacitive strain sensor depending on the different bending angles of the finger (n=3); dynamic response of the capacitive strain sensor during the bending and straightening of the finger. Reproduced from [1], with permission from the American Chemical Society

porosity (Fig. 28) [374, 375]. In these systems, the ink is an emulsion composed of a photocurable macromer as the continuous phase and a dispersed internal phase that acts as a sacrificial template, generating microscale pores upon curing. The emulsion-templated pore architecture is locked in during photopolymerization of each layer in both vat stereolithography [376, 377] and paste extrusion setups [374, 378, 379]. The design of the microscale emulsion-templated pores and the programmed macroscale lattice structure influence transport, swelling, permeability, mechanical properties, and biological integration. Dual control over micro- and macroscale architecture expands the design space of 3D-printed devices beyond what is achievable with nonporous printed materials.

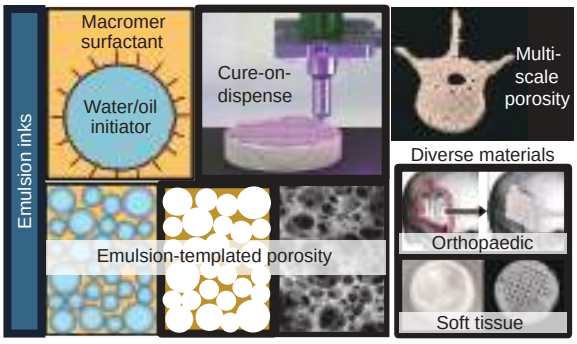

Fig. 28 Emulsion inks used in the design of 3D-printed devices with multiscale porosity for a diverse range of applications, including bone grafts, soft tissue scaffolds, and wound dressings. Fundamental design inputs of emulsion inks (e.g., surfactant concentration and mixing speed) allow for tuning of ink rheology and material microarchitecture, yielding printable emulsion inks and tunable device properties. Reproduced from [40], licensed under CC BY 4.0; reproduced from [374], with permission from WILEY-VCH Verlag GmbH & Co. KGaA, Weinheim; reproduced from [379], with permission from WILEY-VCH Verlag GmbH & Co. KGaA, Weinheim; reproduced from [380], with permission from IOP Publishing Ltd.

The Cosgriff-Hernandez laboratory at the University of Texas at Austin has developed a versatile suite of emulsion inks based on high internal phase emulsions (HIPEs), defined as emulsions in which the dispersed (internal) phase makes up more than 74% of the total volume. HIPEs exhibit shear-thinning behavior, enabling them to act as elastic solids at low shear and to flow once a yield stress is reached. This transition allows them to be readily extruded during printing while still retaining their form after deposition—properties that make them well suited for extrusion-based AM. In the first application of HIPEs as extrudable emulsion inks, the Cosgriff-Hernandez group examined how macromer composition affected low-shear viscosity and, together with cure-on-dispense UV polymerization, influenced extruded layer fidelity [374]. This work established the rheological and curing parameters required for maintaining print fidelity, enabling the fabrication of complex polyHIPE geometries with multiscale porosity. Building on this new platform, they have translated this to biodegradable, fumarate-based macromers for application in the 3D printing of bone grafts [380]. 3D-printed scaffolds generated from propylene fumarate dimethacrylate HIPE inks have displayed multiscale porosity—engineered macropores (approximately 250 μm) and emulsion-templated micropores (5–30 μm)—and have supported robust hMSC viability and proliferation. To overcome the trade-off between porosity and mechanical performance, a multi-material printing strategy has been developed that combines paste extrusion of the emulsion ink with thermal extrusion of a solid polyester shell. These biomimetic constructs have exhibited compressive properties approaching those of trabecular bone while maintaining enhanced permeability, demonstrating how emulsion inks can be integrated into hybrid architectures to simultaneously tailor mechanical and transport properties. Parallel work with cell-releasing hydrogel carriers has provided a simple and effective method for seeding printed scaffolds with hMSCs, further enhancing their capacity to support bone regeneration [381]. This group has further extended emulsion inks to hydrogel platforms for printing soft tissue scaffolds [379] and wound dressings [40]. In contrast to the prior water-in-oil HIPE inks, these systems employ oil-in-water emulsions with a continuous phase based on a hydrogel precursor and a dispersed mineral oil phase. This new class of emulsion inks has enabled high-fidelity printing of porous hydrogels without the need for high polymer concentrations or rheological additives [379]. These material advances have translated into a clinically relevant wound dressing, where the dual porosity facilitated rapid, self-adjusting moisture control [40]. Collectively, this work has established a framework for emulsion inks and facilitated their continued development and application in AM.

3.1.3 Photoinitiators for vat polymerization-based AM

The Narayan group at the University of North Carolina and North Carolina State University has examined the biological properties of photoinitiators that have potential use in vat polymerization-based AM. They studied the polymerization of GelMA using the free radical photoinitiator lithium phenyl(2, 4, 6-trimethylbenzoyl) phosphinate (LAP) and found that a 10-min exposure to 405 nm light (9.6 mW/cm^2) from a light-emitting diode led to full crosslinking of 10% (mass fraction) GelMA with LAP at concentrations greater than 3.4 mmol/L. This study suggests that although no mutagenicity was associated with the use of LAP under typical bioprinting conditions, free radicals from photoexcited LAP can be cytotoxic to cells that are undergoing a vat polymerization-based bioprinting process. In another study, they evaluated acellular 10% (mass fraction) GelMA hydrogels that were

crosslinked with various concentrations of LAP and crosslinking illumination times [382]. They performed the Alamar Blue viability assay and CyQuant Direct Cell viability assay with human primary renal proximal tubule epithelial cells (hRPTECs) that were exposed to extracts of each formulation and showed that LAP concentration did not have an effect on extract cytotoxicity via the Alamar Blue assay but decreased hRPTEC viability via the CyQuant Direct cell assay; in addition, UV light exposure during crosslinking was not noted to affect extract cytotoxicity levels via either assay. The differences in the cytotoxicity results obtained from the two viability assays imply cell membrane damage and would benefit from further evaluation. They have examined the use of diphenyl(2,4,6-trimethylbenzoyl)phosphine oxide (TPO) nanoparticles, which exhibit increased water dispersibility, as a photoinitiator for polymerizing GelMA [383]. Significant cytotoxicity is noted in cells exposed to GelMA with TPO nanoparticles; this result indicates that removal of the photoinitiator may be needed to utilize GelMA crosslinked with TPO nanoparticles for biological applications. In another study, they examined the photopolymerization of allylated gelatin using three photoinitiation systems, namely, ruthenium/sodium persulfate (Ru/SPS; 400–500 nm), Irgacure 2959 (320–500 nm), and LAP (320–500 nm) [41]. It is noted that photopolymerization using the Ru/SPS system was significantly more rapid (<5 s) compared to both Irgacure 2959 (70 s) and LAP (50 s). In addition, the Ru/SPS was noted to polymerize a thicker allylated gelatin construct compared to Irgacure 2959 and LAP (Fig. 29). These results support the utilization of the visible light-based Ru/SPS photoinitiator for allylated gelatin constructs since it offers rapid gelation and a good curing depth. This group has also considered free-radical-generating molecules that are part of biological systems for use as biocompatible photoinitiators [384]. They studied the crosslinking of polyethylene glycol diacrylate with commercially available photoinitiators (Irgacure 369 and Irgacure 2959) and a riboflavin–triethanolamine mixture. The comet assay showed that the two tested photopolymers polymerized with the riboflavin mixture, which contained 50% and 66% polyethylene glycol diacrylate by volume, possessed significantly lower genotoxicity than the photopolymers made with Irgacure 2959 and Irgacure 369. The results of these studies have indicated that novel photoinitiators are needed to facilitate the clinical translation of vat polymerization-based methods for scaffold fabrication without the use of extensive postprocessing steps.

3.2 Metals and ceramics

Biofabrication enables precise control over pore size, shape, and spatial distribution in porous metal and ceramic implants, facilitating the creation of structures that mimic trabecular bone while matching patient-specific anatomy [4, 94–96, 385]. For porous metals such as titanium (Ti) or Ti6Al4V, powder bed fusion processes, selective laser melting/sintering, and directed energy deposition are widely used to build lattice and triply periodic minimal surface (TPMS) architectures with uniform and graded porosity, thereby reducing stiffness to mitigate stress shielding and promoting bone ingrowth and vascularization in load-bearing orthopedic and dental implants [386–388]. These metallic scaffolds can be customized from computed tomography (CT) or magnetic resonance imaging (MRI) data for segmental defect reconstruction, spinal cages, acetabular components, and cranio-maxillofacial implants. For porous ceramics, AM routes such as lithography-based ceramic manufacturing, binder jetting, and extrusion-based printing enable the fabrication of interconnected macroporous structures in hydroxyapatite, tricalcium phosphate, and related bioceramics for bone grafts, cages, and wedges used in bone regeneration and defect filling [389, 390]. In these

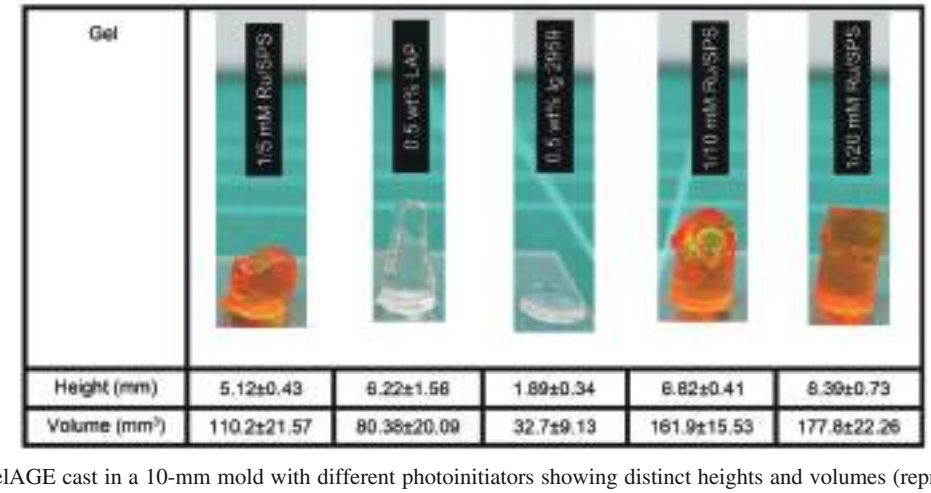

Fig. 29 Image of GelAGE cast in a 10-mm mold with different photoinitiators showing distinct heights and volumes (reproduced from [41], licensed under CC BY 4.0)

systems, controlled pore geometry enhances osteointegration and mechanical performance compared to conventionally foamed ceramics. In both metals and ceramics, AM therefore supports functionally graded porosity, complex internal architectures, and patient bone defect-specific designs that are difficult or impossible to realize using conventional manufacturing methods.

Over nearly three decades, the Bandyopadhyay and Bose groups at Washington State University have conducted pioneering research on first-generation porous metal and ceramic materials for implant applications. Their early efforts concentrated on designing calcium phosphate-based porous ceramic scaffolds using AM. They have extensively investigated how dopant chemistry influences the biological properties of calcium phosphate ceramics for implants and drug delivery, with particular emphasis on early-stage osseointegration, controlling degradation kinetics, and improving mechanical performance [391–393]. Their work on porous metal implants has highlighted the advantages of AM for creating uniform or structurally graded implants that provide superior biological fixation while mitigating stress shielding [3, 394–396]. Figure 30 summarizes their first-generation work on porous ceramic and metal implants. They have also demonstrated that AM can be used to fabricate porous metal implants from Ti, Ti6Al4V, Ta, CoCrMo, and NiTi alloys, and today, more than 500,000 AM-processed, Food and Drug Administration (FDA)-approved devices are implanted each year in the U.S. alone. Their research on 3D printed doped tricalcium phosphate (TCP) in the presence of ZnO, MgO, and SiO_2, and natural medicinal compounds (NMCs), such as curcumin from turmeric, gingerol from ginger, and allicin from garlic, showed early-stage bone formation in the rat distal femur model [397–400]. Curcumin release from 3D printed scaffolds promotes bone formation in a rat distal femur model [397]. Bimodal porosity scaffolds show cancellous-cortical bone-like structures with gradient porosity and a mechanical strength of approximately 12 MPa, where gingerol/allicin-release kinetics are controlled with polymers such as polyethylene glycol (PEG) and PCL [398]. In addition, they have shown that AM enables the incorporation of bioactive coatings on metallic implants to enhance biocompatibility [401] and that titania nanotubes on AM-processed porous Ti structures can further improve biocompatibility [402]. Their recent research has focused on alloy design for metallic implants with inherent antibacterial properties to prevent biofilm formation and reduce the risk of implant failure [39, 403]. Although the application of AM in biomedical device manufacturing is expanding rapidly, concerns related to AM's mechanical properties, particularly fatigue response and post-processing treatments, are becoming critical to ensure reproducibility.

3.3 Composites and others

3.3.1 Advances in bioink formulation and embedded bioprinting

One of the central challenges in 3D bioprinting for tissue engineering is the development of bioinks that simultaneously meet the mechanical, biological, and printability requirements needed for tissue reconstruction. The Annabi laboratory at the University of Los Angeles has been at the forefront of this effort by engineering biomimetic bioinks and printing strategies that enable high biomimicry and print fidelity across diverse tissue types [5, 404, 405]. A major advancement has been the development of elastic bioinks containing GelMA and methacryloyl-substituted tropoelastin (MeTro), a modified recombinant human protein [5]. These bioinks provide the elasticity needed for dynamic soft tissues such as the heart and blood vessels. As a proof of concept, the Annabi laboratory has successfully 3D-bioprinted vascularized cardiac constructs and demonstrated their function in vitro and in vivo. Incorporating MeTro imparted resilience and cytocompatibility, enabling the formation of functional vasculature with endothelial barrier function within contractile cardiac tissue constructs exhibiting synchronized beating of encapsulated cardiomyocytes (Figs. 31a–31f) [5]. The constructs also showed minimal inflammatory responses and were efficiently biodegraded in vivo when implanted subcutaneously in rats. Collectively, this work has highlighted the potential of elastic bioinks for printing 3D functional cardiac tissues, which can eventually be used for cardiac tissue replacement. In parallel, the laboratory has developed conductive bioinks by incorporating poly(3,4-ethylenedioxythiophene):polystyrene sulfonate (PEDOT: PSS) microparticles into GelMA and other biopolymers [405]. By tuning the PEDOT: PSS concentration and ionic crosslinking density, the Annabi laboratory has achieved hydrogels with controllable conductivity, mechanical robustness, and excellent print fidelity, supporting the fabrication of complex, electrically active tissue constructs (Figs. 31g and 31h).

Despite significant progress in 3D bioprinting, the low mechanical stability of cell-laden bioinks often compromises print fidelity and limits the fabrication of complex architectures. To address this, the Annabi laboratory has adopted FRESH, a support-bath technique that provides temporary mechanical stabilization during deposition [5, 405]. The support bath functions as a Bingham plastic, behaving as a solid below a critical yield stress and flowing as a liquid above it [97]. This behavior enables smooth nozzle movement while preserving the printed structure until crosslinking is complete. Notably, FRESH printing also reduces shear stress by allowing the extrusion of low-viscosity bioinks, improving cell viability. The support bath composition

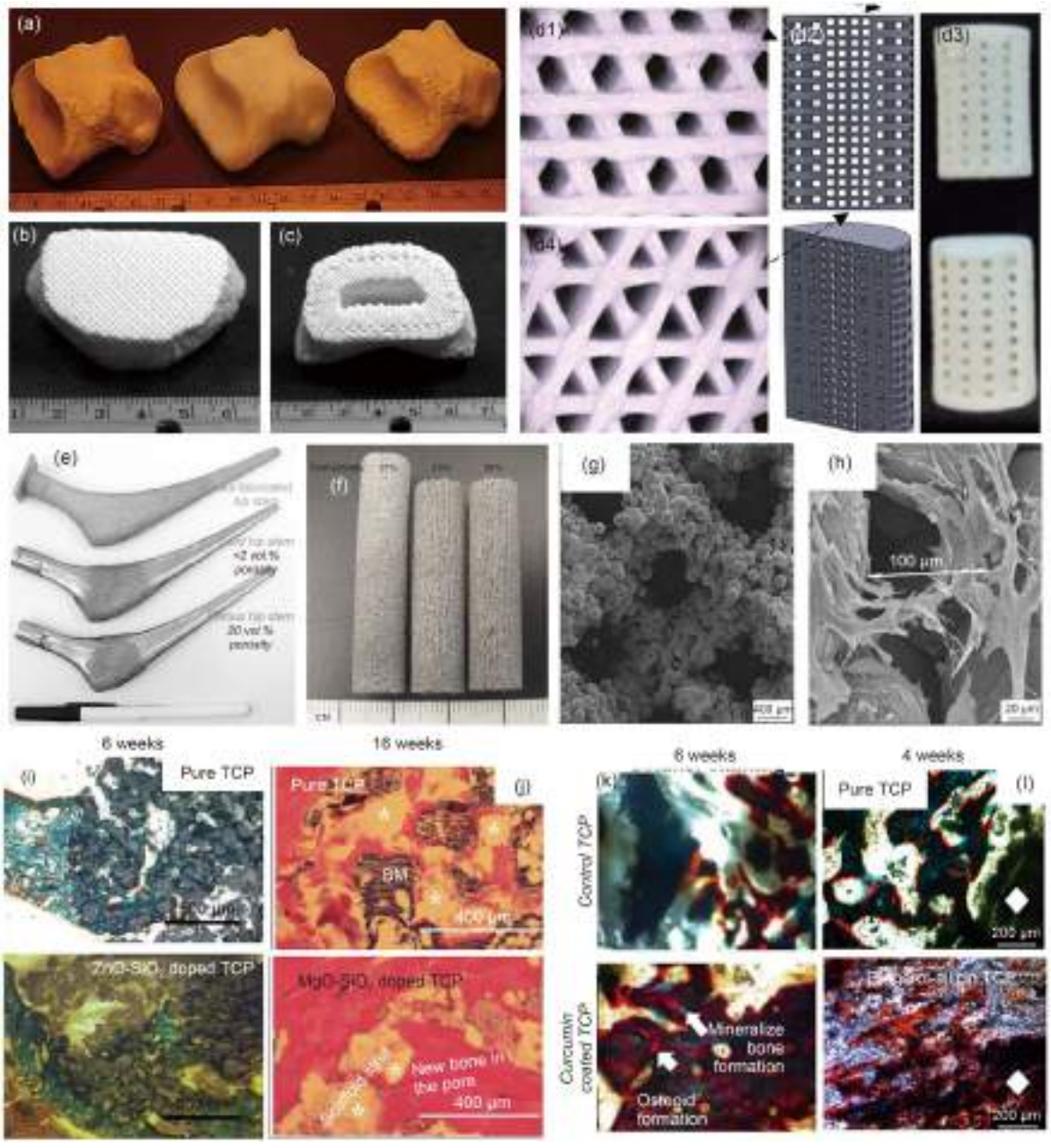

Fig. 30 Additive manufacturing of porous ceramic and metallic scaffolds for bone repair. (a) From CT scan to ceramic bone graft using AM (left: a horse knuckle; middle: a plastic model via FDM; right: a porous patient defect-matched ceramic bone graft printed using FDM). Uniform porosity (b) and gradient porosity (c) patient defect-matched ceramic bone graft. (d1–d4) Various porosity designs for bone grafts made of ceramic-polymer composites. (e) AM porous metal implants made of titanium processed via laser directed energy deposition (DED). (f) Porous metal implants with varying degrees of porosity manufactured via laser DED. (g) Designed porosity titanium implants for enhanced early-stage osseointegration. (h) In vitro studies with human osteoblast cells cultured on laser DED-processed porous titanium implants showing porosity bridging abilities reflecting the early-stage osseointegration possibility. (i) TCP- and ZnO-SiO_2-doped TCP scaffolds using Goldner's trichome showing mineralized and new bone formation after 6 weeks in the rat distal femur model. Implants are shown in gray/brown color with mineralized sections in blue and osteoid formation in orange. (j) H&E-stained images of 3DP TCP and 3DP MgO-SiO_2-doped TCP scaffolds showing new bone formation after 16 weeks in the rat distal femur model. Bone marrow (BM) is shown. The asterisk indicates acellular regions derived from the scaffold. Black—bone marrow, pink/red—new/old bone, yellow—acellular regions derived from the scaffolds. (k) Optical microscopy images of decalcified tissue-implant specimens showing mineralized bone and osteoid formation after 6 weeks of surgery in the rat distal femur model. (l) Gingerol-allicin in bimodal porosity 3D printed scaffolds showing early-stage bone formation with respect to TCP control or osteogenesis in an in vivo rat distal femur model after 4 weeks. For (k, l): modified Masson Goldner trichrome staining (top) and after hematoxylin & eosin (H&E) staining (bottom). (a–c) are reproduced from [4], with permission from the American Ceramic Society; (d1, d4) are reproduced from [95], with permission from Elsevier B.V.; (d2, l) are reproduced from [398], with permission from the American Chemical Society; (d3, j) are reproduced from [400], with permission from the Biomedical Engineering Society; (e) is reproduced from [3], with permission from Acta Materialia Inc.; (f) is reproduced from [388], with permission from Acta Materialia Inc.; (g, h) are reproduced from [395], with permission from Acta Materialia Inc.; (i) is reproduced from [399], with permission from Acta Materialia Inc.; (k) is reproduced from [397], with permission from Elsevier Ltd.

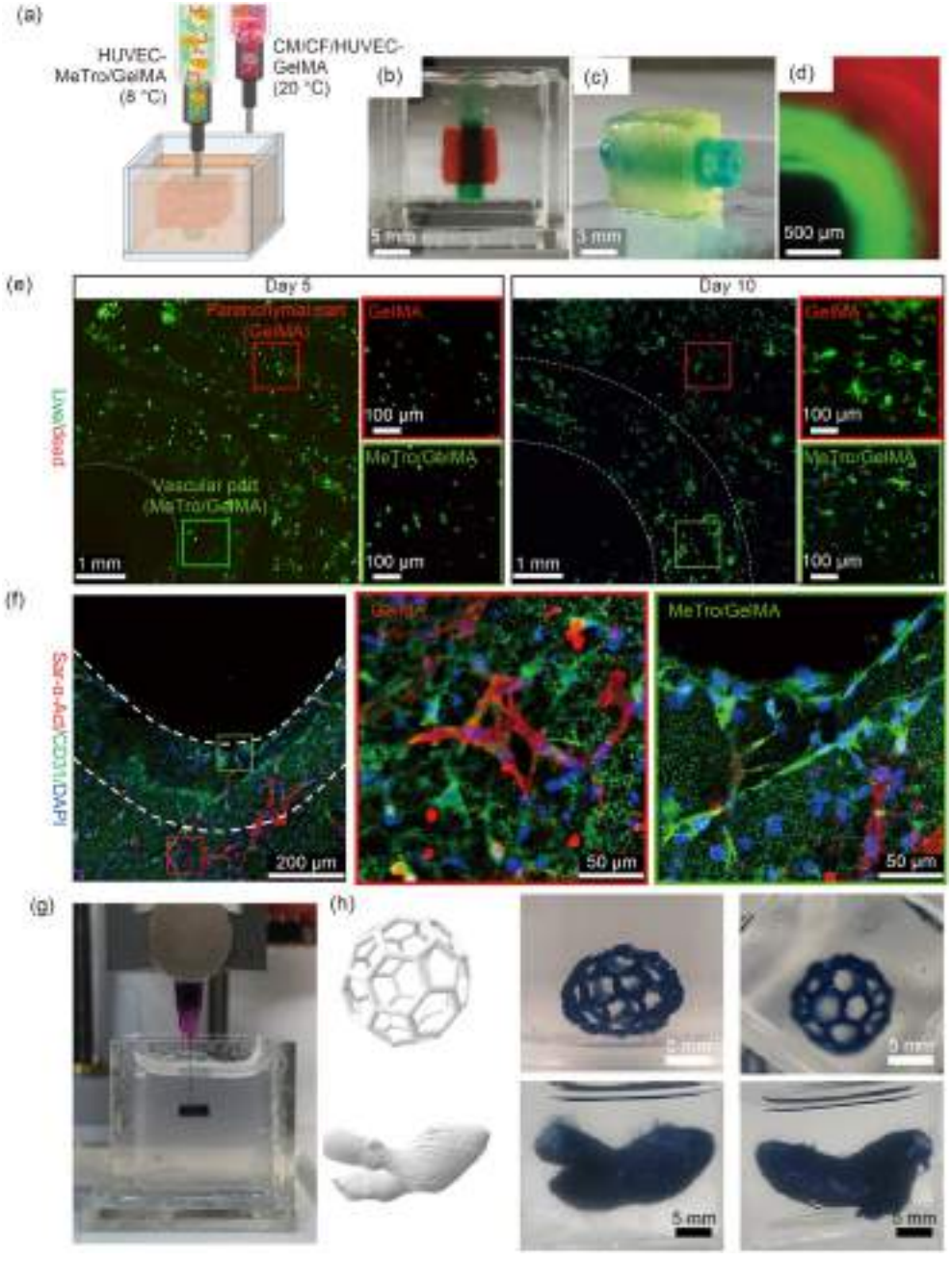

Fig. 31 Embedded 3D bioprinting of soft and elastic tissue. (a) Schematic illustration of 3D bioprinting of vascularized cardiac constructs using cell-laden MeTro/GelMA bioinks. (b) A vascularized cardiac construct immediately after printing within the support bath, and (c) following photocrosslinking and washing steps. (d) Green and red food dyes were incorporated into the MeTro/GelMA and GelMA bioinks, respectively, for visualization purposes. (e) Live/Dead staining of the vascularized cardiac construct on Day 10 post bioprinting. (f) Immunostaining of the vascularized cardiac construct against sarcomeric α-actinin (red), CD31 (green), and DAPI (blue) on Day 10 post bioprinting. Reproduced from [5], with permission from Wiley-VCH GmbH. (g) Conductive GelMA/PEDOT:PSS bioink into the support bath. (h) 3D-printed buckyball structure and left ventricle with the ascending aorta printed using the GelMA/PEDOT:PSS bioink. Reproduced from [405], with permission from the American Chemical Society

can be tuned for specific applications; for example, incorporating calcium ions improved ionic crosslinking of conductive GelMA-based bioinks and enhanced structural resolution [405].

Building upon these advances, the Annabi laboratory is now expanding its bioprinting research toward the development of next-generation biomaterials for extrusion-based 3D bioprinting, with the goal of creating constructs that more closely recapitulate the hierarchical organization of native tissues. Many biological tissues exhibit layered or gradient structures, where each layer supports distinct cell populations and performs specialized physiological functions [406]. To

mimic this complexity, the laboratory is designing multi-material bioinks tailored to the specific microenvironmental needs of individual cell types. A prominent example of this ongoing work is the fabrication of multilayered urethral constructs, where the inner layer is optimized to support urothelial cell growth and barrier formation, while the outer layer is engineered to promote smooth muscle cell growth and contractility. A similar bilayer strategy is being applied to the regeneration of vascular tissues, with bioinks designed to sustain cell functions, thereby recreating the structural and mechanical integration of native vessels.

3.3.2 Hybrid bioinks

Achieving scaffolds that accurately replicate patient-specific anatomy and function requires precise control of geometry, material composition, and biologically responsive features [315, 316]. To meet this need, the Habib laboratory at Rochester Institute of Technology and their collaborators have developed bioinks optimized for fidelity and cytocompatibility to advance high-fidelity, patient-adaptive scaffold manufacturing technologies. They formulated a series of hybrid bioinks composed of alginate, CMC, 2,2,6,6-tetramethyl-1-piperidinyloxy (TEMPO)-mediated nanofibrillated cellulose (TO-NFC), polyethylene glycol diacrylate (PEGDA), and montmorillonite (MMT) nanoclays to enhance the mechanical stability of printed hydrogels [45, 187, 312, 313, 407, 408]. Systematic rheological characterization and filament fusion/collapse tests guided the optimization of this bioink's composition, yielding improved viscoelastic properties for extrusion printing (Figs. 32a and 32b). The optimized bioink supports the fabrication of intricate 3D scaffold geometries with minimal deformation, demonstrating excellent printability and shape fidelity in extrusion-based bioprinting (Fig. 32c). Importantly, cell encapsulation studies have shown that a range of 84%–90% of cells (e.g., BxPC3, HEK 293, Porc1, prostate stem, and hMSCs) remain viable up to 21 days post-bioprinting, indicating a highly cytocompatible environment. This balance of print fidelity and cell viability underscores the hybrid bioink's promise as a robust scaffold material. By mitigating the trade-off between mechanical strength and biocompatibility, this formulation has enabled the fabrication of durable, cell-friendly constructs with reliable shape fidelity.

3.3.3 Yield-stress inks to enable embedded and in-air extrusion printing

YSFs [85] maintain their shape as elastic solids at rest, but flow like liquids when the applied stress is higher than the yield stress. These characteristics can be leveraged to establish a novel and facile technology for the printing of low-viscosity, low-modulus, and slow-solidifying inks in YSF baths, that is, for embedded extrusion printing as well as printing of YSF-based composite inks in air (self-supported printing in air). Different from conventional extrusion printing or DIW processes, YSF-enabled extrusion bioprinting processes decouple the need for in situ rapid solidification during printing, enabling the printing-then-solidification modality. A 3D construct can retain its shape during printing; once the printing process is completed, it is then subjected to a suitable crosslinking mechanism for solidification.

The Huang group at the University of Florida has developed Laponite nanoclay suspensions [411, 412], gellan microgels [413], gelatin microgel-gelatin solution

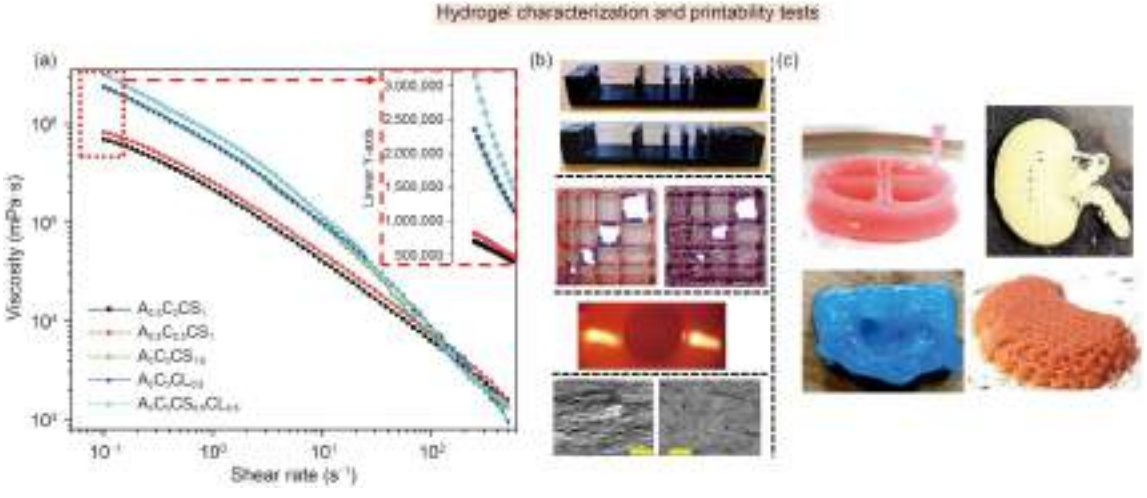

Fig. 32 Rheological and printability characterization of hydrogel bioinks. (a) Hydrogel rheological characterization. (b) Printability and shape fidelity tests, including filament collapse, fusion tests, and scanning electron microscopy (SEM) microstructures. (c) Diverse printed geometries that closely mimic their computer-aided design (CAD) models. Reproduced from [313], with permission from the Society of Manufacturing Engineers; reproduced from [407], licensed under CC BY 4.0; reproduced from [409], licensed under CC BY 4.0; reproduced from [410], with permission from the American Society of Mechanical Engineers

composites [414], and fumed silica suspensions [415] for embedded extrusion printing applications. During printing, the printed structure is stabilized by a YSF support bath that readily flows if an external force higher than its yield stress is applied. Such an external force can be exerted by a moving extrusion nozzle. Once the nozzle moves on, the fluidized support material fills any crevasse in its wake and then returns to its gel-like behavior. This bulk YSF support material successfully holds each printed feature in place if the surface tension and gravitational forces are lower than the yield stress of the support YSF material. After printing is completed, the whole liquid structure is solidified in situ by applying applicable crosslinking mechanisms. Finally, the solidified structure is harvested from the YSF support bath for any further processing as needed.

The group has also developed Laponite nanoclay suspensions [412, 416] and gelatin microgel-gelatin solution composites [417] as YSF materials for self-supported printing-in-air applications. By mixing YSF materials with various hydrogel precursors or living cells, the Huang group has developed various hydrogels or cellular composites with self-supporting capacity, which can be printed into 3D structures directly in air and retain their shapes before crosslinking. After printing is completed, the whole structures are solidified in situ by applying suitable crosslinking stimuli.

3.3.4 PCL/Bioactive borate glass (BBG) composite material for bone scaffold

The Leu group at the Missouri University of Science and Technology has investigated the viability of human adipose stem cells (ASCs) printed on the PCL/BBG scaffold, aiming to create a highly angiogenic 3D environment required for complex and dynamic interactions that govern the cells' behavior in vivo [418]. They have also investigated the viability of ASCs in alginate-gelatin hydrogel printed with or without BBG [419]. The BBG (13–93B3), which was used in their studies, is a highly angiogenic and rapidly dissolving biomaterial, and its physiologically relevant ionic dissolution is known to stimulate cells in vitro and endogenous tissues in vivo. The composite hydrogel was used to suspend ASCs in the bioink. Scaffolds have been investigated in different material compositions, including bioink only, PCL + bioink, and PCL + BBG + bioink, to investigate ASC viability in these various compositions. The viability of ASCs has been further investigated by depositing ASC-laden alginate–gelatin hydrogel between polylactic acid-BBG composite filaments [420], with which to measure the weight loss over time of the composite scaffold, pH change of the surrounding media, and mechanical properties. The assessment results indicated improvement in mechanical properties and glass dissolution, and showed nonuniform cell viability along the scaffold thickness, with lower viability in the bottom region and higher viability in the top layers of the scaffold. To address the challenge of slow degradation of melt-deposited biopolymers in 3D bioprinting, the Leu group developed a solvent-based 3D printing method for fabricating cellularized biopolymer-BBG composite scaffolds for bone repair and other tissue engineering applications [421]. To investigate the effect of pore architecture and porosity on mechanical properties and bone regeneration after implantation, the Leu group has fabricated and compared scaffolds with different architectures (cubic, spherical, x, gyroid, and diamond) at different porosities [422]. Furthermore, they investigated the fabrication of scaffolds with polymer/bioactive glass composites using near-field electrospinning [423] to address the issue of how to incorporate glass particles to achieve a 3D architecture mimicking natural tissues.

4 Physics modeling in biofabrication and biomedical manufacturing

Physics-based modeling, either from the perspective of process dynamics or from the perspective of biomechanics, provides quantitative insights for guiding biofabrication and biomedical manufacturing from empirical and experimental manufacturing toward predictable, controllable, scalable, and safe production. Based on specific objectives, these processes usually integrate complex fluid mechanics, transport kinetics, crosslinking/gelation mechanisms, and cell–material interactions across multiple dimensions and time scales. These mechanistic models are increasingly essential for predicting and optimizing printing fidelity, interpreting failure modes, defining measurable quality attributes, and guiding process and material design. In the U.S., modeling efforts include both process-focused frameworks [424], such as deposition and curing dynamics, stability, and defect formation, and biofocused biophysics models for emergent phenomena that arise after fabrication, such as cell migration, aggregation, and collective mechanics within biofabricated environments.

4.1 Process dynamics modeling

4.1.1 Ink printability study

While bioprinting has been adopted for many biomedical applications, the printability of various bioinks is still largely evaluated based on a trial-and-error approach, hindering the wide adoption of bioprinting. The Huang group at the University of Florida has devoted itself to studying the droplet formation process during dispensing living cell-laden viscoelastic complex fluids and further constructing various phase diagrams to quantify bioink printability. Toward this goal, the Huang group has studied the droplet formation physics underlying various printing processes such

as bubble formation and expansion processes [425, 426] and cell droplet impact processes [427] during LIFT, and proposed hydrodynamic and printability phase diagrams for inkjetting (Fig. 33) [7, 428, 429], LIFT [430–433], and fluid extrusion [434, 435], respectively, using printing conditions and material property-related nondimensional numbers. The Huang group has further studied the upflow and its mitigation [436] and the deposition volume compensation strategy for enhanced printing fidelity [437] during embedded printing.

4.1.2 Modeling and connecting material properties and bioprinting outcomes

At the University of Maine, the Khoda group's research in biofabrication and biomedical manufacturing has focused on the codesign of geometry, materials, and manufacturing processes to enable scalable, high-fidelity fabrication of living and bioactive systems. Their overarching objective is to establish manufacturing-science-driven frameworks that connect intrinsic material properties (e.g., rheology, gelation, and transport) with extrinsic biological outcomes (e.g., cell viability, proliferation, and structural function).

One thrust of this work has been the establishment of a design-driven scaffold architecture for extrusion-based bioprinting, emphasizing continuous deposition, interconnected porosity, and functionally graded internal features. By integrating computer-aided design (CAD)-based slicing, deposition path planning, and topology-aware infill strategies, this research has demonstrated how heterogeneous pore networks can be fabricated reproducibly while preserving mechanical integrity and nutrient transport [438–441]. These contributions have advanced the transition from process-driven to design-centric biofabrication, enabling physiologically relevant scaffold architectures beyond uniform lattices (Fig. 34a).

Building on this architectural framework, the laboratory has developed cellulose-derived and hybrid hydrogel bioinks optimized for extrusion bioprinting [313, 407]. Using alginate, CMC, nanocellulose, and TO-NFC, they demonstrated that low-solid-content (<8%) bioinks can achieve high shape fidelity while maintaining long-term cell viability (approximately 86%–91%). Systematic rheological characterization, filament fusion and collapse metrics, and printability indices were introduced to quantitatively link bioink composition with manufacturability and post-print structural stability [187]. These studies have established cellulose-based bioinks as scalable, biodegradable alternatives for tissue scaffolding and living material fabrication (Fig. 34b).

A key contribution of this body of work is the analytical coupling of nozzle-scale rheology with cell survivability in extrusion bioprinting. By modeling shear stress as a function of viscosity, pressure, and nozzle diameter, they identified critical stress thresholds governing spatial patterns of cell viability within extruded filaments [45]. This framework has provided predictive guidance for balancing printability and biocompatibility across multiple mammalian cell lines, transforming bioink optimization from empirical tuning to a physics-informed design process (Fig. 34c).

Most recently, the Khoda laboratory introduced a machine-learning-enabled framework for bioink precursor optimization,

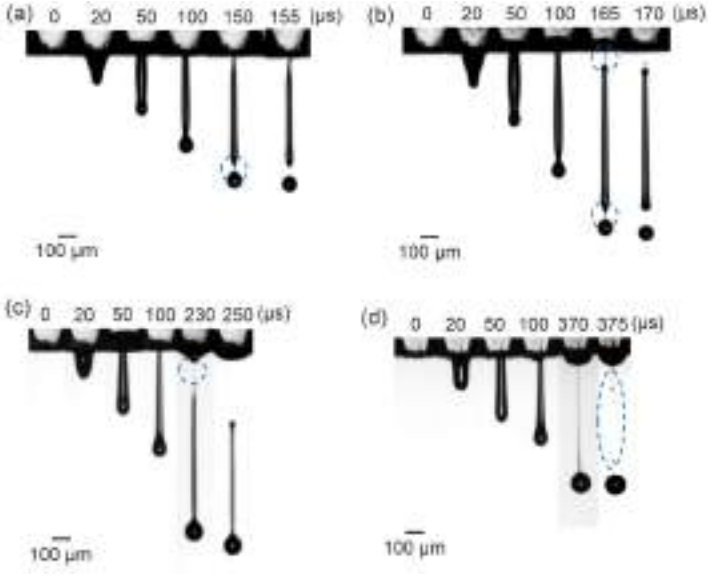

Fig. 33 Four pinch-off types during drop-on-demand (DOD) printing: (a) front pinching; (b) hybrid pinching; (c) exit pinching; (d) middle pinching. The sodium alginate concentration and excitation voltage are listed as follows: (a) 0.30% and 35 V; (b) 0.30% and 42 V; (c) 1.00% and 50 V; (d) 2.00% and 50 V. Each pinch-off location is marked using a dashed circle. Reproduced from [7], with permission from the American Chemical Society

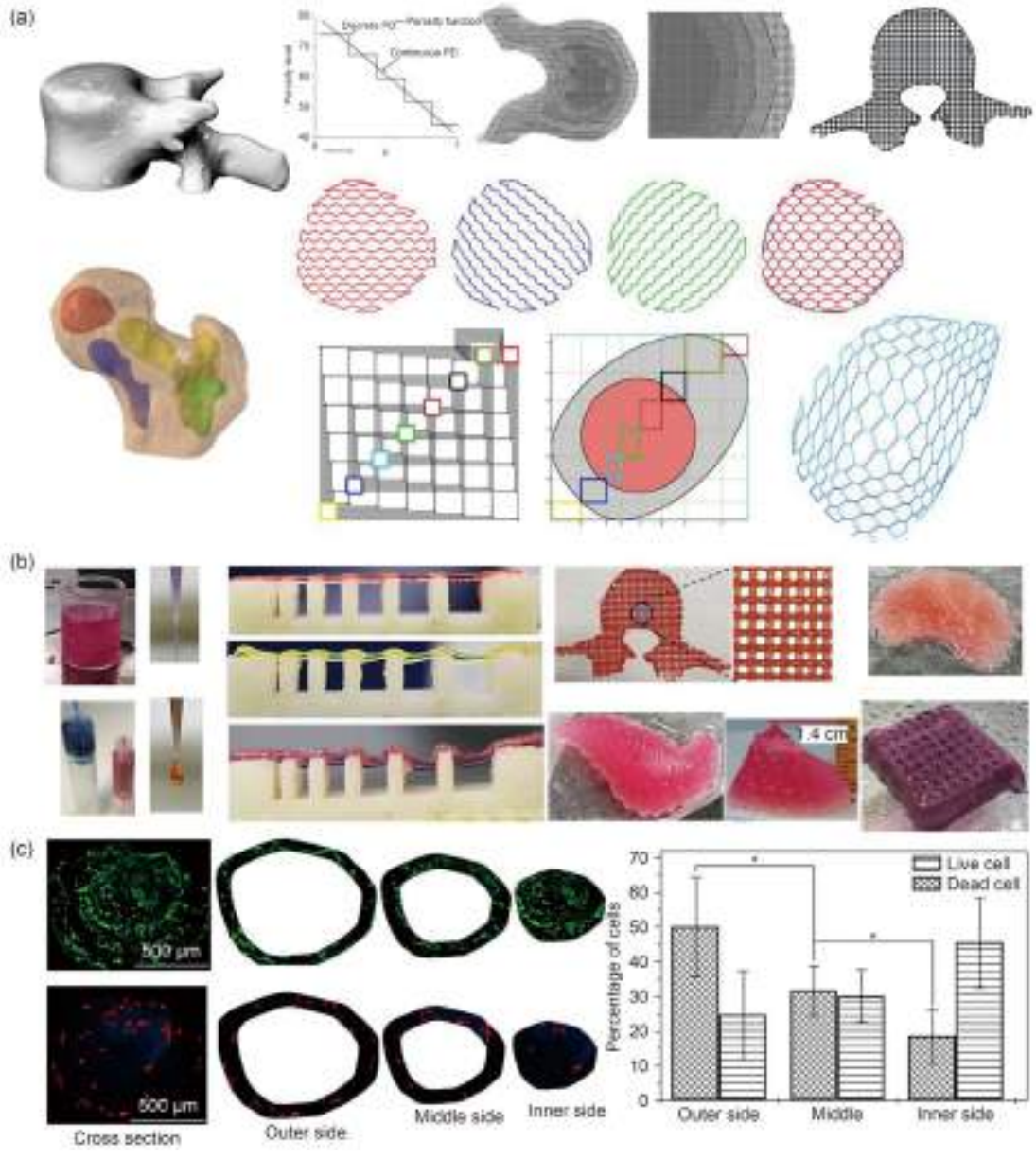

Fig. 34 Modeling-assisted scaffold design, material optimization, and post-print biological evaluation. (a) Computer-aided design-driven scaffold architecture. (b) Optimizing printable natural hydrogel material for extrusion-based bioprinting. (c) Post-printing analysis for cell viability. Reproduced from [45], with permission from the American Society of Mechanical Engineers; reproduced from [187], with permission from the Society of Manufacturing Engineers; reproduced from [313], with permission from the Society of Manufacturing Engineers; reproduced from [407], license under CC BY 4.0; reproduced from [438], with permission from the American Society of Mechanical Engineers; reproduced from [440], with permission from Elsevier Ltd.; reproduced from [444], under exclusive license to Springer Nature Singapore Pte Ltd.

addressing a critical bottleneck in biomanufacturing: the exhaustive experimental search required to identify viable multi-material compositions [442]. In this work, they developed a constraint-based Bayesian optimization approach to predict and optimize the viscosity of heterogeneous bioink precursors composed of alginate, CMC, and TO-NFC using sparse experimental data. A novel mask-based constraint strategy has been introduced to incorporate domain knowledge—such as solid-content limits and cell-viability thresholds—directly into the optimization loop. This approach enables decoupling intrinsic material properties (e.g., viscosity) from extrinsic biological constraints while systematically shrinking the feasible design space. The resulting surrogate model has reduced the experimental workload by orders of magnitude while accurately identifying compositions that support both printability and cell viability, establishing a data-driven paradigm for intelligent bioink design. In addition, Dr. Khoda's laboratory

has extended these biofabrication principles to green bioprinting and microalgae-based biomanufacturing, integrating photosynthetic living cells into 3D-bioprinted hydrogel scaffolds [443].

Collectively, this research has helped to advance biofabrication as a manufacturing science, integrating digital design, rheology, and machine learning to enable reproducible, scalable, and biologically functional biomanufacturing platforms for tissue engineering and sustainable living materials [444].

4.1.3 Process dynamics modeling during extrusion bioprinting

With the multitude of parameters that must be specified for any biofabrication and biomedical manufacturing process, physics-based modeling offers the opportunity to efficiently realize optimized print fidelity without time-intensive trial-and-error experimentation. The Heilshorn laboratory at Stanford University has developed numerous process dynamics modeling works for bioprinting processes. For optimization of embedded extrusion bioprinting processes, models that consider the time-dependent properties of the entire system are essential. As a first requirement, the ink must yield to enable extrusion. A number of traditional polymer physics models can be used to manipulate ink parameters, such as polymer molecular weight and crosslink density, to create an injectable material [42]. An alternative approach is to diffuse catalysts and/or crosslinking reactants into (or out of) the ink to temporarily alter the rheological properties of the ink [43]. This strategy of "diffusion-enabled bioprinting" allows for two distinct sets of rheological parameters to be optimized: one set for the fabrication process and a second set for optimal biological interactions [44]. By measuring and modeling the reaction and diffusion rate constants, the time evolution of the ink rheology and the final viscoelastic scaffold properties can be accurately predicted [445]. In addition to modulating the ink rheology, diffusion-enabled bioprinting can be used to pattern the final scaffold geometry [446]. This is achieved by modulating the diffusivity of the support bath to control the reaction-diffusion time of small molecules and crosslink initiators. This process is particularly adept at constructing cell-laden, perfusable networks with complex, branched geometries that can be accurately predesigned with finite element models (Fig. 35a) [447]. Currently, new models are being developed that take into account the effects of shear-dependent ink viscosity (Fig. 35b). For example, depending on the rate of ink extrusion, the ink viscosity can be designed to either promote or prevent local mixing with the support bath, which can be predictably modeled to create scaffolds with microscale porosity for enhanced cell spreading [448]. Modulation of the ink extrusion rate can also be used to predictably align embedded collagen fibers within printed filaments [449]. Importantly, modeling allowed for the accurate prediction and fabrication of printed scaffold regions with alternating fiber orientations (both parallel and perpendicular to the printing direction), resulting in control over the orientation of adherent cells. Looking ahead, advanced methods to characterize and model real-time scaffold viscoelasticity, including scaffold changes caused by cell-imposed forces [450], will enable more advanced tissue-like structures.

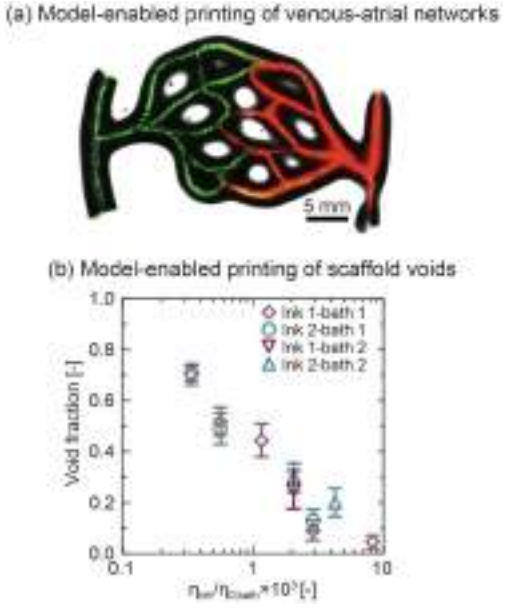

Fig. 35 Modeling-guided design strategies in biofabrication. (a) Finite element modeling accurately predicts the final structure of perfusable venous-atrial-like networks fabricated using the GUIDE-3DP "diffusion out" strategy (reproduced from [447], with permission from IOP Publishing Ltd.). (b) The log ratio of ink to support bath viscosity scales linearly with the scaffold void fraction across four different ink–bath formulations. This simple relationship allows for the design of microstructure within a printed scaffold to improve cell spreading (reproduced from [448], with permission from Wiley-VCH GmbH)

4.1.4 Coaxial extrusion modeling

In native tissues, capillary networks sustain oxygenation and nutrient delivery, whereas bioprinted constructs lacking vascularization suffer necrosis due to diffusion limitations. The inability to maintain large-scale constructs without adequate vascularization has intensified the demand for engineered blood vessels [451]. Although 3D bioprinting can generate complex and sophisticated structures, it remains inefficient in producing hollow vascular channels [452]. Coaxial extrusion provides an effective method for fabricating tubular structures with internal lumens that function as vascular conduits [453]. In this technique, two or more concentric nozzles are employed: the outer nozzle extrudes

matrix material to form the vascular wall, while the inner nozzle delivers crosslinking agents or bioinks to deposit cells onto the tubular scaffold. Research in coaxial extrusion generally falls into two domains [454]: optimization of the extrusion process to achieve precise dimensions and development of bioinks to enhance the functionality of vascular constructs, including mechanical integrity, cell viability, and perfusibility [455]. The Chen group at Washington State University has investigated the flow behavior in coaxial extrusion, which is more complex than that in single-nozzle extrusion and depends on parameters such as flow rate, extrusion speed, material viscosity, and the ratio between inner and outer nozzle outputs [46]. They have also studied the modulation effect of the flow rate ratio between the inner and outer nozzles on the wall thickness of printed tubular structures [456].

4.2 Biomechanical investigation and modeling

4.2.1 Process-induced cell injury

Excessive process-induced damage has been found to cause cell injury and even death during direct bioprinting, and the cell viability and cell injury of post-printing cells have been of concern. The understanding of process-induced cell injury during bioprinting will lead to its safe and efficient implementation, thus enabling its wide application for organ printing and rapid prototyping of cell-based products. While necrotic cells can be identified using dye inclusion/exclusion assays to assess membrane integrity, apoptotic cells cannot be detected by routine inclusion/exclusion cell viability assays and have been largely ignored in studies to date. To mitigate printing-induced cell injury, a better understanding of cellular responses is critical to the success of printing processes by differentiating between post-printing apoptotic and necrotic cells. For the robust implementation of bioprinting, the Huang group at the University of Florida has estimated the cell mechanical profile experienced by living cells during the cell droplet formation [425] and cell droplet landing [427] processes in LIFT, investigated the post-printing cell viability [457], and modeled the cell membrane stability under external normal pressure [48].

In addition, the Pei laboratory at Texas A&M University has begun using 3D printing to recreate extreme environments to study the responses of human cells, particularly bronchial cells, to these environments [458, 459]. With an interdisciplinary team, the Pei laboratory aims to use their manufacturing background to help evaluate and improve the health and performance of flight pilots, as well as to prepare for space travel.

4.2.2 Cell-level research for understanding bioprinting-induced mechanotransduction

The role of mechanotransduction—the process by which cells convert physical forces into biochemical signals—and the subtle effects of shear stress on long-term cellular fate remain poorly characterized. Since mechanical cues govern crucial processes such as embryonic development and wound healing, understanding these forces is paramount for safe clinical translation of bioprinting. The work of Dupont identified the transcriptional coactivators Yes-associated protein (YAP) and transcriptional coactivator with PDZ-binding motif (TAZ) as the primary rheostats of the cell [460]. These factors respond to the mechanical properties of the ECM and fluid flow.

In stiff/stressed environments, YAP/TAZ translocate to the nucleus, activating pro-proliferative and anti-apoptotic genes (e.g., CTGF, CYR61); while in soft/protected environments, they remain sequestered in the cytoplasm, maintaining homeostatic cellular states. In the context of cancer progression, aberrant nuclear localization of YAP/TAZ has been definitively linked to oncogenic transformation and the acquisition of chemoresistance. This raises a provocative question for the bioprinting community: does the transient but intense shear stress of the printing nozzle inadvertently "program" cells toward a pre-malignant phenotype?

Building upon the mechanobiological concerns of bioprinting, work [461] from the Boland group at the University of Texas at El Paso provides a stark empirical warning regarding the molecular consequences of the printing process. Utilizing RNA-seq and phosphoproteomic analysis, they demonstrated that thermal inkjet bioprinting (TIB) acts as a potent mechanical and thermal stimulus that significantly alters the transcriptomic profile of human breast cancer cells. The Boland group's findings have revealed "massive" phosphorylation of critical oncogenic pathways, specifically triggering the activation of proteins associated with multidrug resistance (MDR) and survival.

Crucially, RNA-seq data have identified the upregulation of long noncoding RNAs such as lung cancer associated transcript 1 (*LUCAT1*), along with inflammatory and survival genes such as interleukin-6 (*IL6*) and C-C motif chemokine ligand 26 (*CCL26*). These molecular shifts are not merely transient; they result in a "primed" cellular state where printed cells exhibit increased resistance to standard chemotherapeutic agents and radiation compared to nonprinted controls. This research underscores that the bioprinting process itself can induce a phenotypic shift—characterized by them as a stress-induced "defense mode"—which necessitates a more rigorous evaluation of how biofabrication parameters might inadvertently promote cancer progression or therapeutic evasion in engineered tissues.

The mechanical rigors of TIB induce a spectrum of cellular alterations, ranging from acute transcriptomic shifts to enduring modifications of the epigenetic landscape [49]. Their immunocytochemical longitudinal study (3 to 72 h post-print) revealed a distinct, time-dependent divergence in the localization of the mechanosensitive cofactors YAP and TAZ. While TIB cells initially showed decreased YAP expression at 3 h, a significant "rebound" nuclear surge occurred by 48 h (Fig. 36a). Conversely, TAZ has exhibited consistently elevated nuclear occupancy in printed cells across all time points, peaking between 24 h and 48 h (Fig. 36b).

Intriguingly, this nuclear influx appears to be decoupled from the canonical NUAK2 signaling pathway, which typically governs YAP/TAZ shuttling. The persistence of nuclear YAP, despite phosphorylation, suggests that TIB-induced translocation bypasses standard regulatory checkpoints. This "leakage" into the nucleus is likely driven by physical compromise of the nuclear barrier; the Boland group has observed a significant increase in Lamin A/C at 3 h post-TIB—a hallmark of compensatory mechanical reinforcement—alongside visible nuclear wrinkling in printed populations. These morphological deformities suggest that the printing process physically "squeezes" or stretches nuclear pores, allowing for noncanonical protein entry.

To counter this mechanical bypass, the Boland group has integrated YAP antibodies directly into the bioink as a competitive sequestration strategy. Their findings demonstrated that these antibodies successfully traverse the cell membrane into the cytosol but are size-excluded from the nucleus (Fig. 36d). Once intracellular, the antibodies act as cytosolic anchors, binding to and sequestering YAP proteins. By physically impeding the transport of YAP across the stressed nuclear envelope, this "immuno-bioink" approach effectively blocks the downstream activation of oncogenic pathways, offering a viable method for maintaining cellular homeostasis post-fabrication.

In conclusion, the evolution of bioprinting from a structural fabrication tool to a viable clinical platform depends entirely on the ability to govern the mechanobiological dialog between the printing process and the cell. As evidenced by the noncanonical nuclear translocation of YAP/TAZ and the subsequent risk of transcriptomic reprogramming, sublethal printing stress represents a "silent" barrier to safe tissue engineering and must be considered when designing bioinks to mitigate this response.

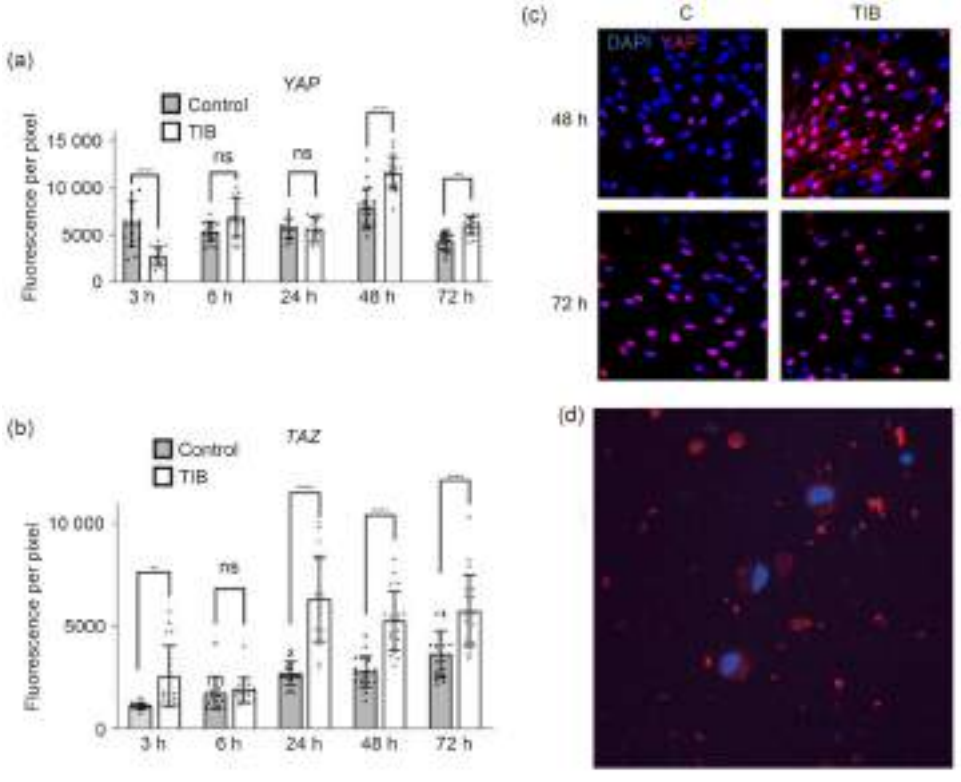

Fig. 36 Nuclear expression of the transcription factors YAP/TAZ in bioprinted vs. control cells. (a) Averaged fluorescence per pixel of YAP in bioprinted and control cells post-TIB. (b) Averaged fluorescence per pixel of TAZ in bioprinted and control cells post-TIB. (c) Representative fluorescent images of cell nuclei at 48 and 72 h post-printing. Images were taken at 40× magnification and created in ImageJ. Increased YAP nuclear expression was observed at 48 and 72 h for TIB cells. (d) YAP immunoreactivity in the nucleus in TIB cells at 1 h post-printing. The image shows no YAP in the nucleus of TIB cells

4.2.3 Physics of cell migration, aggregation, and collective mechanics in 3D embedded bioprinting materials

Embedded 3D printing eliminates the need for self-supporting inks, providing stability while printing with soft materials and complex fluids including colloids, living cells, polymer solutions, and silicone [424]. The Angelini laboratory at the University of Florida has developed a diversity of embedding media made from packed microscopic hydrogel particles (microgels) that serve as both bioprinting support medium and a 3D culture environment (Figs. 37a and 37b). Aqueous microgels can be synthesized from charged or uncharged polymers and swollen in liquid growth media, enabling biomanufacturing across scales down to the single-cell level [462, 463]. Oily microgels have been used to 3D-print droplet arrays for encapsulating and sequencing individual extracellular vesicles [464]. Microgels' use in embedded printing applications has led to a thorough investigation of their yielding and flow behaviors under various solvent conditions [462, 465]. However, the complexity of a cell's response to its physical microenvironment creates the need to study cell behavior in embedded printing materials and related technologies such as cell-laden injectable biomaterials [466].

The physical properties of microgel embedding media have led to novel mechanisms of cell migration and aggregation in biofabrication contexts (Figs. 37c and 37g). For example, T cells dispersed in microgel media use pores to migrate without rearranging microgels, traversing smaller pores more quickly (Figs. 37d and 37e) [467]. The porosity of packed microgels also facilitates molecular transport, as found with albumin secreted by 3D printed liver discoids [468]. Both migration and molecular transport play roles in 3D-printed immunotherapy models of glioblastoma where T cells migrate in response to signals diffusing from the tumoroid (Fig. 37g) [469]. Microgel reconfiguration, by contrast, is central to the aggregation of cohesive nonmigratory cells, where two aggregation transitions are found: dispersed cells form clusters at volume fractions above 4%, and a system-spanning percolated cell network emerges at

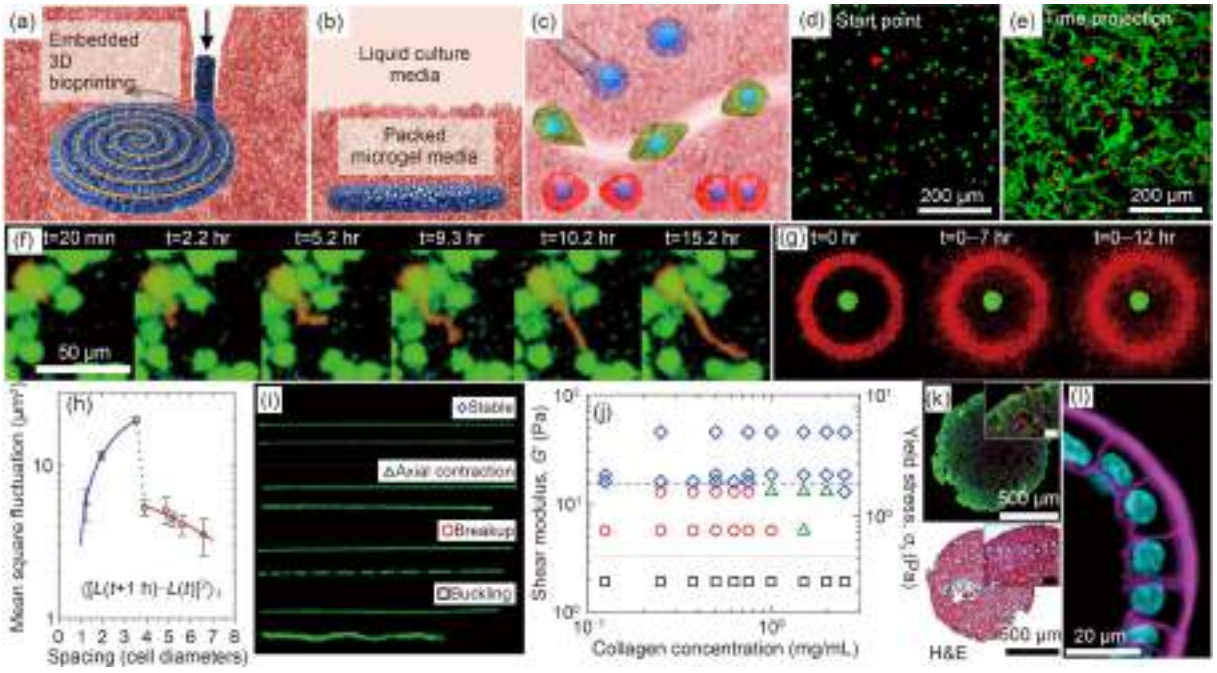

Fig. 37 Cell migration, aggregation, and collective mechanics in packed microgel media. (a) Embedded 3D printing enables soft materials including cells to be directly printed into packed microgel support materials. (b) The packed microgel media serves as a printing support material and 3D culture environment. (c) The reconfigurability and porous structure of microgel packs enable single-cell manipulation, migration, and aggregation. (d, e) T cells migrate through existing pores without rearranging the microgels. (f) MCF10A cells extend long filopodia, reaching through the microgel media and contacting neighboring cells. (g) In a 3D bioprinted immunotherapy model of glioblastoma, tumor reactive T cells migrate and respond to the nearby tumoroid. (h) Cell length, L, fluctuates dramatically in time, t, and exhibits a strong dependence on the average cell–cell spacing. (i) 3D bioprinted "microbeams" made from collagen filled with contractile cells exhibit instabilities controlled by their composition and the packing density of the embedding microgel medium (top image in each group: t=0; bottom image in each group: t=24 h). (j) A stability diagram determined from beams made with different collagen concentrations embedded in microgel media prepared at different packing densities. (k) Self-compaction in 3D bioprinted human liver tissue model correlates with function. (l) Glandular acini develop normally in packed microgel media. (a, b, k) are reproduced from [472], with permission from Elsevier B.V.; (d, e) are reproduced from [467], with permission from IOP Publishing Ltd.; (f, h) are reproduced from [471], with permission from the American Chemical Society; (g) is reproduced from [469], with permission from Elsevier B.V.; (i, j) are reproduced from [47], licensed under CC BY 4.0; (l) is reproduced from [463], with permission from the American Chemical Society

25% [470]. Here, both transition boundaries can be shifted by microgel yield stress and cell cohesiveness. The clustering transition is also set by the amplitude of fluctuations in cell length that overcome physical barriers created by microgels. Such fluctuations were found to depend on cell proximity, reaching a maximum when the average cell–cell surface spacing was approximately 3.5 cell lengths (Fig. 37h) [471].

The roles of cell migration and aggregation are lessened when 3D printing continuously structured cell populations, where collective mechanical behaviors dominate. For example, living "microbeams" made from collagen networks filled with contractile cells can exhibit mechanical instabilities depending on their composition and the yield stress of the embedding material (Figs. 37i and 37j). The cell-driven instabilities include buckling, failure, and axial contraction [47]. Stable self-compaction was linked to improved function in 3D-printed human liver discoids, measured through liver marker secretion, gene expression, and drug metabolism (Fig. 37k) [472]. The yield-stress threshold for mechanical stability is very low—less than approximately 2 Pa—reducing constraints on potential expansion of mechanically stable tissues. Indeed, within such materials, spheroid expansion was measured [471] and growing glandular acini appeared to develop normally (Fig. 37l) [463].

Over approximately 100 years, countless careful microscopic investigations have built understanding of cell mechanics on 2D surfaces [473]. Thus, while recent work has uncovered several new 3D mechanical behaviors in microgel media, researchers are just beginning to understand the physics of cell migration, aggregation, and collective mechanics in new engineering contexts such as embedded bioprinting materials.

5 Applications

Innovations in the manufacturing process, materials development, and process modeling lay the foundation for translating technological advances into anatomically precise and biological function-relevant applications [75]. These applications not only play a role in evaluating the performance of laboratory-created constructions but also demonstrate measurable progress and impact in biofabrication and biomedical manufacturing. In the U.S., research teams have achieved remarkable progress in application-driven research, which increasingly forms a reverse design logic that starts from clinical or experimental requirements and then systematically optimizes fabrication strategy, material system, and physics-informed process designs. This section highlights representative U.S. application frontiers across engineered tissue models as in vitro platforms for disease modeling and therapeutic testing, engineered tissue constructs for in vivo use, and clinical and commercial translational successes, illustrating how the field is moving from laboratory-scale proof-of-concept constructs toward reproducible, scalable, and clinically translational biomedical products and systems.

5.1 Engineered tissue models as in vitro platforms

Engineered in vitro tissue models are becoming a major translational module for biofabrication by providing human-relevant platforms with controlled architecture, perfusion, and quantitative functional readouts, helping bridge gaps between 2D culture and animal studies. In the U.S., progress is propelled by the convergence of bioprinting, microfluidics, and stem-cell biology, alongside imaging-enabled and computation-enabled patient specificity. In this section, select developments in the biofabrication and biomanufacturing of cardiac models, bone models, neural models, vascular models, breast cancer models, and other in vitro models are highlighted. For example, Vunjak-Novakovic's group at Columbia University developed iPSC-derived cardiac tissues with electromechanical conditioning and multiorgan microphysiological systems connected by vascular channels to capture organ crosstalk [52, 73]. The Serpooshan-Bauser group at Emory University has bioprinted perfusable, anatomically faithful cardiovascular replicas to model congenital heart disease and related vascular pathology [366, 474]. Beyond the heart, the Bertassoni laboratory's work on mineralized, cell-laden hydrogels and precision patterning at Oregon Health and Science University has enabled bone-relevant hierarchy and multicellular complexity [475], while the Ning group at Cleveland State University [55, 476] and the Kamm group at Massachusetts Institute of Technology [477–483] have advanced embedded and microvascularized cancer and barrier platforms to interrogate tumor microenvironments, metastasis, and blood–brain barrier transport. Other efforts, including embedded tumor organoids [59] and tunable ECM architectures that guide cell behavior [484], illustrate a shift toward standardizable, functionally validated in vitro models suitable for mechanistic discovery, therapeutic screening, and personalized medicine. Beyond the in vitro platforms highlighted in this section, there are also some other researchers' work that is indispensable in this field. For example, Skardal's laboratory, now at the Ohio State University, developed an integrated three-tissue organ-on-a-chip platform that couples bioprinted liver, heart, and lung tissues in a shared perfusion loop to study interorgan drug responses, illustrating how biofabrication can enable multi-tissue in vitro physiology [485]. The Raman group, now at Massachusetts Institute of Technology, has helped establish biohybrid robotics by coupling engineered skeletal muscle actuators with 3D-printed flexible skeletons, demonstrating optogenetically controlled biological machines that connect tissue engineering

with responsive soft robotic systems [486]. The Butcher group at Cornell University developed rapid 3D printing/photocrosslinking strategies for anatomically accurate and mechanically heterogeneous aortic valve scaffolds, helping define biofabrication routes for structurally complex cardiovascular tissues [487].

5.1.1 Cardiac models

Cardiac tissues are an area of intense research within TERM, representing an environment with enormous implications for human outcomes in both healthy and diseased states, but also one that requires conditions for mature tissue development that are difficult to recreate in vitro. Work included within this section highlights some key developments regarding approaches that researchers in the U.S. have taken for in vitro cardiac model development, recreating functional tissue.

5.1.1.1 Multi-organ microfluidic devices to recreate complex tissue niches

The Vunjak-Novakovic group seeks to address TERM needs with a special focus on utilizing stem cells and organ-on-a-chip technology to recreate human physiology across different scales, for both modeling and personalized medicine applications. They researched the development of iPSC-derived cardiac tissue showing mature markers, accomplished in only 4 weeks of culture, using a specialized bioreactor designed to provide electromechanical stimulation to early-stage iPSC-derived cardiomyocytes (Fig. 38a) [52, 488]. The fabricated bioreactor, using an increasing electromechanical stimulation frequency, has been able to create tissue that did not have mature electrical mechanical coupling, but did exhibit a positive force–frequency relationship, as well as adult-like mitochondrial density, sarcomere length, and ultrastructure, which are all key metrics in mature cardiac tissue. This approach to culturing mature-marker cardiac tissue has further been used to study more complex cell systems, such as the effect of macrophages on tissue contractile force [489], as well as for personalized medicine, simulating cardiomyopathy using iPSCs derived from patients [490].

Work on accurate cardiac tissue culture has been further expanded to be used in a multi-organ microfluidic device with compartments for liver, bone, and skin cultures in addition to a heart compartment, linked by a vascular channel to allow for organ crosstalk (Fig. 38b) [73]. Each of these organ compartments could maintain its respective phenotypes for over 4 weeks of culture within the platform (Fig. 38c) and possessed a high degree of overlap of expressed genes compared to available data from adult organs (Fig. 38d1) and had expression of proteins of particular interest for their respective tissues (Fig. 38d2). Furthermore, these organ recreations were able to exhibit pharmacokinetic

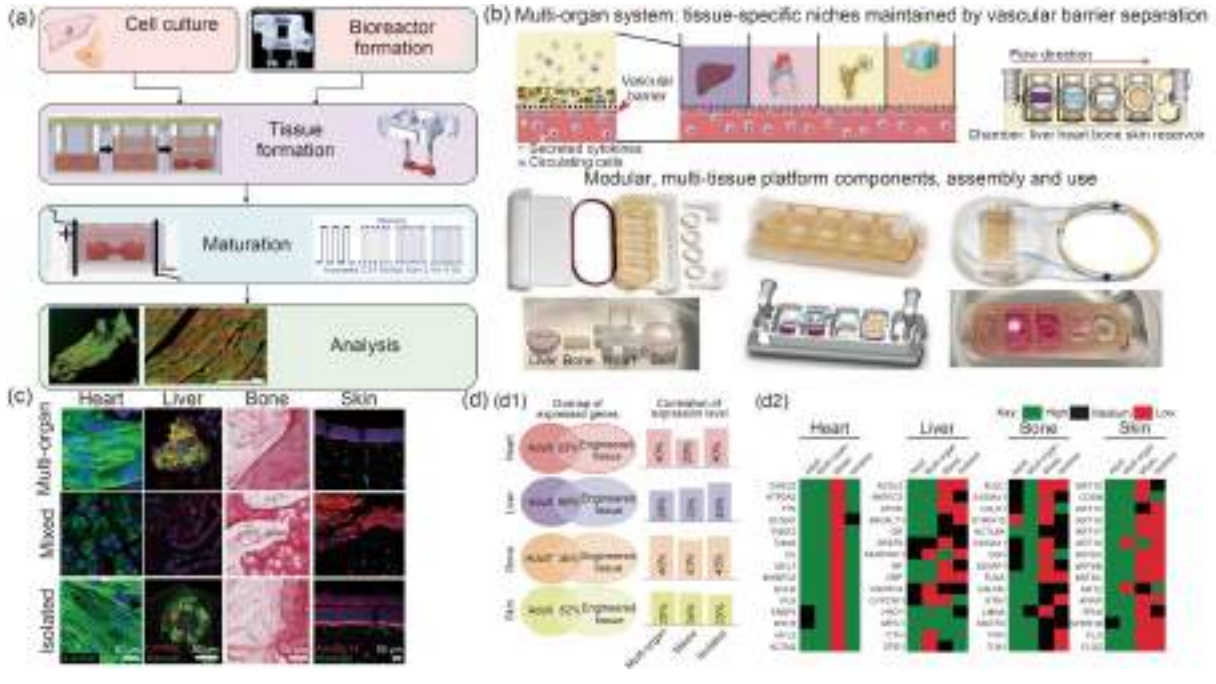

Fig. 38 iPSC cardiac tissue engineering and incorporation into a matured-tissue multi-organ chip. (a) Approach for culture and maturation of iPSC-derived cardiac tissue within a bioreactor designed for electromechanical stimulation (reproduced from [488], under exclusive licence to Springer Nature Limited). (b) Schematic detailing the organization of the multi-tissue chip used to culture liver, heart, bone, and skin niches, linked by a channel with a vascular barrier. (c) Representative immunofluorescence staining of each organ compartment. (d) Gene expression of each investigated organ, showing overlap of expressed genes with available adult datasets (d1) and presence of proteins of specific interest for each organ (d2). Reproduced from [73], under exclusive licence to Springer Nature Limited

and pharmacodynamic trends resembling what is seen in vivo in response to the administration of doxorubicin. A modified version of this bioreactor platform has been utilized to explore key organ responses to both acute [491, 492] and protracted [492] neutron radiation, in order to simulate and mitigate the impact of radiation on astronauts during space travel.

Both in terms of progress made in recreating in vivo behavior and applying this progress to advance medical research, this group works at the cutting edge of iPSC-based biofabrication.

5.1.1.2 3D bioprinted platforms for modeling heart development and congenital heart disease

Congenital heart disease (CHD) remains the most common cause of birth-related mortality, arising from complex disruptions in cardiac morphogenesis. Understanding these processes requires experimental models that accurately recapitulate the dynamic and multicellular architecture of the developing human heart [366, 493–495]. The Serpooshan-Bauser group, now at UTHealth Houston, has integrated 3D bioprinting, patient-specific iPSC technologies, and perfusion bioreactor systems to engineer next-generation in vitro systems for modeling heart development and congenital cardiovascular disorders (Fig. 39) [51, 366, 367, 474, 496–498].

This laboratory's research has introduced human iPSC-derived, bioprinted constructs that emulate early embryonic heart tube formation [366, 367]. Using optimized GelMA-based hydrogels and DLP bioprinting, they fabricated perfusable, chamber-like microtissues composed of cardiomyocytes, endocardial, and fibroblast lineages arranged in physiologically relevant patterns. These embryonic heart tube models demonstrate synchronized contraction, lumen formation, and mechano-responsive gene expression (e.g., *KLF2*, *KLF4*, *ITGB5*), recapitulating biomechanical signaling central to heart morphogenesis [367]. Integration of microfluidic perfusion bioreactors enables controlled application of shear stress, driving maturation of endocardial–myocardial interfaces and promoting tissue alignment and metabolic switching toward oxidative phosphorylation.

Building on this developmental framework, disease-specific bioprinted models have been engineered using patient-derived iPSCs from children with hypoplastic left heart syndrome (HLHS) and other CHDs [51, 366, 367, 474, 496–498]. These constructs exhibit disease-linked phenotypes, including altered calcium handling and proliferation, and reduced contractility, mirroring clinical observations. High-resolution photon-counting computed tomography (PCCT) and micro-CT imaging allow nondestructive monitoring of bioprinted tissue structure, degradation, lumen patency, and perfusion [499, 500], while single-cell transcriptomic and immunohistochemical analyses elucidate molecular dysregulation at cell-type resolution [367, 497].

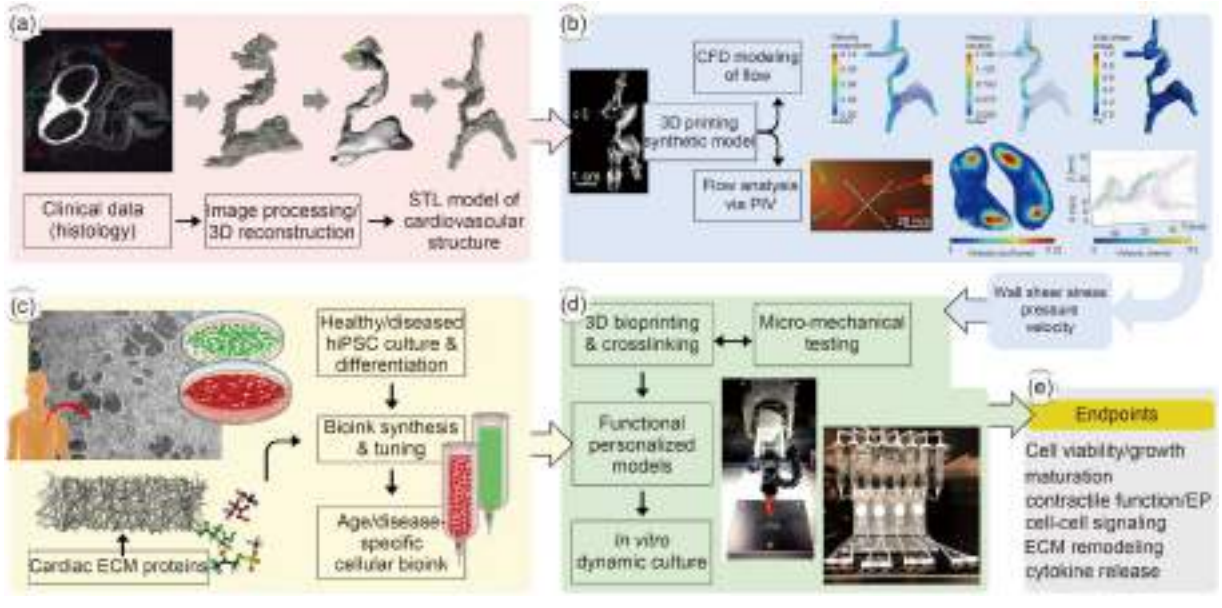

Fig. 39 Integrated biofabrication workflow for modeling heart development and congenital heart disease. (a) Clinical imaging and/or histological data are processed to generate stereolithography (STL) models of patient-specific cardiovascular structures. (b) The digital reconstructions inform 3D printing of synthetic models that are used for computational fluid dynamics (CFD) modeling (top), as well as particle–image velocimetry (PIV) flow analysis (bottom), to quantify hemodynamic parameters in 3D. Reproduced from [366], with permission from Wiley-VCH GmbH. (c) In parallel, age- and/or disease-specific cellular bioinks will be prepared using healthy and diseased human iPSCs encapsulated in hydrogel solutions. Bioink properties are tuned to optimize biomimetic function. (d) The 3D STL design will be bioprinted using optimized cellular bioinks. The resulting constructs undergo dynamic perfusion culture for functional maturation and studying physiological and pathophysiological processes. Together, these integrated analyses define the relationship between hemodynamic forces and biological endpoints (e) toward developing functional, patient-specific cardiovascular tissue models

Together, these approaches have established a pipeline for genotype-to-phenotype discovery and preclinical drug screening in personalized congenital disease models.

Complementary to developmental systems, the group has leveraged bioprinting for vascular disease modeling in CHD. Using patient imaging and computational design, they have created perfusable, anatomically faithful replicas of pulmonary veins and arteries to study stenosis, atresia, and surgical recanalization [51, 474, 496–498]. Endothelialized, bifurcated vein constructs cultured under physiologic flow reproduce the hemodynamic microenvironment associated with restenosis. By combining particle–image velocimetry (PIV) and computational fluid dynamics (CFD), they mapped wall shear-stress distributions and correlated disturbed flow with endothelial-to-mesenchymal transition (EndMT) and neointimal proliferation [51, 474, 496–498]. Integration of magnetic nanoparticle-mediated drug targeting has demonstrated localized delivery of rapamycin to stenotic regions, effectively suppressing pathological cell proliferation without systemic toxicity [496].

These patient-specific vascular models provide a controllable, high-throughput testbed to evaluate mechanical and pharmacologic interventions and to refine surgical planning for pediatric CHD. Beyond vasculature, similar bioprinting and perfusion strategies are being extended to fabricate chambered cardiac tissues and organoid-on-chip systems incorporating vascular, stromal, and neural crest components [501–503].

Collectively, these efforts position the Serpooshan-Bauser laboratory for work in biofabrication for cardiovascular developmental biology. By merging high-fidelity 3D bioprinting, stem-cell biology, and experimental and computational biomechanics, they are establishing a mechanistically informed platform that bridges in silico, in vitro, and clinical realms, advancing personalized modeling, regenerative therapy development, and the future of CHD research.

5.1.1.3 Optimized ECM-based bioinks enable an advanced human cardiac model

The limited proliferative capacity of adult cardiomyocytes is a major obstacle in cardiovascular disease modeling and therapeutic development. While iPSC-derived cardiomyocytes (iPSC-CMs) have emerged as a promising cell source for in vitro cardiac tissues, engineering living human heart models with complex geometry and physiologically relevant fluid dynamics has proven challenging. In particular, the formation of robust cell–cell connections within high-resolution, 3D constructs is difficult to achieve using terminally differentiated, nonproliferative iPSC-CMs.

An alternative strategy involves the use of early-stage iPSCs that are highly proliferative, combined with microenvironments that support controlled expansion and lineage specification in 3D. Central to this approach is the identification of ECM cues that guide cardiac development. Building on comprehensive analyses of ECM composition during human development, the Ogle group at the University of Minnesota has established an integrated biomaterial optimization platform to identify ECM formulations that enhance cardiac differentiation [504, 505]. Using ECM-encapsulated hydrogels and response surface statistical modeling, optimized ECM compositions have been predicted and validated. This optimized formulation (opt) significantly enhanced cardiac differentiation and improved calcium dynamics compared to the control group without ECM and the group with maximized ECM concentrations (Fig. 40a1), underscoring the importance of ECM composition rather than bulk content.

Using a similar strategy, an optimized ECM formulation supporting iPSC-derived endothelial differentiation has also been identified (Fig. 40a2), highlighting the potential to engineer multi-lineage cardiovascular tissues through spatially controlled ECM deposition [506, 507]. Together, these findings have enabled the development of an ECM-based bioink that supports both iPSC expansion and cardiac differentiation while maintaining printability and structural fidelity. This bioink has been subsequently used to fabricate a chambered structure [50]. The resultant human chambered muscle pump (hChaMP) has exhibited a contiguous outer muscle layer of approximately 500 μm, robust expression of proteins associated with mature CM phenotypes, and physiologically relevant pressure–volume dynamics. Importantly, hChaMPs have responded to pharmacological stimulation, demonstrating the clinical relevance of the platform (Fig. 40b).

Despite advances in dynamic culture and cloning reagent supplementation [508] to promote iPSC expansion in bioprinted constructs, uniform muscle formation throughout the chamber wall requires active perfusion. To address this limitation, a 3D-printed perfusion bioreactor has been designed to deliver nutrients throughout the hChaMP [509]. Perfused constructs exhibited a 1.9-fold increase in colony density after seven days compared to static controls, indicating improved nutrient accessibility and cellular uniformity. Furthermore, the bioreactor design has enabled the integration of a valve system to recapitulate physiological pressure–volume loops. Preliminary data from the Ogle group have shown improved pressure–volume relationships relative to nonvalved constructs, suggesting the platform's potential for modeling early single-ventricular cardiac diseases (Fig. 40c). Beyond disease modeling, ECM-based bioinks have been applied to generate centimeter-scale cardiac testbeds to evaluate medical device–tissue interactions [510]. When coupled with hydrogel-based piezoelectric sensors, these constructs have enabled real-time mapping of contact pressure during

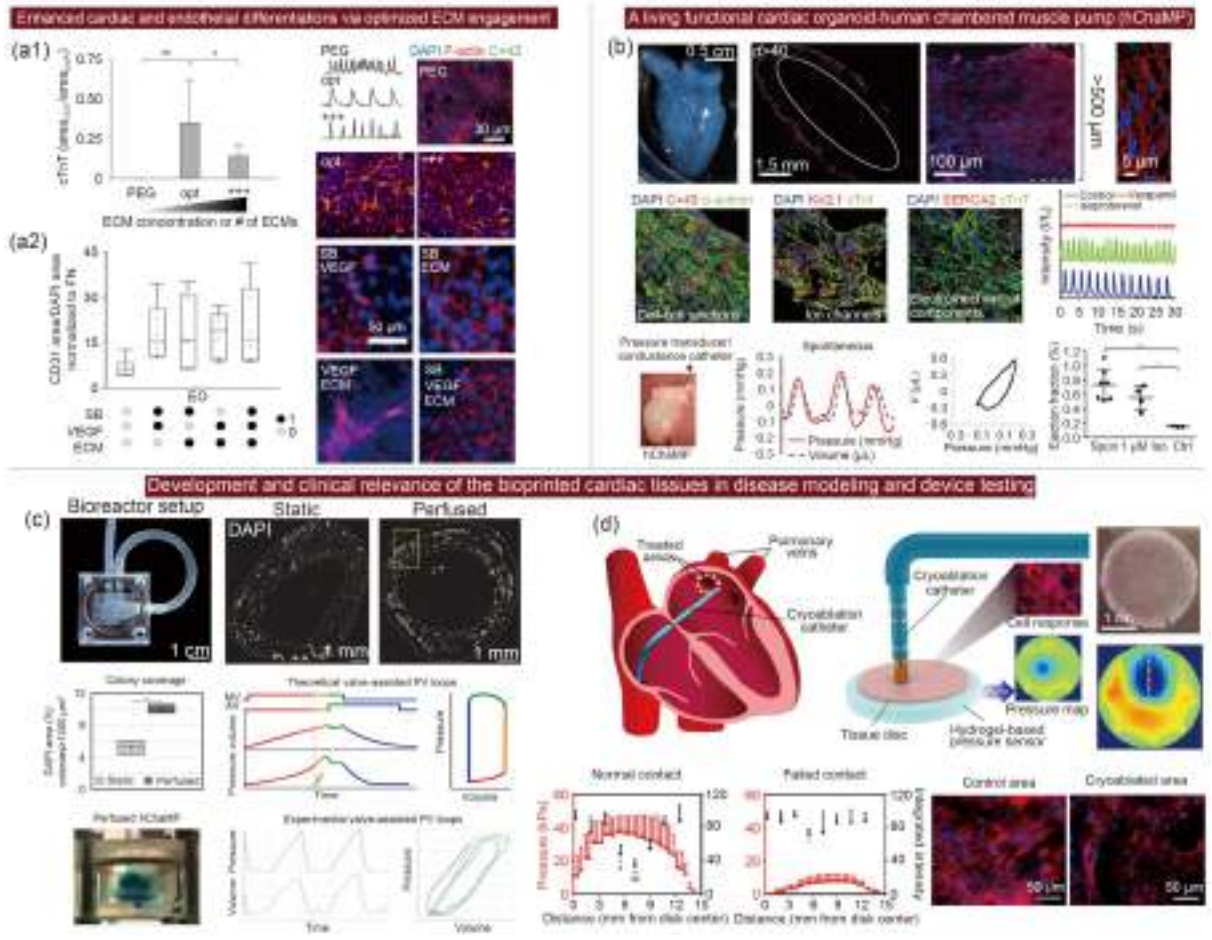

Fig. 40 Optimized ECM-based bioinks enable advanced human cardiac model systems. (a1) Enhancement of cardiac troponin T (cTnT) expression with optimized ECM formulation (opt) compared to the control (PEG) and the maximized ECM (+++) groups (left); validation of the opt by calcium dynamics and connexin 43 (Cx43) expression (right). Reproduced from [505], licensed under CC BY 4.0. (a2) Optimized ECM for endothelial differentiation showing cluster of differentiation 31 (CD31) expression with/without transforming growth factor beta (TGFβ) inhibitor (SB) and vascular endothelial growth factor (VEGF). Reproduced from [506], licensed under CC BY-NC-ND. (b) An hChaMP created by 3D bioprinting (top row, left); contiguous muscle formation in the hChaMP, as indicated by cTnT staining (top row middle and right); immunostaining of hChaMP for cardiac maturation markers and calcium dynamics of the hChaMP with drug stimulation (middle row); the setup for measuring pressure and volume changes generated by the hChaMP and the corresponding pressure–volume loop (bottom row, left and middle); the ejection fractions of the hChaMP with drug stimulation (bottom row, right). Reproduced from [50], with permission from American Heart Association Inc. (c) A 3D-printed bioreactor designed for culturing hChaMPs (top row, left); the side view of a bioreactor with a fully perfused hChaMP (bottom row, left); cell colony distribution in static (top row, middle) and perfused (top row, right) hChaMPs revealed by DAPI staining; quantified cell colony coverage (middle row, left); theoretical pressure–volume dynamics of hChaMPs with an external valve system (middle row, right); experimental pressure–volume dynamics of an acellular hChaMP with a valve system (bottom row, right). Reproduced from [509], licensed under CC BY 4.0. (d) Schematic image showing the process of pulmonary vein ablation and the bionic myocardial testbed with pressure-sensing capability (top left and middle); a bioprinted cardiac testbed and the corresponding pressure map with normal catheter contact. The gray-dotted line indicates the area for assessing pressure and cell activity profiles (top right); calcium intensities after cryoablation and recorded pressure profiles along the radius of testbeds (bottom left); the cryoablated testbed and the control testbed stained with cTnT to reveal the cryo-damage at the cellular level (bottom right). Reproduced from [510], licensed under CC BY 4.0

cryoablation. Reduced correlations between applied pressure and cellular response were observed under failed contact conditions, along with localized cellular damage following ablation (Fig. 40d). Collectively, these platforms provide critical insights into human cardiac tissue dynamics during therapeutic intervention and offer a translational framework for bridging device design with clinically relevant use conditions.

5.1.2 Bone model

Despite promising progress, significant challenges remain before routine clinical translation can be realized. Achieving sufficient mechanical strength for load-bearing applications while maintaining cell viability remains a central hurdle. The development of gradient and multiphasic constructs that replicate cortical and cancellous bone architecture is an ongoing

area of investigation. Vascularization strategies must be further refined to support nutrient diffusion and integration in large-scale constructs. Standardization of bioink formulations, scalability of manufacturing processes, and regulatory considerations also require attention. Future directions include the integration of bioreactor systems for dynamic conditioning, incorporation of gene-activated matrices, and application of artificial intelligence-guided design to optimize scaffold architecture. Ultimately, the convergence of advanced biomaterials, stem cell science, and precision biomanufacturing positions 3D bioprinting as a powerful platform for next-generation bone regenerative therapies within the broader framework of regenerative engineering.

Bone cells are predominantly embedded within collagen fibrils that are mineralized in a highly coordinated manner at the nanoscale [475]. As a result, osteons, which are the functional units of bone, are vascularized, innervated, lined with active osteoblasts and osteoprogenitor stromal cells, and embedded with osteocytes. Similarly, both native organs and cancers rely on precise spatial organization of multiple cell types to confer function. In healthy tissues, this organization enables coordinated cell–cell interactions that give rise to emergent tissue- and organ-level performance [511]. In cancer, this principle is recapitulated in the tumor microenvironment, where malignant cells are arranged within highly structured and heterogeneous cellular neighborhoods alongside stromal, vascular, and immune cells [512]. Cells assembled without this spatial and biological organization are arguably cellular agglomerates that poorly recapitulate meaningful function or disease behavior.

Historically, recreating the nano-, micro-, and macroscale patterns that emerge during native organogenesis using engineering-inspired biofabrication approaches has required complementary strategies. The Bertassoni group at Oregon Health and Science University has progressively addressed these challenges by tackling ECM complexity, the fabrication of vascular capillaries, and the development of methods enabling tissue construction with single-cell spatial resolution and high heterogeneity.

At the first order of precision, this group has developed methods to mineralize cell-laden hydrogels to address the nanostructural hierarchy of cell-laden bone tissue in bioprinted [513], micropatterned [53, 514], and on-chip tissue structures [515], enabling bone mimicry with precision down to approximately 2 nm for individual apatite crystallites (Figs. 41a1 and 41a2). Early extrusion-based bioprinting approaches for fabricating sacrificial channels and cell-laden hydrogels (Figs. 41b1–41b3) enabled some of the first vascularized tissue constructs (Figs. 41b4–41b7) [516–518], as well as the biofabrication of simple tissue-like architectures [519, 520].

Recognizing that extrusion bioprinting alone could not replicate the precise cellular organization of complex organs, research has pivoted to DLP-based printing that offers finer resolution (Fig. 41c) [511]. These efforts have leveraged studies to define biological requirements for forming robust, pericyte-supported vascular capillaries within bioprinted microgels that could be injected with built-in vessels and rapidly integrate with host vasculature [521, 522] or be cultured on-a-chip [523]. They have also developed innervated tissue structures that support neurite connectivity [227, 514]. The microgeometrical control afforded by vat polymerization further enabled commercial efforts to translate microgels for dental regeneration [524] and LEGO-like scaffolds for bone regeneration (Fig. 41d) [525].

5.1.3 Neural models

Neural models are another example of complex environments with a wide range of cell types and specific environmental demands. Developing in vitro models that recreate key aspects of different sections of the brain microenvironment poses many challenges, but fortunately, researchers in the U.S. have been able to develop models for neural studies, both for healthy and a variety of disease conditions. Some of these advancements are highlighted within this section.

5.1.3.1 Establishing effective, high-throughput models for neural environment modeling

The National Center for Advancing Translational Sciences (NCATS) 3D Tissue Bioprinting Laboratory (3DTBL) is a multidisciplinary hub of advanced research technologies that works with the biomedical community to harness and advance the production, validation, and use of 3D tissue models to accelerate the development of new medicines. 3DTBL aims to create a versatile platform of both healthy and diseased 3D tissue models and integrate their use as predictive assays into biomedical research, early discovery, and preclinical development pipelines to enable regulatory filings and make the translational process more efficient. The different 3D tissue models are developed using a fit-for-purpose approach: as physiologically complex as needed for the intended context of use of each model, but as simple as possible to ensure practical assembly and robustness of use. With this approach in mind, models for varied tissues, such as skin [526–528] and neural environments [54, 529–532], have been developed and applied to study disease states.

Some recent work from this group has focused on developing models that recreate aspects of the neural environment for disease research. Neural model approaches have involved the use of spheroids, organ-on-a-chip devices, and extrusion bioprinting. A method for generating functional neural spheroids designed for use in high-throughput platforms was used [54, 533]. These models have been effectively used to model neurotropic virus infections and screen

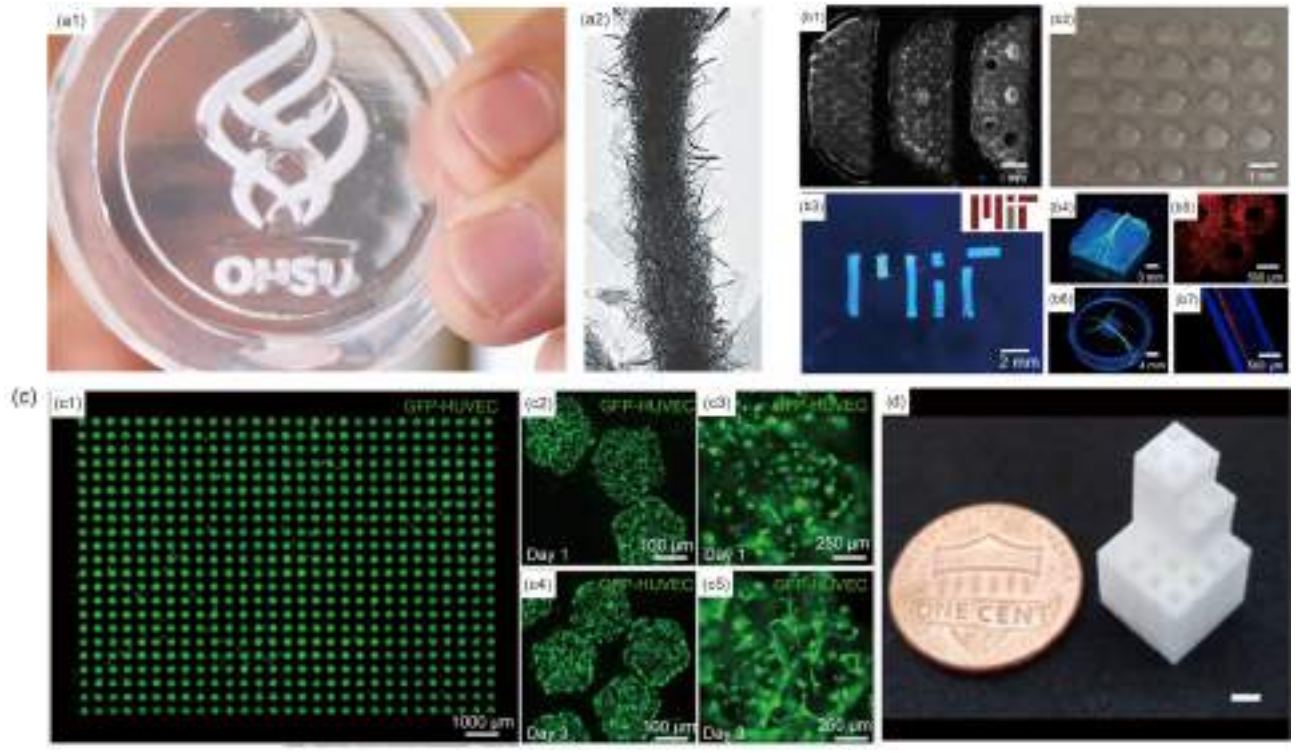

Fig. 41 Biofabrication of tissue structures using microengineering and bioprinting methods. (a1) Micro-molded bone tissue constructs with (a2) nanometer-scale biomineralization (reproduced from [53], with permission from Wiley-VCH GmbH). (b1) Extrusion bioprinted cell-laden GelMA hydrogels in fibers, (b2) microdot arrays, (b3) MIT logo, and (b4–b7) various formats of vascular patterns (reproduced from [519], with permission from IOP Publishing Ltd.). (c) DLP vat polymerization for high-throughput biofabrication of cell-laden hydrogels forming vascular capillaries (reproduced from [522], with permission from Wiley-VCH GmbH). (d) DLP printing of beta tricalcium phosphate LEGO-like scaffolds for bone regeneration (reproduced from [525], with permission from WILEY-VCH Verlag GmbH & Co. KGaA, Weinheim)

drugs for their treatment [531], being able to support productive infection, demonstrate time- and virus-dependent changes in disease profiles, and show response to different therapeutics to gauge potential as a screening platform. Relatedly, an organ-on-chip (OOC) approach was used to investigate the brain microvascular network response to flavivirus infection [530]. Using brain microvascular ECs and pericytes, a perfusable network resembling the blood–brain barrier was created, which was able to demonstrate flavivirus-induced pathophysiological phenotypes.

Bioprinting has also been used by the 3DTBL to fabricate neural environments, for model establishment and for investigation into cancer. In one example, bioprinting was also used to modify a previous approach to neural model creation [532], where the addition of AM was used to guide network formation to form a neural circuit [534]. The resulting network had significantly enhanced directionality and activity, demonstrating potential for future use as both a method of enhancing cell organization and as a testing platform [529, 534]. In another model, the neurovascular unit was recreated with ECs, pericytes, and astrocytes to introduce glioblastoma spheroids and examine cancer progression and response to therapeutics [529]. Using this high-throughput model, they were able to observe changes in angiogenesis and gene expression as a result of the glioblastoma spheroid, and epithelial-to-mesenchymal transition, and screen 18 different therapeutics targeting different pathways. Overall, 3DTBL has demonstrated effective methods for creating and testing high-throughput models that have great potential for rapid preclinical testing and evaluation.

5.1.3.2 Embedded printing to facilitate neuroblastoma study

At Cleveland State University, the Ning laboratory's research in biomanufacturing is dedicated to creating human tissue constructs for regenerative medicine and disease modeling [535–537]. One unique illustration is the effort to model neuroblastoma (NB), the most prevalent extracranial pediatric solid tumor [538]. Effective treatment of NB remains elusive, partly due to the limited understanding of its TME, which plays a critical role in orchestrating disease progression. Ning and colleagues utilized an embedded bioprinting strategy to develop a human-based in vitro NB platform that enables systematic interrogation of TME-mediated effects on tumor behavior [55]. The construct is fabricated using biocompatible, mechanically tunable hydrogels to recapitulate key ECM characteristics in

NB (Fig. 42). Additionally, it incorporates perfusable inner channels with a central cavity engineered to accommodate human ECs and patient-derived NB spheroids, thereby mimicking essential features of NB–EC–ECM interactions. Quantitative analyses demonstrated that under dynamic culture, the model sustains vigorous NB spheroid viability and expansion while promoting a more aggressive tumor phenotype. In addition, the platform has enabled controlled evaluation of metabolic activity, cytokine secretion, and gene expression profiles of NB spheroids across defined microenvironmental contexts. Together, these findings have established a physiologically relevant system for dissecting TME-driven cellular and molecular mechanisms that regulate NB growth, invasion, and therapeutic response.

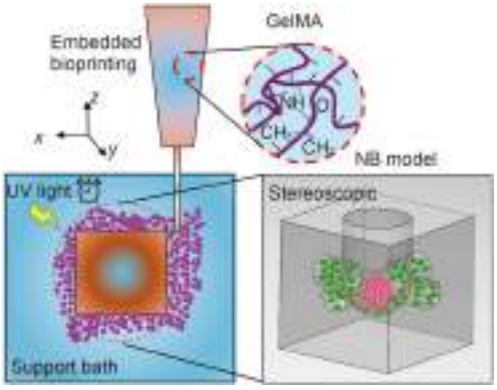

Fig. 42 NB model used to investigate how the tumor microenvironment regulates NB progression (reproduced from [55], licensed under CC BY)

5.1.4 Vascular models

The vascular system serves as a "highway" throughout the body that enables, via advection, the transport of key nutrients, gases, and waste products to support the metabolic needs of cells within tissue. For in vitro models, recreation of this system remains one of the most prevalent issues in the field, as multiscale, hierarchical vasculature is necessary for effective recapitulation of many tissues. Although many tissue and organ models include vasculature as a necessity, this section is dedicated to highlighting platforms that focus on vascularization, approaching this problem from a variety of perspectives.

5.1.4.1 Perfusable vascularized tissue biofabrication and microvascular network engineering

The Lewis group at Harvard University and coworkers have made foundational contributions to the development of biofabrication strategies for creating perfusable living tissues with increasing structural, cellular, and manufacturing sophistication [58, 539–543]. In early work, they established a multimaterial bioprinting approach for fabricating thick vascularized tissues that exceeded 1 cm in thickness, integrated parenchymal, stromal, and endothelial compartments, and remained actively perfusable on chip for more than 6 weeks [542]. This study was important not only because it demonstrated long-term viability in thick constructs, but also because it showed that embedded vascular channels could be used as functional conduits for biochemical delivery and in situ tissue maturation. The Lewis group's later work has extended this concept from "cells-in-gels" toward densely cellular living matrices by introducing sacrificial writing into functional tissue (SWIFT), in which hundreds of thousands of organ building blocks are compacted into high-cell-density tissues and patterned with embedded vascular channels through sacrificial writing [58]. More recently, they have advanced the manufacturing resolution of perfusable architectures by developing high-resolution DLP strategies for embedding microchannel networks in cytocompatible photoclickable bioresins [540]. Taken together, these studies define a clear trajectory from centimeter-scale vascularized tissue printing to dense organ-specific tissue assembly and, more recently, to finer-feature microvascular manufacturing.

5.1.4.2 Biofabricating in vitro models for cardiovascular disease modeling

Pulmonary vein stenosis (PVS) is characterized by abnormal vascular cell proliferation that progressively narrows the vascular lumen [544]. This life-threatening cardiovascular disorder can elevate pulmonary venous pressure, induce pulmonary hypertension, and ultimately lead to heart failure. Outcomes for PVS interventions remain suboptimal, primarily because the mechanisms governing disease progression and precipitating its serious complications are not yet fully elucidated. Therefore, developing physiologically relevant PVS models that recapitulate its complex pathophysiology becomes significant. The Ning laboratory at Cleveland State University and its collaborators have integrated DLP printing, nanoparticles, and bioreactors to develop an in vitro PVS model [496]. The construct incorporates bifurcating vascular branches to recapitulate the structural features of PVS and is subsequently seeded with human ECs to mimic pulmonary venous anatomy (Fig. 43). Under perfusion with physiologically relevant flow dynamics, the system supports the formation of a uniform, confluent endothelium. Computational analyses have revealed that the bifurcation region experiences significantly more disturbed flow. Consistent with these predictions, experimental studies have confirmed that disturbed flow at the bifurcation promotes pronounced EC overgrowth. To regulate this pathological EC proliferation, an externally applied magnetic field to direct rapamycin-loaded superparamagnetic iron oxide nanoparticles was

designed. This targeted delivery strategy effectively localized the nanoparticles to the bifurcation region, resulting in a substantial reduction in EC overproliferation without detectable adverse effects. These findings have established a robust 3D-printed in vitro platform for investigating pulmonary venous homeostasis and disease and highlight its potential for evaluating new or more effective therapies for PVS and other vascular disorders.

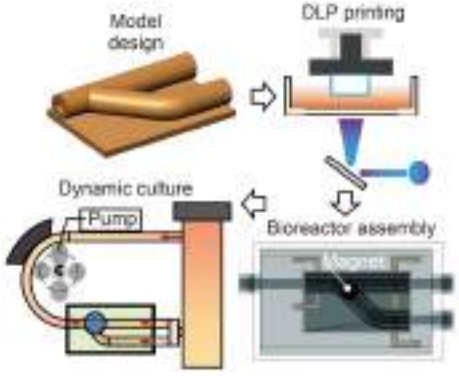

Fig. 43 PVS model designed to examine how flow dynamics influence EC function and to support the development of targeted therapeutic strategies (reproduced from [496], licensed under CC BY)

5.1.4.3 Vascular, cancer, and blood–brain barrier (BBB) models

Microphysiological systems, including OOCs, hold promise for improving drug testing and disease modeling. A major emphasis of the Kamm laboratory at the Massachusetts Institute of Technology is the development of self-assembling microvascular networks (MVNs) within microfluidic devices to bioengineer human tissues that advance this promise. Microfluidic devices, fabricated using soft lithography [479], are injected with a mixture of ECs and stromal cells suspended in fibrin hydrogels [479, 545], and these cells self-assemble within days into lumenized, perfusable microvessels via vasculogenesis. Early systems used adjacent channels for ECs and stromal cells [477, 478], while later iterations cocultured them together within one compartment (Figs. 44a and 44b) [546] and integrated tissue-specific cell types [480, 545]. The resulting MVNs retain physiologically-relevant junctional proteins [547], recapitulate passive and active transport across the endothelium [546], and exhibit in vivo-like vascular permeability (Fig. 44c) and size- and charge-dependent selectivity [547]. These features, along with the ability to apply intravascular and transmural flow to recapitulate fluid convection, directly sample interstitial fluid [546], and visualize transport into the surrounding ECM and cell uptake [548], position MVN technology as a powerful tool for drug distribution studies. Interstitial flow enhances network formation [57, 549], and continuous intravascular flow applied using a microfluidic pump [550] drives vascular remodeling (Figs. 44d and 44e) [551, 552] and supports long-term culture [553].

To advance disease modeling, the Kamm group has developed cancer metastasis platforms, in which tumor cells perfused through MVNs can be visualized in detail as they recapitulate steps of the metastatic cascade, including intravasation, cancer cell arrest, extravasation, and outgrowth (Fig. 44f) [479, 481]. These systems have been used to study multiple biological components and mechanisms affecting extravasation, including polyploidy [554], hypercoagulability [555], CCL2-CCR2 signaling [482], the glycocalyx [556], luminal and transendothelial flows [557], hypoxia [558], neutrophil interactions [559], tumor integrin beta-1 [481], and A3 adenosine receptors [560]. More recently, tumor spheroids embedded within MVNs further model the tumor microenvironment (Fig. 44g and 44h), enabling studies of cancer-related endothelial dysfunction, drug delivery, tumor-associated macrophages, therapeutic antibodies, and patient-specific responses [483, 561, 562].

The Kamm group has also engineered physiologically accurate and complex models of the BBB to study drug transport and to evaluate its compromise in neurodegenerative diseases. Initial BBB MVNs incorporating human induced pluripotent stem cell-derived ECs and brain pericytes and astrocytes (Fig. 44i) expressed physiologically relevant cellular transporters, tight junctional proteins, and ECM components, and exhibited pericyte and astrocyte contact with microvessels, along with permeabilities similar to those of in vivo brain vasculature [480, 545]. Additional systems have combined neural cells with endothelial monolayers [563] or MVNs [564] to model Alzheimer's disease (AD) BBB dysfunction. The microfluidic device housing the integrated BBB MVN-neural system features one compartment for the MVN with a separate central chamber for the culture of neurons, allowing for separate seeding and culture of each system in its own optimized medium (Fig. 44j) [564, 565]. Culture of AD neurospheres has resulted in impaired vascular morphology and barrier function, along with beta-amyloid depositions in the vasculature [564]. Further studies have revealed that prolonged coculture of BBB MVNs with AD neurons in the central channel resulted in dysregulation of endothelial and pericyte markers and increases in soluble beta-amyloid in both neuronal and vascular compartments (Figs. 44k and 44l) [565]. These studies have established in vitro models for probing links between vascular dysfunction and neurodegenerative disease.

While MVN systems effectively recapitulate salient vascular features in multiple organ systems and disease states, future efforts focused on incorporating organ-specific parenchyma through the inclusion of organoids will require new strategies for organoid vascularization [566] and for connecting these structures with the surrounding MVNs.

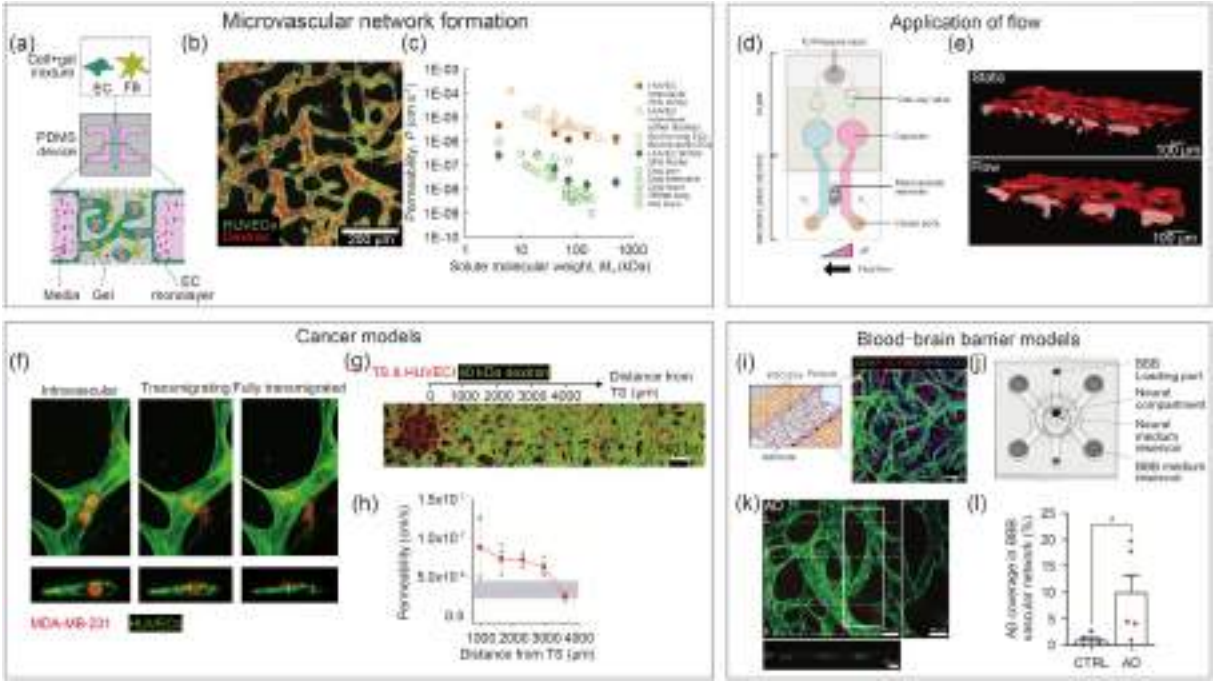

Fig. 44 Engineered microvascular networks and applications to tissue-specific models. (a) Schematic of a microfluidic device with ECs and fibroblasts (FB) suspended within a gel in the central channel, forming a microvascular network (MVN). (b) Confocal image of MVN perfused with fluorescent dextran. (c) Permeability of MVNs (solid circles) to a range of solutes with different molecular weights compared to permeabilities of other in vitro and in vivo preparations. (d) Schematic of microfluidic pump that circulates flow through MVNs. (e) 3D reconstructions of MVNs cultured under static conditions or after 48 h of flow (white outlines indicate vascular perimeters from orthogonal sections). (f) Confocal image of perfused MVN with tumor cells. Snapshots over time of cross-sectional views of a single tumor cell as it transmigrates across the endothelium. (g) Confocal image of a tumor spheroid embedded in MVN that has been perfused with fluorescent dextran (green). (h) Vascular permeability at increasing distances from the tumor spheroid. (i) Schematic and confocal image of a BBB model composed of ECs (green), pericytes (red), and astrocytes (magenta). (j) Schematic of microfluidic device with a BBB channel and neural compartment. (k) Confocal image and orthogonal views of an AD vascular model with staining for beta-amyloid (magenta). (l) Beta-amyloid in the BBB vasculature is increased in the AD model compared to the healthy control . (a, c) are reproduced from [547], with permission from Elsevier Ltd.; (b) is reproduced from [546], with permission from WILEY-VCH Verlag GmbH & Co. KGaA, Weinheim; (d) is reproduced from [553], licensed under CC BY-NC-ND; (e) is reproduced from [551], with permission from Elsevier Ltd.; (f) is reproduced from [479], with permission from Springer Nature Limited; (g, h) are reproduced from [483], with permission from WILEY-VCH Verlag GmbH & Co. KGaA, Weinheim; (i) is reproduced from [480], with permission from Elsevier Ltd.; (j) is reproduced from [564], licensed under CC BY 4.0; (k, l) are reproduced from [565], with permission from Elsevier Ltd.

5.1.4.4 Sacrificial biofabrication of complex vascular constructs

Vascularization strategies historically focused on growth factor delivery, controlled-release biomaterials, or gene and cell therapies to stimulate host angiogenesis, but have largely failed [567–574]. Although the approaches induce vessel ingrowth, the resulting networks were often disorganized, hyperbranched, and ultimately inadequate to sustain perfusion in large tissue volumes. These experiences suggested that building effective tissues requires not only more vessels but also control over the architecture of the vasculature [567].

To tackle this challenge, the Chen laboratory at Boston University and the Wyss Institute, along with others, have developed a class of sacrificial manufacturing tools that use dissolvable elements to pre-structure vascular conduits within natural and synthetic ECMs prior to or in parallel with cellular organization. Early work showed that 3D-printed sacrificially cast carbohydrate glass lattices could be embedded in cell-laden hydrogels and removed to leave behind perfusable vascular networks, which, when endothelialized, sustained thick constructs of highly metabolic parenchymal cells [575]. Extending this work, they introduced sacrificial percolation of anisotropic networks (SPAN), in which pipettable alginate microfibers are mixed into pre-gel solutions, allowed to form a percolated network at physiologic vascular volume fractions, and then enzymatically degraded to yield a distributed, perfusable network in minutes, independent of construct size and compatible with diverse hydrogels and fabrication formats (Fig. 45a) [56]. In SPAN constructs, perfusion through the percolated void network dramatically improves convective and diffusive transport, eliminating hypoxia in regions that remain oxygen-limited in bulk gels,

and providing a platform in which ECs seeded in the bulk matrix preferentially exit the gel to line the void surfaces, forming an interconnected endothelialized microvasculature while perfusion is maintained throughout the construct. The technique also allows for rapid generation of perfused networks, but if combined with 3D printing, can also build more complex network geometries. Recently, they established that subtractive approaches could be extended across multiple scales to achieve substantially higher resolution vascular networks than those achieved using typical 3D printing methods [576]. Using gallium-based engineered sacrificial capillary pumps for evacuation (ESCAPE) to generate high-fidelity, hierarchical vascular trees from arterioles down to near-capillary dimensions provides a means to create multiscalar conduits that can be endothelialized and integrated into larger tissue platforms (Fig. 45b) [576]. By enabling the generation of multiscalar trees with precise control over branching geometry, caliber transitions, and alignment, one can study how geometric features regulate flow distribution, shear stress, and remodeling in engineered networks. Overall, these sacrificial strategies provide a toolbox for rapidly establishing perfusion and for building vascular architectures that can support tissue assembly.

These pre-structured vascular architectures have been shown not only to support perfusion and function of engineered tissues in culture, but also to enhance engraftment and function following implantation. Micropatterned endothelial cords embedded in fibrin guide host angiogenesis along predefined trajectories, accelerating host–graft anastomosis and improving perfusion and survival of co-implanted hepatocyte aggregates compared with unpatterned constructs [577]. Building on this principle, 3D-printed vascular patches with centimeter-scale organized channels direct host collateral formation and rescue perfusion and function

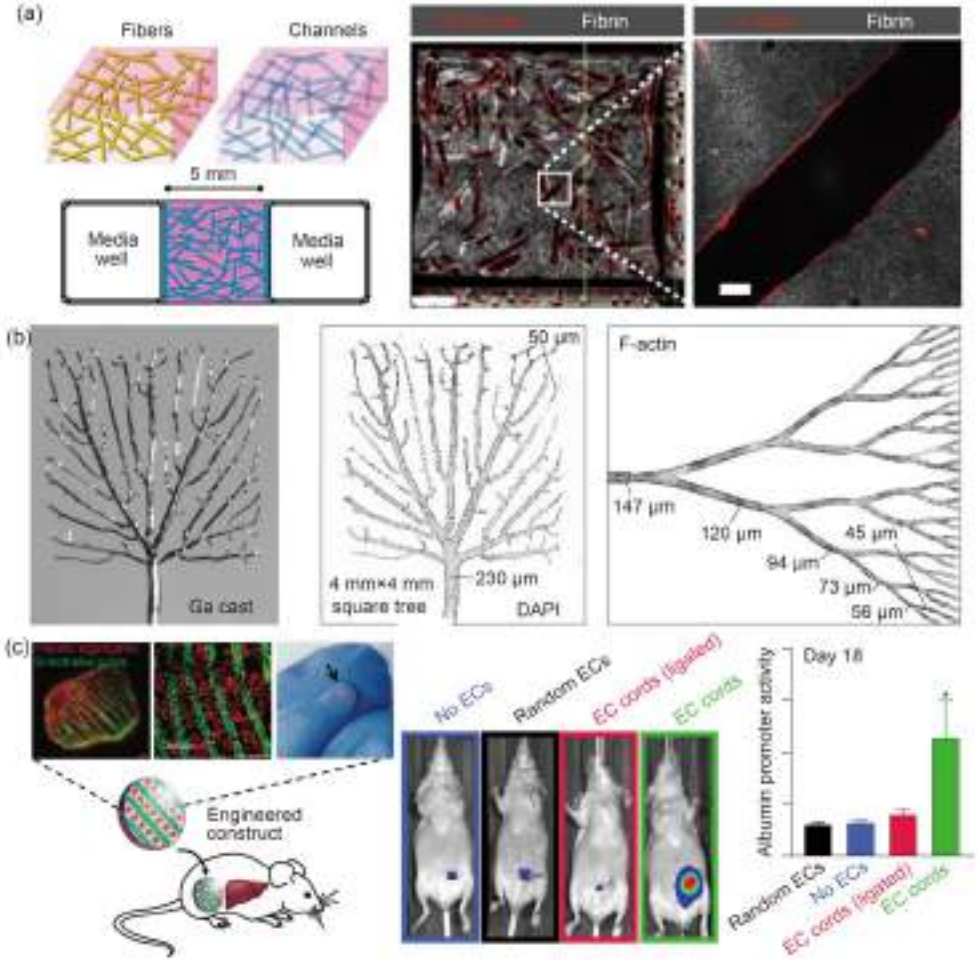

Fig. 45 Examples of sacrificial biofabrication of complex vascular constructs. (a) SPAN: percolated network of endothelialized cavities that are generated by casting and degrading alginate fibers (reproduced from [56], with permission from Elsevier Inc.). (b) ESCAPE: hierarchical vascular trees that are patterned using gallium (reproduced from [576], under exclusive licence to Springer Nature Limited). (c) Patterned constructs featuring hepatocyte aggregates (red) and parallel vascular cords (green), upon implantation, enhance engraftment, vascularization, and tissue function (reproduced from [577], with permission from National Academy of Sciences; reproduced from [579], under exclusive licence to the American Association for the Advancement of Science

in hindlimb and myocardial ischemia, whereas randomly embedded ECs or nonpatterned channels fail to achieve comparable benefit, emphasizing the importance of vascular geometry in therapeutic outcomes [578]. These technologies have also demonstrated benefit in a tissue engineering context. Synthetic liver "seeds" in which primary human hepatocytes and stromal cells are organized around parallel endothelial cords exhibit rapid host vascular invasion, superior hepatic survival and function, and the capacity to expand in response to regenerative cues after liver injury, highlighting how initial vascular patterning and multicellular architecture can program both acute integration and long-term growth of engineered tissues (Fig. 45c) [577, 579]. Together, these efforts position sacrificially defined and pre-organized vasculature as a central design paradigm for biofabrication and biomedical manufacturing of thick, metabolically demanding tissues.

5.1.5 Breast cancer models

Breast cancer is one of the most prevalent cancer types and remains a high-mortality condition. It is challenging to faithfully recapitulate the breast cancer microenvironment in a way that supports various cancer-associated cell types and heterogeneity while effectively reflecting cancer progression. Highlights within this section are notable advancements in models used to study breast cancer.

5.1.5.1 Embedded bioprinting of breast cancer model

The Duan group at the University of Nebraska Medical Center has produced embedded, bioprinted breast cancer cells and tumor organoid models using low-concentration collagen I-based bioinks [59]. The composition of collagen I-based bioink is optimized with a thermoresponsive HA-based polymer to maintain the phenotypes of both noninvasive epithelial and invasive breast cancer cells, as well as cancer-associated fibroblasts. Mouse breast tumor organoids have been bioprinted using optimized collagen bioink to better mimic in vivo tumor morphology compared to Matrigel and collagen I alone (Fig. 46a). Adipocytes and adipose-derived mesenchymal stromal cells (ADMSCs) also play an important role in breast cancer metastasis and drug resistance. The Duan group has developed several 3D bioprinted adipose models [580–582] and cocultured breast cancer models [583, 584]. In one study, breast cancer cells were 3D bioprinted within ADMSC layers of varying thickness to mimic obesity and to examine the effects of ADMSC thickness on doxorubicin (DOX) resistance and lysyl oxidase (LOX) secretion (Fig. 46b). In the moderate and thick-layered ADMSC constructs, significantly more cells were stained negative for cleaved Caspase-3, indicating less apoptosis (Fig. 46c). Both ADMSCs and breast cancer cells intrinsically expressed LOX, regardless of changes in thickness or DOX administration. Notably, treatment with a LOX inhibitor significantly decreased stiffness in the ADMSC region but did not affect stiffness in the breast cancer cell region. In addition, LOX inhibitor treatment enhanced the DOX sensitivity of breast cancer cells in the bioprinted constructs, as seen by a decrease in LOX secretion and downregulation of adenosine triphosphate-binding cassette transporter gene expression. Increasing ADMSC layer thickness also induced the upregulation of hypoxia-inducible factor 1-alpha (HIF1α), indicating hypoxia, which in turn promotes epithelial-to-mesenchymal transition [584] and vasculature formation [59]. Taken together, 3D bioprinted breast cancer models can faithfully reproduce in vivo conditions and provide improved platforms for studying breast cancer biology and for drug screening. These models offer the potential to improve the understanding of tumor–stroma–vessel interactions, therapeutic resistance, and the influence of the TME on cancer progression.

5.1.5.2 Breast cancer study enabled by single-cell bioprinting

Despite advances in high-precision biofabrication, recreating the cell–cell communication that defines complex organ function and disease states such as cancer requires even greater control, including precise single-cell placement. The Bertassoni laboratory at Oregon Health and Science University has adapted microfluidic technologies to enable jetting of individual cells with <2 μm positional accuracy, incorporating up to eight distinct cell phenotypes per print. This capability enabled near-exact phenocopies of patient-derived TMEs (Fig. 47) [585] and developed methods to study how spatial organization regulates tumor transcriptomics [586], opening new avenues for precision biofabrication of tissues and disease models.

5.1.6 Other in vitro models

Many in vitro models fall outside of the categories that have already been discussed. This section highlights some notable developments in the application of biomanufacturing and biofabrication methods for in vitro construct creation.

5.1.6.1 Engineering physiologically relevant mesoscale ECM architectures

In stromal environments, collagen fibers are often thick, tortuous, and geometrically diverse, with properties that extend across subcellular to multicellular scales. Such structural heterogeneity plays a critical role in shaping cellular behavior yet has traditionally been difficult to replicate in tissue model systems. Conventional methods for generating

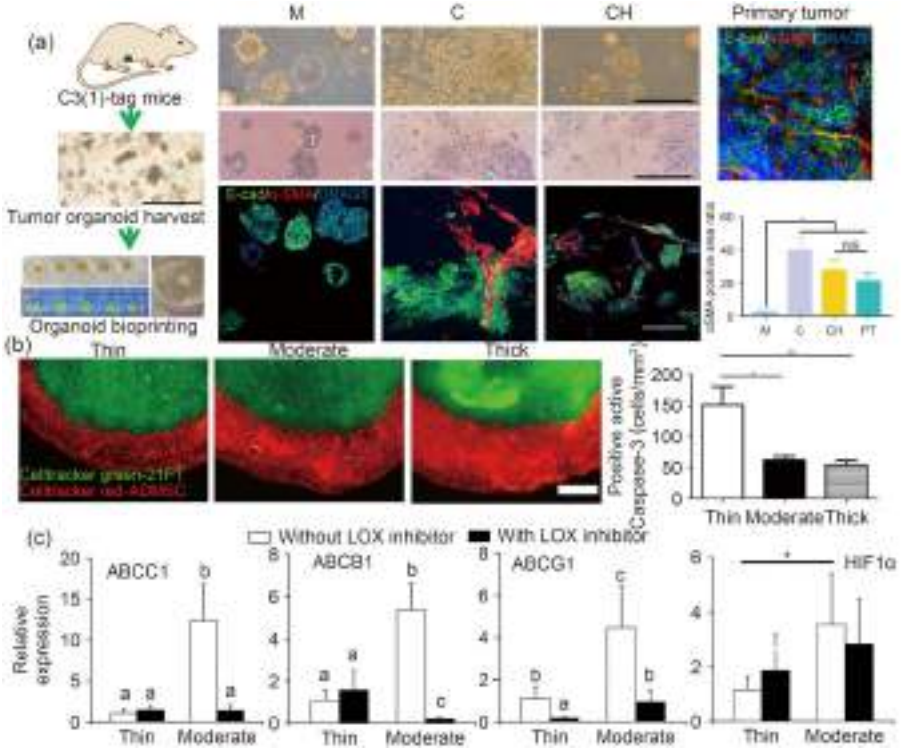

Fig. 46 3D-bioprinted breast cancer model to recapitulate the in vivo microenvironment and study the effects of stromal cells on tumor growth, invasion, and therapeutic response. (a) The bioink consisting of collagen I and HA-poly(N-isopropylacrylamide) (pNIPAM) supported the growth of tumor organoids with cancer-associated stromal cells. Breast tumor organoids were harvested from the tumor sample and can be high-throughput bioprinted in the support bath. Morphology of breast tumor organoids in three bioinks on Day 1 is shown. Bioprinted tumor organoids in the Matrigel and CH models remained in the spheroid structure from Day 1 to Day 7; however, in the collagen, cells became more invasive and quickly spread to the surrounding area on Day 1, leading to the loss of the original spheroid structure. Hematoxylin & eosin (H&E) staining of breast tumor organoids on Day 7 in three bioinks is shown (M: Matrigel; C: collagen I only; CH: collagen I with HA-pNIPAM). Immunofluorescence staining of E-cadherin and α-SMA proteins on breast tumor organoids and mouse tumor samples demonstrated a similar morphology to the bioprinted tumor organoids in the CH model compared to the primary tumor (PT) tissue based on the cell phenotype and ratio. Quantification of the α-SMA-positive area ratio from organoid samples in three bioinks and the primary tumor is shown. Scale bars: pink 5 mm; black 250 μm; white 100 μm. These results suggested that the bioprinted tumor organoids using the CH bioink enabled better spatial organization and phenotype maintenance of both the cancer cells and the stromal cells from the organoids, resembling the in vivo tumor tissue. Reproduced from [59], licensed under CC BY-NC-ND. (b) 3D-bioprinted breast cancer models with various ADMSC layer thicknesses; positive cleaved Caspase-3 cell density in the middle region in the bioprinted constructs with different ADMSC layer thicknesses. (c) Effects of LOX inhibitor on bioprinted construct stiffness and DOX response: quantitative polymerase chain reaction (qPCR) analysis of adenosine triphosphate (ATP)-binding cassette transporter genes (i.e., ABCC1, ABCB1, and ABCG1) and HIF1α expression in bioprinted constructs with and without the LOX inhibitor. Reproduced from [583], with permission from the American Chemical Society

collagen I hydrogels typically yield networks composed of relatively thin fibers. While modest tunability in fiber thickness has been achieved, the resulting range is limited, generally spanning approximately 100 nm to a few micrometers [587–589]. Moreover, many collagen gel properties (e.g., concentration, porosity, and stiffness) are intrinsically coupled, restricting the ability to independently tune scaffold features and posing challenges for engineering tissue models that require precise control over microenvironmental cues without relying on artificial crosslinking or chemical modifications.

Recent advances from the Mak laboratory at Stony Brook University have introduced new strategies for producing collagen matrices with robust and tunable mesoscale architectures. These approaches leverage controlled biophysical stimulation during collagen assembly. Upon neutralization, collagen molecules undergo fibrillogenesis; if mechanical mixing forces are applied during this process, localized clustering occurs, generating spatially distributed mesoscopic collagen "islands" (Fig. 48a) [484]. Such clusters exhibit tunable porosity and size while preserving the interconnected network structure and strain-stiffening behavior characteristic of biopolymer systems. Furthermore, the introduction of macromolecular crowding agents, such as polyethylene glycol, during mixing promotes additional architectural features. Under these conditions, collagen fibrils bundle into thick, continuous fibers that can exceed 30 μm in diameter (Fig. 48b) [277]. These fibers can be collected

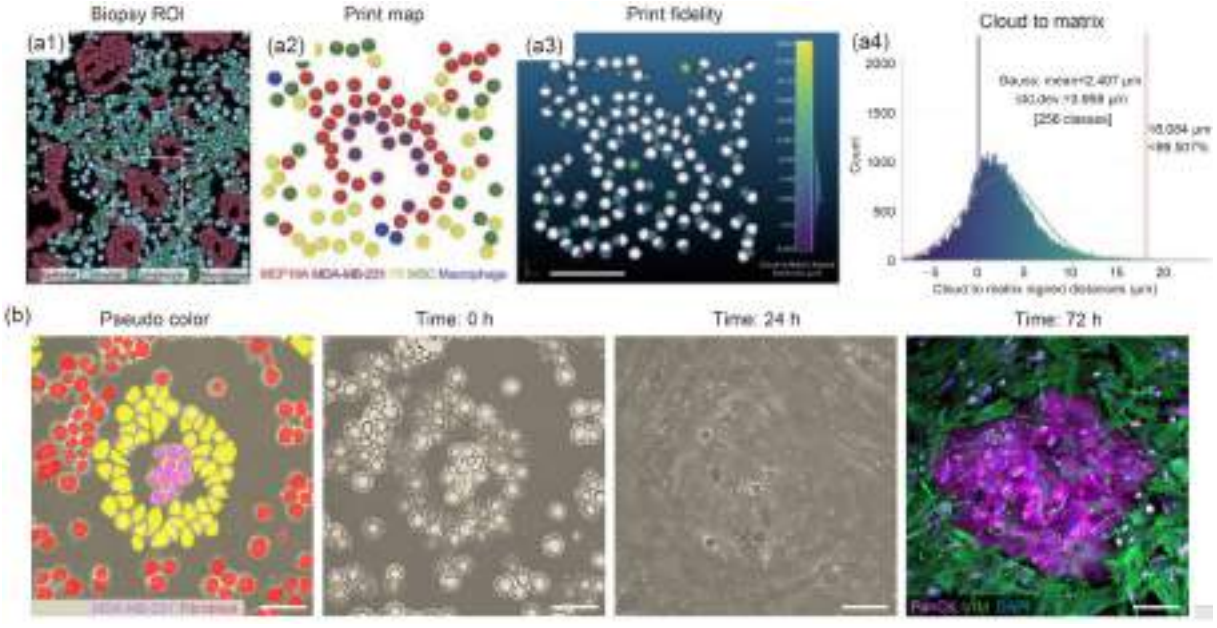

Fig. 47 High-precision bioprinting for spatially defined tumor microenvironments. (a1) Single-cell resolution mapping of a tumor microenvironment, (a2) printing map, and (a3, a4) printing fidelity plots demonstrating high accuracy of cell positioning via microfluidic dispensing. (b) Pseudocolored breast tumor cells immediately after bioprinting with high precision, showing time evolution of printed patterns forming an invasive ductal carcinoma-like organization. Reproduced from [585], licensed under CC BY-NC-ND

via centrifugation and resuspended at desired densities or embedded within alternative ECM backgrounds (e.g., fibrin), enabling the construction of hybrid matrices with customizable bundle-level concentrations [590].

Importantly, these methods allow key parameters to be decoupled. For example, network-level porosity can be tuned independently of local collagen density, permitting the design of globally soft and porous matrices that contain locally stiff, dense regions. Such architectures have revealed that cells respond strongly to mesoscale properties, which can override bulk substrate mechanics. This principle has been exploited to generate soft collagen gels that promote osteogenesis, highlighting the importance of mesoscale architectures in lineage specification [484].

Applications of these tunable architectures extend across multiple tissue types. Mesenchymal stem cells (MSCs) cultured within clustered or bundled collagen networks have demonstrated enhanced osteogenic differentiation [277, 484]; iPSCs have been guided toward mesodermal fates [484]; engineered microvascular networks and vascularized organoids have been successfully biofabricated with local guidance by bundle geometries [590]; and tumors or fibrosis models with clustered or bundled collagen architectures have been shown to exhibit alterations in morphodynamics, spreading, molecular profiles, cell–matrix interactions, and responses to mechanical stimulation [277, 591–593]. Collectively, these findings underscore the functional significance of mesoscale ECM architectures in regulating cell differentiation, tissue organization, and critical processes in disease and development. By enabling precise control over structural features that mimic native tissue complexity, these emerging methods advance the biomimicry of engineered microenvironments and open new avenues for translational tissue engineering.

5.1.6.2 Interplay between materials structure and light-assisted biofabrication parameters for tunable disease model

Microtissues provide an effective and cost-efficient tool in personalized medicine [594, 595]. The major design criteria in making microtissues include controlling ECM morphology, establishing quality-control thresholds, and ensuring the safety of biological cell processing [596, 597]. When applied to disease modeling, additional challenges arise, including uncontrolled spheroid growth, limited real-time monitoring capabilities, and gaps in understanding the optimal ECM properties needed to support disease-specific cell functions [594, 598]. The Miri laboratory at the New Jersey Institute of Technology has addressed some of these challenges by exploring how 3D bioprinting parameters and bioink microstructure influence cellular behavior. In the first step, they developed a custom DLP bioprinting system to fabricate hydrogel-based microfluidic devices (Fig. 49a) [599]. PEGDA and GelMA were used to demonstrate the potential of the DLP platform for creating microtissue models and microfluidic devices (Fig. 49b). GelMA, compared to PEGDA, resulted in lower printing resolution [598]. The DLP bioprinter's capacity was achieved by using PEGDA

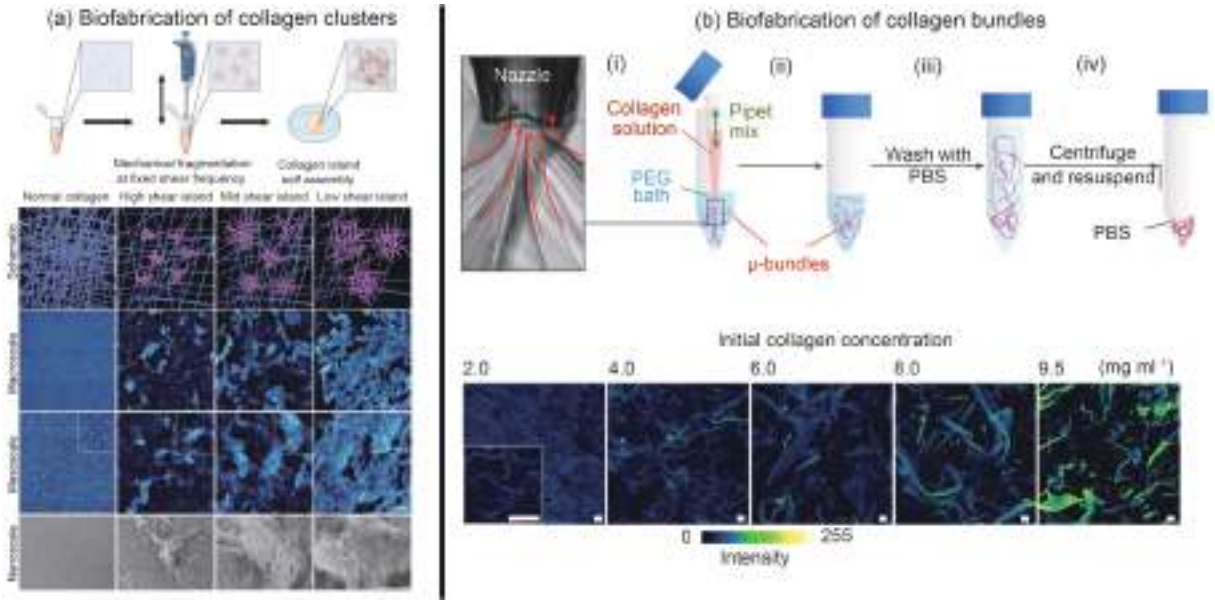

Fig. 48 Biofabrication of collagen networks with cluster and bundle architectures. (a) Collagen clusters: mechanical mixing forces during collagen gelation led to spatially distributed collagen clusters that formed an intact collagen network. Scale bars from top to bottom: 100, 30, 50, and 20 μm. Reproduced from [484], with permission from Wiley-VCH GmbH. (b) Collagen bundles: macromolecular crowding coupled with controlled mechanical mixing led to thick continuous collagen bundles, including large bundles over 30 μm in diameter. Scale bars: 30 μm. Reproduced from [277], under exclusive licence to Springer Nature Limited

(20%–40% volume fraction) [124] and GelMA (0.03–0.07 g/mL) to print different shapes and structures. The stiffness of the resulting printed structures can be controlled by varying the ink composition, the UV curing process parameters, and the geometry. LAP was selected as the photoinitiator, and a concentration of 0.1% (1 mg/mL) LAP was shown to support cell viability while enabling precise light-assisted bioprinting [600]. Cell density has also been optimized in this material system using DLP parameters to ensure cell viability and biotransport reliability (Fig. 49c) [601]. The group then developed a reliable protocol for creating fibrosarcoma cell spheroids as depicted in Fig. 49d [602]. After three days of spheroid formation in an incubator, they quantified spheroid diameter and roundness using ImageJ. In addition, quantitative reverse transcription polymerase chain reaction (qRT-PCR) measurements were used to study the role of bulk stiffness on the gene expression of tumor cells (Fig. 49e). Softer GelMA scaffolds, characterized by larger pore sizes (Fig. 49c), resulted in increased expression of mesenchymal markers such as cluster of differentiation 44 (CD44) on Day 5 [602]. They also observed that the ECM microstructure can impact the mesenchymal behavior of tumor cells within spheroid-laden GelMA microtissues [602]. Similarly, the breast tumor cells formed spheroids when embedded in a stiffer bioink, characterized by smaller pore sizes (Fig. 49f), over three weeks [603]. The softer bioink resulted in more elongated tumor cells. In parallel, the team has developed a real-time monitoring system using conductive ink to track spheroid expansion in their microfluidic chips [604]. Real-time monitoring enables the study of cell responses in bioprinted microtissues.

5.1.6.3 Porous and perfusable tissue device creation

The Li laboratory at the University of Texas at Austin has developed a solvent-free fabrication method for tissue engineering scaffolds [606]. Traditional scaffold fabrication methods rely on organic solvents, which can be difficult to fully remove even after extensive washing and leaching. The Li laboratory's method integrates solid-state foaming with ultrasonic cavitation to create a porous structure using only inert gas and water, eliminating the need for organic solvents. Building on this approach, the laboratory has developed a selective ultrasonic foaming process to fabricate miniaturized tissue engineering scaffolds on polymeric biochips [607] (Figs. 50a and 50b). This technique bridges the gap between microfluidic technology and tissue engineering, enabling the creation of microscale, 3D engineered tissue model systems essential for human biology research and drug testing. Two notable examples of these innovative devices are a 3D microdevice for cell migration study [608] and a perfusion-based two-chamber tissue model for personalized medicine [609].

Cell migration in response to chemoattractants is a key biological process in cancer metastasis. While numerous in vitro assays have been developed to investigate the mechanisms and potential inhibitors of cancer cell migration, most previous studies have relied on 2D cell cultures, where cells form a monolayer that does not accurately

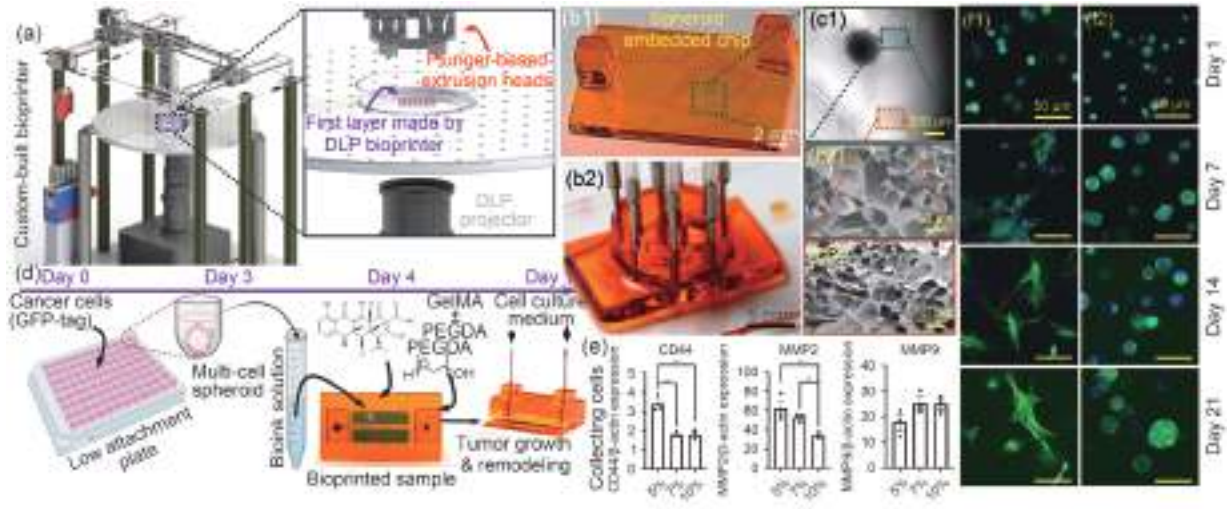

Fig. 49 Biofabricated tumor-on-a-chip platform and cancer models. (a) Schematics of the bioprinter and a zoomed picture of the extrusion heads (reproduced from [599], with permission from IOP Publishing Ltd.). (b) Examples made by the system: 3D-bioprinted PEGDA-40% (volume fraction) chip filled with dyed water (reproduced from [599], with permission from IOP Publishing Ltd.; reproduced from [605], with permission from the American Chemical Society). (c) A light microscopy image of the selected area with the spheroid-laden gel (c1), along with the scanning electron microscopy (SEM) images of the microstructure in GelMA 5% (0.05 g/mL, c2) and 10% (0.10 g/mL, c3). Reproduced from [602], with permission from Acta Materialia Inc. (d) Sarcoma tumor cell (HT1080) spheroid protocol along with creating tumor-on-a-chip. (e) CD44, MMP2, and MMP9 mRNA expressions in the sarcoma tumor cell (HT1080) spheroids normalized to β-actin expression for different concentrations of GelMA. Reproduced from [602], with permission from Acta Materialia Inc. (f) Immunofluorescence images of F-actin (green, phalloidin) and nuclei (blue, DAPI) for the carcinoma tumor cells (MDA-MB-231) in GelMA 5.7% (57 mg/mL, f1) and 7% (70 mg/mL, f2) over 21 days (reproduced from [603], licensed under CC BY)

replicate in vivo behavior. Utilizing the selective ultrasonic foaming process, the Li laboratory has developed a 3D microdevice to enable cancer cell growth and migration within a porous channel, closely mimicking the 3D environment of human biological systems and providing a more physiologically relevant model for studying cancer metastasis [608] (Fig. 50c).

The perfusion-based two-chamber tissue model system has been developed as an alternative to animal models for drug testing. Drug discovery and development is a lengthy and costly process, with animal testing serving as a critical yet problematic step due to its inaccuracy in predicting human responses, high costs, and ethical concerns. A promising solution is the development of engineered tissue model systems that more accurately replicate the complex environment and interactions of human organs. The liver, a key organ in drug metabolism, contains enzymes that vary significantly based on genotype, leading to differing drug responses. However, current in vitro models fail to effectively capture these variations. While some research groups have developed 2D cell culture systems, these models, with cells growing on flat surfaces, do not sufficiently mimic the physiological conditions of the human body.

To address this gap, the laboratory has developed a perfusion-based 3D tissue model system consisting of two chambers, each containing a tissue engineering scaffold, connected by a microfluidic channel. One scaffold is seeded with liver cells and the other is seeded with cancer cells, both of which can be patient-specific and customized to individual genotypes. By using genetically similar cells or a patient's own cells, this system has enabled the prediction of individual drug responses, providing critical data for personalized medicine [610] (Fig. 50d). The Li laboratory has continued to contribute to the biomanufacturing field, with current research focusing on high-strength bone implant design and fabrication [610–614].

5.2 Engineered tissue constructs for in vivo use

Engineered tissue constructs intended for in vivo implantation impose the most demanding and clinically relevant requirements on biofabrication and biomedical engineering: constructs must be biocompatible and functional, while supporting host tissue integration, which needs to meet rigorous requirements for cell proliferation, migration, and differentiation, as well as vascular and neural growth, appropriate mechanical integrity, and long-term safety [616, 617]. Consequently, U.S. research in this area increasingly emphasizes application-specific construct designs, in which the fabrication process and biomaterial system are optimized to achieve tissue-relevant architecture, appropriate cell organization, and function with clinical translational considerations. The subsections below highlight representative advances in major target tissues (notably bone and skin)

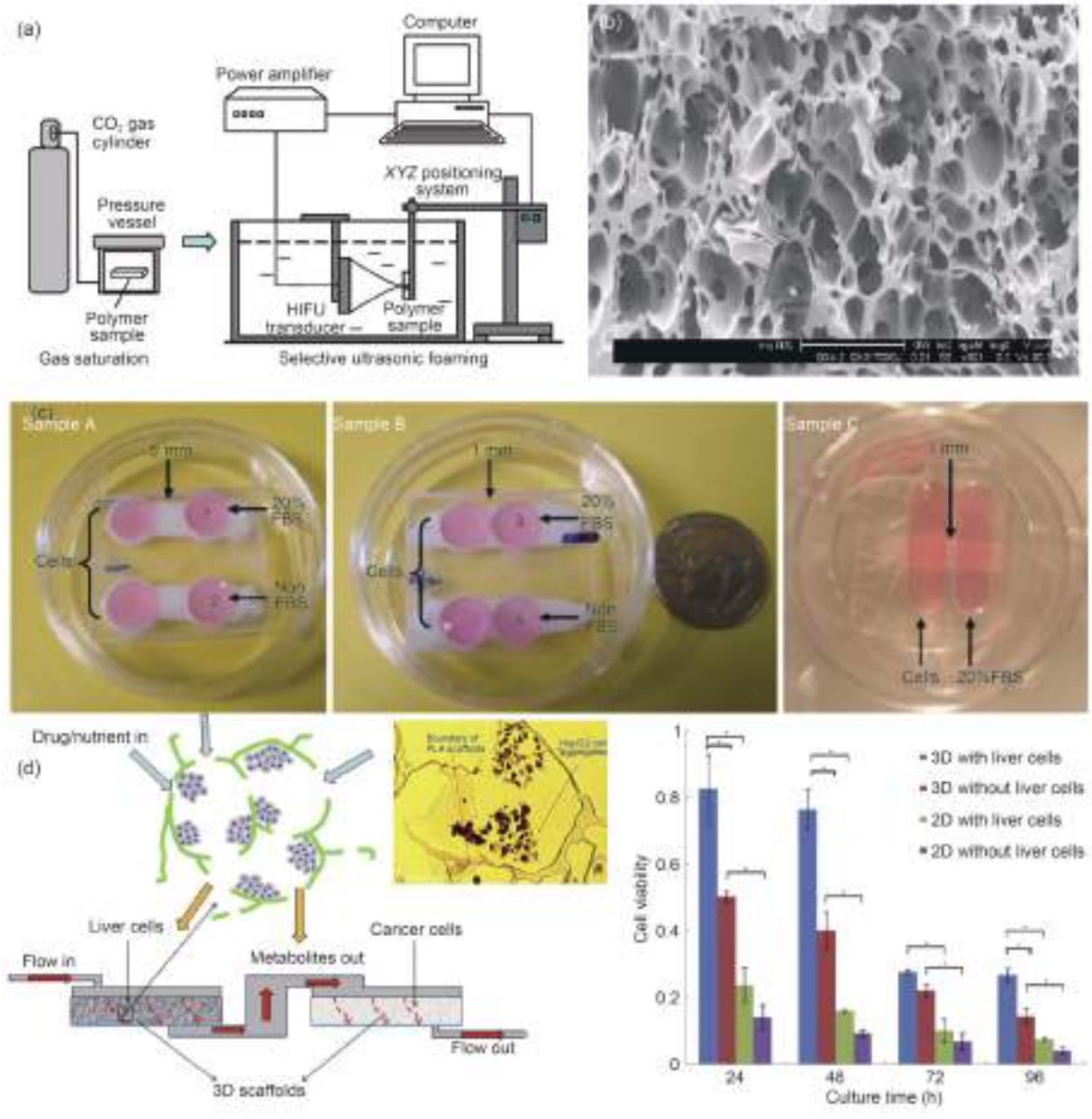

Fig. 50 Porous polymer fabrication and chip-based cell culture platforms. (a) The setup of the selective ultrasonic foaming process (reproduced from [615]). (b) The scanning electron microscopy (SEM) image of an open-celled polymethyl methacrylate specimen (scale bar: 200 μm). Reproduced from [607], with permission from the American Society of Mechanical Engineers. (c) 3D porous cell migration biochip samples (reproduced from [608], with permission from Springer Science Business Media, LLC). (d) Porous polymer chip used for the study of liver and cancer cells (reproduced from [609], with permission from Elsevier Ltd.)

and enabling strategies for fabricating complex regenerative constructs.

5.2.1 Integrated tissue and organ bioprinting for anatomical recreation

The team at the Wake Forest Institute for Regenerative Medicine has developed the integrated tissue–organ printer (ITOP), enabling the simultaneous deposition of multiple components, including cells, biomaterials, and bioactive molecules, to generate structurally stable and biologically relevant tissue constructs [75]. The system combines a mechanically supportive polymeric framework with precisely positioned cells, allowing the recreation of native tissue architecture. In 2016, ITOP was successfully applied to generate human-scale tissue constructs, marking a significant advance toward clinical translation [75]. Since then, ITOP has been employed to engineer a wide range of tissues, including shape-defined structures such as bone [618, 619], cartilage [75], and skin [76]; hollow organs such as blood

vessels [620], urethras [621], and tracheas [622, 623]; organized tissues, including skeletal muscle [624, 625], innervated muscle [626], and cardiac muscle [627]; composite tissues such as osteochondral (bone cartilage) and musculotendinous (muscle-tendon) [562] constructs; and even whole organs, including the kidney [628, 629] and liver [630] (Fig. 51). This platform allows precise control over tissue shape, cellular organization, and integration, offering unprecedented opportunities for complex tissue engineering.

As bioprinting is increasingly applied to a wider range of tissues and organs, the demand for advanced bioink systems continues to grow. These systems must provide high-resolution fidelity, mechanical stability, and tissue-specific functionality [616]. To accelerate bioink development, the research team at the Wake Forest Institute for Regenerative Medicine has previously established a quantitative bioink artifact designed to assess printability and elucidate the relationship between rheological properties and printing outcomes [631–634]. This framework enables predictable performance during bioprinting and supports reproducible fabrication, which is critical for translational research and eventual commercialization of bioprinted tissues. To recapitulate tissue-specific microenvironments, they have developed bioinks incorporating growth factor-mimetic peptide tethering [635] as well as decellularized ECM-derived components [621, 628, 629, 636]. These formulations closely mimic in vivo conditions, delivering essential biochemical cues that promote cell survival, engraftment, and functional maturation.

From a clinical perspective, a comprehensive bioprinting workflow begins with patient-specific medical imaging, progresses through computer-aided design/computer-aided manufacturing (CAD/CAM)-based tissue design, and culminates in the automated fabrication of 3D constructs that replicate native tissue architecture [573]. This workflow has been

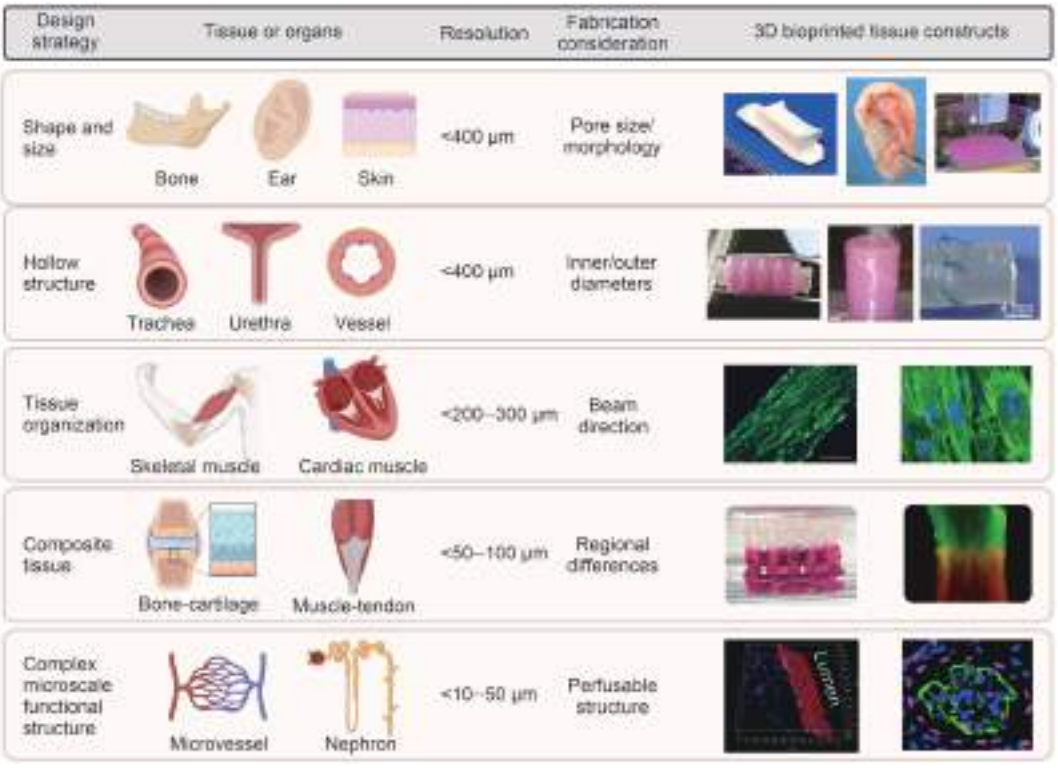

Fig. 51 Wake Forest Institute for Regenerative Medicine (WFIRM) bioprinting applications. 3D bioprinting technology enables the creation of constructs of various shapes and sizes, including human-scale bone (reproduced from [74], with permission from Wiley-VCH GmbH), ear cartilage (reproduced from [75], with permission from Springer Nature America, Inc.), and multilayered skin (reproduced from [76], under exclusive licence to the American Association for the Advancement of Science), as well as hollow tubular structures such as the trachea (reproduced from [623], with permission from Elsevier Ltd.), urethra (reproduced from [621], with permission from Acta Materialia Inc.), and blood vessels (reproduced from [620], with permission from IOP Publishing Ltd.). At the tissue organization level, precise cellular alignment is achievable, particularly in the construction of skeletal tissue (reproduced from [75], with permission from Springer Nature America, Inc.) and cardiac muscle (reproduced from [74], with permission from Wiley-VCH GmbH). Further innovation extends to the fabrication of composite tissues, including the osteochondral (bone cartilage) structure (reproduced from [74], with permission from Wiley-VCH GmbH) and the musculotendinous (muscle tendon) structure (reproduced from [628], with permission from IOP Publishing Ltd.). As the field progresses, the integration of functional inner structures, including vascularization (reproduced from [630], licensed under CC BY-NC) and functional units (reproduced from [638], licensed under CC BY-NC), is becoming increasingly essential to meet the demands of whole organ bioprinting

applied to diverse tissues and organs, enabling the reproducible generation of anatomically precise constructs suitable for preclinical evaluation and, ultimately, therapeutic application [75, 618, 619]. By integrating advanced bioinks, standardized processes, precise tissue design, and artificial intelligence (AI) -driven optimization, bioprinting platforms can address the multifaceted challenges of regenerative medicine, paving the way for patient-specific tissue therapies and functional organ replacement [74, 637]. Continued innovation in bioink development [638], workflow standardization, and AI integration will be essential to fully realize the translational potential of 3D bioprinting, thereby accelerating the path toward clinical adoption of regenerative therapies.

5.2.2 Bone

The regeneration of large bone defects in vivo is a complex process that requires the coordination of numerous cell types to enable vascularization, innervation, immune cell infiltration, and bone ECM deposition and mineralization, especially in the craniofacial region. For large gaps in the skeleton, the standard-of-care treatment for a critical size or larger is either an autologous bone graft or an inert, often metallic, replacement device. Both types of devices require at least 2 months of immobilization and have a number of associated complications, including donor site deficit, pain, and morbidity. Current metallic skeletal fixation or replacement devices may lead to stress shielding-induced bone loss and/or stress concentration-induced device failure. The research highlighted in this section is focused on biofabrication and biomanufacturing approaches that facilitate enhanced regeneration of bone defects.

5.2.2.1 Biofabrication for craniofacial bone regeneration

The Grayson laboratory at Johns Hopkins University has focused on multifunctional biomaterials designed to facilitate craniofacial bone regeneration. 3D-printed composite materials are advantageous as the individual components may target distinct elements of the regenerative cascade. Prior studies demonstrated that a PCL base is advantageous for FDM printing, given its low melting point, biodegradability, clearance from the body, and amenability to forming composites. Porous PCL scaffolds can also be 3D-printed with good mechanical integrity and anatomic fidelity to reconstruct geometrically complex facial bones [617].

Decellularized bone (DCB) has been used clinically for dental applications and can be shaped into porous scaffolds for bone regeneration. PCL-DCB composite scaffolds [639–641] have been used to successfully regenerate bone injuries in pigs [642, 643]. The gross geometry of each scaffold used to treat 2 cm full-thickness, bilateral injuries in the zygoma was customized based on CT images of each pig. A point-of-care surgical process has been adopted to mimic the proposed clinical scenarios for personalized treatments. PCL-DCB tabs were used to affix the scaffolds to the adjacent bone and CT imaging over the course of 1 year demonstrated bone regeneration in and around PCL-DCB scaffolds (Fig. 52a). Upon harvest, mechanical testing has demonstrated functional integration. Histologic assessment has revealed adequate vascularization and mild foreign-body response. Data at 1 year in this large preclinical model have strongly supported the potential for clinical application to human patients.

Calcium peroxide (CPO) also enhances bone regeneration capacity when blended with PCL to fabricate PCL-CPO composites [644]. CPO reacts with water to release oxygen. Prior studies demonstrated that oxygen-eluting scaffolds significantly enhanced mineral deposition in vivo [60]. PCL-CPO scaffolds provide sustained release of oxygen for more than 1 week, and scaffolds containing up to 25% by weight of CPO were made with good structural and mechanical integrity while also accelerating the degradation rates of the composites. While oxygen is not directly osteoinductive, PCL-CPO scaffolds stimulated enhanced osteogenesis following 3 weeks of in vitro culture and led to increased mineral deposition relative to PCL-only scaffolds after 8 weeks when placed in murine calvarial injuries in vivo.

Advanced imaging modalities [645–647] have provided useful tools to better understand the mechanisms by which biomaterial implants mediate de novo bone formation. Real-time multimodal imaging provides unique insight into the kinetics of vascularization that precedes mineral deposition. Vascular structure, saturated oxygen levels (Fig. 52b), and relative blood flow data can be correlated with spatial patterns of mineral deposition, and the data are ultimately used to guide scaffold design [648]. Alternatively, end-point fluorescent light sheet and micro-CT images reveal the intricate interplay between the vasculature (Fig. 52c) [644] and minerals (Fig. 52d) [642, 643], and the biomaterial implant. Imaging data will ultimately feed into design considerations, leading to additional composites and fabrication techniques to biomanufacture scaffolds with greater functionality and versatility.

5.2.2.2 Inductive materials for bone regenerative engineering

In bone critical size defects, autografts from patients remain the gold standard, followed by allografts from donors, yet challenges, including donor site morbidity, limited supply, secondary infection, and immune complications, create a clear need for alternative ways to tissue regeneration [650]. Regenerative engineering, a field developed by the Laurencin laboratory, now at the University of Connecticut [651–656],

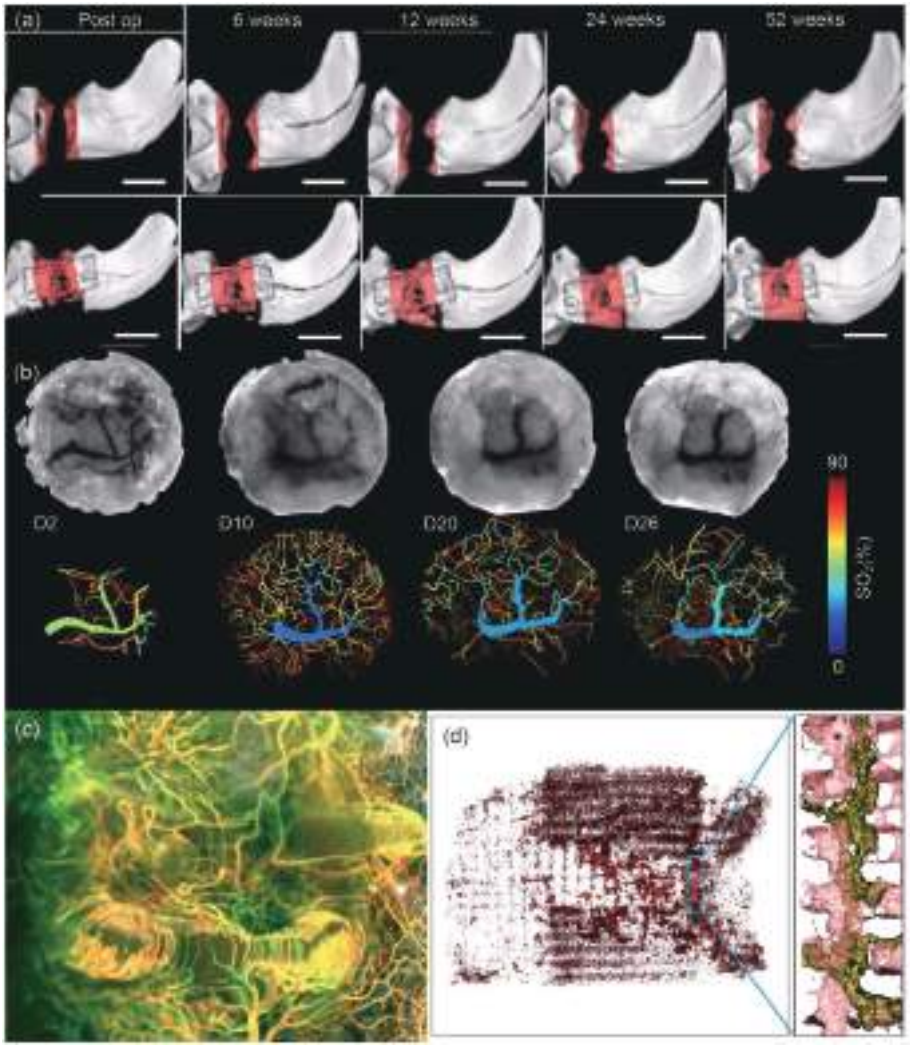

Fig. 52 3D-printed scaffolds for craniofacial bone regeneration. (a) Time course of bone healing in untreated (top) or PCL-DCB-treated (bottom) 2 cm full-thickness zygoma injury in skeletally mature Yucatan minipigs over 1 year. (b) Multimodal real-time imaging in skull injury in a mouse over 26 days, showing vascular structure and bone healing (top) and corresponding intravascular saturated oxygen levels. (c) Light sheet microscope image of blood vessels in a murine skull defect growing in the pore spaces and around PCL-CPO struts. (d) Micro-CT image of spatial patterns of mineral deposition relative to scaffolds implanted in the midface of minipigs. (a, d) are reproduced from [642], licensed under CC BY-NC-ND; (b) is reproduced from [649], with permission from Elsevier Inc.; (c) is reproduced from [644], with permission from Acta Materialia Inc.

has potential solutions for addressing these issues by integrating materials science, stem cell biology, and clinical translation to regenerate complex tissues. Recent work toward addressing these needs in the Laurencin laboratory has focused on the use of inductive materials for osseous regenerative engineering, a class of materials that includes polymers, calcium phosphate ceramics, metals, and graphene-family materials [657]. They have recently incorporated inductive materials such as graphene oxide [658], calcium phosphate graphene [8, 659], and magnesium phosphate graphene [61], as well as small-molecule forskolin [660], into their matrices, all of which have demonstrated the ability to significantly impact osteogenic differentiation and the potential to heal critical-size bone defects.

5.2.2.3 Novel methods for bone tissue function and mechanical property regenerative medicine

The Dean laboratory at the University of Wisconsin-Madison has studied novel biofabrication strategies for bone and vascular tissue engineering as well as novel design strategies for personalized skeletal graft, graft fixation, or replacement device geometry, materials, and location, with an emphasis on novel point-of-care manufacturing processes.

Together with the Becker laboratory at Duke University, the Dean laboratory has studied the utility of tethering (conjugating) growth factor ligands (i.e., cell-signaling peptides) to the surface of 3D-printed poly(propylene fumarate-co-propylene succinate) tissue-engineered bone grafts [661]. To

provide immediate perfusion to those grafts, the Dean laboratory is collaborating with the laboratory of Grissel Trujillo-de Santiago and Mario Alvarez at Tecnológico de Monterrey (Monterrey, Mexico) to conjugate ligands in chaotic printed [662] hydrogels to produce microvasculature appendage sheets (MASs). These MASs have internal channels formed using a fugitive hydrogel, hydroxyethyl cellulose. This results in channels as thin as the smallest arteries (150 μm) that then rapidly branch to capillary size and diameter (i.e., 10–30 μm diameter) (Figs. 53a and 53b) [663]. The Dean laboratory envelopes MAS with resorbable, woven, 10–50 μm in diameter, polymer microfibers produced by MEW [664]. In summer 2025, the Dean laboratory and the Dalton laboratory at the University of Oregon, sponsored by the National Science Foundation (NSF)-supported HAMMER Engineering Research Center, trained graduate students and postdoctoral researchers to design MEW weaves, program those designs in G code, and print them using an open-source MEW machine that they built for less than $4000 U.S. [665]. For perspective, commercial MEW machines cost $150,000 U.S. or more.

Once placed, bone grafts are typically immobilized by a metallic (e.g., Grade 23 Ti6Al4V) skeletal fixation device. Graft healing is intended to restore load-bearing competence.

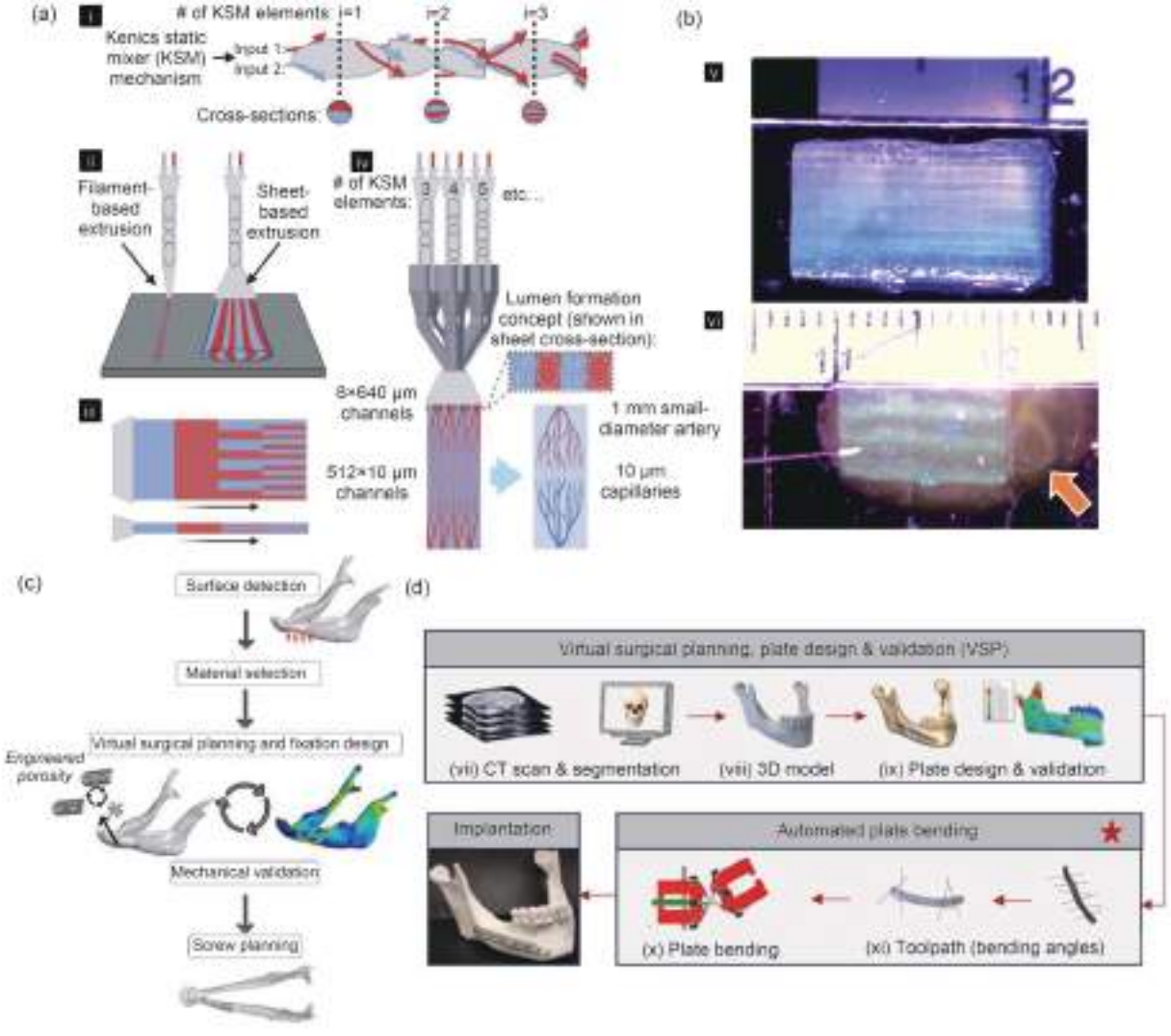

Fig. 53 Biofabrication for microvasculature and patient-specific skeletal repair. (a) Biofabrication of microvasculature. Kenics static mixer (KSM) can create microchannel layers as thin as a single cell thick (i) in a filament or a sheet (ii). (iii) Microchannels formed from fugitive hydrogels can be evacuated and used to provide vascular perfusion. (iv) Multiple KSMs can be arrayed to produce rapidly branching channels that can be as thin as an arteriole or a capillary. (b) (v) A MEW fiber net is used to hold and implant the MAS. (vi) Fluorescent dye injected (on the right) into rapidly branching channels that release a diffuse (i.e., perfusing) flow at the other side of the MAS (right). Reproduced from [663], licensed under CC BY 4.0. (c) The steps needed to plan the properties of this personalized mandibular fixation plate (reproduced from [666], with permission from Acta Materialia Inc.). (d) (vii) Skeletal repair virtual surgical planning begins with segmentation of relevant anatomy to obtain (viii) a digital model used to design the plate (ix) shape and function. (x) An off-the-shelf plate can be robotically bent to match that optimal design at the point of care following the (xi) bending angles determined. Reproduced from [670], licensed under CC BY-NC-ND

To avoid stress shielding or concentration, it is important that fixation hardware does not interrupt the normal loading pattern [666]. The Dean group has studied the use of personalization to optimize skeletal fixation size, shape, location, and material properties, especially in areas under the highest loads, such as the jaws [62] and lower limbs [667]. In collaboration with the Elahinia Laboratory at the University of Toledo, the Dean group conducted an in vivo sheep model study (Fig. 53c) of personalized, 3D printed, superelastic NiTi mandibular graft fixation hardware [668]. Separately, the Dean laboratory and Luo laboratory at The Ohio State University have also developed a magnesium-based alloy for skeletal fixation devices that is intended to resorb once the reconstructed bone has healed [669]. Finally, the Dean laboratory collaborated with the Hoelzle laboratory at Ohio State University on point-of-care manufacturing strategies to robotically bend off-the-shelf, metallic skeletal fixation devices (Fig. 53d) [670, 671].

5.2.2.4 Intraoperative bioprinting (IOB)

IOB, also known as in vivo or in situ bioprinting, is an effective process, in which defect information can be rapidly acquired via 3D scanning and then repaired by bioprinting, which reduces manual interventions such as culturing bioprinted constructs or modifying prefabricated constructs to conform to defect shapes [672, 673]. The Ozbolat laboratory at Penn State University has made considerable contributions in the context of IOB. For example, IOB for hard and soft tissues in a stratified manner precisely to repair composite bone/skin defects in rats has been demonstrated for the first time in the literature [674]. More recently, genetic engineering has been utilized to advance the regeneration of intraoperatively bioprinted bone. In this regard, controlled release of BMP-2 and platelet-derived growth factor (PDGF) encoding bioprinted plasmid DNA (pBMP-2 and pPDGF, respectively) enabled improved bone regeneration in rat calvarial defects [675]. In another study, the delivery of pBMP-2 in situ was more effective than transfecting progenitors ex situ and then bioprinting them intraoperatively in bone regeneration [676]. The Ozbolat laboratory has also demonstrated adipose-derived extracellular matrix (ad-ECM) from human liposuction surgeries as a bioink with de novo adipogenic properties that supports the differentiation of progenitors into adipocytes, which has enabled the reconstruction of the adipose layer of skin in calvarial areas in rats and supported hair follicle downgrowth when the ad-ECM was cobioprinted with adipose-derived stem cells into the skin defects intraoperatively [677]. Despite the attempts made by the Ozbolat laboratory and other researchers, the viability of IOB-generated thick tissues heavily depends on effective vascularization. In this regard, IOB has been recently integrated with a microsurgery technique, called "micropuncture (MP)," for rapid and effective vascularization of intraoperatively bioprinted thick tissue constructs (Fig. 54a1) [678] along with the successful execution of IOB (Figs. 54a2 and 54b) in both small and large animal models [9], validating the translation potential of IOB for automated surgical interventions. Overall, IOB is unique in the clinical realm and is expected to have a significant impact on the reconstructive algorithm for challenging clinical dilemmas.

5.2.3 Skin

5.2.3.1 Bioprinting for bone and skin tissue engineering

The Leu group at the Missouri University of Science and Technology has investigated 3D-printed dressings using clinically relevant hydrogels for wound healing, particularly for healing of deep partial-thickness burn wounds, notably second-degree burn wounds [63]. Different ratios of gelatin and alginate mixtures have been printed and examined in terms of rheological and mechanical properties, degradation rate, and hydration activity to tune the hydrogel composition for the best functionality. The cell-laden dressings were bioprinted to evaluate the effect of the gelatin: alginate ratio on the proliferation and growth of human dermal fibroblasts. Their findings confirmed that higher alginate content is associated with higher viscosity and Young's modulus, while higher gelatin content is associated with faster degradation and higher cell viability. Since prolonged healing, pain, and traumatic removal due to the lack of long-term wound hydration are some of the main challenges in the treatment of second-degree burn wounds, they have fabricated 3D-printed dressings with gelatin, alginate, and BBG, and characterized their mechanical properties, degradation rate, hydration activity, and in vitro cell viability [679]. The in vivo wound healing functionality of the dressings was investigated with histological analysis, using a rat model with a second-degree burn wound. The animal study has shown that the printed dressings with BBG exhibited faster wound closure, nonadhesive contact, noninvasive debridement, and nontraumatic dressing removal. Additionally, histological analysis results have demonstrated that printed dressings contributed to more uniform re-epithelialization and tissue remodeling compared to nonprinted hydrogels of the same compositions.

5.2.4 Others

Outside of the discussed categories, many notable advancements have been made in engineered constructs intended for in vivo use. Highlights in this section are some notable developments in the application of biomanufacturing and biofabrication methods for in vivo construct use.

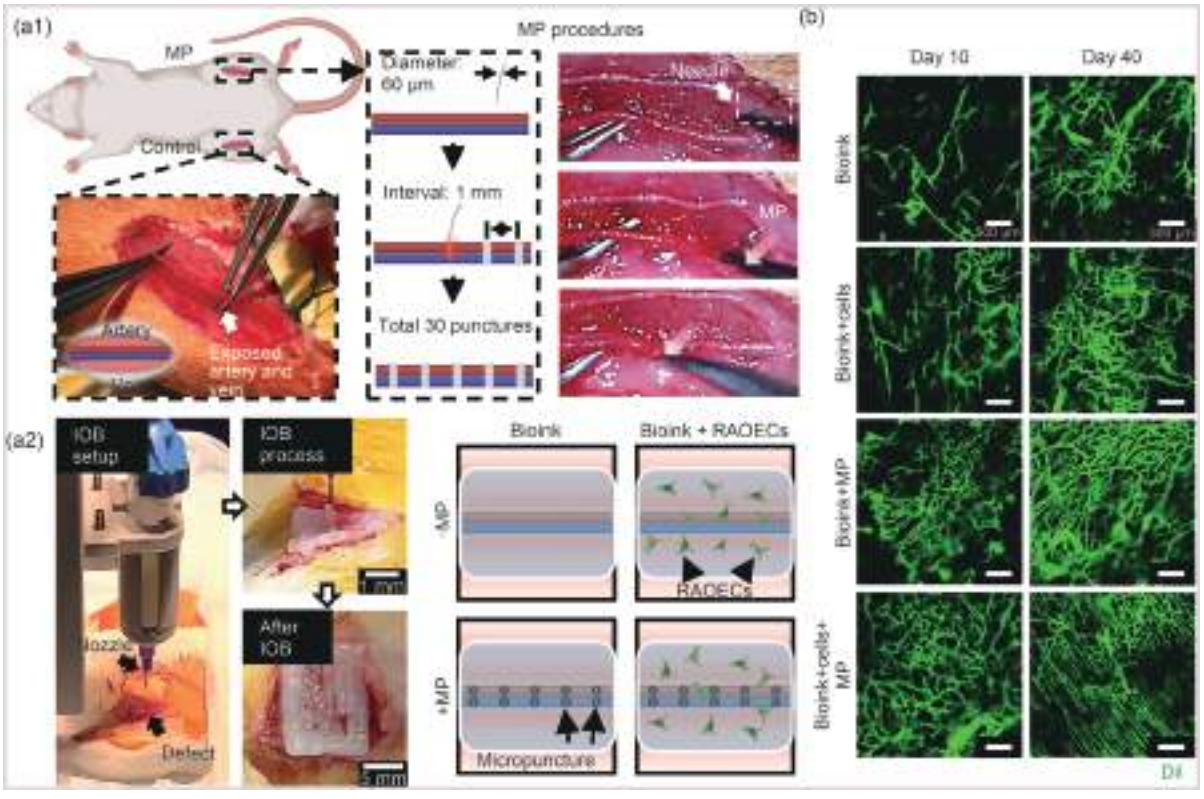

Fig. 54 Integration of micropuncture and IOB. (a1) Micropuncture was performed on the right femoral artery and vein of rats using a 60-μm microneedle at 1-mm intervals. (a2) IOB of a collagen-based bioink loaded with or without rat ECs. The presence of MPs and cells yielded four different groups including (i) Bioink, (ii) Bioink+cells, (iii) Bioink+MP, and (iv) Bioink+cells+MP. (b) Evaluation of vascularization via fluorescence angiography taken of whole-mount constructs. Reproduced from [678], with permission from Elsevier Ltd.

5.2.4.1 3D bioprinting of complex tissues for regenerative medicine

The Fisher laboratory at the University of Maryland utilizes bioprinting and bioreactors to create in vitro models or implants, focusing on bone, cartilage, vascular, soft tissue, placenta, and thin-membranous tissues, to study biological functions, disease progression, wound healing, and organ development.

This laboratory has employed bioprinting to engineer a wide range of clinically relevant tissue constructs, from soft tissues such as the nipple-areolar complex (Fig. 55a) [64], periosteum, and placental barrier, to vascular grafts and musculoskeletal tissues such as bone and cartilage (Fig. 55b) [64, 680–686]. To support vascularized bone regeneration, they have developed a toolbox for the design, characterization, and evaluation of 3D-printed scaffolds, combining modular design, nondestructive scaffold evaluation, biocompatibility, and mechanical testing and in silico modeling to predict host vessel integration [64, 680–687].

To model the placental barrier, they bioprinted a cylindrical GelMA hydrogel scaffold loaded with relevant placental cells, ECM components, and growth factors at defined radial positions. This has allowed them to study trophoblast and stem cell migration, maternal-fetal transport, and pathologies such as preeclampsia (Fig. 55c) [683, 686]. In vascular tissue engineering, they have fabricated fully printed, biodegradable grafts using poly(propylene fumarate) resins and DLP stereolithography, enabling patient-specific customization, controlled microscale architecture, and demonstrating in vivo functionality (Fig. 55d) [684].

For soft tissue reconstruction, they developed a hybrid printing strategy combining degradable bioinks, such as GelMA, with a nondegradable methylcellulose and poly(ethylene) glycol (MC-PEG) network to fabricate stable, biomimetic constructs that support tissue integration and maintain structural integrity [681, 682]. To advance musculoskeletal tissue engineering, they have combined computational modeling with extrusion-based printing to create biphasic osteochondral units with mechanically robust interfaces and layer-specific biomechanical properties [687].

To address the challenge of fabricating thin membranous tissues (Fig. 55e), they have implemented an innovative 4D extrusion-based bioprinting strategy that leverages post-printing contraction to produce a biomimetic, multilayered periosteum with precise architecture and controlled thickness, overcoming the limitations of traditional approaches [681, 688]. Across all tissue types, the Fisher laboratory integrates hybrid and multimaterial printing,

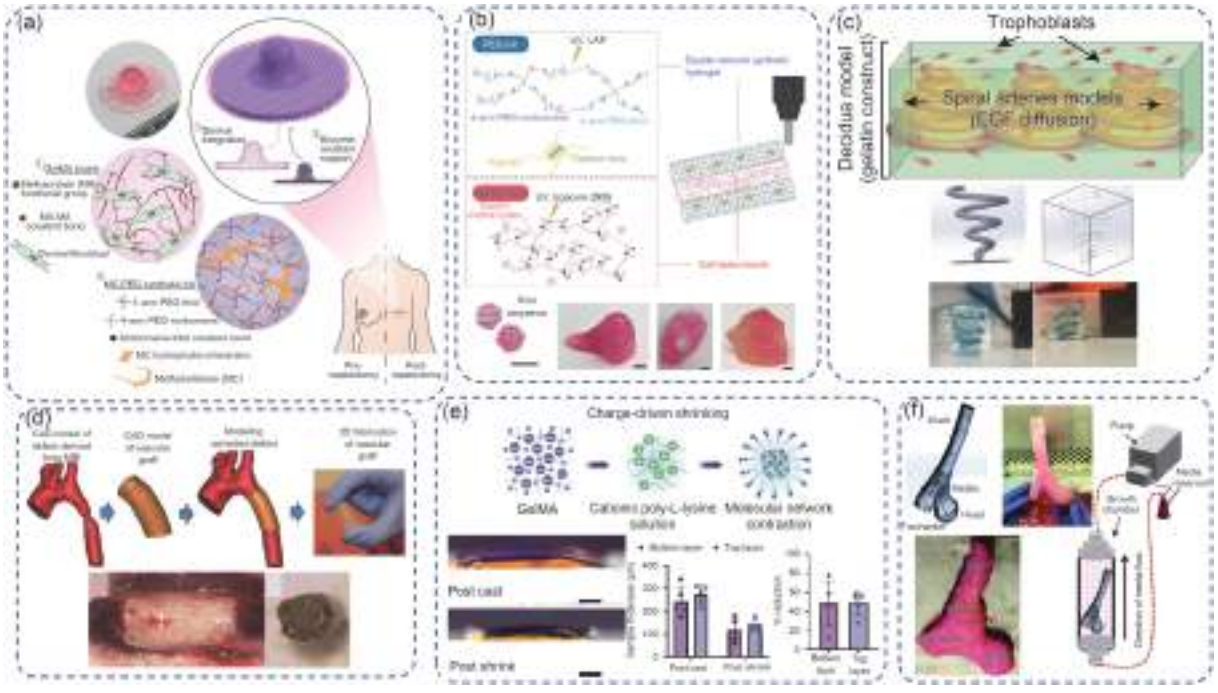

Fig. 55 Biofabricating complex tissues for regenerative medicine. (a) Hybrid nipple-areola scaffolds are created by coprinting GelMA and MC-PEG bioinks (reproduced from [64], with permission from Wiley-VCH GmbH). (b) Additional hybrid constructs are generated by printing PEG and GelMA bioinks into complex architectures, including nose, ear, and thyroid cartilage constructs (reproduced from [682], with permission from WILEY-VCH Verlag GmbH & Co. KGaA, Weinheim). (c) Spiral microchannel structures printed as embedded spirals within transparent support matrices (reproduced from [683], with permission from the American Chemical Society). (d) Patient-specific vascular grafts are generated, CAD-refined, then DLP-printed and evaluated for fibrosis after implantation (reproduced from [684], with permission from WILEY-VCH Verlag GmbH & Co. KGaA, Weinheim). (e) Charge-based shrinking of GelMA allows for the printing of thin membranous tissues (reproduced from [681], with permission from Wiley-VCH GmbH). (f) Large-scale bone graft fabrication demonstration, including CAD design of the mold, filling with alginate-encapsulated hMSC, culture in a perfusion bioreactor, and the resulting anatomical femur construct (reproduced from [690], with permission from Mary Ann Liebert, Inc.)

precise architectural control, and the incorporation of physical and chemical gradients to produce constructs with enhanced cellular responses, tissue integration, and translational potential for regenerative medicine, disease modeling, and patient-specific therapies.

Perfusion bioreactors are valuable tools for culturing in vitro tissue-engineered constructs, as they enable improved control of oxygen and shear stress, thereby promoting cellular growth and differentiation. Using stereolithography, the Fisher laboratory has manufactured custom-designed bioreactors to advance research across a variety of topics, including bone regeneration and extracellular vesicle production (Fig. 55f). They have developed a tubular perfusion system that promotes osteoblastic differentiation of mesenchymal stem cells cultured in alginate [689, 690], collagen [691], and biphasic calcium phosphate zirconia scaffolds [692]. They utilized a tubular perfusion system bioreactor design to culture MSC-laden poly(lactic-co-glycolic acid)/poly(ε-caprolactone) scaffolds that promoted in vivo bone regeneration compared to static and acellular constructs [693]. Additionally, they developed a large-scale tubular perfusion system bioreactor and successfully cultured a construct the size of a human femur, demonstrating proof of concept for full-scale bone engineering [690]. Recently, the laboratory has designed bioreactor systems to enhance mesenchymal stem cell extracellular vesicle production via mechanical confinement, resulting in a 40- to 80-fold increase over conventional cell culture [694]. The extracellular vesicles exhibited strong wound-healing capacity, opening the door to good manufacturing practice (GMP)-compliant, scalable production of extracellular vesicle therapeutics.

The Fisher laboratory has developed biofabrication strategies using 3D bioprinting and perfusion bioreactors to address challenges in both soft and hard tissues. Together, these innovations advance the development of translational implants and in vitro functional models. Moving forward, the laboratory plans to use its biofabrication tools to build GMP-grade nipple-areolar complexes, disease models of the placental barrier, and bioreactor-based kidney tissue models.

5.3 Clinical and commercial translational successes

Clinical and commercial translation is the critical test of biofabrication and biomedical manufacturing, requiring that

laboratory innovations mature into robust, scalable, and regulatory-aligned products that deliver measurable clinical or societal value. Key challenges in this area include integrating biofabrication technologies into regulatory frameworks and ensuring consistency and quality in the resulting products, especially at the manufacturing process scale. This subsection highlights representative U.S. translational successes, including medical devices and interventional cardiovascular technologies [65, 695, 696], 3D-printed resorbable implants and advanced scaffold architectures, including emerging shape-memory/4D printing strategies and tissue-mimicking materials [697–699] that support biofabricated consumer bioproducts such as engineered leather and cultivated meat that demonstrate manufacturing scale-up beyond traditional biomedical markets [700], to name a few. These examples illustrate how the U.S. efforts are moving from proof-of-concept demonstrations toward validated products supported by manufacturability, quality systems, and adoption pathways.

5.3.1 Medical device and impacts on healthcare: interventional neurocardiovascular devices

Interventional neurocardiovascular devices use blood vessels as corridors to access the brain, lung, heart, kidney, liver, extremities, and others for minimally invasive diagnosis or treatment of conditions without major surgery. Guidewire, catheter, balloon, stent, and driveshaft are major components of interventional devices, which are inserted through small incisions in the wrist or groin and guided to the target area using medical imaging. The first interventional procedure was performed by a German physician, Werner Forssmann, in 1929 by inserting a catheter via the vein in his arm to his heart. In the 1960s, coaxial guidewires and catheters were invented, and the first procedure in a patient to restore blood flow in the leg was performed. Coronary balloon angioplasty was invented in the 1970s to restore blood flow in the heart; rotational atherectomy was invented in the 1980s to remove hardened calcified plaques, transcatheter aortic valve replacement was first performed in an animal lab in 1989 and commercialized in 2013, and mechanical thrombectomy to remove brain clots for stroke treatment was invented in the 1990s. These inventions have a significant impact on human health.

In the 2010s, the Shih laboratory at the University of Michigan investigated the fundamentals of diamond grinding of calcified plaque within blood vessels, as shown in Fig. 56a [65, 695, 696, 701–705]. A small, high-speed, rotating diamond wheel, driven by a motor located outside the body via a driveshaft, orbits the vessel due to the fluid force providing the pressure to lift and support the orbital motion [701]. Based on this observation, a two-phase atherectomy device was proposed. A small diamond wheel first penetrates a hole in the calcified plaque in the coronary or popliteal artery and then enlarges using this orbiting motion [696, 702, 703]. A small wheel has less force and heat build-up, which is safer for patients due to clot generation. This research has laid the foundation for research on interventional devices.

Based on this concept, the innovation continues to cut and remove blood clots [65, 706–715]. Due to the thin vessel

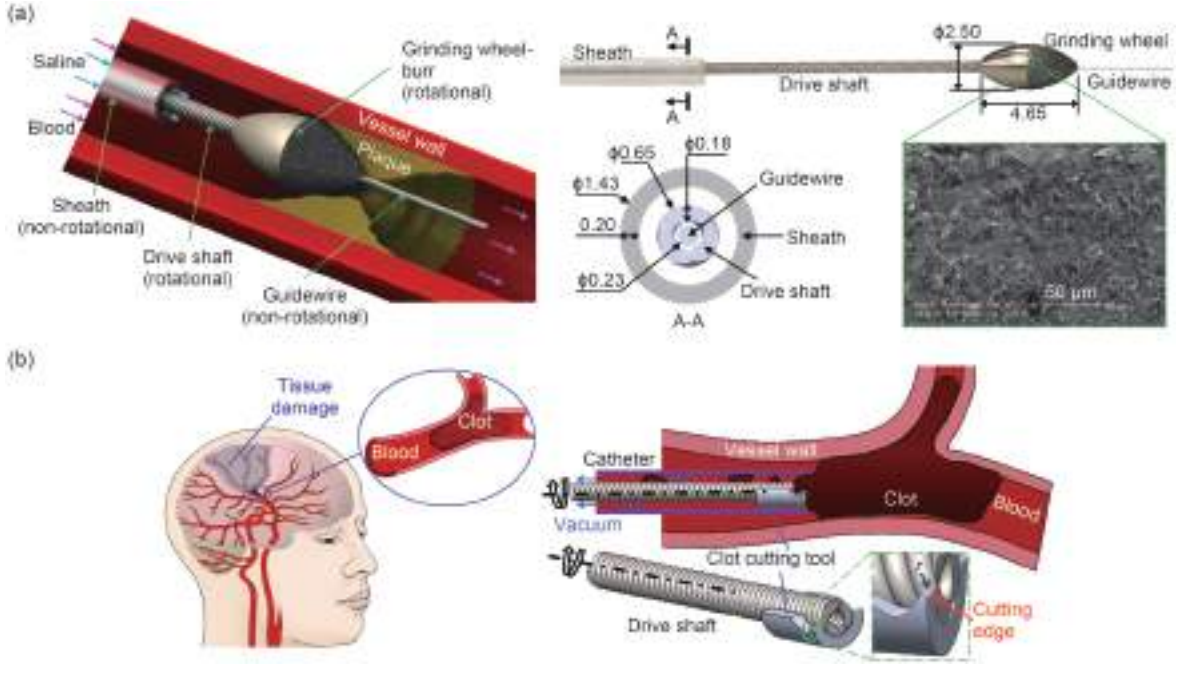

Fig. 56 Interventional neurocardiovascular devices. (a) Device developed for atherectomy (reproduced from [696], with permission from CIRP). (b) Device developed for thrombectomy (reproduced from [706], with permission from CIRP)

walls in the brain and lungs, the cutting tool is inside the tip of the catheter. The soft clot (Fig. 56b) is deformed by vacuum suction and cut into small pieces, which are removed by the vacuum outside the body. This cutting-based interventional thrombectomy device is for the treatment of stroke and pulmonary embolism. A startup, Endovascular Engineering, has been established and has completed a clinical trial to treat pulmonary embolism.

Another interventional device idea is to oscillate the pressure inside the balloon to fracture and expand calcified plaque blockages in the knee and coronary arteries. The pressure from the carbon dioxide canister is converted into short, high-peak hydraulic pressure waves, which travel from outside of the body via a small catheter to the balloon and calcified plaques that have many microcracks as a source for stress concentration [715]. Amplitude Vascular Systems was a startup (acquired by Stryker in 2026) based on this intravascular lithotripsy technique and completed a clinical trial on calcified plaque in the knee.

5.3.2 Clinical translation of 3D-printed resorbable implants, 4D printing shape memory PGD, 3D printing advanced scaffold architectures, and 3D printing tissue mimicking materials

The Hollister laboratory at the Georgia Institute of Technology aims to develop in vitro and in vivo implantable biologic systems for tissue reconstruction, diagnostics, and procedural planning, leveraging computational design and 3D biomaterial printing.

The Hollister laboratory has developed and robustly characterized a 3D-printed PCL resorbable airway splint for pediatric tracheobronchomalacia (Figs. 57a–57c), used in over 30 patients with improved clinical outcomes—restored airway patency, reduced ventilation dependence, and, in some cases, avoided tracheostomy altogether [697, 699, 716–721]. In porcine models (1–2 years), airway splint PCL degradation caused elastic stiffening, increased yield and failure stress, and reduced plastic strain (Fig. 57d), linked to molecular chain reorganization and hydrolytic embrittlement [722–724]. They further showed that the PCL starting form (pellets vs. powder) and printing modality (extrusion vs. laser sintering) significantly influence device properties—printability, elasticity, plasticity, degradation, and cell interactions [725]. Laser-sintered PCL produced bimodal porosity and permeability, enhancing cell survival and compliance for soft tissue regeneration [66]. Laser-sintering PCL also enabled the fabrication of complex architectures (Fig. 57e), including 3D auxetic [66, 726, 727] and topology-optimized architectures [728–730], which improved tissue regeneration in preclinical models [726, 729].

Another frontier is 4D printing—shape-changing devices using shape-memory materials supporting minimally invasive surgery. The Hollister laboratory has developed poly(glycerol dodecanedioate) (PGD), a photopolymerizable, 3D-printable (DLP, SLA, extrusion) bioresorbable elastomer for soft tissue reconstruction (Fig. 57f) [698, 721–739]. 4D-printed PGD demonstrated shape transformation post-implantation and strong tissue integration in animal models (Figs. 57g and 57h) [737].

Translation of 3D-printed reconstruction approaches requires robust models for bench, preclinical, and clinical trial testing. Realistic anatomical phantoms can be created using

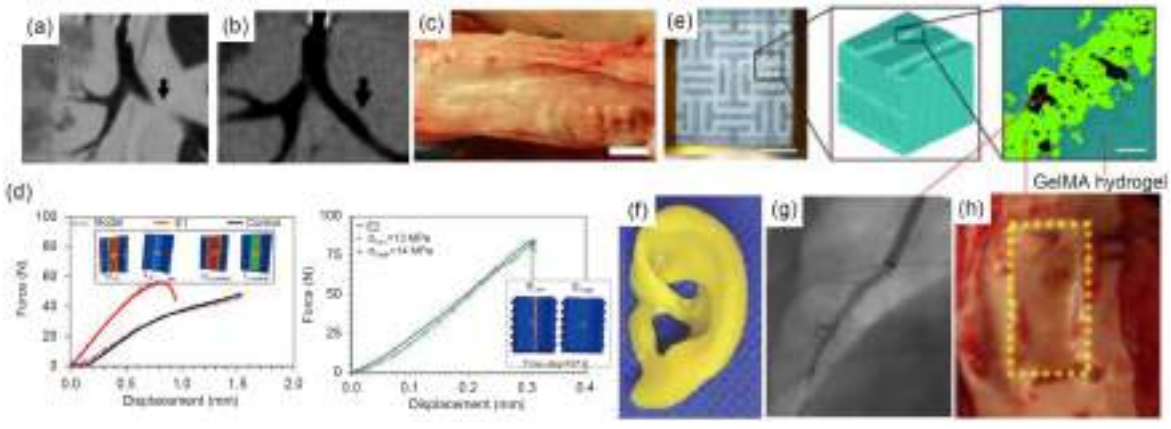

Fig. 57 Printing, preclinical, and clinical results with 3D- and 4D-printed materials. (a) Patient with malacic bronchial collapse presurgery. (b) Patient post implantation showing patent bronchi. (c) Implanted 3D-printed PCL splint after 2 years on porcine trachea. (d) Force–displacement testing of splint retrieved from porcine model showing initial plastic ductility after printing (left, solid black curve), stiffening and loss of plastic ductility (left, solid red curve) after 1 year, and complete brittleness with damaging behavior at 2 years (right). (e) Example laser-sintered PCL auxetic structure and resulting permeability at strut level. (f) DLP-printed PGD ear. (g) Delivery of the PGD device in the porcine model. (h) Resulting integration of the PGD device in the porcine arterial wall at 3 months. (a, b) are reproduced from [719], with permission from the American Association for the Advancement of Science; (c, d) are reproduced from [722], with permission from Elsevier Ltd.; (e) is reproduced from [66], with permission from Wiley-VCH GmbH; (f) is reproduced from [698], with permission from Elsevier Ltd.; (g, h) are reproduced from [737], with permission from Elsevier Ltd.

tissue-mimicking materials to enhance this testing. The Hollister laboratory has extensively characterized 3D-printed model materials and developed algorithms for optimal selection for mimicking tissue properties [740, 741]. In summary, 3D-printed biomaterials hold immense promise for clinical translation and tissue reconstruction. However, achieving this potential demands a rigorous understanding of input material properties, printing processes, and comprehensive testing of three-dimensional printing (3DP) constructs in vitro and in vivo.

5.3.3 Biomaterial vaccines

The Mooney laboratory at Harvard University has focused on the innovative use of biomaterials to investigate and modulate cell behavior on a number of different fronts. This group was one of the first to investigate 3D material interactions with cell fate and differentiation [742]. Their recent work has focused on immunomodulatory material fabrication and development. A recent study, representing the first clinical trial of a macroscale biomaterial-based vaccine, used a materials system developed by the Mooney laboratory for patient-specific treatment of metastatic melanoma [743]. The vaccine, dubbed WDVAX, is created using a poly(lactic-*co*-glycolic acid)-based scaffold with immunostimulatory components cytokine GM-CSF, CpG oligonucleotides, and autologous tumor lysate. The scaffold functions as a large, degradable, antigen-presenting structure capable of recruiting and activating dendritic cells to enhance antitumor response. Having previously been demonstrated to be effective in treating tumors in mice [744], these scaffolds have been applied to human trials and implanted subcutaneously in patients with metastatic melanoma. The WDVAX treatment was generally able to be manufactured in the target quantities for almost all patients in this small study, and the physical properties of the scaffolds were able to be manufactured with relative consistency. Although it is difficult to draw conclusions from a relatively small clinical trial, the data suggest that the vaccine was able to elicit $CD4^+$ T cell and innate immune system responses, and 43% of patients treated with the vaccine exhibited stable disease. Overall, this trial serves as both a milestone use of biomaterial vaccines as well as a promising cancer therapeutic option, especially if paired with other treatment modalities, such as checkpoint blockade.

5.3.4 Biofabricated leather and meat

Traditionally, the term biofabrication is used in the context of tissue engineering and regenerative medicine and refers to the generation of biologically functional products with living cells, bioactive molecules, and biomaterials as building blocks [17]. The Forgacs laboratory at the University of Missouri and companies launched around the ideas developed there have demonstrated that methods of biofabrication apply well beyond tissue engineering and regenerative medicine. The laboratory's academic activity in the early 2000s included the development of extrusion bioprinting [11, 745] that culminated in the launching of the company Organovo, Inc. [746], the first commercial entity in the bioprinting space. The company focused on the fabrication of physiologically relevant 3D human tissue models for drug development and testing (Fig. 58a) [747]. It was soon realized that leather and meat originating from two specific animal tissues could be produced by similar methods. This led to the founding of Modern Meadow, Inc. [748] in 2011 with the mission to produce leather and meat sustainably, without slaughter. They recognized that leather and meat, as consumer products, do not require the full complexity of the underlying skin and muscle tissue. Leather on a high level comprises only the collagen ECM, just one compartment of the hide of the animal. Unstructured meat products, such as hamburgers, dumplings, and sausages, can also be made using just components of full meat cuts, such as the muscle cellular biomass, without the need to engineer, e.g., bone.

By 2013, Modern Meadow successfully produced aesthetically appealing leather and edible meat products, notably the celebrated 'meat chip' (Fig. 58b) [749], but the economics did not work, especially for the latter category. The company abandoned working on cultivated meat in 2014 and kept focusing on biofabricated leather. The process has gone through several iterations [700] to arrive at Innovera, a truly transformative leather alternative [750]. Innovera is indistinguishable from animal-derived leather in regard to material properties, but contrary to leather, it can be produced sustainably and ethically through a process that produces no waste. Innovera's true success is demonstrated by the recent announcement that the car maker Mercedes will use it for the interior of its newest concept car (Fig. 58c) [10].

For cultivated meat, the number of companies started massively growing soon after Modern Meadow stopped its activity in the space. Realizing the value of the earlier lessons, in 2018 the project was reignited by some of the Modern Meadow researchers through a new company, Fork & Good, Inc. [77], to focus on pork products (Fig. 58d). Making cultivated meat economically at scale is truly challenging. It requires an approach that is not orthogonal to that practiced by the pharmaceutical industry, except that the price points are totally different. Whereas pharma can charge practically any price for its products, cultivated meat needs to compete with the 'Walmart' price of meat. To be successful in this endeavor requires serious innovations in multiple disciplines, such as cell line development, cell culture medium production, and bioprocessing. For this reason, cultivated meat represents one of the latest and most exciting developments in biofabrication.

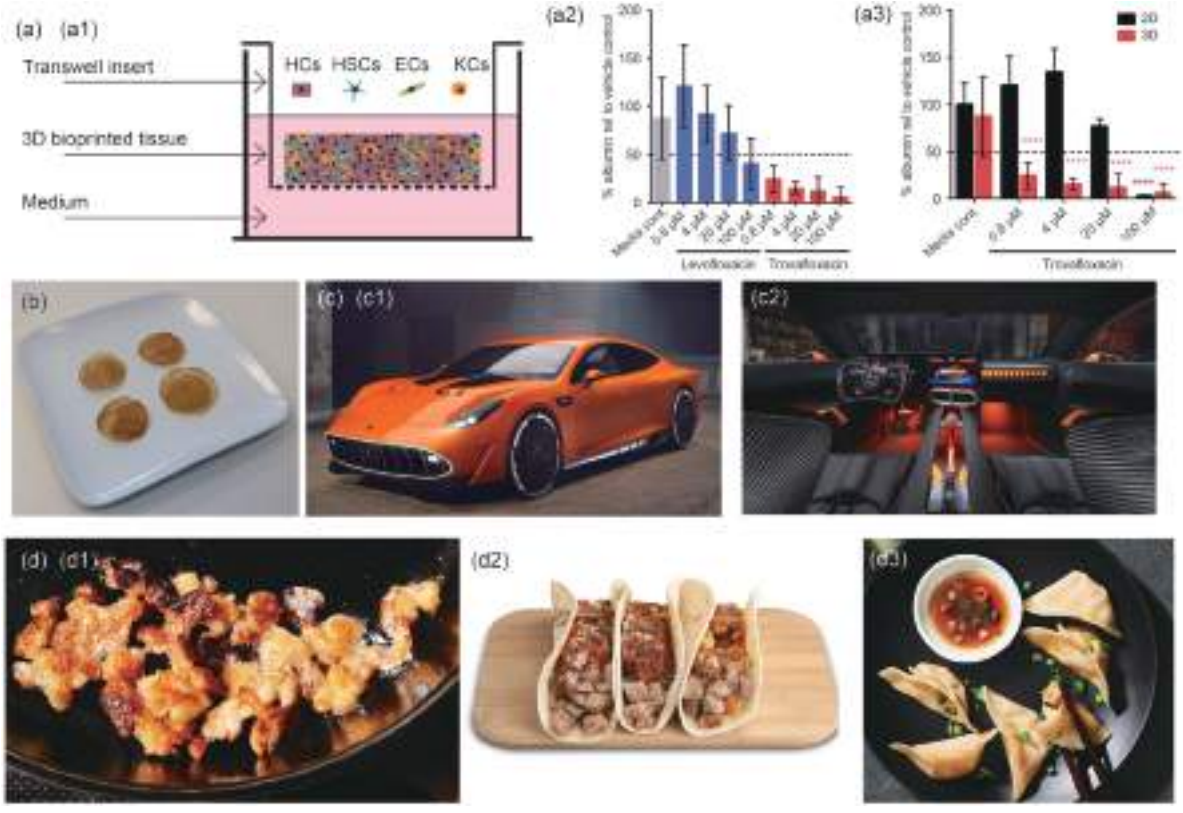

Fig. 58 Translational and commercial successes in biofabrication and biomedical manufacturing. (a) Bioprinted 3D models are physiologically relevant: (a1) schematic of a transwell assay with Organovo's 3D-printed human liver construct (HC: human hepatocyte; HSC: hepatic stellate cell; EC: endothelial cell; KC: Kupffer cell); (a2) measurement of secreted albumin in the supernatant of 3D liver tissues treated with two chemically similar antibiotics, showing that Trovafloxacin is hepatotoxic, whereas Levofloxacin is not; (a3) levels of albumin in 3D liver tissues and standard 2D hepatocyte cultures treated with Trovafloxacin (whereas the 2D cultures do not show toxicity, the 3D cultures do at elevated concentrations). Reproduced from [747], licensed under CC BY. (b) Modern Meadow's meat chip, containing up to 90% bovine muscle cells (image courtesy of Modern Meadow). (c) The recently introduced Mercedes Concept AMG XX car (c1) whose interior is made fully of Modern Meadow's Innovera leather alternative (c2) (image courtesy of Modern Meadow [749]; image courtesy of Mercedes-AMG [751]). (d) Various unstructured meat products prepared using Fork & Good's biofabricated cultivated meat (images courtesy of Fork & Good [77])

6 Outlook

Across the U.S., the future impact of biofabrication and biomedical manufacturing depends on addressing a set of tightly interconnected gaps in process innovation and validation, biomaterial engineering and cell manufacturing, physics-informed modeling and control, and application-driven performance assessment and quality control. While these fields have advanced rapidly, broader and more sustained translation requires a shift from impressive proof-of-concept demonstrations to predictable, reproducible, and scalable manufacturing systems supported by clearly defined quality attributes and translation-aligned workflows. Addressing these challenging needs requires coordinated advances in manufacturing science, biomaterials, process modeling, monitoring, and control, cellular and molecular biology, and translational infrastructure, along with scale-up production strategies that improve productivity without sacrificing functional performance or reproducibility. The further development of the field is expected to be accelerated by emerging technologies such as digital twins for the monitoring of bioprinted living systems and AI for the design of bioinks for specific printing applications.

6.1 Process innovation, selection, and validation

U.S. research has greatly expanded the biofabrication and biomedical manufacturing toolbox through a wide range of process innovations [752], as highlighted in Section 2. These advances are opening new possibilities for the fabrication of biomedical devices and biological systems, ranging from custom orthopedic implants, stents, tissue/organ constructs, and drug screening models to integrated wearable platforms with embedded sensing functions. At the same time, new process innovations are needed to reliably process difficult-to-print/fabricate biomaterials and biological materials while maintaining geometric fidelity, cell compatibility, and functional performance.

Despite substantial progress, process selection in biofabrication and biomedical manufacturing remains largely empirical. The field still lacks robust material–process–property–functionality relationships [15] that connect fabrication conditions and material evolution during printing to constructs or device performance. In tissue engineering using biofabrication, these relationships govern printing fidelity, transport behavior, and long-term biological function, especially in thick, heterogeneous, and dynamically remodeling systems. In biomedical devices, they similarly control dimensional precision, interfacial quality, mechanical robustness, surface characteristics, and operational reliability. As a result, there are still no well-accepted digital-twin frameworks for matching specific fabrication modalities and conditions to tissue-, device-, and function-related requirements, or for defining the trade-offs among process parameters, geometric fidelity, cytocompatibility, throughput, mechanical performance, and post-fabrication maturation.

Process validation is another important gap, especially for multimaterial and multifunctional constructs and devices, where interfacial behavior, feature resolution, and time-dependent structural evolution can strongly affect performance. At the same time, the field still needs more effective in-line monitoring and feedback-control strategies to correct printing defects and mitigate printing-induced injuries during fabrication. More broadly, as in other advanced manufacturing applications, persistent needs remain to reduce cost, increase speed, and improve robustness and part quality.

6.2 Biomaterials engineering and cell manufacturing

Biomaterials remain one of the main bottlenecks in biofabrication and biomedical engineering. For tissue engineering using biofabrication, next-generation bioinks must be engineered not only for printability, but also to support cell loading, migration, maturation, and long-term function while meeting practical demands such as reproducibility, sterilization compatibility, storage stability, and scalable manufacturing. For biomedical devices, material demands include mechanical compatibility, surface functionality, durability, and compatibility with the implementing environment. Although many bioinks and printable formulations have been reported [85, 417, 431], the pool of truly translation-ready materials remains limited. Major barriers include high cost, compositional variability, incomplete compatibility with sterilization and storage, and the lack of standardized reference materials and formulation protocols, all of which hinder cross-laboratory reproducibility, meaningful comparison across fabrication systems, and eventual commercial translation. More broadly, the field still needs the development and standardization of a wider range of economically viable, printable materials for biofabrication and biomedical use, including new classes of biocompatible polymers that enable advanced functional biological constructs and medical devices. Establishing one or more benchmark materials that can be used across laboratories and fabrication systems would provide a common baseline for comparing fabrication systems and material performance, help unify datasets across the field, and potentially facilitate regulatory evaluation.

Such datasets can also be shared to facilitate the adoption of AI for bioprinting. Beyond bioink innovations, the integration of AI and machine learning into bioprinting workflows has the potential to emerge as a transformative strategy. AI-driven platforms might enable real-time process optimization, automated error detection and correction, and improved reproducibility.

A particularly significant need in biofabrication is the scale-up production of living cells as manufacturing inputs, a challenge fundamentally different from preparing conventional material feedstocks. Bioprinting, particularly for high cell density and large tissue printing, requires cell production and processing workflows that are scalable, cost-effective, and compatible with GMP [15] and with the intended recipient; however, process development, monitoring, quality control, and supply chain management remain insufficiently mature when living cells are treated as dynamic, heterogeneous materials rather than static inputs. In addition, the limited shelf life of cell-laden tissue constructs, especially thick, vascularized tissue models intended to function as self-sustaining living systems, creates an urgent need for practical production, preservation, storage, and distribution strategies. Furthermore, progress remains constrained by an incomplete understanding of how material composition, cell type, cell density, and spatial and temporal cell–material interactions jointly determine construct maturation and function, highlighting the need for better-defined materials and cellular principles to improve both biological performance and manufacturing efficiency.

6.3 Physical modeling of printing dynamics and cell injury

The field needs the development and broader adoption of predictive digital-twin frameworks that integrate process physics, material behavior, biological responses, and functional performance to capture not only how constructs and devices are fabricated but also how they evolve after fabrication. Advancing biofabrication and biomedical manufacturing from empirical optimization toward predictive manufacturing requires a deeper mechanistic understanding of printing dynamics, material behavior, and post-fabrication behavior. For cell-laden systems, this includes modeling the behavior of complex fluids, such as viscoelastic polymer solutions, yield-stress support baths, and soft cell-laden suspensions, as well as fundamental phenomena such as droplet formation in

drop-on-demand systems and filament stability in extrusion-based processes. For biomedical devices, comparable modeling challenges include predicting curing or consolidation behavior, interfacial integrity, residual stress development, dimensional accuracy, and long-term structural and functional stability. Representative U.S. contributions, as presented in Section 4, have already demonstrated the value of such approaches.

At the same time, predictive modeling must extend beyond geometric fidelity alone. For bioprinted constructs, success cannot focus solely on shape fidelity, because process-induced stresses may compromise cell health and long-term function even if the printed geometry appears acceptable. Current assessments often rely on cell viability and necrotic damage, while apoptotic damage is less investigated. Beyond routine viability assays, future studies should investigate the cellular and molecular mechanisms underlying fabrication-induced damage and quantify how specific process exposures, such as stress magnitude and history, extensional deformation, and thermal or photochemical dose, affect cell health, phenotype stability, and long-term function. Such efforts are essential to enable the modeling and mitigation of bioprinting-induced damage [187, 431, 753].

Predictive frameworks are also needed to capture post-fabrication properties and biological development. Biofabricated tissue constructs include processes such as tissue fusion, maturation, remodeling, and degradation. Biomedical devices include the evolution of mechanical integrity, interfacial stability, degradation behavior (when applicable), and long-term functional reliability under physiological conditions. Such models are essential not only for improving fabrication strategies but also for determining the level of structural, material, and biological complexity truly required to achieve meaningful clinical benefit. A better understanding is needed regarding how cellular constructs and implanted devices interact with their host environment over time, particularly with respect to tissue integration, chronic inflammation, foreign-body response, infection risk, and long-term performance. These gaps motivate a tighter integration of physics-based modeling, biological modeling, in situ monitoring, and closed-loop control, enabling model-informed process windows and more rigorous quality assurance beyond trial-and-error optimization. A critical missing component is the establishment of standardized data infrastructures, including shared databases, metadata standards, and interoperable formats to enable cross-platform learning and model development.

6.4 Application-driven construct performance assessment and quality control

Process performance assessment of biofabrication and biomedical manufacturing is still frequently limited by the lack of rigorous and standardized performance assessment frameworks, due to the complex structure of the data collected during fabrication [754, 755]. For biofabricated constructs, assessment must extend beyond structural fidelity to performance metrics, such as mass transport, perfusion, vascularization and innervation, cell viability, maturation, and tissue-specific functional and long-term stable performance after implantation. These considerations become especially pronounced in clinically relevant applications and in physiologically relevant in vitro models, where sustained perfusion and multicellular interactions are essential. Although fabrication technologies have advanced greatly in recreating some tissue structures, biomimetic function evaluation remains elusive in some cases, despite some significant progress. To enable meaningful clinical and commercial translation, the field requires more than assessing anatomical fidelity. Instead, it requires improved patient specificity, mechanical properties, and standardized methods to evaluate whether a construct performs as intended. Related evaluation frameworks should include validated benchmarks for perfusion efficiency, vascular and nervous integration, mechanical durability, degradation behavior, cell viability and maturation, and tissue-specific functional readouts.

Furthermore, evaluation of printed constructs and devices remains a major bottleneck. Spatially resolved characterization typically has a space-time-varying distribution and is thus challenging to properly describe and analyze [756, 757], and the incorporation of living cells introduces additional time-dependent performance dimensions that must be monitored temporally. Heterogeneous cell populations and evolving tissue properties demand advanced characterization methods capable of quantifying geometry, interfaces, transport pathways, mechanical behavior, and functional readouts over time, mathematically and statistically. The field would benefit greatly from standardized benchmarks that connect "as-fabricated" attributes to in vitro and in vivo performance, enabling more rigorous comparisons across platforms and accelerating translation.

Even when constructs or devices are fabricated with similar initial geometries, their biological outcomes can diverge substantially because of differences in cell composition, organization, remodeling, and maturation. For many soft tissues, the mechanisms governing tissue fusion, collective cell mechanics, and the evolution of the local microenvironment, including mechanical conditioning, nutrient and oxygen transport, and biochemical signaling, remain insufficiently understood. Addressing these gaps requires time-resolved experimental and modeling frameworks that include maturation as an integral part of the manufacturing process rather than a secondary step, particularly for constructs in which vascularization and innervation are critical to function.

6.5 Application-oriented design as a priority

A major need in U.S. biofabrication and biomedical manufacturing is a shift from technology-first development to application-driven design [758]. In practice, this means starting with the intended use, such as a vascularized implant, organoid model, microphysiological system, or implantable device, and translating that use into a set of quantifiable design requirements, for example permeability, mechanical load-bearing needs, anatomical fidelity, electrical coupling, barrier function, or sterilization constraints. This design logic can sharpen material development by defining which properties truly matter and can improve process development by clarifying when a specific fabrication process offers the most appropriate balance of resolution, throughput, and multimaterial integration [759]. Design does not sit downstream of process or material selection; rather, it should provide the mechanism for linking application targets to material behavior, manufacturing capability, and validated functional performance.

6.6 Ethical biofabrication and biomedical manufacturing

Ethical manufacturing has recently emerged as an important topic with the goal of forming a set of ethical principles that guide the actions and decisions of individuals and organizations involved across the product life cycle to deliver both economic and social values from manufacturing while maintaining manufacturing legality, integrity, and accountability in the age of the internet and AI. The scope of ethical biofabrication and biomedical manufacturing may be even broader due to the use of living cells as a starting material and the making of living systems as the final product in many applications.

In addition to the envisioned organ printing application, biofabricated tissues, organoids, and microphysiological systems are expected to complement, reduce, and, where scientifically appropriate, partially replace animal models in preclinical research [760–762] as recently encouraged as a type of new approach methodologies (NAMs) in the U.S. As biofabrication and biomedical manufacturing continue to advance, additional ethical considerations must evolve in parallel with technical capabilities, including human relevance, cell source traceability, fit-for-purpose validation, patient safety, equitable translation, public acceptance, and governmental regulations, to name a few. For soft tissue constructs and other biofabricated systems, careful ethical attention should be given to cell and tissue sourcing, donor consent, biomaterial composition, xeno-derived components, construct safety, intended use, and accessibility, while ensuring that validation strategies are selected according to the application rather than defaulting to conventional fabrication studies without sufficient scientific justification. It is noted that this ethical issue may become even more debatable for increasingly sophisticated in vitro systems, such as in vitro brain models [763] and cultivated meat.

6.7 Other directions for U.S. biofabrication and biomedical manufacturing

Among the many opportunities ahead, two other priorities appear especially important for the continued development of U.S. biofabrication and biomedical manufacturing. The first is scalability: many technologies can now produce sophisticated small-scale constructs, but the field still faces major challenges in scaling construct size, production rate, and manufacturing robustness while preserving biological and functional quality [223]. The second is standardization, including the development of shared material benchmarks, reproducible process windows, and application-relevant quality metrics that allow meaningful comparison across platforms and laboratories.

In summary, the continued advancement of biofabrication and biomedical manufacturing in the U.S. depends on coordinated progress in manufacturing processes, materials, predictive modeling, and application-driven validation within an ethical framework, together with stronger standards, translational infrastructure, and workforce development. The field is now at a stage where future impact will be determined less by isolated demonstrations and more by the ability to deliver predictable, reproducible, scalable, and clinically relevant systems.

Acknowledgements YXC, KRP, and YH would like to acknowledge Ms. Lielle E. Daniel's contributions to reference management. TEA would like to acknowledge the contributions of Tia Monjure. DD would like to acknowledge pivotal contributions to the collaborative work reported here by current and recent affiliates of the Osteo Engineering Laboratory: Dr. Ciro Rodriguez, Tecnológico de Monterrey; Dr. Agnieszka Chmielewska-Wysocka, Cardinal Stefan Wyszynski University; Dr. Javier Vazquez, Department of Integrated Systems Engineering, The Ohio State University; Dr. Luis Olivas, Dr. Tanya Djemal, and Joshua Alexander, Department of Biomedical Engineering, University of Wisconsin-Madison. SJH would like to acknowledge the work of Harsha Ramaraju, PhD; Jeong Hun Park, PhD; Adam Verga; Glenn Green, MD; Rick Ohye, MD; Steven Goudy, MD; Kevin Maher, MD; Subhadra Shashidharan, MD; Ryan Akman, PhD; Martin Bocks, MD; and Jakari Harris. BMO would like to acknowledge the contributions of Wei-Han Lin, Ph.D. LGZ acknowledges the contributions of Bing Ren, PhD. The authors particularly thank Dr. Qian Wu for her support with the copyright permission requests.

DD also wishes to acknowledge partial support from a U.S. National Science Foundation Engineering Research Center grant EEC-2133630 (HAMMER) as well as partial support from a U.S. Department of Defense grant number WSlXWH-15-9-0001, Project MTF4. The views and conclusions contained herein are those of the author and should not be interpreted as necessarily representing the official policies or endorsements, either expressed or implied, of the U.S. Government. PDD is supported by the Bradshaw and

Holzapfel Research Professor in Transformational Science and Mathematics Fund. The contributions of MF were made as part of their official duties as National Institutes of Health (NIH) federal employees, are in compliance with agency policy requirements, and are considered Works of the United States Government. However, the findings and conclusions presented in this paper are those of the author(s) and do not necessarily reflect the views of the NIH or the U.S. Department of Health and Human Services. Work at the National Center for Advancing Translational Sciences (NCATS) was funded by the NIH Intramural Research Program and the NIH Helping to End Addiction Long-term (HEAL) initiative. MG acknowledges support from NSF (NSF DMR 2044479)". SJH would also like to acknowledge funding support from the NIH (NIH/NICHD R01 086201; NIH/NHLBI R01 179686; NIH/NIAMS R01 082523; NIH/NHLBI R21 126004; NIH/NICHD R21 110874) and the National Science Foundation (NSF) (NSF PFI 2314241) for work reported here. MM acknowledges support from the National Institutes of Health National Institute of General Medical Sciences grant R35GM142875. LGZ acknowledges the support of the NSF Advanced Manufacturing (AM) program Grant 2427645 and the NSF Engineering of Biomedical Systems (EBMS) program Grant 2110842. YSZ acknowledges the support by the Brigham Research Institute.

Author contributions Conceptualization: YH, YSZ, SCC, and JJY. Writing—original draft: all authors. Writing—review & editing: YXC, KRP, YH, YSZ, SCC, and JJY. Supervision: YH, YSZ, SCC, and JJY.

Declarations

Conflict of interest YSZ is a deputy editor of *Bio-Design and Manufacturing* (*BDM*); ECH, WL, JJY, SCC, and YH are editorial board members of *BDM*; YFJ is an associate editor of *BDM*. They were not involved in the editorial review or the decision to publish this article. GF is a co-founder of Organovo, Modern Meadow and Fork & Good and presently serves as the Chief Scientific Officer of the latter company. PDD is a co-founder of VivoTex LLC and holds equity in the company. The University of Oregon remains PDD's primary place of employment and the contribution here can be attributed to the University of Oregon. WG is founder and CEO of Bespoke Bone. SJH receives patient royalties from Materialise for Airway work. He is co-founder of Reformis Surgical which seeks to commercialize 3D printing of poly(glycerol dodecanedioate). RDK is a co-founder of AIM Biotech and receives research support from Amgen, AbbVie, Novartis, Takeda and Daiichi-Sankyo. AT is a cofounder of InPrint Bio and the conflict of interest is managed by the University of Connecticut. MWT is on the scientific advisory boards of Apersys, InkVivo Technologies, and AcousticaBio. YSZ consulted for Allevi by 3D Systems; consults for PepGel; cofounded, consults for, and holds options in Linton Lifesciences and Criocore; and sits on the scientific advisory board of and holds options in Xellar Biosystems; the relevant interests are managed by the Brigham and Women's Hospital. The other authors declare that they have no conflict of interest.

Ethical approval This article does not contain any studies with human or animal subjects performed by any of the authors.

Use of generative AI tools No generative AI tools were used during the preparation of this paper.

References

1. Shi W, Jang S, Kuss MA et al (2024) Digital light processing 4D printing of poloxamer micelles for facile fabrication of multifunctional biocompatible hydrogels as tailored wearable sensors. *ACS Nano* 18(10):7580–7595. https://doi.org/10.1021/acsnano.3c12928
2. Weygant J, Entezari A, Koch F et al (2024) Droplet 3D cryobioprinting for fabrication of free-standing and volumetric structures. *Aggregate* 5(5):e599. https://doi.org/10.1002/agt2.599
3. Krishna BV, Bose S, Bandyopadhyay A (2007) Low stiffness porous Ti structures for load-bearing implants. *Acta Biomater* 3(6):997–1006. https://doi.org/10.1016/j.actbio.2007.03.008
4. Darsell J, Bose S, Hosick HL et al (2003) From CT scan to ceramic bone graft. *J Am Ceram Soc* 86(7):1076–1080. https://doi.org/10.1111/j.1151-2916.2003.tb03427.x
5. Lee S, Sani ES, Spencer AR et al (2020) Human-recombinant-elastin-based bioinks for 3D bioprinting of vascularized soft tissues. *Adv Mater* 32(45):2003915. https://doi.org/10.1002/adma.202003915
6. Reizabal A, Devlin BL, Paxton NC et al (2023) Melt electrowriting of nylon-12 microfibers with an open-source 3D printer. *Macromol Rapid Commun* 44(24):2300424. https://doi.org/10.1002/marc.202300424
7. Xu CX, Zhang ZY, Fu JZ et al (2017) Study of pinch-off locations during drop-on-demand inkjet printing of viscoelastic alginate solutions. *Langmuir* 33(20):5037–5045. https://doi.org/10.1021/acs.langmuir.7b00874
8. Hosseini FS, Whitfield T, Orlando JD et al (2025) Osteoinductive low-dose 3D porous calcium phosphate graphene oxide–integrated matrices enhance osteogenesis and mechanical properties. *Proc Natl Acad Sci USA* 122(28):e2427124122. https://doi.org/10.1073/pnas.2427124122
9. Yeo M, Gupta D, Derman ID et al (2025) Intraoperative bioprinting for craniomaxillofacial bone reconstruction in rats and sheep. *Small Sci* 5(11):2400621. https://doi.org/10.1002/smsc.202400621
10. The SHOP Staff (2025) Modern Meadow enters development partnership with Mercedes-Benz. https://theshopmag.com/news/modern-meadow-development-partnership-mercedes-benz/ [Accessed on 2 March 2026]
11. Jakab K, Neagu A, Mironov V et al (2004) Engineering biological structures of prescribed shape using self-assembling multicellular systems. *Proc Natl Acad Sci USA* 101(9):2864–2869. https://doi.org/10.1073/pnas.0400164101
12. Boland T, Mironov V, Gutowska A et al (2003) Cell and organ printing 2: fusion of cell aggregates in three-dimensional gels. *Anat Rec Part A Discov Mol Cell Evol Biol* 272A(2):497–502. https://doi.org/10.1002/ar.a.10059
13. Mironov V, Boland T, Trusk T et al (2003) Organ printing: computer-aided jet-based 3D tissue engineering. *Trends Biotechnol* 21(4):157–161. https://doi.org/10.1016/S0167-7799(03)00033-7
14. Atala A, Bauer SB, Soker S et al (2006) Tissue-engineered

autologous bladders for patients needing cystoplasty. *Lancet* 367(9518):1241–1246. https://doi.org/10.1016/S0140-6736(06)68438-9
15. Huang Y, Schmid SR (2018) Additive manufacturing for health: state of the art, gaps and needs, and recommendations. *J Manuf Sci Eng* 140(9):094001. https://doi.org/10.1115/1.4040430
16. Mironov V, Trusk T, Kasyanov V et al (2009) Biofabrication: a 21st century manufacturing paradigm. *Biofabrication* 1(2):022001. https://doi.org/10.1088/1758-5082/1/2/022001
17. Groll J, Boland T, Blunk T et al (2016) Biofabrication: reappraising the definition of an evolving field. *Biofabrication* 8: 013001. https://doi.org/10.1088/1758-5090/8/1/013001
18. Groll J, Burdick JA, Cho DW et al (2019) A definition of bioinks and their distinction from biomaterial inks. *Biofabrication* 11:013001. https://doi.org/10.1088/1758-5090/aaec52
19. Malda J, Visser J, Melchels FP et al (2013) 25th Anniversary Article: Engineering hydrogels for biofabrication. *Adv Mater* 25(36):5011–5028. https://doi.org/10.1002/adma.201302042
20. Moroni L, Burdick JA, Highley C et al (2018) Biofabrication strategies for 3D in vitro models and regenerative medicine. *Nat Rev Mater* 3(5):21–37. https://doi.org/10.1038/s41578-018-0006-y
21. Shih AJ (2008) Biomedical manufacturing: a new frontier of manufacturing research. *J Manuf Sci Eng* 130(2):021009. https://doi.org/10.1115/1.2896116
22. Chen R, Chang RC, Tai B et al (2020) Biomedical manufacturing: a review of the emerging research and applications. *J Manuf Sci Eng* 142(11):110807. https://doi.org/10.1115/1.4048043
23. Guillemot F, Mironov V, Nakamura M (2010) Bioprinting is coming of age: report from the International Conference on Bioprinting and Biofabrication in Bordeaux (3B'09). *Biofabrication* 2:010201. https://doi.org/10.1088/1758-5082/2/1/010201
24. Murphy SV, Atala A (2014) 3D bioprinting of tissues and organs. *Nat Biotechnol* 32:773–785. https://doi.org/10.1038/nbt.2958
25. Huang Y, Leu MC, Mazumder J et al (2015) Additive manufacturing: current state, future potential, gaps and needs, and recommendations. *J Manuf Sci Eng* 137:014001. https://doi.org/10.1115/1.4028725
26. Jeon O, Lee YB, Hinton TJ et al (2019) Cryopreserved cell-laden alginate microgel bioink for 3D bioprinting of living tissues. *Mater Today Chem* 12:61–70. https://doi.org/10.1016/j.mtchem.2018.11.009
27. Jeon O, Bin Lee Y, Lee SJ et al (2022) Stem cell-laden hydrogel bioink for generation of high resolution and fidelity engineered tissues with complex geometries. *Bioact Mater* 15:185–193. https://doi.org/10.1016/j.bioactmat.2021.11.025
28. Miao SD, Cui HT, Nowicki M et al (2018) Stereolithographic 4D bioprinting of multiresponsive architectures for neural engineering. *Adv Biosyst* 2(9):1800101. https://doi.org/10.1002/adbi.201800101
29. Reizabal A, Kangur T, Saiz PG et al (2023) MEWron: an open-source melt electrowriting platform. *Addit Manuf* 71:103604. https://doi.org/10.1016/j.addma.2023.103604
30. Reizabal A, Saiz PG, Luposchainsky S et al (2024) Cryo-electrohydrodynamic jetting of aqueous silk fibroin solutions. *ACS Biomater Sci Eng* 10(3):1843–1855. https://doi.org/10.1021/acsbiomaterials.3c00851
31. Ragelle H, Tibbitt MW, Wu SY et al (2018) Surface tension-assisted additive manufacturing. *Nat Commun* 9:1184. https://doi.org/10.1038/s41467-018-03391-w
32. Roth JG, Brunel LG, Huang MS et al (2023) Spatially controlled construction of assembloids using bioprinting. *Nat Commun* 14:4346. https://doi.org/10.1038/s41467-023-40006-5
33. Kim MH, Ozbolat IT (2026) Aspiration-assisted bioprinting of spheroids. *Nat Protoc* 21(4):1325–1373. https://doi.org/10.1038/s41596-025-01240-x
34. Ravanbakhsh H, Luo ZY, Zhang X et al (2022) Freeform cell-laden cryobioprinting for shelf-ready tissue fabrication and storage. *Matter* 5(2):573–593. https://doi.org/10.1016/j.matt.2021.11.020
35. Chansoria P, Narayanan LK, Schuchard K et al (2019) Ultrasound-assisted biofabrication and bioprinting of preferentially aligned three-dimensional cellular constructs. *Biofabrication* 11(3):035015. https://doi.org/10.1088/1758-5090/ab15cf
36. Sadak O, Kuss MA, Shi W et al (2025) Development of a 3D printed liquid-core hydrogel platform for real-time carbon nanotube sensors. *Emergent Mater* 8(2):1111–1120. https://doi.org/10.1007/s42247-024-00818-7
37. Saeedinejad F, Alipanah F, Toro S et al (2025) In situ-formed tissue-adhesive macroporous scaffolds enhance cell infiltration and tissue regeneration. *Acta Biomater* 200:358–377. https://doi.org/10.1016/j.actbio.2025.04.049
38. Rodriguez-Rivera GJ, Sharma S, Maduka CV et al (2025) Microgel aspect ratio influences injectable granular hydrogel scaffold pore structure and cellular invasion for tissue repair. *Adv Sci* 12(43):e11513. https://doi.org/10.1002/advs.202511513
39. Bandyopadhyay A, Mitra I, Ciliveri S et al (2024) Additively manufactured Ti–Ta–Cu alloys for the next-generation load-bearing implants. *Int J Extreme Manuf* 6(1):015503. https://doi.org/10.1088/2631-7990/ad07e7
40. Cereceres S, Lan ZY, Bryan L et al (2019) Bactericidal activity of 3D-printed hydrogel dressing loaded with gallium maltolate. *APL Bioeng* 3(2):026102. https://doi.org/10.1063/1.5088801
41. Yang KH, Lindberg G, Soliman B et al (2021) Effect of photoinitiator on precursory stability and curing depth of thiol-ene clickable gelatin. *Polymers* 13(11):1877. https://doi.org/10.3390/polym13111877
42. de Paiva Narciso N, Navarro RS, Gilchrist AE et al (2023) Design parameters for injectable biopolymeric hydrogels with dynamic covalent chemistry crosslinks. *Adv Healthc Mater* 12(27): 2301265. https://doi.org/10.1002/adhm.202301265
43. Hull SM, Lou JZ, Lindsay CD et al (2023) 3D bioprinting of dynamic hydrogel bioinks enabled by small molecule modulators. *Sci Adv* 9(13):eade7880. https://doi.org/10.1126/sciadv.ade7880
44. Cai B, Kilian D, Ramos Mejia D et al (2024) Diffusion-based 3D bioprinting strategies. *Adv Sci* 11(8):2306470. https://doi.org/10.1002/advs.202306470
45. Habib A, Khoda B (2021) Fiber-filled hybrid hydrogel for biomanufacturing. *J Manuf Sci Eng* 143(4):041013. https://doi.org/10.1115/1.4049479
46. Yu I, Chen R (2021) An experimental and numerical study on coaxial extrusion of a non-Newtonian hydrogel material. *J Manuf Sci Eng* 143(8):081008. https://doi.org/10.1115/1.4050181
47. Morley CD, Ellison ST, Bhattacharjee T et al (2019) Quantitative characterization of 3D bioprinted structural elements under cell generated forces. *Nat Commun* 10:3029. https://doi.org/10.1038/s41467-019-10919-1

48. Yin J, Huang Y (2011) Study of process-induced cell membrane stability in cell direct writing. *J Manuf Sci Eng* 133(5):054501. https://doi.org/10.1115/1.4004685
49. Ablanedo Morales P, Rodriguez B, Furth ME et al (2023) Thermal inkjet bioprinting drastically alters cell phenotype. *Biofabrication* 15(3):031001. https://doi.org/10.1088/1758-5090/acd3b3
50. Kupfer ME, Lin WH, Ravikumar V et al (2020) In situ expansion, differentiation, and electromechanical coupling of human cardiac muscle in a 3D bioprinted, chambered organoid. *Circ Res* 127(2):207–224. https://doi.org/10.1161/circresaha.119.316155
51. Devlin C, Tomov ML, Chen H et al (2024) Patient-specific 3D *in vitro* modeling and fluid dynamic analysis of primary pulmonary vein stenosis. *Front Cardiovasc Med* 11:1432784. https://doi.org/10.3389/fcvm.2024.1432784
52. Ronaldson-Bouchard K, Ma SP, Yeager K et al (2018) Advanced maturation of human cardiac tissue grown from pluripotent stem cells. *Nature* 556(7700):239–243. https://doi.org/10.1038/s41586-018-0016-3
53. Subbiah R, Lin EY, Athirasala A et al (2023) Engineering of an osteoinductive and growth factor-free injectable bone-like microgel for bone regeneration. *Adv Healthc Mater* 12(11):2200976. https://doi.org/10.1002/adhm.202200976
54. Strong CE, Zhang JJ, Carrasco M et al (2023) Functional brain region-specific neural spheroids for modeling neurological diseases and therapeutics screening. *Commun Biol* 6:1211. https://doi.org/10.1038/s42003-023-05582-8
55. Ning LQ, Shim J, Tomov ML et al (2022) A 3D bioprinted in vitro model of neuroblastoma recapitulates dynamic tumor-endothelial cell interactions contributing to solid tumor aggressive behavior. *Adv Sci* 9(23):2200244. https://doi.org/10.1002/advs.202200244
56. Lammers A, Hsu HH, Sundaram S et al (2024) Rapid tissue perfusion using sacrificial percolation of anisotropic networks. *Matter* 7(6):2184–2204. https://doi.org/10.1016/j.matt.2024.04.001
57. Zhang S, Wan ZP, Pavlou G et al (2022) Interstitial flow promotes the formation of functional microvascular networks in vitro through upregulation of matrix metalloproteinase-2. *Adv Funct Mater* 32(43):2206767. https://doi.org/10.1002/adfm.202206767
58. Skylar-Scott MA, Uzel SGM, Nam LL et al (2019) Biomanufacturing of organ-specific tissues with high cellular density and embedded vascular channels. *Sci Adv* 5(9):eaaw2459. https://doi.org/10.1126/sciadv.aaw2459
59. Shi W, Mirza S, Kuss M et al (2023) Embedded bioprinting of breast tumor cells and organoids using low-concentration collagen-based bioinks. *Adv Healthc Mater* 12(26):2300905. https://doi.org/10.1002/adhm.202300905
60. Farris AL, Lambrechts D, Zhou YX et al (2022) 3D-printed oxygen-releasing scaffolds improve bone regeneration in mice. *Biomaterials* 280:121318. https://doi.org/10.1016/j.biomaterials.2021.121318
61. Whitfield T, Hosseini FS, Orlando JD et al (2025) Magnesium phosphate functionalized graphene oxide and PLGA composite matrices with enhanced mechanical and osteogenic properties for bone regeneration. *Regen Biomater* 12:rbaf074. https://doi.org/10.1093/rb/rbaf074
62. Moghaddam NS, Skoracki R, Miller M et al (2016) Three dimensional printing of stiffness-tuned, nitinol skeletal fixation hardware with an example of mandibular segmental defect repair. *Procedia CIRP* 49:45–50. https://doi.org/10.1016/j.procir.2015.07.027
63. Fayyazbakhsh F, Khayat MJ, Leu MC (2022) 3D-printed gelatin-alginate hydrogel dressings for burn wound healing: a comprehensive study. *Int J Bioprinting* 8(4):618. https://doi.org/10.18063/ijb.v8i4.618
64. Van Belleghem S, Mahadik B, Snodderly K et al (2021) Dual extrusion patterning drives tissue development aesthetics and shape retention in 3D printed nipple-areola constructs. *Adv Healthc Mater* 10(23):2101249. https://doi.org/10.1002/adhm.202101249
65. Zhang ZK, Lyu JJ, Zheng YH et al (2025) Miniature Ni-diamond wheel for drilling and grinding of calcified plaque surrogate in chronic total occlusion treatment. *Bio-Des Manuf* 8(6): 1009–1023. https://doi.org/10.1631/bdm.2500004
66. Park JH, Park HJ, Tucker SJ et al (2023) 3D printing of poly-ε-caprolactone (PCL) auxetic implants with advanced performance for large volume soft tissue engineering. *Adv Funct Mater* 33(24):2215220. https://doi.org/10.1002/adfm.202215220
67. Stryker (2026) Stryker completes acquisition of Amplitude Vascular Systems to add next-generation IVL technology to peripheral vascular portfolio. https://investors.stryker.com/press-releases/news-details/2026/Stryker-completes-acquisition-of-Amplitude-Vascular-Systems-to-add-next-generation-IVL-technology-to-peripheral-vascular-portfolio/default.aspx [Accessed on 7 June 2026]
68. Stryker (2026) AVS, now part of Stryker, enrolls first patient in first-in-human coronary intravascular lithotripsy study. https://www.stryker.com/us/en/about/news/2026/avs-now-part-of-stryker-enrolls-first-patient-in-first-in-human-coronary-intravascular-lithotripsy-study.html [Accessed on 18 May 2026]
69. Hua WJ, Zhang C, Cui HR et al (2025) High-speed embedded ink writing of anatomic-size organ constructs. *Adv Sci* 12(13): 2405980. https://doi.org/10.1002/advs.202405980
70. Liu JC, Shahriar M, Xu HQ et al (2022) Cell-laden bioink circulation-assisted inkjet-based bioprinting to mitigate cell sedimentation and aggregation. *Biofabrication* 14(4):045020. https://doi.org/10.1088/1758-5090/ac8fb7
71. Guo SB, Agarwal T, Song SQ et al (2025) Development of novel multi-responsive 4D printed smart nanocomposites with polypyrrole coated iron oxides for remote and adaptive transformation. *Mater Horiz* 12(11):3907–3917. https://doi.org/10.1039/D4MH01804D
72. O'Neal J, Villasmil-Urdaneta LA, Woods P et al (2025) Lungprint: robot-assisted 3D bioprinting of lung models with cellulose-derivative bioinks. In: Proceedings of the ASME International Mechanical Engineering Congress and Exposition, p.1–9. https://doi.org/10.1115/imece2025-166723
73. Ronaldson-Bouchard K, Teles D, Yeager K et al (2022) A multi-organ chip with matured tissue niches linked by vascular flow. *Nat Biomed Eng* 6(4):351–371. https://doi.org/10.1038/s41551-022-00882-6
74. Lee SJ, Jeong W, Atala A (2024) 3D bioprinting for engineered tissue constructs and patient-specific models: current progress and prospects in clinical applications. *Adv Mater* 36(49):2408032. https://doi.org/10.1002/adma.202408032
75. Kang HW, Lee SJ, Ko IK et al (2016) A 3D bioprinting system to produce human-scale tissue constructs with structural integrity. *Nat Biotechnol* 34(3):312–319. https://doi.org/10.1038/nbt.3413
76. Jorgensen AM, Gorkun A, Mahajan N et al (2023) Multicellular bioprinted skin facilitates human-like skin architecture in vivo. *Sci Transl Med* 15(716):eadf7547. https://doi.org/10.1126/scitranslmed.adf7547
77. Fork & Good (2026) Fork & Good.

https://forkandgood.com/ [Accessed on 19 April 2026]
78. Ligon SC, Liska R, Stampfl J et al (2017) Polymers for 3D printing and customized additive manufacturing. *Chem Rev* 117(15):10212–10290. https://doi.org/10.1021/acs.chemrev.7b00074
79. Ngo TD, Kashani A, Imbalzano G et al (2018) Additive manufacturing (3D printing): a review of materials, methods, applications and challenges. *Compos Part B Eng* 143:172–196. https://doi.org/10.1016/j.compositesb.2018.02.012
80. Gao W, Zhang YB, Ramanujan D et al (2015) The status, challenges, and future of additive manufacturing in engineering. *Comput Aided Des* 69:65–89. https://doi.org/10.1016/j.cad.2015.04.001
81. Dizon JRC, Espera AH, Chen QY et al (2018) Mechanical characterization of 3D-printed polymers. *Addit Manuf* 20:44–67. https://doi.org/10.1016/j.addma.2017.12.002
82. Kunwar P, Xiong Z, Zhu Y et al (2019) Hybrid laser printing of 3D, multiscale, multimaterial hydrogel structures. *Adv Opt Mater* 7(21):1900656. https://doi.org/10.1002/adom.201900656
83. Saksena J (2023) Utilizing laser direct writing to fabricate in vitro bioengineered systems for elucidating cellular dynamics in breast tumor and wound microenvironments. Dissertation, Tulane University, USA
84. Zhang YS, Haghiashtiani G, Hübscher T et al (2021) 3D extrusion bioprinting. *Nat Rev Meth* Primers 1:75. https://doi.org/10.1038/s43586-021-00073-8
85. Wu Q, Song KD, Zhang DM et al (2022) Embedded extrusion printing in yield-stress-fluid baths. *Matter* 5(11):3775–3806. https://doi.org/10.1016/j.matt.2022.09.003
86. Ji S, Almeida E, Guvendiren M (2019) 3D bioprinting of complex channels within cell-laden hydrogels. *Acta Biomater* 95: 214–224. https://doi.org/10.1016/j.actbio.2019.02.038
87. Uzel SGM, Weeks RD, Eriksson M et al (2022) Multimaterial multinozzle adaptive 3D printing of soft materials. *Adv Mater Technol* 7(8):2101710. https://doi.org/10.1002/admt.202101710
88. Highley CB, Rodell CB, Burdick JA (2015) Direct 3D printing of shear-thinning hydrogels into self-healing hydrogels. *Adv Mater* 27(34):5075–5079. https://doi.org/10.1002/adma.201501234
89. Nakamura K, Di Caprio N, Taasan JT et al (2026) Dynamic regulation of granular hydrogels through guest-host interactions to spatiotemporally guide cellular migration. *Adv Sci* 13(5):e12971. https://doi.org/10.1002/advs.202512971
90. Skylar-Scott MA, Mueller J, Visser CW et al (2019) Voxelated soft matter via multimaterial multinozzle 3D printing. *Nature* 575(7782):330–335. https://doi.org/10.1038/s41586-019-1736-8
91. Rosalia L, Sinha S, Weiss JD et al (2026) Gradient multinozzle 3D printing. bioRxiv. https://doi.org/10.64898/2026.03.21.712762
92. Zhu ZJ, Park HS, McAlpine MC (2020) 3D printed deformable sensors. *Sci Adv* 6(25):eaba5575. https://doi.org/10.1126/sciadv.aba5575
93. Griffin MR, Bertram SE, Robison NP et al (2025) 3D vector field-guided toolpathing for 3D bioprinting. *Commun Eng* 4:154. https://doi.org/10.1038/s44172-025-00489-0
94. Bose S, Darsell J, Hosick HL et al (2002) Processing and characterization of porous alumina scaffolds. *J Mater Sci Mater Med* 13(1):23–28. https://doi.org/10.1023/a:1013622216071
95. Kalita SJ, Bose S, Hosick HL et al (2003) Development of controlled porosity polymer-ceramic composite scaffolds via fused deposition modeling. *Mater Sci Eng C* 23(5):611–620. https://doi.org/10.1016/S0928-4931(03)00052-3
96. Bose S, Suguira S, Bandyopadhyay A (1999) Processing of controlled porosity ceramic structures via fused deposition. *Scr Mater* 41(9):1009–1014. https://doi.org/10.1016/S1359-6462(99)00250-X
97. Hinton TJ, Jallerat Q, Palchesko RN et al (2015) Three-dimensional printing of complex biological structures by freeform reversible embedding of suspended hydrogels. *Sci Adv* 1(9):e1500758. https://doi.org/10.1126/sciadv.1500758
98. Lee A, Hudson AR, Shiwarski DJ et al (2019) 3D bioprinting of collagen to rebuild components of the human heart. *Science* 365(6452):482–487. https://doi.org/10.1126/science.aav9051
99. Tashman JW, Shiwarski DJ, Feinberg AW (2021) A high performance open-source syringe extruder optimized for extrusion and retraction during FRESH 3D bioprinting. *HardwareX* 9: e00170. https://doi.org/10.1016/j.ohx.2020.e00170
100. Tashman JW, Shiwarski DJ, Feinberg AW (2022) Development of a high-performance open-source 3D bioprinter. *Sci Rep* 12: 22652. https://doi.org/10.1038/s41598-022-26809-4
101. Pusch K, Hinton TJ, Feinberg AW (2018) Large volume syringe pump extruder for desktop 3D printers. *HardwareX* 3:49–61. https://doi.org/10.1016/j.ohx.2018.02.001
102. Bliley J, Tashman J, Stang M et al (2022) FRESH 3D bioprinting a contractile heart tube using human stem cell-derived cardiomyocytes. *Biofabrication* 14(2):024106. https://doi.org/10.1088/1758-5090/ac58be
103. Sun WH, Williamson AS, Sukhnandan R et al (2023) Biodegradable, sustainable hydrogel actuators with shape and stiffness morphing capabilities via embedded 3D printing. *Adv Funct Mater* 33(36):2303659. https://doi.org/10.1002/adfm.202303659
104. Hudson AR, Shiwarski DJ, Kramer AJ et al (2025) Enhancing viability in static and perfused 3D tissue constructs using sacrificial gelatin microparticles. *ACS Biomater Sci Eng* 11(5):2888–2897. https://doi.org/10.1021/acsbiomaterials.4c02169
105. Shiwarski DJ, Hudson AR, Tashman JW et al (2025) 3D bioprinting of collagen-based high-resolution internally perfusable scaffolds for engineering fully biologic tissue systems. *Sci Adv* 11(17):eadu5905. https://doi.org/10.1126/sciadv.adu5905
106. Hua WJ, Mitchell K, Raymond L et al (2021) Fluid bath-assisted 3D printing for biomedical applications: from pre- to postprinting stages. *ACS Biomater Sci Eng* 7(10):4736–4756. https://doi.org/10.1021/acsbiomaterials.1c00910
107. Zhang C, Hua WJ, Mitchell K et al (2024) Multiscale embedded printing of engineered human tissue and organ equivalents. *Proc Natl Acad Sci USA* 121(9):e2313464121. https://doi.org/10.1073/pnas.2313464121
108. Hua WJ, Mitchell K, Kariyawasam LS et al (2022) Three-dimensional printing in stimuli-responsive yield-stress fluid with an interactive dual microstructure. *ACS Appl Mater Interfaces* 14(34):39420–39431. https://doi.org/10.1021/acsami.2c12465
109. LeBlanc KJ, Niemi SR, Bennett AI et al (2016) Stability of high speed 3D printing in liquid-like solids. *ACS Biomater Sci Eng* 2(10):1796–1799. https://doi.org/10.1021/acsbiomaterials.6b00184
110. Hua WJ, Zhang C, Raymond L et al (2025) Embedded 3D printing of engineered lung cancer model for assisting fine-needle

aspiration biopsy. *Biofabrication* 17:015042. https://doi.org/10.1088/1758-5090/ad9fe0
111. Hua WJ, Zhang C, Mitchell K et al (2025) Advanced design and 3D printing strategies with alginate-nanoclay nanocomposites: from microstructure to bioprinting. *Adv Mater Technol* 10(5): 2401167. https://doi.org/10.1002/admt.202401167
112. Zhang C, Hua WJ, Juarez K et al (2025) Ink-bath interactions in embedded ink writing for producing functional parts. *Adv Mater Technol* 10(6):2401693. https://doi.org/10.1002/admt.202401693
113. Hua WJ, Zhang C, Mitchell K et al (2024) Filament formation mechanisms in yield-stress fluid-enabled embedded ink writing. *Addit Manuf* 91:104353. https://doi.org/10.1016/j.addma.2024.104353
114. Abaci A, Camci-Unal G, Guvendiren M et al (2023) Three-dimensional bioprinting for medical applications. *MRS Bull* 48(6):624–631. https://doi.org/10.1557/s43577-023-00546-z
115. Abaci A, Guvendiren M (2024) 3D bioprinting of dense cellular structures within hydrogels with spatially controlled heterogeneity. *Biofabrication* 16(3):035027. https://doi.org/10.1088/1758-5090/ad52f1
116. Truong H, Abaci A, Gharacheh H et al (2025) Embedded bioprinting of dense cellular constructs in bone allograft-enhanced hydrogel matrices for bone tissue engineering. *Biomater Sci* 13(12):3213–3222. https://doi.org/10.1039/D4BM01616E
117. Gharacheh H, Guvendiren M (2022) Cell-laden composite hydrogel bioinks with human bone allograft particles to enhance stem cell osteogenesis. *Polymers* 14(18):3788. https://doi.org/10.3390/polym14183788
118. Ji S, Abaci A, Morrison T et al (2020) Novel bioinks from UV-responsive norbornene-functionalized carboxymethyl cellulose macromers. *Bioprinting* 18:e00083. https://doi.org/10.1016/j.bprint.2020.e00083
119. Levato R, Dudaryeva O, Garciamendez-Mijares CE et al (2023) Light-based vat-polymerization bioprinting. *Nat Rev Meth Primers* 3:47. https://doi.org/10.1038/s43586-023-00231-0
120. Dhariwala B, Hunt E, Boland T (2004) Rapid prototyping of tissue-engineering constructs, using photopolymerizable hydrogels and stereolithography. *Tissue Eng* 10(9–10):1316–1322. https://doi.org/10.1089/ten.2004.10.1316
121. You ST, Xiang Y, Hwang HH et al (2023) High cell density and high-resolution 3D bioprinting for fabricating vascularized tissues. *Sci Adv* 9(8):eade7923. https://doi.org/10.1126/sciadv.ade7923
122. Kunwar P, Poudel A, Aryal U et al (2025) Multi-material gradient printing using meniscus-enabled projection stereolithography (MAPS). *Adv Mater Technol* 10(6):2400675. https://doi.org/10.1002/admt.202400675
123. Lu Y, Mapili G, Suhali G et al (2006) A digital micro-mirror device-based system for the microfabrication of complex, spatially patterned tissue engineering scaffolds. *J Biomed Mater Res* 77A(2):396–405. https://doi.org/10.1002/jbm.a.30601
124. Miri AK, Nieto D, Iglesias L et al (2018) Microfluidics-enabled multimaterial maskless stereolithographic bioprinting. *Adv Mater* 30(27):1800242. https://doi.org/10.1002/adma.201800242
125. Kunwar P, Aryal U, Poudel A et al (2024) Droplet bioprinting of acellular and cell-laden structures at high-resolutions. *Biofabrication* 16(3):035019. https://doi.org/10.1088/1758-5090/ad4c09
126. Crosby CO, Dhand AP, Taasan JT et al (2025) Fabrication of microgel-reinforced hydrogels via vat photopolymerization. *ACS Macro Lett* 14(5):603–609. https://doi.org/10.1021/acsmacrolett.5c00086
127. Lu Y, Chen SC (2004) Micro and nano-fabrication of biodegradable polymers for drug delivery. *Adv Drug Deliv Rev* 56(11): 1621–1633. https://doi.org/10.1016/j.addr.2004.05.002
128. Mapili G, Lu Y, Chen SC et al (2005) Laser-layered microfabrication of spatially patterned functionalized tissue-engineering scaffolds. *J Biomed Mater Res Part B Appl Biomater* 75B(2): 414–424. https://doi.org/10.1002/jbm.b.30325
129. Zhang AP, Qu X, Soman P et al (2012) Rapid fabrication of complex 3D extracellular microenvironments by dynamic optical projection stereolithography. *Adv Mater* 24(31):4266–4270. https://doi.org/10.1002/adma.201202024
130. Hwang HH, You ST, Ma XY et al (2021) High throughput direct 3D bioprinting in multiwell plates. *Biofabrication* 13(2): 025007. https://doi.org/10.1088/1758-5090/ab89ca
131. Freeman S, Ramos R, Alexis Chando P et al (2019) A bioink blend for rotary 3D bioprinting tissue engineered small-diameter vascular constructs. *Acta Biomater* 95:152–164. https://doi.org/10.1016/j.actbio.2019.06.052
132. Kunwar P, Poudel A, Aryal U et al (2026) Shaping soft hydrogels into 3D, multiscale, perfusable models using multimodal printing. *Biofabrication* 18(2):025026. https://doi.org/10.1088/1758-5090/ae5b29
133. Merife AB, Poudel A, Polshikova A et al (2025) 3D osteocyte networks under pulsatile unidirectional fluid flow stimuli (PUFFS). *ACS Biomater Sci Eng* 11(10):6216–6233. https://doi.org/10.1021/acsbiomaterials.5c00730
134. Zhang KR, Ogando C, Filip A et al (2022) *In vitro* model to study confined osteocyte networks exposed to flow-induced mechanical stimuli. *Biomed Mater* 17(6):065027. https://doi.org/10.1088/1748-605X/aca37c
135. Merife AB, Seitz MP, Polshikova A et al (2026) Bone multicellular unit on a chip (BMU-chip) subjected to cyclic mechanical loading. *ACS Biomater Sci Eng* 12(4):2301–2314. https://doi.org/10.1021/acsbiomaterials.5c01798
136. Jackett KN, DaPonte DL, Soman P et al (2025) Modeling the effects of radiation on the bone tumor microenvironment: opportunities for exploring combination therapies in microphysiologic systems. *Cell Mol Biol Lett* 30(1):97. https://doi.org/10.1186/s11658-025-00774-y
137. Sawyer SW, Shridhar SV, Zhang KR et al (2018) Perfusion directed 3D mineral formation within cell-laden hydrogels. *Biofabrication* 10(3):035013. https://doi.org/10.1088/1758-5090/aacb42
138. Sawyer SW, Zhang KR, Horton JA et al (2020) Perfusion-based co-culture model system for bone tissue engineering. *AIMS Bioeng* 7(2):91–105. https://doi.org/10.3934/bioeng.2020009
139. Geffert ZJ, Fougnier D, Van Durme B et al (2026) Assembly of cell-seeded 3D printed hydrogel modules with perfusable channel networks. *Adv Funct Mater* 36(44):e75239. https://doi.org/10.1002/adfm.75239
140. Xiong Z, Kunwar P, Soman P (2021) Hydrogel-based diffractive optical elements (hDOEs) using rapid digital photopatterning. *Adv Opt Mater* 9(2):2001217. https://doi.org/10.1002/adom.202001217
141. Kunwar P, Jannini AVS, Xiong Z et al (2020) High-resolution 3D printing of stretchable hydrogel structures using optical projection lithography. *ACS Appl Mater Interfaces* 12(1):1640–1649.

https://doi.org/10.1021/acsami.9b19431
142. Kunwar P, Andrada BL, Poudel A et al (2023) Printing double-network tough hydrogels using temperature-controlled projection stereolithography (TOPS). *ACS Appl Mater Interfaces* 15(25):30780–30792. https://doi.org/10.1021/acsami.3c04661
143. Kunwar P, Xiong Z, McLoughlin ST et al (2020) Oxygen-permeable films for continuous additive, subtractive, and hybrid additive/subtractive manufacturing. *3D Print Addit Manuf* 7(5): 216–221. https://doi.org/10.1089/3dp.2019.0166
144. Geffert ZJ, Xiong Z, Grutzmacher J et al (2024) Multipath projection stereolithography for three-dimensional printing microfluidic devices. *ACS Appl Mater Interfaces* 16(50):69807–69817. https://doi.org/10.1021/acsami.4c10547
145. Xiong Z, Li HY, Kunwar P et al (2019) Femtosecond laser induced densification within cell-laden hydrogels results in cellular alignment. *Biofabrication* 11(3):035005. https://doi.org/10.1088/1758-5090/ab0f8b
146. Poudel A, Kunwar P, Aryal U et al (2025) Cellnet technology to generate 3D, functional, single-cell networks in custom architectures within collagen. *Biofabrication* 17(2):025036. https://doi.org/10.1088/1758-5090/adc48f
147. Gupta D, Derman ID, Xu CX et al (2025) Droplet-based bioprinting. *Nat Rev Meth Primers* 5:25. https://doi.org/10.1038/s43586-025-00394-y
148. Wilson WC Jr, Boland T (2003) Cell and organ printing 1: protein and cell printers. *Anat Rec* 272A(2):491–496. https://doi.org/10.1002/ar.a.10057
149. Schiele NR, Corr DT, Huang Y et al (2010) Laser-based direct-write techniques for cell printing. *Biofabrication* 2(3):032001. https://doi.org/10.1088/1758-5082/2/3/032001
150. Li XD, Liu BX, Pei B et al (2020) Inkjet bioprinting of biomaterials. *Chem Rev* 120(19):10793–10833. https://doi.org/10.1021/acs.chemrev.0c00008
151. Xu HQ, Liu JC, Zhang ZY et al (2022) Cell sedimentation during 3D bioprinting: a mini review. *Bio-Des Manuf* 5(3):617–626. https://doi.org/10.1007/s42242-022-00183-6
152. Xu HQ, Liu JC, Shahriar M et al (2023) Investigation of cell aggregation on the printing performance in inkjet-based bioprinting of cell-laden bioink. *Langmuir* 39(1):545–555. https://doi.org/10.1021/acs.langmuir.2c02817
153. Xu T, Jin J, Gregory C et al (2005) Inkjet printing of viable mammalian cells. *Biomaterials* 26(1):93–99. https://doi.org/10.1016/j.biomaterials.2004.04.011
154. Xu CX, Chai WX, Huang Y et al (2012) Scaffold-free inkjet printing of three-dimensional zigzag cellular tubes. *Biotechnol Bioeng* 109(12):3152–3160. https://doi.org/10.1002/bit.24591
155. Christensen K, Compaan A, Chai WX et al (2017) In situ printing-then-mixing for biological structure fabrication using intersecting jets. *ACS Biomater Sci Eng* 3(12):3687–3694. https://doi.org/10.1021/acsbiomaterials.7b00752
156. Xiong RT, Zhang ZY, Chai WX et al (2015) Freeform drop-on-demand laser printing of 3D alginate and cellular constructs. *Biofabrication* 7(4):045011. https://doi.org/10.1088/1758-5090/7/4/045011
157. Xu HQ, Martinez Salazar DM, Shahriar M et al (2022) Investigation and characterization of cell aggregation during and after inkjet-based bioprinting of cell-laden bioink. *J Manuf Sci Eng* 144(10):104501. https://doi.org/10.1115/1.4054640
158. Xu HQ, Xu CX, Zhang ZY (2019) Sedimentation study of bioink containing living cells. In: Proceedings of the ASME 14th International Manufacturing Science and Engineering Conference, p.1–7. https://doi.org/10.1115/msec2019-2747
159. Liu JC, Xu HQ, Wang ZY et al (2024) Numerical modeling of inkjet cell output under the interplay of cell-laden bioink consumption and sedimentation. *J Manuf Syst* 74:826–840. https://doi.org/10.1016/j.jmsy.2024.05.009
160. Xu HQ, Casillas J, Krishnamoorthy S et al (2020) Effects of Irgacure 2959 and lithium phenyl-2,4,6-trimethylbenzoylphosphinate on cell viability, physical properties, and microstructure in 3D bioprinting of vascular-like constructs. *Biomed Mater* 15(5): 055021. https://doi.org/10.1088/1748-605x/ab954e
161. Krishnamoorthy S, Wadnap S, Noorani B et al (2020) Investigation of gelatin methacrylate working curves in dynamic optical projection stereolithography of vascular-like constructs. *Eur Polym J* 124:109487. https://doi.org/10.1016/j.eurpolymj.2020.109487
162. Xu CX, Zhang ZY, Christensen K et al (2014) Freeform vertical and horizontal fabrication of alginate-based vascular-like tubular constructs using inkjetting. *J Manuf Sci Eng* 136(6):061020. https://doi.org/10.1115/1.4028578
163. Liu JC, Xu CX (2024) Improving uniformity of cell distribution in post-inkjet-based bioprinting. *J Manuf Sci Eng* 146:014501. https://doi.org/10.1115/1.4063134
164. Liu JC, Xu HQ, Shahriar M et al (2023) Modeling of cell distribution dynamics in cell-laden bioink with active circulation. *Addit Manuf* 73:103669. https://doi.org/10.1016/j.addma.2023.103669
165. Liu JC, Xu CX (2024) Spatial distribution of encapsulated cells dramatically alters biomechanical properties and microstructure of 3D printed cellular structures. *J Manuf Process* 120:1203–1212. https://doi.org/10.1016/j.jmapro.2024.05.029
166. Shahriar M, Molinares M, Acharya G et al (2025) 3D bioprinting of a perfusable tumor microenvironment model to investigate perfusion and chemotherapeutic responses in ovarian cancer cells. *Int J Bioprinting* 11(6):260–278. https://doi.org/10.36922/ijb025320316
167. Molinares M, Wolpert N, Gollahon L et al (2025) Effect of micropillar density on morphology and migration of low and high metastatic potential breast cancer cells. *Colloids Surf B Biointerfaces* 245:114214. https://doi.org/10.1016/j.colsurfb.2024.114214
168. Saksena J, Sklare SC, Phamduy TB et al (2022) The power of CAD/CAM laser bioprinting at the single-cell level: evolution of printing. In: Zhang LJG, Fisher JP, Leong KW (Eds.), 3D Bioprinting and Nanotechnology in Tissue Engineering and Regenerative Medicine (2nd Ed.). Elsevier, p.93–121. https://doi.org/10.1016/b978-0-12-824552-1.00004-9
169. Baldacchini T, Saksena J, Sklare SC et al (2021) Translation of laser-based three-dimensional printing technologies. *MRS Bull* 46(2):174–185. https://doi.org/10.1557/s43577-021-00042-2
170. Schiele NR, Chrisey DB, Corr DT (2011) Gelatin-based laser direct-write technique for the precise spatial patterning of cells. *Tissue Eng Part C Meth* 17(3):289–298. https://doi.org/10.1089/ten.tec.2010.0442
171. Burks HE, Phamduy TB, Azimi MS et al (2016) Laser direct-write onto live tissues: a novel model for studying cancer cell migration. *J Cell Physiol* 231(11):2333–2338. https://doi.org/10.1002/jcp.25363
172. Hicks MR, Pyle AD (2023) The emergence of the stem cell niche. *Trends Cell Biol* 33(2):112–123. https://doi.org/10.1016/j.tcb.2022.07.003

173. Raof NA, Schiele NR, Xie YB et al (2011) The maintenance of pluripotency following laser direct-write of mouse embryonic stem cells. *Biomaterials* 32(7):1802–1808. https://doi.org/10.1016/j.biomaterials.2010.11.015
174. Tan ML, Jenkins-Johnston N, Huang S et al (2023) Endothelial cells metabolically regulate breast cancer invasion toward a microvessel. *APL Bioeng* 7(4):046116. https://doi.org/10.1063/5.0171109
175. Monteran L, Zait Y, Erez N (2024) It's all about the base: stromal cells are central orchestrators of metastasis. *Trends Cancer* 10(3):208–229. https://doi.org/10.1016/j.trecan.2023.11.004
176. Phamduy TB, Sweat RS, Azimi MS et al (2015) Printing cancer cells into intact microvascular networks: a model for investigating cancer cell dynamics during angiogenesis. *Integr Biol* 7(9): 1068–1078. https://doi.org/10.1039/c5ib00151j
177. Phamduy TB, Raof NA, Schiele NR et al (2012) Laser direct-write of single microbeads into spatially-ordered patterns. *Biofabrication* 4(2):025006. https://doi.org/10.1088/1758-5082/4/2/025006
178. Vinson BT, Phamduy TB, Shipman J et al (2017) Laser direct-write based fabrication of a spatially-defined, biomimetic construct as a potential model for breast cancer cell invasion into adipose tissue. *Biofabrication* 9(2):025013. https://doi.org/10.1088/1758-5090/aa6bad
179. Ozbek II, Saybasili H, Ulgen KO (2024) Applications of 3D bioprinting technology to brain cells and brain tumor models: special emphasis to glioblastoma. *ACS Biomater Sci Eng* 10(5): 2616–2635. https://doi.org/10.1021/acsbiomaterials.3c01569
180. Curley JL, Sklare SC, Bowser DA et al (2016) Isolated node engineering of neuronal systems using laser direct write. *Biofabrication* 8(1):015013. https://doi.org/10.1088/1758-5090/8/1/015013
181. Christensen K, Xu CX, Chai WX et al (2015) Freeform inkjet printing of cellular structures with bifurcations. *Biotechnol Bioeng* 112(5):1047–1055. https://doi.org/10.1002/bit.25501
182. Christensen K, Zhang ZY, Xu CX et al (2018) Deformation compensation during buoyancy-enabled inkjet printing of three-dimensional soft tubular structures. *J Manuf Sci Eng* 140:011011. https://doi.org/10.1115/1.4037996
183. Guo SB, Cui HT, Agarwal T et al (2024) Nanomaterials in 4D printing: expanding the frontiers of advanced manufacturing. *Small* 20(30):2307750. https://doi.org/10.1002/smll.202307750
184. Jeon O, Bin Lee Y, Jeong H et al (2019) Individual cell-only bioink and photocurable supporting medium for 3D printing and generation of engineered tissues with complex geometries. *Mater Horiz* 6(8):1625–1631. https://doi.org/10.1039/c9mh00375d
185. Ravanbakhsh H, Zhang YS (2022) Cryobioprinting for biomedical applications. *J 3D Print Med* 6(4):163–166. https://doi.org/10.2217/3dp-2022-0017
186. Correia FP, Monteiro MV, Borralho M et al (2025) Advanced toolboxes for cryobioprinting human tissue analogs. *Adv Healthc Mater* 14(10):2405011. https://doi.org/10.1002/adhm.202405011
187. Habib MA, Khoda B (2022) Rheological analysis of bio-ink for 3D bio-printing processes. *J Manuf Process* 76:708–718. https://doi.org/10.1016/j.jmapro.2022.02.048
188. Ding AX, Tang F, Alsberg E (2025) 4D printing: a comprehensive review of technologies, materials, stimuli, design, and emerging applications. *Chem Rev* 125(7):3663–3771. https://doi.org/10.1021/acs.chemrev.4c00070
189. Ding AX, Tang F, Alsberg E (2025) The emerging 4D printing of shape-memory thermomorphs for self-adaptative biomedical implants. *Adv Funct Mater* 35(28):2418348. https://doi.org/10.1002/adfm.202418348
190. Wang Y, Cui HT, Esworthy T et al (2022) Emerging 4D printing strategies for next-generation tissue regeneration and medical devices. *Adv Mater* 34(20):2109198. https://doi.org/10.1002/adma.202109198
191. Cui HT, Miao SD, Esworthy T et al (2019) A novel near-infrared light responsive 4D printed nanoarchitecture with dynamically and remotely controllable transformation. *Nano Res* 12(6):1381–1388. https://doi.org/10.1007/s12274-019-2340-9
192. Miao SD, Cui HT, Esworthy T et al (2020) 4D self-morphing culture substrate for modulating cell differentiation. *Adv Sci* 7(6):1902403. https://doi.org/10.1002/advs.201902403
193. Cui HT, Yu ZX, Huang YM et al (2023) 3D printing of thick myocardial tissue constructs with anisotropic myofibers and perfusable vascular channels. *Biomater Adv* 153:213579. https://doi.org/10.1016/j.bioadv.2023.213579
194. Cui HT, Liu CY, Esworthy T et al (2020) 4D physiologically adaptable cardiac patch: a 4-month in vivo study for the treatment of myocardial infarction. *Sci Adv* 6(26):eabb5067. https://doi.org/10.1126/sciadv.abb5067
195. Hann SY, Cui HT, Nowicki M et al (2020) 4D printing soft robotics for biomedical applications. *Addit Manuf* 36:101567. https://doi.org/10.1016/j.addma.2020.101567
196. Cui HT, Zhu W, Miao SD et al (2024) 4D printed nerve conduit with in situ neurogenic guidance for nerve regeneration. *Tissue Eng Part A* 30(11–12):293–303. https://doi.org/10.1089/ten.tea.2023.0194
197. Wang Y, Cui HT, Wang YC et al (2021) 4D printed cardiac construct with aligned myofibers and adjustable curvature for myocardial regeneration. *ACS Appl Mater Interfaces* 13(11):12746–12758. https://doi.org/10.1021/acsami.0c17610
198. Lee YB, Jeon O, Lee SJ et al (2021) Induction of four-dimensional spatiotemporal geometric transformations in high cell density tissues via shape-changing hydrogels. *Adv Funct Mater* 31(24):2010104. https://doi.org/10.1002/adfm.202010104
199. Ding AX, Jeon O, Tang R et al (2021) Cell-laden multiple-step and reversible 4D hydrogel actuators to mimic dynamic tissue morphogenesis. *Adv Sci* 8(9):2004616. https://doi.org/10.1002/advs.202004616
200. Ding AX, Lee SJ, Ayyagari S et al (2022) 4D biofabrication via instantly generated graded hydrogel scaffolds. *Bioact Mater* 7: 324–332. https://doi.org/10.1016/j.bioactmat.2021.05.021
201. Ding AX, Tang F, Ayyagari S et al (2026) Reprogrammable 4D tissue engineering hydrogel scaffold via reversible ion printing. *Bioact Mater* 62:282–293. https://doi.org/10.1016/j.bioactmat.2026.03.011
202. Ding AX, Jeon O, Cleveland D et al (2022) Jammed microflake hydrogel for four-dimensional living cell bioprinting. *Adv Mater* 34(15):2109394. https://doi.org/10.1002/adma.202109394
203. Ding AX, Lee SJ, Tang R et al (2022) 4D cell-condensate bioprinting. *Small* 18(36):2202196. https://doi.org/10.1002/smll.202202196
204. Gasvoda KL, Ding A, Sterenberg A et al (2025) A 4D biokirigami strategy for engineering complex tissue curvatures. bioRxiv.

https://doi.org/10.1101/2025.06.28.662122
205. Ding AX, Cleveland DS, Gasvoda KL et al (2025) Cell contractile forces drive spatiotemporal morphogenesis in 4D bioprinted living constructs. *Matter* 8(11):102413. https://doi.org/10.1016/j.matt.2025.102413
206. Ding AX, Gasvoda KL, Cleveland DS et al (2025) Cell contractile force-mediated morphogenetic tissue engineering via 4D printed degradable hydrogel scaffolds. *Adv Sci* 12(48):e07288. https://doi.org/10.1002/advs.202507288
207. Sun AX, Lin H, Fritch MR et al (2017) Chondrogenesis of human bone marrow mesenchymal stem cells in 3-dimensional, photocrosslinked hydrogel constructs: effect of cell seeding density and material stiffness. *Acta Biomater* 58:302–311. https://doi.org/10.1016/j.actbio.2017.06.016
208. Zhang JH, Wehrle E, Adamek P et al (2020) Optimization of mechanical stiffness and cell density of 3D bioprinted cell-laden scaffolds improves extracellular matrix mineralization and cellular organization for bone tissue engineering. *Acta Biomater* 114: 307–322. https://doi.org/10.1016/j.actbio.2020.07.016
209. Banerjee D, Singh YP, Datta P et al (2022) Strategies for 3D bioprinting of spheroids: a comprehensive review. *Biomaterials* 291:121881. https://doi.org/10.1016/j.biomaterials.2022.121881
210. Derman ID, Kim MH, Sarikaya MD et al (2026) Unconventional bioprinting modalities for advanced tissue biofabrication. *Biomaterials* 326:123704. https://doi.org/10.1016/j.biomaterials.2025.123704
211. Ayan B, Celik N, Zhang ZF et al (2020) Aspiration-assisted freeform bioprinting of pre-fabricated tissue spheroids in a yield-stress gel. *Commun Phys* 3:183. https://doi.org/10.1038/s42005-020-00449-4
212. Kim MH, Banerjee D, Celik N et al (2022) Aspiration-assisted freeform bioprinting of mesenchymal stem cell spheroids within alginate microgels. *Biofabrication* 14(2):024103. https://doi.org/10.1088/1758-5090/ac4dd8
213. Wu Y, Ayan B, Moncal KK et al (2020) Hybrid bioprinting of zonally stratified human articular cartilage using scaffold-free tissue strands as building blocks. *Adv Healthc Mater* 9(22): 2001657. https://doi.org/10.1002/adhm.202001657
214. Heo DN, Ayan B, Dey M et al (2021) Aspiration-assisted bioprinting of co-cultured osteogenic spheroids for bone tissue engineering. *Biofabrication* 13(1):015013. https://doi.org/10.1088/1758-5090/abc1bf
215. Banerjee D, Ivanova MM, Celik N et al (2023) Biofabrication of an *in-vitro* bone model for Gaucher disease. *Biofabrication* 15(4):045023. https://doi.org/10.1088/1758-5090/acf95a
216. Ayan B, Wu Y, Karuppagounder V et al (2020) Aspiration-assisted bioprinting of the osteochondral interface. *Sci Rep* 10: 13148. https://doi.org/10.1038/s41598-020-69960-6
217. Celik N, Kim MH, Yeo M et al (2022) miRNA induced 3D bioprinted-heterotypic osteochondral interface. *Biofabrication* 14(4):044104. https://doi.org/10.1088/1758-5090/ac7fbb
218. Celik N, Kim MH, Hayes DJ et al (2021) miRNA induced co-differentiation and cross-talk of adipose tissue-derived progenitor cells for 3D heterotypic pre-vascularized bone formation. *Biofabrication* 13(4):044107. https://doi.org/10.1088/1758-5090/ac23ae
219. Alioglu MA, Yilmaz YO, Singh YP et al (2024) Nested biofabrication: matryoshka-inspired intra-embedded bioprinting. *Small Meth* 8(8):2301325. https://doi.org/10.1002/smtd.202301325
220. Dey M, Ayan B, Yurieva M et al (2021) Studying tumor angiogenesis and cancer invasion in a three-dimensional vascularized breast cancer micro-environment. *Adv Biol* 5(7):2100090. https://doi.org/10.1002/adbi.202100090
221. Dey M, Kim MH, Dogan M et al (2022) Chemotherapeutics and CAR-T cell-based immunotherapeutics screening on a 3D bioprinted vascularized breast tumor model. *Adv Funct Mater* 32(52): 2203966. https://doi.org/10.1002/adfm.202203966
222. Dey M, Kim MH, Nagamine M et al (2022) Biofabrication of 3D breast cancer models for dissecting the cytotoxic response of human T cells expressing engineered MAIT cell receptors. *Biofabrication* 14(4):044105. https://doi.org/10.1088/1758-5090/ac925a
223. Kim MH, Singh YP, Celik N et al (2024) High-throughput bioprinting of spheroids for scalable tissue fabrication. *Nat Commun* 15:10083. https://doi.org/10.1038/s41467-024-54504-7
224. Ayan B, Heo DN, Zhang ZF et al (2020) Aspiration-assisted bioprinting for precise positioning of biologics. *Sci Adv* 6(10): eaaw5111. https://doi.org/10.1126/sciadv.aaw5111
225. Huang MS, Christakopoulos F, Roth JG et al (2025) Organoid bioprinting: from cells to functional tissues. *Nat Rev Bioeng* 3(2):126–142. https://doi.org/10.1038/s44222-024-00268-0
226. Zhang DY, Huerta-López C, Heilshorn SC (2025) Organoid bioprinting to pattern the matrix microenvironment. *Curr Opin Biomed Eng* 35:100607. https://doi.org/10.1016/j.cobme.2025.100607
227. Fredrikson JP, Roth DM, Cosgrove JA et al (2025) Engineering neuronal networks in granular microgels to innervate bioprinted cancer organoids on-a-chip. *Lab Chip* 25(14):3467–3481. https://doi.org/10.1039/D5LC00134J
228. LeSavage BL, Zhang DY, Huerta-López C et al (2024) Engineered matrices reveal stiffness-mediated chemoresistance in patient-derived pancreatic cancer organoids. *Nat Mater* 23(8): 1138–1149. https://doi.org/10.1038/s41563-024-01908-x
229. Liu YM, Gilchrist AE, Johansson PK et al (2025) Engineered hydrogels for organoid models of human nonalcoholic fatty liver disease. *Adv Sci* 12(22):e17332. https://doi.org/10.1002/advs.202417332
230. Huang MS, LeSavage BL, Ghorbani S et al (2025) Viscoelastic N-cadherin-like interactions maintain neural progenitor cell stemness within 3D matrices. *Nat Commun* 16:5213. https://doi.org/10.1038/s41467-025-60540-8
231. Johansson PK, Liu YM, Klett KC et al (2025) Polarized distribution of lipid droplets with long acyl chains and unsaturation are hallmarks of human intestinal enteroid differentiation. *Anal Chem* 97(49):27076–27090. https://doi.org/10.1021/acs.analchem.5c02648
232. Narazaki G, Miura Y, Pavlov SD et al (2025) Scalable production of human cortical organoids using a biocompatible polymer. *Nat Biomed Eng* 9(12):2115–2123. https://doi.org/10.1038/s41551-025-01427-3
233. Snow F, Doyle SE, Liu E et al (2025) A detailed guide to melt electro-writing for tissue engineering applications. *Biofabrication* 17(4):042004. https://doi.org/10.1088/1758-5090/adfbc4
234. O'Neill KL, Dalton PD (2023) A decade of melt electrowriting. *Small Meth* 7(7):2201589. https://doi.org/10.1002/smtd.202201589
235. Brown TD, Dalton PD, Hutmacher DW (2011) Direct writing

by way of melt electrospinning. *Adv Mater* 23(47):5651–5657. https://doi.org/10.1002/adma.201103482
236. Hochleitner G, Jüngst T, Brown TD et al (2015) Additive manufacturing of scaffolds with sub-micron filaments via melt electrospinning writing. *Biofabrication* 7(3):035002. https://doi.org/10.1088/1758-5090/7/3/035002
237. Hollister SJ (2009) Scaffold design and manufacturing: from concept to clinic. *Adv Mater* 21(32/33):3330–3342. https://doi.org/10.1002/adma.200802977
238. Hutmacher DW, Woodfield TBF, Dalton PD (2014) Scaffold design and fabrication. In: Blitterswijk JDB (Eds.), Tissue Engineering (2nd Ed.). Elsevier, p.311–346. https://doi.org/10.1016/b978-0-12-420145-3.00010-9
239. Martine LC, Holzapfel BM, McGovern JA et al (2017) Engineering a humanized bone organ model in mice to study bone metastases. *Nat Protoc* 12(4):639–663. https://doi.org/10.1038/nprot.2017.002
240. Schuurman W, Khristov V, Pot MW et al (2011) Bioprinting of hybrid tissue constructs with tailorable mechanical properties. *Biofabrication* 3(2):021001. https://doi.org/10.1088/1758-5082/3/2/021001
241. Domb A, Mikos AG (2007) Matrices and scaffolds for drug delivery in tissue engineering. *Adv Drug Deliv Rev* 59(4−5):185–186. https://doi.org/10.1016/j.addr.2007.05.001
242. Bas O, Gorissen B, Luposchainsky S et al (2021) Ultrafast, miniature soft actuators. *Multifunct Mater* 4(4):045001. https://doi.org/10.1088/2399-7532/ac2faf
243. Schaefer N, Janzen D, Bakirci E et al (2019) 3D electrophysiological measurements on cells embedded within fiber-reinforced matrigel. *Adv Healthc Mater* 8(5):1801226. https://doi.org/10.1002/adhm.201801226
244. Saidy NT, Shabab T, Bas O et al (2020) Melt electrowriting of complex 3D anatomically relevant scaffolds. *Front Bioeng Biotechnol* 8:793. https://doi.org/10.3389/fbioe.2020.00793
245. Paxton NC, Luposchainsky S, Reizabal A et al (2024) Manufacture of biomimetic auricular surgical implants using 3D printed high density polyethylene microfibers. *Adv Mater Technol* 9(3): 2301190. https://doi.org/10.1002/admt.202301190
246. Tourlomousis F, Ding HZ, Kalyon DM et al (2017) Melt electrospinning writing process guided by a "printability number". *J Manuf Sci Eng* 139(8):081004. https://doi.org/10.1115/1.4036348
247. Cao K, Zhang FC, Wang BJ et al (2022) Analytical interpretation of microscale fiber deviation in designing for polymer melt electrohydrodynamic-based additive manufacturing. *Addit Manuf* 58:103035. https://doi.org/10.1016/j.addma.2022.103035
248. Cao K, Zhang FC, Zaeri A et al (2022) Advancing a real-time image-based jet lag tracking methodology for optimizing print parameters and assessing melt electrowritten fiber quality. *Addit Manuf* 54:102764. https://doi.org/10.1016/j.addma.2022.102764
249. Cao K, Zhang FC, Zaeri A et al (2021) A charge-based mechanistic study into the effect of collector temperature on melt electrohydrodynamic printing outcomes. *Adv Mater Technol* 6(7): 2100251. https://doi.org/10.1002/admt.202100251
250. Ding HZ, Cao K, Zhang FC et al (2019) A fundamental study of charge effects on melt electrowritten polymer fibers. *Mater Des* 178:107857. https://doi.org/10.1016/j.matdes.2019.107857
251. Cao K, Zhang FC, Zaeri A et al (2022) Quantitative investigation into the design and process parametric effects on the fiber-entrapped residual charge for a polymer melt electrohydrodynamic printing process. *Macro Mater Eng* 307(3):2100766. https://doi.org/10.1002/mame.202100766
252. Cao K, Zhang FC, Zaeri A et al (2023) A holistic model for melt electrowritten three-dimensional structured materials based on residual charge. *Int J Bioprinting* 9(2):656. https://doi.org/10.18063/ijb.v9i2.656
253. Tourlomousis F, Jia C, Karydis T et al (2019) Machine learning metrology of cell confinement in melt electrowritten three-dimensional biomaterial substrates. *Microsyst Nanoeng* 5:15. https://doi.org/10.1038/s41378-019-0055-4
254. Zaeri A, Cao K, Zhang FC et al (2024) Design and fabrication of fibrous spindle-like constructs using a melt electrohydrodynamic writing process. *Macro Mater Eng* 309(11):2400080. https://doi.org/10.1002/mame.202400080
255. Luo ZY, Lian LM, Stocco T et al (2024) 3D assembly of cryo(bio)printed modular units for shelf-ready scalable tissue fabrication. *Adv Funct Mater* 34(4):2309173. https://doi.org/10.1002/adfm.202309173
256. Luo ZY, Tang GS, Ravanbakhsh H et al (2022) Vertical extrusion cryo(bio)printing for anisotropic tissue manufacturing. *Adv Mater* 34(12):2108931. https://doi.org/10.1002/adma.202108931
257. Andolfi A, Cai L, González Martínez MV et al (2026) Hyaluronic acid-based bioink for anisotropic neural tissue cryobioprinting. *Int J Extreme Manuf* 8(1):015003. https://doi.org/10.1088/2631-7990/adfeee
258. Shirwaiker R, Chansoria P, Narayanan L (2024) Ultrasound-based patterning of particles and cells within fluid matrices. US Patent 12179194
259. Chansoria P, Shirwaiker R (2019) Characterizing the process physics of ultrasound-assisted bioprinting. *Sci Rep* 9:13889. https://doi.org/10.1038/s41598-019-50449-w
260. Chansoria P, Shirwaiker R (2019) Ultrasonically-induced patterning of viable cells in viscous bioinks during 3D biofabrication. In: Proceedings of the ASME 14th International Manufacturing Science and Engineering Conference, p.1–6. https://doi.org/10.1115/msec2019-2816
261. Chansoria P, Shirwaiker R (2020) 3D bioprinting of anisotropic engineered tissue constructs with ultrasonically induced cell patterning. *Addit Manuf* 32:101042. https://doi.org/10.1016/j.addma.2020.101042
262. Chansoria P, Asif S, Polkoff K et al (2021) Characterizing the effects of synergistic thermal and photo-cross-linking during biofabrication on the structural and functional properties of gelatin methacryloyl (GelMA) hydrogels. *ACS Biomater Sci Eng* 7(11):5175–5188. https://doi.org/10.1021/acsbiomaterials.1c00635
263. Chansoria P, Asif S, Gupta N et al (2022) Multiscale anisotropic tissue biofabrication via bulk acoustic patterning of cells and functional additives in hybrid bioinks. *Adv Healthc Mater* 11(10): e2102351. https://doi.org/10.1002/adhm.202102351
264. Asif S, Chansoria P, Shirwaiker R (2020) Ultrasound-assisted vat photopolymerization 3D printing of preferentially organized carbon fiber reinforced polymer composites. *J Manuf Process* 56:1340–1343. https://doi.org/10.1016/j.jmapro.2020.04.029
265. Chansoria P, Yousefian O, Muller M et al (2018) Ultrasound-assisted manipulation of micro-particles in fluid matrix to create highly aligned anisotropic composite structures. In: Proceedings of the IISE Annual Conference
266. Ahmed N, Shirwaiker R (2025) Digital light processing (DLP) bioprinting of collagen-riboflavin hydrogels for cultivated meat

applications. *Manuf Lett* 44:877–883. https://doi.org/10.1016/j.mfglet.2025.06.104
267. Kuang X, Rong Q, Belal S et al (2023) Self-enhancing sono-inks enable deep-penetration acoustic volumetric printing. *Science* 382(6675):1148–1156. https://doi.org/10.1126/science.adi1563
268. Kuang X, Rong Q, Belal S et al (2026) Sonicated inks and focused-ultrasound writing enable deep-penetration acoustic volumetric printing. *Nat Protoc* 21:2919–2959. https://doi.org/10.1038/s41596-025-01258-1
269. Xie M, Lian L, Zhang Z et al (2026) Rapid volumetric bioprinting of pristine protein-based (bio)inks. *Nat Protoc* (early access). https://doi.org/10.1038/s41596-026-01341-1
270. Xie M, Lian L, Mu X et al (2023) Volumetric additive manufacturing of pristine silk-based (bio)inks. *Nat Commun* 14:210. https://doi.org/10.1038/s41467-023-35807-7
271. Lian L, Xie M, Luo Z et al (2024) Rapid volumetric bioprinting of decellularized extracellular matrix bioinks. *Adv Mater* 36(34): 2304846. https://doi.org/10.1002/adma.202304846
272. Bernal PN, Florczak S, Inacker S et al (2025) The road ahead in materials and technologies for volumetric 3D printing. *Nat Rev Mater* 10:826–841. https://doi.org/10.1038/s41578-025-00785-3
273. Zhang TY, Huang YM, Kukulski P et al (2023) Support generation for robot-assisted 3D printing with curved layers. In: IEEE International Conference on Robotics and Automation, p.12338–12344. https://doi.org/10.1109/icra48891.2023.10161432
274. Ozbolat IT, Khoda AKMB (2014) Design of a new parametric path plan for additive manufacturing of hollow porous structures with functionally graded materials. *J Comput Inf Sci Eng* 14(4):041005. https://doi.org/10.1115/1.4028418
275. Habib A, Quigley C, Sarah R et al (2024) Design and fabrication of in-house nozzle system to extrude multi-hydrogels for 3D bioprinting process. *J Manuf Sci Eng* 146(2):021003. https://doi.org/10.1115/1.4063357
276. Quigley C, Tuladhar S, Habib A (2022) A roadmap to fabricate geometrically accurate three-dimensional scaffolds CO-printed by natural and synthetic polymers. *J Micro Nano Manuf* 10(2): 021001. https://doi.org/10.1115/1.4055474
277. Gong XY, Wen Z, Liang ZX et al (2025) Instant assembly of collagen for tissue engineering and bioprinting. *Nat Mater* 24(8): 1307–1318. https://doi.org/10.1038/s41563-025-02241-7
278. Corbett DC, Olszewski E, Stevens K (2019) A FRESH take on resolution in 3D bioprinting. *Trends Biotechnol* 37(11):1153–1155. https://doi.org/10.1016/j.tibtech.2019.09.003
279. Jordan SN, Li XM, Rossello-Martinez A et al (2025) Macromolecular crowding-based biofabrication utilizing unmodified extracellular matrix bioinks. *Acta Biomater* 198:37–48. https://doi.org/10.1016/j.actbio.2025.02.052
280. Xiao H, Liang ZX, Gong XY et al (2025) Application of instant assembly of collagen to bioprint cardiac tissues. *APL Bioeng* 9(2):026124. https://doi.org/10.1063/5.0252746
281. Figueroa-Milla AE, DeMaria W, Wells D et al (2024) Vascular tissues bioprinted with smooth muscle cell-only bioinks in support baths mimic features of native coronary arteries. *Biofabrication* 16(4):045033. https://doi.org/10.1088/1758-5090/ad6d8f
282. Jeon O, Park H, Leach JK et al (2025) Biofabrication of engineered tissues by 3D bioprinting of tissue specific high cell-density bioinks. *Mater Today* 86:172–182. https://doi.org/10.1016/j.mattod.2025.03.021
283. Jeon O, Park H, Lee MS et al (2025) In situ cell-only bioprinting of patterned prevascular tissue into bioprinted high-density stem cell-laden microgel bioinks for vascularized bone tissue regeneration. bioRxiv. https://doi.org/10.1101/2025.03.17.643708
284. Ostrovidov S, Salehi S, Costantini M et al (2019) 3D bioprinting in skeletal muscle tissue engineering. *Small* 15(24):1805530. https://doi.org/10.1002/smll.201805530
285. Wu SH, Duan B, Qin XH et al (2017) Living nano-micro fibrous woven fabric/hydrogel composite scaffolds for heart valve engineering. *Acta Biomater* 51:89–100. https://doi.org/10.1016/j.actbio.2017.01.051
286. Akbari M, Tamayol A, Laforte V et al (2014) Composite living fibers for creating tissue constructs using textile techniques. *Adv Funct Mater* 24(26):4060–4067. https://doi.org/10.1002/adfm.201303655
287. Singh S, Choudhury D, Yu F et al (2020) In situ bioprinting – bioprinting from benchside to bedside? *Acta Biomater* 101: 14–25. https://doi.org/10.1016/j.actbio.2019.08.045
288. Seyedsalehi A, Saeedinejad F, Toro S et al (2024) Benefits of in situ foamed and printed porous scaffolds in wound healing. *Adv Healthc Mater* 13(31):2401944. https://doi.org/10.1002/adhm.202401944
289. Quint JP, Mollocana-Lara E, Samandari M et al (2024) A robotic arm with open-source reconstructive workflow for *in vivo* bioprinting of patient-specific scaffolds. *Appl Phys Rev* 11(4):041402. https://doi.org/10.1063/5.0197123
290. Xie MJ, Shi Y, Zhang C et al (2022) In situ 3D bioprinting with bioconcrete bioink. *Nat Commun* 13:3597. https://doi.org/10.1038/s41467-022-30997-y
291. Urciuolo A, Poli I, Brandolino L et al (2020) Intravital three-dimensional bioprinting. *Nat Biomed Eng* 4(9):901–915. https://doi.org/10.1038/s41551-020-0568-z
292. Chen YW, Zhang JM, Liu X et al (2020) Noninvasive in vivo 3D bioprinting. *Sci Adv* 6(23):eaba7406. https://doi.org/10.1126/sciadv.aba7406
293. Liu HZ, Zhang Y, Jian ZA et al (2023) A novel portable *in situ* printer for hydrogel multi-structure molding and cell printing. *APL Bioeng* 7(4):046119. https://doi.org/10.1063/5.0176301
294. Quint JP, Mostafavi A, Endo Y et al (2021) In vivo printing of nanoenabled scaffolds for the treatment of skeletal muscle injuries. *Adv Healthc Mater* 10(10):2002152. https://doi.org/10.1002/adhm.202002152
295. Russell CS, Mostafavi A, Quint JP et al (2020) *In situ* printing of adhesive hydrogel scaffolds for the treatment of skeletal muscle injuries. *ACS Appl Bio Mater* 3(3):1568–1579. https://doi.org/10.1021/acsabm.9b01176
296. Bernal PN, Delrot P, Loterie D et al (2019) Volumetric bioprinting of complex living-tissue constructs within seconds. *Adv Mater* 31(42):1904209. https://doi.org/10.1002/adma.201904209
297. Tumbleston JR, Shirvanyants D, Ermoshkin N et al (2015) Continuous liquid interface production of 3D objects. *Science* 347(6228):1349–1352. https://doi.org/10.1126/science.aaa2397
298. Langer R, Vacanti JP (1993) Tissue engineering. *Science* 260(5110): 920–926. https://doi.org/10.1126/science.8493529
299. Casavant BP, Berthier E, Theberge AB et al (2013) Suspended microfluidics. *Proc Natl Acad Sci USA* 110(25):10111–10116.

https://doi.org/10.1073/pnas.1302566110
300. Haack AJ, Brown LG, Goldstein AJ et al (2025) Suspended tissue open microfluidic patterning (STOMP). *Adv Sci* 12(25): 2501148. https://doi.org/10.1002/advs.202501148
301. Lee UN, Day JH, Haack AJ et al (2020) Layer-by-layer fabrication of 3D hydrogel structures using open microfluidics. *Lab Chip* 20(3):525–536. https://doi.org/10.1039/C9LC00621D
302. Shanjani Y, Pan CC, Elomaa L et al (2015) A novel bioprinting method and system for forming hybrid tissue engineering constructs. *Biofabrication* 7(4):045008. https://doi.org/10.1088/1758-5090/7/4/045008
303. Li JN, Kim C, Pan CC et al (2022) Hybprinting for musculoskeletal tissue engineering. *iScience* 25(5):104229. https://doi.org/10.1016/j.isci.2022.104229
304. Li JN, Kim C, Alizadeh HV et al (2025) Hybrid bioprinting for functionally graded tissue engineering constructs with patterned and localized biochemical signals. *Adv Compos Hybrid Mater* 9(1):11. https://doi.org/10.1007/s42114-025-01546-0
305. Elomaa L, Kang YQ, Seppälä JV et al (2014) Biodegradable photocrosslinkable poly(depsipeptide-co-ε-caprolactone) for tissue engineering: synthesis, characterization, and *in vitro* evaluation. *J Polym Sci Part A Polym Chem* 52(23):3307–3315. https://doi.org/10.1002/pola.27400
306. Elomaa L, Pan CC, Shanjani Y et al (2015) Three-dimensional fabrication of cell-laden biodegradable poly(ethylene glycol-*co*-depsipeptide) hydrogels by visible light stereolithography. *J Mater Chem B* 3(42):8348–8358. https://doi.org/10.1039/c5tb01468a
307. Bruyas A, Lou F, Stahl AM et al (2018) Systematic characterization of 3D-printed PCL/β-TCP scaffolds for biomedical devices and bone tissue engineering: influence of composition and porosity. *J Mater Res* 33(14):1948–1959. https://doi.org/10.1557/jmr.2018.112
308. Li JN, Moeinzadeh S, Kim C et al (2023) Development and systematic characterization of GelMA/alginate/PEGDMA/xanthan gum hydrogel bioink system for extrusion bioprinting. *Biomaterials* 293:121969. https://doi.org/10.1016/j.biomaterials.2022.121969
309. Anada T, Pan CC, Stahl AM et al (2019) Vascularized bone-mimetic hydrogel constructs by 3D bioprinting to promote osteogenesis and angiogenesis. *Int J Mol Sci* 20(5):1096. https://doi.org/10.3390/ijms20051096
310. Shanjani Y, Siebert SM, Ker DFE et al (2020) Acoustic patterning of growth factor for three-dimensional tissue engineering. *Tissue Eng Part A* 26(11–12):602–612. https://doi.org/10.1089/ten.TEA.2019.0271
311. Sakthiabirami K, Kang JH, Jang JG et al (2021) Hybrid porous zirconia scaffolds fabricated using additive manufacturing for bone tissue engineering applications. *Mater Sci Eng C* 123:111950. https://doi.org/10.1016/j.msec.2021.111950
312. Nelson C, Tuladhar S, Habib A (2023) Designing an interchangeable multi-material nozzle system for the three-dimensional bioprinting process. *J Med Devices* 17(2):020901. https://doi.org/10.1115/1.4055249
313. Habib A, Khoda B (2019) Development of clay based novel hybrid bio-ink for 3D bio-printing process. *J Manuf Process* 38:76–87. https://doi.org/10.1016/j.jmapro.2018.12.034
314. Liu Y, Wan Y, Li CJ et al (2025) Gradient scaffolds in bone-soft tissue interface engineering: structural characteristics, fabrication techniques, and emerging trends. *J Orthop Transl* 50:333–353. https://doi.org/10.1016/j.jot.2024.10.015
315. Podgórski R, Wojasiński M, Małolepszy A et al (2024) Fabrication of 3D-printed scaffolds with multiscale porosity. *ACS Omega* 9(27):29186–29204. https://doi.org/10.1021/acsomega.3c09035
316. Zhou JC, See CW, Sreenivasamurthy S et al (2023) Customized additive manufacturing in bone scaffolds: the gateway to precise bone defect treatment. *Research* 6:239. https://doi.org/10.34133/research.0239
317. Colosi C, Shin SR, Manoharan V et al (2016) Microfluidic bioprinting of heterogeneous 3D tissue constructs using low-viscosity bioink. *Adv Mater* 28(4):677–684. https://doi.org/10.1002/adma.201503310
318. Traore MA, George SC (2017) Tissue engineering the vascular tree. *Tissue Eng Part B Rev* 23(6):505–514. https://doi.org/10.1089/ten.teb.2017.0010
319. Weinberg CB, Bell E (1986) A blood vessel model constructed from collagen and cultured vascular cells. *Science* 231(4736): 397–400.
320. Cabodi M, Choi NW, Gleghorn JP et al (2005) A microfluidic biomaterial. *J Am Chem Soc* 127(40):13788–13789. https://doi.org/10.1021/ja054820t
321. Borenstein JT, Terai H, King KR et al (2002) Microfabrication technology for vascularized tissue engineering. *Biomed Microdevices* 4(3):167–175. https://doi.org/10.1023/A:1016040212127
322. Kaihara S, Borenstein J, Koka R et al (2000) Silicon micromachining to tissue engineer branched vascular channels for liver fabrication. *Tissue Eng* 6(2):105–117. https://doi.org/10.1089/107632700320739
323. Fidkowski C, Kaazempur-Mofrad MR, Borenstein J et al (2005) Endothelialized microvasculature based on a biodegradable elastomer. *Tissue Eng* 11(1–2):302–309. https://doi.org/10.1089/ten.2005.11.302
324. Bellan LM, Singh SP, Henderson PW et al (2009) Fabrication of an artificial 3-dimensional vascular network using sacrificial sugar structures. *Soft Matter* 5(7):1354–1357. https://doi.org/10.1039/B819905A
325. Bellan LM, Kniazeva T, Kim ES et al (2012) Fabrication of a hybrid microfluidic system incorporating both lithographically patterned microchannels and a 3D fiber-formed microfluidic network. *Adv Healthc Mater* 1(2):164–167. https://doi.org/10.1002/adhm.201100052
326. Bellan LM, Pearsall M, Cropek DM et al (2012) A 3D interconnected microchannel network formed in gelatin by sacrificial shellac microfibers. *Adv Mater* 24(38):5187–5191. https://doi.org/10.1002/adma.201200810
327. Lee JB, Wang XT, Faley S et al (2016) Development of 3D microvascular networks within gelatin hydrogels using thermoresponsive sacrificial microfibers. *Adv Healthc Mater* 5(7):781–785. https://doi.org/10.1002/adhm.201500792
328. Rector JA, McBride L, Weber CM et al (2025) Fabrication of endothelialized capillary-like microchannel networks using sacrificial thermoresponsive microfibers. *Biofabrication* 17(1):015023. https://doi.org/10.1088/1758-5090/ad867d
329. Hu YZ, He ZY, Hao Y et al (2019) Kinetic control in assembly of plasmid DNA/polycation complex nanoparticles. *ACS Nano* 13(9):10161–10178. https://doi.org/10.1021/acsnano.9b03334
330. Qiao DD, Liu LX, Chen Y et al (2018) Potency of a scalable nanoparticulate subunit vaccine. *Nano Lett* 18(5):3007–3016. https://doi.org/10.1021/acs.nanolett.8b00478
331. Hu HZ, Yang C, Zhang F et al (2021) A versatile and robust platform for the scalable manufacture of biomimetic nanovaccines. *Adv Sci* 8(15):2002020.

https://doi.org/10.1002/advs.202002020
332. Chen XN, Shi TF, Yang C et al (2022) Scalable biomimetic SARS-CoV-2 nanovaccines with robust protective immune responses. *Signal Transduct Target Ther* 7:96. https://doi.org/10.1038/s41392-022-00942-y
333. He ZY, Liu ZJ, Tian HK et al (2018) Scalable production of core–shell nanoparticles by flash nano complexation to enhance mucosal transport for oral delivery of insulin. *Nanoscale* 10(7): 3307–3319. https://doi.org/10.1039/c7nr08047f
334. He ZY, Hu YZ, Nie TQ et al (2018) Size-controlled lipid nanoparticle production using turbulent mixing to enhance oral DNA delivery. *Acta Biomater* 81:195–207. https://doi.org/10.1016/j.actbio.2018.09.047
335. He ZY, Santos JL, Tian HK et al (2017) Scalable fabrication of size-controlled chitosan nanoparticles for oral delivery of insulin. *Biomaterials* 130:28–41. https://doi.org/10.1016/j.biomaterials.2017.03.028
336. Patel KK, Tariveranmoshabad M, Kadu S et al (2025) From concept to cure: the evolution of CAR-T cell therapy. *Mol Ther* 33(5):2123–2140. https://doi.org/10.1016/j.ymthe.2025.03.005
337. Ramamurthy A, Tommasi A, Saha K (2024) Advances in manufacturing chimeric antigen receptor immune cell therapies. *Semin Immunopathol* 46(5):12. https://doi.org/10.1007/s00281-024-01019-4
338. Levine BL, Miskin J, Wonnacott K et al (2017) Global manufacturing of CAR T cell therapy. *Mol Ther Meth Clin Dev* 4:92–101. https://doi.org/10.1016/j.omtm.2016.12.006
339. Kliegman M, Zaghlula M, Abrahamson S et al (2024) A roadmap for affordable genetic medicines. *Nature* 634(8033):307–314. https://doi.org/10.1038/s41586-024-07800-7
340. Tommasi A, Cappabianca D, Bugel M et al (2025) Efficient nonviral integration of large transgenes into human T cells using Cas9-CLIPT. *Mol Ther Meth Clin Dev* 33(1):101437. https://doi.org/10.1016/j.omtm.2025.101437
341. Xu J, Melenhorst JJ, Fraietta JA (2018) Toward precision manufacturing of immunogene T-cell therapies. *Cytotherapy* 20(5): 623–638. https://doi.org/10.1016/j.jcyt.2017.12.007
342. Kabra M, Shahi PK, Wang YY et al (2023) Nonviral base editing of KCNJ13 mutation preserves vision in a model of inherited retinal channelopathy. *J Clin Invest* 133(19):e171356. https://doi.org/10.1172/JCI171356
343. Wei SC, Cantor AJ, Walleshauser J et al (2025) Evaluation of subretinally delivered Cas9 ribonucleoproteins in murine and porcine animal models highlights key considerations for therapeutic translation of genetic medicines. *PLoS ONE* 20(6):e0317387. https://doi.org/10.1371/journal.pone.0317387
344. Saha K, Sontheimer EJ, Brooks PJ et al (2021) The NIH somatic cell genome editing program. *Nature* 592(7853):195–204. https://doi.org/10.1038/s41586-021-03191-1
345. Gillmore JD, Gane E, Täubel J et al (2025) Nexiguran ziclumeran gene editing in hereditary ATTR with polyneuropathy. *N Engl J Med* 393(14):1375–1386. https://doi.org/10.1056/nejmoa2510209
346. Musunuru K, Grandinette SA, Wang X et al (2025) Patient-specific in vivo gene editing to treat a rare genetic disease. *N Engl J Med* 392(22):2235–2243. https://doi.org/10.1056/NEJMoa2504747
347. Bot A, Scharenberg A, Friedman K et al (2026) In vivo chimeric antigen receptor (CAR)-T cell therapy. *Nat Rev Drug Discov* 25 (2):116–137. https://doi.org/10.1038/s41573-025-01291-5
348. Freedman BS, Bulte JWM, Conklin BR et al (2026) Monitoring biological effects of somatic cell genome editing. *Nat Rev Genet* 27(4):323–342. https://doi.org/10.1038/s41576-025-00916-0
349. Chaikof EL, Chen JC, Gillette MU et al (2025) Integrating synthetic biology to understand and engineer the heart, lung, blood, and sleep systems. *Cell Syst* 16(12):101446. https://doi.org/10.1016/j.cels.2025.101446
350. Angelini Stewart A, Ahrens-Nicklas RC, Tsai SQ et al (2026) Measurement and clinical interpretation of CRISPR off-targets. *Nat Genet* 58(1):20–27. https://doi.org/10.1038/s41588-025-02428-3
351. Mandal BB, Grinberg A, Seok Gil E et al (2012) High-strength silk protein scaffolds for bone repair. *Proc Natl Acad Sci USA* 109(20):7699–7704. https://doi.org/10.1073/pnas.1119474109
352. Clark AY, Martin KE, García JR et al (2020) Integrin-specific hydrogels modulate transplanted human bone marrow-derived mesenchymal stem cell survival, engraftment, and reparative activities. *Nat Commun* 11:114. https://doi.org/10.1038/s41467-019-14000-9
353. Brown TE, Carberry BJ, Worrell BT et al (2018) Photopolymerized dynamic hydrogels with tunable viscoelastic properties through thioester exchange. *Biomaterials* 178:496–503. https://doi.org/10.1016/j.biomaterials.2018.03.060
354. Cooke ME, Di Caprio N, Killgore J et al (2025) Tailoring agarose fluid gels for use in suspension bath bioprinting and culture of spheroid-based bioinks. *Biofabrication* 17(4):045020. https://doi.org/10.1088/1758-5090/ae0aff
355. DeFoe A, Toth J, Dhand AP et al (2025) Digital light processing of hydrogel molds to guide cell mechanosensing and the fabrication of meniscal tissue constructs. *APL Bioeng* 9(4):046111. https://doi.org/10.1063/5.0289256
356. Riffe MB, Di Caprio N, Davidson MD et al (2026) Injectable bilayered cryogel scaffolds for targeted adhesion to tissues. *ACS Macro Lett* 15(2):244–251. https://doi.org/10.1021/acsmacrolett.5c00265
357. Trindade D, Di Caprio N, Maurício AC et al (2026) Bioactive and injectable granular hydrogels incorporating decellularized extracellular matrix. *ACS Biomater Sci Eng* 12(3):1787–1798. https://doi.org/10.1021/acsbiomaterials.5c02060
358. Ouyang LL, Highley CB, Rodell CB et al (2016) 3D printing of shear-thinning hyaluronic acid hydrogels with secondary cross-linking. *ACS Biomater Sci Eng* 2(10):1743–1751. https://doi.org/10.1021/acsbiomaterials.6b00158
359. Guvendiren M, Burdick JA (2012) Stiffening hydrogels to probe short- and long-term cellular responses to dynamic mechanics. *Nat Commun* 3:792. https://doi.org/10.1038/ncomms1792
360. Guvendiren M, Lu HD, Burdick JA (2012) Shear-thinning hydrogels for biomedical applications. *Soft Matter* 8(2):260–272. https://doi.org/10.1039/c1sm06513k
361. Daly AC, Riley L, Segura T et al (2020) Hydrogel microparticles for biomedical applications. *Nat Rev Mater* 5(1):20–43. https://doi.org/10.1038/s41578-019-0148-6
362. Burdick JA, Anseth KS (2002) Photoencapsulation of osteoblasts in injectable RGD-modified PEG hydrogels for bone tissue engineering. *Biomaterials* 23(22):4315–4323. https://doi.org/10.1016/S0142-9612(02)00176-X
363. Khetan S, Guvendiren M, Legant WR et al (2013) Degradation-mediated cellular traction directs stem cell fate in covalently crosslinked three-dimensional hydrogels. *Nat Mater* 12(5):458–465. https://doi.org/10.1038/nmat3586
364. Burdick JA, Prestwich GD (2011) Hyaluronic acid hydrogels for biomedical applications. *Adv Mater* 23(12):H41–H56.

https://doi.org/10.1002/adma.201003963
365. Caliari SR, Burdick JA (2016) A practical guide to hydrogels for cell culture. *Nat Methods* 13(5):405–414. https://doi.org/10.1038/nmeth.3839
366. Cetnar AD, Tomov ML, Ning LQ et al (2021) Patient-specific 3D bioprinted models of developing human heart. *Adv Healthc Mater* 10(15):2001169. https://doi.org/10.1002/adhm.202001169
367. Jin LQ, Tomov ML, Chen H et al (2023) Abstract P1067: A perfused in vitro model of embryonic heart tube: leveraging 3D bioprinting and human induced pluripotent stem cell technologies to study heart development. *Circ Res* 133(Suppl_1):AP1067. https://doi.org/10.1161/res.133.suppl_1.p1067
368. Annabi N, Tamayol A, Uquillas JA et al (2014) 25th Anniversary Article: Rational design and applications of hydrogels in regenerative medicine. *Adv Mater* 26(1):85–124. https://doi.org/10.1002/adma.201303233
369. Tamayol A, Akbari M, Annabi N et al (2013) Fiber-based tissue engineering: progress, challenges, and opportunities. *Biotechnol Adv* 31(5):669–687. https://doi.org/10.1016/j.biotechadv.2012.11.007
370. Eugenis I, Wu D, Hu C et al (2022) Scalable macroporous hydrogels enhance stem cell treatment of volumetric muscle loss. *Biomaterials* 290:121818. https://doi.org/10.1016/j.biomaterials.2022.121818
371. Mostafavi A, Samandari M, Karvar M et al (2021) Colloidal multiscale porous adhesive (bio)inks facilitate scaffold integration. *Appl Phys Rev* 8(4):041415. https://doi.org/10.1063/5.0062823
372. Shi W, Fang F, Kong YF et al (2022) Dynamic hyaluronic acid hydrogel with covalent linked gelatin as an anti-oxidative bioink for cartilage tissue engineering. *Biofabrication* 14(1):014107. https://doi.org/10.1088/1758-5090/ac42de
373. Wei L, Wu SH, Kuss M et al (2019) 3D printing of silk fibroin-based hybrid scaffold treated with platelet rich plasma for bone tissue engineering. *Bioact Mater* 4:256–260. https://doi.org/10.1016/j.bioactmat.2019.09.001
374. Sears NA, Dhavalikar PS, Cosgriff-Hernandez EM (2016) Emulsion inks for 3D printing of high porosity materials. *Macromol Rapid Commun* 37(16):1369–1374. https://doi.org/10.1002/marc.201600236
375. Sengokmen-Ozsoz N, Claeyssens F (2025) Designing tomorrow's polymers: enabling multiscale porous structures from high internal phase emulsions *via* additive manufacturing. *Curr Opin Colloid Interface Sci* 77:101921. https://doi.org/10.1016/j.cocis.2025.101921
376. Johnson DW, Sherborne C, Didsbury MP et al (2013) Macrostructuring of emulsion-templated porous polymers by 3D laser patterning. *Adv Mater* 25(23):3178–3181. https://doi.org/10.1002/adma.201300552
377. Sušec M, Ligon SC, Stampfl J et al (2013) Hierarchically porous materials from layer-by-layer photopolymerization of high internal phase emulsions. *Macromol Rapid Commun* 34(11):938–943. https://doi.org/10.1002/marc.201300016
378. Wang AJ, Paterson T, Owen R et al (2016) Photocurable high internal phase emulsions (HIPEs) containing hydroxyapatite for additive manufacture of tissue engineering scaffolds with multiscale porosity. *Mater Sci Eng C* 67:51–58. https://doi.org/10.1016/j.msec.2016.04.087
379. Sears NA, Wilems TS, Gold KA et al (2019) Hydrocolloid inks for 3D printing of porous hydrogels. *Adv Mater Technol* 4(2): 1800343. https://doi.org/10.1002/admt.201800343
380. Sears N, Dhavalikar P, Whitely M et al (2017) Fabrication of biomimetic bone grafts with multi-material 3D printing. *Biofabrication* 9(2):025020. https://doi.org/10.1088/1758-5090/aa7077
381. Whitely M, Cereceres S, Dhavalikar P et al (2018) Improved in situ seeding of 3D printed scaffolds using cell-releasing hydrogels. *Biomaterials* 185:194–204. https://doi.org/10.1016/j.biomaterials.2018.09.027
382. Nguyen AK, Goering PL, Reipa V et al (2019) Toxicity and photosensitizing assessment of gelatin methacryloyl-based hydrogels photoinitiated with lithium phenyl-2,4,6-trimethylbenzoylphosphinate in human primary renal proximal tubule epithelial cells. *Biointerphases* 14(2):021007. https://doi.org/10.1116/1.5095886
383. Yang KH, Liu YZ, Skoog SA et al (2024) Physico-chemical properties and cytotoxicity of gelatin methacryloyl crosslinked with nanoparticle photoinitiator. *J Mater Res* 39(13):1852–1861. https://doi.org/10.1557/s43578-024-01369-7
384. Nguyen AK, Gittard SD, Koroleva A et al (2013) Two-photon polymerization of polyethylene glycol diacrylate scaffolds with riboflavin and triethanolamine used as a water-soluble photoinitiator. *Regen Med* 8(6):725–738. https://doi.org/10.2217/rme.13.60
385. Bose S, Ke DX, Sahasrabudhe H et al (2018) Additive manufacturing of biomaterials. *Prog Mater Sci* 93:45–111. https://doi.org/10.1016/j.pmatsci.2017.08.003
386. Vamsi Krishna B, Xue WC, Bose S et al (2008) Engineered porous metals for implants. *JOM* 60(5):45–48. https://doi.org/10.1007/s11837-008-0059-2
387. Bandyopadhyay A, Krishna BV, Xue WC et al (2009) Application of Laser Engineered Net Shaping (LENS) to manufacture porous and functionally graded structures for load bearing implants. *J Mater Sci Mater Med* 20(1):29–34. https://doi.org/10.1007/s10856-008-3478-2
388. Bandyopadhyay A, Espana F, Balla VK et al (2010) Influence of porosity on mechanical properties and in vivo response of Ti6Al4V implants. *Acta Biomater* 6(4):1640–1648. https://doi.org/10.1016/j.actbio.2009.11.011
389. Bose S, Roy M, Bandyopadhyay A (2012) Recent advances in bone tissue engineering scaffolds. *Trends Biotechnol* 30(10): 546–554. https://doi.org/10.1016/j.tibtech.2012.07.005
390. Bose S, Vahabzadeh S, Bandyopadhyay A (2013) Bone tissue engineering using 3D printing. *Mater Today* 16(12):496–504. https://doi.org/10.1016/j.mattod.2013.11.017
391. Bose S, Fielding G, Tarafder S et al (2013) Understanding of dopant-induced osteogenesis and angiogenesis in calcium phosphate ceramics. *Trends Biotechnol* 31(10):594–605. https://doi.org/10.1016/j.tibtech.2013.06.005
392. Bandyopadhyay A, Bernard S, Xue WC et al (2006) Calcium phosphate-based resorbable ceramics: influence of MgO, ZnO, and SiO_2 dopants. *J Am Ceram Soc* 89(9):2675–2688. https://doi.org/10.1111/j.1551-2916.2006.01207.x
393. Bose S, Bandyopadhyay A (2015) Resorbable ceramics with controlled strength loss rates. US Patent 9028871
394. Bandyopadhyay A (2007) Bone replacement materials. US Patent 9327056
395. Xue WC, Krishna BV, Bandyopadhyay A et al (2007) Processing and biocompatibility evaluation of laser processed porous titanium. *Acta Biomater* 3(6):1007–1018. https://doi.org/10.1016/j.actbio.2007.05.009
396. Balla VK, Bodhak S, Bose S et al (2010) Porous tantalum structures for bone implants: fabrication, mechanical and in vitro biological properties. *Acta Biomater* 6(8):3349–3359. https://doi.org/10.1016/j.actbio.2010.01.046
397. Bose S, Sarkar N, Banerjee D (2018) Effects of PCL, PEG and

PLGA polymers on curcumin release from calcium phosphate matrix for *in vitro* and *in vivo* bone regeneration. *Mater Today Chem* 8:110–120. https://doi.org/10.1016/j.mtchem.2018.03.005
398. Bose S, Banerjee D, Vu AA (2022) Ginger and garlic extracts enhance osteogenesis in 3D printed calcium phosphate bone scaffolds with bimodal pore distribution. *ACS Appl Mater Interfaces* 14(11):12964–12975. https://doi.org/10.1021/ACSAMI.1C19617
399. Fielding G, Bose S (2013) SiO_2 and ZnO dopants in three-dimensionally printed tricalcium phosphate bone tissue engineering scaffolds enhance osteogenesis and angiogenesis in vivo. *Acta Biomater* 9(11):9137–9148. https://doi.org/10.1016/j.actbio.2013.07.009
400. Bose S, Tarafder S, Bandyopadhyay A (2017) Effect of chemistry on osteogenesis and angiogenesis towards bone tissue engineering using 3D printed scaffolds. *Ann Biomed Eng* 45(1):261–272. https://doi.org/10.1007/s10439-016-1646-y
401. Roy M, Vamsi Krishna B, Bandyopadhyay A et al (2008) Laser processing of bioactive tricalcium phosphate coating on titanium for load-bearing implants. *Acta Biomater* 4(2):324–333. https://doi.org/10.1016/j.actbio.2007.09.008
402. Bose S, Banerjee D, Shivaram A et al (2018) Calcium phosphate coated 3D printed porous titanium with nanoscale surface modification for orthopedic and dental applications. *Mater Des* 151:102–112. https://doi.org/10.1016/j.matdes.2018.04.049
403. Bandyopadhyay A, Mitra I, Goodman SB et al (2023) Improving biocompatibility for next generation of metallic implants. *Prog Mater Sci* 133:101053. https://doi.org/10.1016/j.pmatsci.2022.101053
404. Zandi N, Sani ES, Mostafavi E et al (2021) Nanoengineered shear-thinning and bioprintable hydrogel as a versatile platform for biomedical applications. *Biomaterials* 267:120476. https://doi.org/10.1016/j.biomaterials.2020.120476
405. Spencer AR, Shirzaei Sani E, Soucy JR et al (2019) Bioprinting of a cell-laden conductive hydrogel composite. *ACS Appl Mater Interfaces* 11(34):30518–30533. https://doi.org/10.1021/acsami.9b07353
406. De Maeseneer T, Zhou F, Annabi N (2025) Advanced fabrication techniques to engineer cell-laden multilayered hollow tubular structures. *Adv Mater Technol* 10(22):e00864. https://doi.org/10.1002/admt.202500864
407. Habib A, Sathish V, Mallik S et al (2018) 3D printability of alginate-carboxymethyl cellulose hydrogel. *Materials* 11(3):454. https://doi.org/10.3390/ma11030454
408. Rohauer R, Schimmelpfennig K, Mei V et al (2025) Characterization and prediction of properties of polymeric materials for extrusion-based bioprinting process. In: Proceedings of the ASME 20th International Manufacturing Science and Engineering Conference, p.1–9. https://doi.org/10.1115/MSEC2025-155176
409. Nelson C, Tuladhar S, Launen L et al (2021) 3D bio-printability of hybrid pre-crosslinked hydrogels. *Int J Mol Sci* 22(24):13481. https://doi.org/10.3390/ijms222413481
410. Nelson C, Tuladhar S, Habib A (2022) Physical modification of hybrid hydrogels to fabricate full-scale construct using three-dimensional bio-printing process. *J Micro Nano-Manuf* 10(1):011005. https://doi.org/10.1115/1.4055230
411. Jin YF, Compaan A, Chai WX et al (2017) Functional nanoclay suspension for printing-then-solidification of liquid materials. *ACS Appl Mater Interfaces* 9(23):20057–20066. https://doi.org/10.1021/acsami.7b02398
412. Jin YF, Xiong RT, Antonelli PJ et al (2021) Nanoclay suspension-enabled extrusion bioprinting of three-dimensional soft structures. *J Manuf Sci Eng* 143(12):121004. https://doi.org/10.1115/1.4051010
413. Compaan AM, Song KD, Huang Y (2019) Gellan fluid gel as a versatile support bath material for fluid extrusion bioprinting. *ACS Appl Mater Interfaces* 11(6):5714–5726. https://doi.org/10.1021/acsami.8b13792
414. Compaan AM, Song KD, Chai WX et al (2020) Cross-linkable microgel composite matrix bath for embedded bioprinting of perfusable tissue constructs and sculpting of solid objects. *ACS Appl Mater Interfaces* 12(7):7855–7868. https://doi.org/10.1021/ACSAMI.9B15451
415. Jin YF, Song KD, Gellermann N et al (2019) Printing of hydrophobic materials in fumed silica nanoparticle suspension. *ACS Appl Mater Interfaces* 11(32):29207–29217. https://doi.org/10.1021/acsami.9b07433
416. Jin YF, Liu CC, Chai WX et al (2017) Self-supporting nanoclay as internal scaffold material for direct printing of soft hydrogel composite structures in air. *ACS Appl Mater Interfaces* 9(20):17456–17465. https://doi.org/10.1021/acsami.7b03613
417. Song KD, Compaan AM, Chai WX et al (2020) Injectable gelatin microgel-based composite ink for 3D bioprinting in air. *ACS Appl Mater Interfaces* 12(20):22453–22466. https://doi.org/10.1021/acsami.0c01497
418. Murphy C, Kolan K, Li WB et al (2017) 3D bioprinting of stem cells and polymer/bioactive glass composite scaffolds for bone tissue engineering. *Int J Bioprint* 3(1):53–63. https://doi.org/10.18063/ijb.2017.01.005
419. Kolan KCR, Semon JA, Bromet B et al (2019) Bioprinting with human stem cell-laden alginate-gelatin bioink and bioactive glass for tissue engineering. *Int J Bioprinting* 5(2):204. https://doi.org/10.18063/ijb.v5i2.2.204
420. Kolan KCR, Semon JA, Bindbeutel AT et al (2020) Bioprinting with bioactive glass loaded polylactic acid composite and human adipose stem cells. *Bioprinting* 18:e00075. https://doi.org/10.1016/j.bprint.2020.e00075
421. Kolan K, Liu Y, Baldridge J et al (2017) Solvent based 3D printing of biopolymer/bioactive glass composite and hydrogel for tissue engineering applications. *Procedia CIRP* 65:38–43. https://doi.org/10.1016/j.procir.2017.04.022
422. Kolan KCR, Huang YW, Semon JA et al (2020) 3D-printed biomimetic bioactive glass scaffolds for bone regeneration in rat calvarial defects. *Int J Bioprinting* 6(2):274. https://doi.org/10.18063/ijb.v6i2.274
423. Kolan KCR, Li J, Roberts S et al (2019) Near-field electrospinning of a polymer/bioactive glass composite to fabricate 3D biomimetic structures. *Int J Bioprinting* 5(1):163. https://doi.org/10.18063/ijb.v5i1.163
424. Bhattacharjee T, Zehnder SM, Rowe KG et al (2015) Writing in the granular gel medium. *Sci Adv* 1(8):e1500655. https://doi.org/10.1126/sciadv.1500655
425. Wang W, Li G, Huang Y (2009) Modeling of bubble expansion-induced cell mechanical profile in laser-assisted cell direct writing. *J Manuf Sci Eng* 131(5):051013. https://doi.org/10.1115/1.4000101
426. Xiong RT, Zhang ZY, Shen JX et al (2015) Bubble formation modeling during laser direct writing of glycerol solutions. *J Micro Nano Manuf* 3:011004. https://doi.org/10.1115/1.4029264
427. Wang W, Huang Y, Grujicic M et al (2008) Study of impact-induced mechanical effects in cell direct writing using smooth particle hydrodynamic method. *J Manuf Sci Eng* 130(2):021012. https://doi.org/10.1115/1.2896118

428. Xu CX, Zhang ZY, Huang Y et al (2019) Phase diagram of pinch-off behaviors during drop-on-demand inkjetting of alginate solutions. *J Manuf Sci Eng* 141(9):091013. https://doi.org/10.1115/1.4044252
429. Sole-Gras M, Christensen K, Chen YX et al (2022) Effects of spatial and temporal offset during landing on mixing performance in intersecting-jets printing. *Addit Manuf* 55:102829. https://doi.org/10.1016/j.addma.2022.102829
430. Zhang ZY, Xiong RT, Corr DT et al (2016) Study of impingement types and printing quality during laser printing of viscoelastic alginate solutions. *Langmuir* 32(12):3004–3014. https://doi.org/10.1021/acs.langmuir.6b00220
431. Zhang ZY, Xu CX, Xiong RT et al (2017) Effects of living cells on the bioink printability during laser printing. *Biomicrofluidics* 11(3):034120. https://doi.org/10.1063/1.4985652
432. Zhang ZY, Xiong RT, Mei RW et al (2015) Time-resolved imaging study of jetting dynamics during laser printing of viscoelastic alginate solutions. *Langmuir* 31(23):6447–6456. https://doi.org/10.1021/acs.langmuir.5b00919
433. Sole-Gras M, Xiong RT, Liang CX et al (2021) Study of overlapping adjacent jets for effective laser-induced forward transfer printing. *J Manuf Sci Eng* 143(4):041001. https://doi.org/10.1115/1.4048440
434. Jin YF, Chai WX, Huang Y (2017) Printability study of hydrogel solution extrusion in nanoclay yield-stress bath during printing-then-gelation biofabrication. *Mater Sci Eng C* 80:313–325. https://doi.org/10.1016/j.msec.2017.05.144
435. Jin YF, Zhao DY, Huang Y (2018) Study of extrudability and standoff distance effect during nanoclay-enabled direct printing. *Bio-Des Manuf* 1(2):123–134. https://doi.org/10.1007/s42242-018-0009-y
436. Chen YX, Allo SC, Ren B et al (2024) Upflow mitigation strategy for nested printing. *CIRP Ann* 73(1):181–184. https://doi.org/10.1016/j.cirp.2024.04.047
437. Chen YX, Samouce C, Shlafer SE et al (2025) Deposition volume compensation for enhanced shape fidelity in nested printing. *J Manuf Sci Eng* 147(11):111003. https://doi.org/10.1115/1.4069661
438. Khoda AKMB, Ozbolat IT, Koc B (2011) Engineered tissue scaffolds with variational porous architecture. *J Biomech Eng* 133(1):011001. https://doi.org/10.1115/1.4002933
439. Khoda AKM, Ozbolat IT, Koc B (2011) A functionally gradient variational porosity architecture for hollowed scaffolds fabrication. *Biofabrication* 3(3):034106. https://doi.org/10.1088/1758-5082/3/3/034106
440. Khoda AKM, Koc B (2013) Functionally heterogeneous porous scaffold design for tissue engineering. *Comput Aided Des* 45(11):1276–1293. https://doi.org/10.1016/j.cad.2013.05.005
441. Khoda AKM, Ozbolat IT, Koc B (2013) Designing heterogeneous porous tissue scaffolds for additive manufacturing processes. *Comput Aided Des* 45(12):1507–1523. https://doi.org/10.1016/j.cad.2013.07.003
442. Xu YH, Sarah R, Habib A et al (2024) Constraint based Bayesian optimization of bioink precursor: a machine learning framework. *Biofabrication* 16(4):045031. https://doi.org/10.1088/1758-5090/ad716e
443. Ayowole O, Lapp J, Khoda B (2025) Evaluation of custom microalgae-based bioink formulations for optimized green bioprinting. *Materials* 18(4):753. https://doi.org/10.3390/ma18040753
444. Khoda B, Habib A (2026) 3D bioprinting with cellulose-derived bio-ink and precursors. In: Klemmt C, Beaucage G (Eds.), Biodegradable 3D-Printing (1st Ed.). Springer, Singapore, p.71–98. https://doi.org/10.1007/978-981-95-4025-9_5
445. Gilchrist AE, Liu YM, Klett K et al (2023) Transient competitors to modulate dynamic covalent cross-linking of recombinant hydrogels. *Chem Mater* 35(21):8969–8983. https://doi.org/10.1021/acs.chemmater.3c01575
446. Shin S, Brunel LG, Cai B et al (2023) Gelation of uniform interfacial diffusant in embedded 3D printing. *Adv Funct Mater* 33(50): 2307435. https://doi.org/10.1002/adfm.202307435
447. Cai B, Kilian D, Ghorbani S et al (2025) One-step bioprinting of endothelialized, self-supporting arterial and venous networks. *Biofabrication* 17(2):025012. https://doi.org/10.1088/1758-5090/adab26
448. Brunel LG, Christakopoulos F, Kilian D et al (2024) Embedded 3D bioprinting of collagen inks into microgel baths to control hydrogel microstructure and cell spreading. *Adv Healthc Mater* 13(25):2303325. https://doi.org/10.1002/adhm.202303325
449. Singhal D, Christakopoulos F, Brunel LG et al (2026) Dual-orientation of collagen fibers to guide cell alignment in 3D-printed constructs. *Acta Biomater* 209:167–182. https://doi.org/10.1016/j.actbio.2025.11.013
450. Krajina BA, LeSavage BL, Roth JG et al (2021) Microrheology reveals simultaneous cell-mediated matrix stiffening and fluidization that underlie breast cancer invasion. *Sci Adv* 7(8):eabe1969. https://doi.org/10.1126/sciadv.abe1969
451. Wang PJ, Sun YZ, Shi XQ et al (2021) 3D printing of tissue engineering scaffolds: a focus on vascular regeneration. *Bio-Des Manuf* 4(2):344–378. https://doi.org/10.1007/s42242-020-00109-0
452. Shao L, Gao Q, Xie CQ et al (2020) Directly coaxial 3D bioprinting of large-scale vascularized tissue constructs. *Biofabrication* 12(3):035014. https://doi.org/10.1088/1758-5090/ab7e76
453. Shyam Mohan T, Datta P, Nesaei S et al (2022) 3D coaxial bioprinting: process mechanisms, bioinks and applications. *Prog Biomed Eng* 4(2):022003. https://doi.org/10.1088/2516-1091/ac631c
454. Sun JR, Gong YP, He YC et al (2025) Process optimization for coaxial extrusion-based bioprinting: a comprehensive analysis of material behavior, structural precision, and cell viability. *Addit Manuf* 100:104682. https://doi.org/10.1016/j.addma.2025.104682
455. Bosch-Rué È, Díez-Tercero L, Delgado LM et al (2022) Biofabrication of collagen tissue-engineered blood vessels with direct co-axial extrusion. *Int J Mol Sci* 23(10):5618. https://doi.org/10.3390/ijms23105618
456. Yu I, Grindrod S, Chen R (2020) Controllability over wall thickness of tubular structures and encapsulation during co-axial extrusion of a thermal-crosslinking hydrogel. *J Manuf Sci Eng* 142(8):081006. https://doi.org/10.1115/1.4047091
457. Zhang ZY, Chai WX, Xiong RT et al (2017) Printing-induced cell injury evaluation during laser printing of 3T3 mouse fibroblasts. *Biofabrication* 9(2):025038. https://doi.org/10.1088/1758-5090/aa6ed9
458. Rahman TT, Wood N, Pei ZJ et al (2024) Effects of extreme temperature on human bronchial epithelial cells in 3D printed samples. *Bioengineering* 11(12):1201. https://doi.org/10.3390/bioengineering11121201
459. Rahman TT, Wood N, Pei ZJ et al (2025) Effects of extrusion pressure during 3D printing on viability of human bronchial epithelial cells in 3D printed samples. *Biomimetics* 10(5):297. https://doi.org/10.3390/biomimetics10050297

460. Dupont S, Morsut L, Aragona M et al (2011) Role of YAP/TAZ in mechanotransduction. *Nature* 474(7350):179–183. https://doi.org/10.1038/nature10137
461. Campbell A, Mohl JE, Gutierrez DA et al (2020) Thermal bioprinting causes ample alterations of expression of LUCAT1, IL6, CCL26, and NRN1L genes and massive phosphorylation of critical oncogenic drug resistance pathways in breast cancer cells. *Front Bioeng Biotechnol* 8:82. https://doi.org/10.3389/fbioe.2020.00082
462. O'Bryan CS, Kabb CP, Sumerlin BS et al (2019) Jammed polyelectrolyte microgels for 3D cell culture applications: rheological behavior with added salts. *ACS Appl Bio Mater* 2(4):1509–1517. https://doi.org/10.1021/acsabm.8b00784
463. Ellison ST, Duraivel S, Subramaniam V et al (2022) Cellular micromasonry: biofabrication with single cell precision. *Soft Matter* 18(45):8554–8560. https://doi.org/10.1039/d2sm01013e
464. Brock AA, Duraivel S, Jiang J et al (2025) RNA sequencing at single vesicle resolution via 3D printed embedded droplet arrays. *ACS Appl Mater Interfaces* 17(38):53110–53121. https://doi.org/10.1021/acsami.5c09959
465. Bhattacharjee T, Kabb CP, O'Bryan CS et al (2018) Polyelectrolyte scaling laws for microgel yielding near jamming. *Soft Matter* 14(9):1559–1570. https://doi.org/10.1039/c7sm01518f
466. Widener AE, Duraivel S, Angelini TE et al (2022) Injectable microporous annealed particle hydrogel based on guest–host-interlinked polyethylene glycol maleimide microgels. *Adv NanoBiomed Res* 2(10):2200030. https://doi.org/10.1002/anbr.202200030
467. Bhattacharjee T, Angelini TE (2019) 3D T cell motility in jammed microgels. *J Phys D Appl Phys* 52(2):024006. https://doi.org/10.1088/1361-6463/aae813
468. Anjum MR, Subramaniam V, Higgins BR et al (2024) Determining rates of molecular secretion from supernatant concentration measurements in a 3D-bioprinted human liver tissue model. *ACS Biomater Sci Eng* 10(10):6711–6720. https://doi.org/10.1021/acsbiomaterials.4c01086
469. Morley CD, Flores CT, Drake JA et al (2022) Spatiotemporal T cell dynamics in a 3D bioprinted immunotherapy model. *Bioprinting* 28:e00231. https://doi.org/10.1016/j.bprint.2022.e00231
470. Morley CD, Tordoff J, O'Bryan CS et al (2020) 3D aggregation of cells in packed microgel media. *Soft Matter* 16(28):6572–6581. https://doi.org/10.1039/d0sm00517g
471. Bhattacharjee T, Gil CJ, Marshall SL et al (2016) Liquid-like solids support cells in 3D. *ACS Biomater Sci Eng* 2(10):1787–1795. https://doi.org/10.1021/acsbiomaterials.6b00218
472. Subramaniam V, Abrahan C, Higgins BR et al (2025) A functional human liver tissue model: 3D bioprinted co-culture discoids. *Biomater Adv* 173:214288. https://doi.org/10.1016/j.bioadv.2025.214288
473. Crick FHC, Hughes AFW (1950) The physical properties of cytoplasm: a study by means of the magnetic particle method. Part I. Experimental. *Exp Cell Res* 1(1):37–80. https://doi.org/10.1016/0014-4827(50)90048-6
474. Tomov ML, Cetnar A, Do K et al (2019) Patient-specific 3-dimensional–bioprinted model for in vitro analysis and treatment planning of pulmonary artery atresia in tetralogy of fallot and major aortopulmonary collateral arteries. *J Am Heart Assoc* 8(24):e014490. https://doi.org/10.1161/jaha.119.014490
475. Mansoorifar A, Subbiah R, de Souza Balbinot G et al (2020) Embedding cells within nanoscale, rapidly mineralizing hydrogels: a new paradigm to engineer cell-laden bone-like tissue. *J Struct Biol* 212(3):107636. https://doi.org/10.1016/j.jsb.2020.107636
476. Schroyer KAR, Schmitz KM, Raheja G et al (2025) Bioprinting of GelMA-based hydrogels to aid in creation of biomimetic 3D models for glioblastoma. *Micromachines* 16(6):654. https://doi.org/10.3390/mi16060654
477. Whisler JA, Chen MB, Kamm RD (2014) Control of perfusable microvascular network morphology using a multiculture microfluidic system. *Tissue Eng Part C Meth* 20(7):543–552. https://doi.org/10.1089/ten.tec.2013.0370
478. Chen MB, Whisler JA, Jeon JS et al (2013) Mechanisms of tumor cell extravasation in an *in vitro* microvascular network platform. *Integr Biol* 5(10):1262–1271. https://doi.org/10.1039/C3IB40149A
479. Chen MB, Whisler JA, Fröse J et al (2017) On-chip human microvasculature assay for visualization and quantification of tumor cell extravasation dynamics. *Nat Protoc* 12(5):865–880. https://doi.org/10.1038/nprot.2017.018
480. Campisi M, Shin Y, Osaki T et al (2018) 3D self-organized microvascular model of the human blood–brain barrier with endothelial cells, pericytes and astrocytes. *Biomaterials* 180:117–129. https://doi.org/10.1016/j.biomaterials.2018.07.014
481. Chen MB, Lamar JM, Li R et al (2016) Elucidation of the roles of tumor integrin β1 in the extravasation stage of the metastasis cascade. *Cancer Res* 76(9):2513–2524. https://doi.org/10.1158/0008-5472.can-15-1325
482. Hajal C, Shin Y, Li L et al (2021) The CCL2-CCR2 astrocyte-cancer cell axis in tumor extravasation at the brain. *Sci Adv* 7(26):eabg8139. https://doi.org/10.1126/sciadv.abg8139
483. Haase K, Offeddu GS, Gillrie MR et al (2020) Endothelial regulation of drug transport in a 3D vascularized tumor model. *Adv Funct Mater* 30(48):2002444. https://doi.org/10.1002/adfm.202002444
484. Nguyen RY, Cabral AT, Rossello-Martinez A et al (2023) Tunable mesoscopic collagen island architectures modulate stem cell behavior. *Adv Mater* 35(16):2207882. https://doi.org/10.1002/adma.202207882
485. Skardal A, Murphy SV, Devarasetty M et al (2017) Multi-tissue interactions in an integrated three-tissue organ-on-a-chip platform. *Sci Rep* 7:8837. https://doi.org/10.1038/s41598-017-08879-x
486. Raman R, Cvetkovic C, Uzel SGM et al (2016) Optogenetic skeletal muscle-powered adaptive biological machines. *Proc Natl Acad Sci USA* 113(13):3497–3502. https://doi.org/10.1073/pnas.1516139113
487. Hockaday LA, Kang KH, Colangelo NW et al (2012) Rapid 3D printing of anatomically accurate and mechanically heterogeneous aortic valve hydrogel scaffolds. *Biofabrication* 4(3):035005. https://doi.org/10.1088/1758-5082/4/3/035005
488. Ronaldson-Bouchard K, Yeager K, Teles D et al (2019) Engineering of human cardiac muscle electromechanically matured to an adult-like phenotype. *Nat Protoc* 14(10):2781–2817. https://doi.org/10.1038/s41596-019-0189-8
489. Lock RI, Graney PL, Tavakol DN et al (2024) Macrophages enhance contractile force in iPSC-derived human engineered cardiac tissue. *Cell Rep* 43(6):114302. https://doi.org/10.1016/j.celrep.2024.114302
490. Morsink MAJ, Wang BZ, Watkins JM et al (2025) A patient-specific engineered tissue model of BAG3-mediated cardiomyopathy. *J Tissue Eng* 16:20417314251371296. https://doi.org/10.1177/20417314251371296
491. Tavakol DN, Nash TR, Kim Y et al (2023) Modeling and countering the effects of cosmic radiation using bioengineered

human tissues. *Biomaterials* 301:122267. https://doi.org/10.1016/j.biomaterials.2023.122267
492. Tavakol DN, Nash TR, Kim Y et al (2024) Modeling the effects of protracted cosmic radiation in a human organ-on-chip platform. *Adv Sci* 11(42):2401415. https://doi.org/10.1002/advs.202401415
493. Jin LQ, Hwang B, Rezapourdamanab S et al (2025) Bioengineering approaches to in vitro modeling of genetic and acquired cardiac diseases. *Curr Cardiol Rep* 27(1):72. https://doi.org/10.1007/s11886-025-02218-7
494. Drakhlis L, Zweigerdt R (2023) Heart in a dish – choosing the right *in vitro* model. *Dis Models Mech* 16(5):dmm049961. https://doi.org/10.1242/dmm.049961
495. Hofbauer P, Jahnel SM, Mendjan S (2021) *In vitro* models of the human heart. *Development* 148(16):dev199672. https://doi.org/10.1242/dev.199672
496. Ning LQ, Zanella S, Tomov ML et al (2024) Targeted rapamycin delivery via magnetic nanoparticles to address stenosis in a 3D bioprinted in vitro model of pulmonary veins. *Adv Sci* 11(26): 2400476. https://doi.org/10.1002/advs.202400476
497. Saadeh MR, Tomov ML, Dasi LP et al (2023) Abstract P3024: Endothelial to mesenchymal transition frequency increases in Williams syndrome pulmonary artery endothelial cells in novel 3D bioprinted *in vitro* arterial model. *Circ Res* 133(Suppl_1): AP3024. https://doi.org/10.1161/res.133.suppl_1.p3024
498. Tomov ML, Perez L, Ning LQ et al (2021) A 3D bioprinted in vitro model of pulmonary artery atresia to evaluate endothelial cell response to microenvironment. *Adv Healthc Mater* 10(20): 2100968. https://doi.org/10.1002/adhm.202100968
499. Gil CJ, Allphin AJ, Jin LQ et al (2025) Image-guided cardiac regeneration via a 3D bioprinted vascular patch with built-in CT visibility. *Chem Eng J* 520:165926. https://doi.org/10.1016/j.cej.2025.165926
500. Gil CJ, Evans CJ, Li L et al (2023) Leveraging 3D bioprinting and photon-counting computed tomography to enable noninvasive quantitative tracking of multifunctional tissue engineered constructs. *Adv Healthc Mater* 12(31):2302271. https://doi.org/10.1002/adhm.202302271
501. Majumdar U, Yasuhara J, Garg V (2021) In vivo and in vitro genetic models of congenital heart disease. *Cold Spring Harb Perspect Biol* 13(4):a036764. https://doi.org/10.1101/cshperspect.a036764
502. Novakovic GV, Eschenhagen T, Mummery C (2014) Myocardial tissue engineering: in vitro models. *Cold Spring Harb Perspect Med* 4(3):a014076. https://doi.org/10.1101/cshperspect.a014076
503. Rufaihah AJ, Chen CK, Yap CH et al (2021) Mending a broken heart: *in vitro*, *in vivo* and *in silico* models of congenital heart disease. *Dis Models Mech* 14(3):dmm047522. https://doi.org/10.1242/dmm.047522
504. Hanson KP, Jung JP, Tran QA et al (2013) Spatial and temporal analysis of extracellular matrix proteins in the developing murine heart: a blueprint for regeneration. *Tissue Eng Part A* 19(9–10): 1132–1143. https://doi.org/10.1089/ten.tea.2012.0316
505. Jung JP, Hu DJ, Domian IJ et al (2015) An integrated statistical model for enhanced murine cardiomyocyte differentiation via optimized engagement of 3D extracellular matrices. *Sci Rep* 5: 18705. https://doi.org/10.1038/srep18705
506. Hall ML, Lin WH, Ogle BM (2025) Optimizing extracellular matrix for endothelial differentiation using a design of experiments approach. *Sci Rep* 15:24479. https://doi.org/10.1038/s41598-025-09256-9
507. Hall ML, Givens S, Santosh N et al (2022) Laminin 411 mediates endothelial specification via multiple signaling axes that converge on β-catenin. *Stem Cell Rep* 17(3):569–583. https://doi.org/10.1016/j.stemcr.2022.01.005
508. Komosa ER, Lin WH, Ogle BM (2025) Toward robust and reproducible pluripotent stem cell expansion in bioprinted GelMA constructs. *Int J Bioprinting* 11(1):363–381. https://doi.org/10.36922/ijb.4633
509. Komosa ER, Lin WH, Mahadik B et al (2024) A novel perfusion bioreactor promotes the expansion of pluripotent stem cells in a 3D-bioprinted tissue chamber. *Biofabrication* 16(1):014101. https://doi.org/10.1088/1758-5090/ad084a
510. Lin WH, Zhu ZJ, Ravikumar V et al (2022) A bionic testbed for cardiac ablation tools. *Int J Mol Sci* 23(22):14444. https://doi.org/10.3390/ijms232214444
511. Bertassoni LE (2022) Bioprinting of complex multicellular organs with advanced functionality-recent progress and challenges ahead. *Adv Mater* 34(3):e2101321. https://doi.org/10.1002/adma.202101321
512. Helms HR, Davies AE, Schutt CE et al (2026) Engineering and biofabrication of early cancer models. *Nat Rev Bioeng* 4(2):134–152. https://doi.org/10.1038/s44222-025-00371-w
513. da Costa Sousa MG, de Souza Balbinot G, Subbiah R et al (2024) *In vitro* development and optimization of cell-laden injectable bioprinted gelatin methacryloyl (GelMA) microgels mineralized on the nanoscale. *Biomater Adv* 159:213805. https://doi.org/10.1016/j.bioadv.2024.213805
514. Thrivikraman G, Athirasala A, Gordon R et al (2019) Rapid fabrication of vascularized and innervated cell-laden bone models with biomimetic intrafibrillar collagen mineralization. *Nat Commun* 10:3520. https://doi.org/10.1038/s41467-019-11455-8
515. Mansoorifar A, Gordon R, Bergan RC et al (2021) Bone-on-a-chip: microfluidic technologies and microphysiologic models of bone tissue. *Adv Funct Mater* 31(6):2006796. https://doi.org/10.1002/adfm.202006796
516. Bertassoni LE, Cecconi M, Manoharan V et al (2014) Hydrogel bioprinted microchannel networks for vascularization of tissue engineering constructs. *Lab Chip* 14(13):2202–2211. https://doi.org/10.1039/c4lc00030g
517. Mansoorifar A, Tahayeri A, Bertassoni LE (2020) Bioinspired reconfiguration of 3D printed microfluidic hydrogels via automated manipulation of magnetic inks. *Lab Chip* 20(10):1713–1719. https://doi.org/10.1039/d0lc00280a
518. Twohig C, Helsinga M, Mansoorifar A et al (2021) A dual-ink 3D printing strategy to engineer pre-vascularized bone scaffolds in-vitro. *Mater Sci Eng C* 123:111976. https://doi.org/10.1016/j.msec.2021.111976
519. Bertassoni LE, Cardoso JC, Manoharan V et al (2014) Direct-write bioprinting of cell-laden methacrylated gelatin hydrogels. *Biofabrication* 6(2):024105. https://doi.org/10.1088/1758-5082/6/2/024105
520. Athirasala A, Tahayeri A, Thrivikraman G et al (2018) A dentin-derived hydrogel bioink for 3D bioprinting of cell laden scaffolds for regenerative dentistry. *Biofabrication* 10(2):024101. https://doi.org/10.1088/1758-5090/aa9b4e
521. Parthiban SP, Athirasala A, Tahayeri A et al (2021) BoneMA—synthesis and characterization of a methacrylated bone-derived hydrogel for bioprinting of *in-vitro* vascularized tissue constructs. *Biofabrication* 13(3):035031. https://doi.org/10.1088/1758-5090/abb11f
522. Franca CM, Athirasala A, Subbiah R et al (2023) High-throughput

bioprinting of geometrically-controlled pre-vascularized injectable microgels for accelerated tissue regeneration. *Adv Healthc Mater* 12(22):e2202840. https://doi.org/10.1002/adhm.202202840
523. Franca CM, Verde MEL, Silva-Sousa AC et al (2025) Perivascular cells function as key mediators of mechanical and structural changes in vascular capillaries. *Sci Adv* 11(2):eadp3789. https://doi.org/10.1126/sciadv.adp3789
524. Cunha D, Souza N, Moreira M et al (2023) 3D-printed microgels supplemented with dentin matrix molecules as a novel biomaterial for direct pulp capping. *Clin Oral Investig* 27(3):1215–1225. https://doi.org/10.1007/s00784-022-04735-z
525. Subbiah R, Hipfinger C, Tahayeri A et al (2020) 3D printing of microgel-loaded modular microcages as instructive scaffolds for tissue engineering. *Adv Mater* 32(36):2001736. https://doi.org/10.1002/adma.202001736
526. Liu X, Michael S, Bharti K et al (2020) A biofabricated vascularized skin model of atopic dermatitis for preclinical studies. *Biofabrication* 12(3):035002. https://doi.org/10.1088/1758-5090/ab76a1
527. Derr K, Zou JY, Luo KR et al (2019) Fully three-dimensional bioprinted skin equivalent constructs with validated morphology and barrier function. *Tissue Eng Part C Methods* 25(6):334–343. https://doi.org/10.1089/ten.TEC.2018.0318
528. Ellison ST, Hayman I, Derr K et al (2025) Limitations of acyclovir and identification of potent HSV antivirals using 3D bioprinted human skin equivalents. *Nat Commun* 16:9200. https://doi.org/10.1038/s41467-025-64245-w
529. Tung YT, Chen YC, Derr K et al (2024) A 3D bioprinted human neurovascular unit model of glioblastoma tumor growth. *Adv Healthc Mater* 13(15):2302831. https://doi.org/10.1002/adhm.202302831
530. Rajput M, Tung YT, Chen YC et al (2025) Perfusable brain microvascular network-on-chip model to study flavivirus NS1-induced endothelial dysfunction. *Adv Funct Mater* 35(50):e04476. https://doi.org/10.1002/adfm.202504476
531. Medina A, Chen YC, Zhang JJ et al (2025) Modeling neurotropic virus infection with functional human neural spheroids as a platform for high-throughput antiviral screening and pathogenesis. *Antivir Res* 242:106248. https://doi.org/10.1016/j.antiviral.2025.106248
532. Kundu S, Boutin ME, Strong CE et al (2022) High throughput 3D gel-based neural organotypic model for cellular assays using fluorescence biosensors. *Commun Biol* 5:1236. https://doi.org/10.1038/s42003-022-04177-z
533. Zhang JJ, Medina A, Ferrer M et al (2025) Generation of functional brain region-specific neural spheroids for high throughput screening. In: Walker JM (Eds.), Methods in Molecular Biology (1st Ed.). Springer, New York, USA. https://doi.org/10.1007/7651_2024_593
534. Antich C, Kundu S, Frebert S et al (2025) Bioprinting spatially guided functional 3D neural circuits with agarose-xanthan gum copolymer hydrogels. *Biomaterials* 318:123156. https://doi.org/10.1016/j.biomaterials.2025.123156
535. Schmitz KM, Larson TL, Borovich MW et al (2025) Development of GelMA-based hydrogel scaffolds with tunable mechanical properties for applications in peripheral nerve regeneration. *ACS Biomater Sci Eng* 11(9):5467–5481. https://doi.org/10.1021/acsbiomaterials.5c00023
536. Ning LQ, Mehta R, Cao C et al (2020) Embedded 3D bioprinting of gelatin methacryloyl-based constructs with highly tunable structural fidelity. *ACS Appl Mater Interfaces* 12(40):44563–44577. https://doi.org/10.1021/acsami.0c15078
537. Ning LQ, Zhu N, Smith A et al (2021) Noninvasive three-dimensional *in situ* and *in vivo* characterization of bioprinted hydrogel scaffolds using the X-ray propagation-based imaging technique. *ACS Appl Mater Interfaces* 13(22):25611–25623. https://doi.org/10.1021/acsami.1c02297
538. Maris JM, Hogarty MD, Bagatell R et al (2007) Neuroblastoma. *Lancet* 369(9579):2106–2120. https://doi.org/10.1016/S0140-6736(07)60983-0
539. Wolf KJ, van Gaal RC, Uzel SGM et al (2026) Perfusable 3D models of ureteric bud and collecting duct tubules. *Cell Biomater* 2(3):100297. https://doi.org/10.1016/j.celbio.2025.100297
540. Rizzo R, Sampon T, Wilt JK et al (2026) Embedding perfusable microchannel networks in photoclickable bioresins via high-resolution digital light processing. *Adv Mater Technol* 11(10):e02466. https://doi.org/10.1002/admt.202502466
541. van Gaal RC, Wolf KJ, Rubins JE et al (2025) Perfusable three-dimensional (3D) models of ureteric bud and collecting duct tubules: TH-PO0532. *J Am Soc Nephrol* 36(10S):10.1681/ASN.2025nynhk311. https://doi.org/10.1681/asn.2025nynhk311
542. Kolesky DB, Homan KA, Skylar-Scott MA et al (2016) Three-dimensional bioprinting of thick vascularized tissues. *Proc Natl Acad Sci USA* 113(12):3179–3184. https://doi.org/10.1073/pnas.1521342113
543. Homan KA, Gupta N, Kroll KT et al (2019) Flow-enhanced vascularization and maturation of kidney organoids in vitro. *Nat Methods* 16(3):255–262. https://doi.org/10.1038/s41592-019-0325-y
544. Pazos-López P, García-Rodríguez C, Guitián-González A et al (2016) Pulmonary vein stenosis: etiology, diagnosis and management. *World J Cardiol* 8(1):81–88. https://doi.org/10.4330/wjc.v8.i1.81
545. Hajal C, Offeddu GS, Shin Y et al (2022) Engineered human blood–brain barrier microfluidic model for vascular permeability analyses. *Nat Protoc* 17(1):95–128. https://doi.org/10.1038/s41596-021-00635-w
546. Offeddu GS, Possenti L, Loessberg-Zahl JT et al (2019) Application of transmural flow across in vitro microvasculature enables direct sampling of interstitial therapeutic molecule distribution. *Small* 15(46):1902393. https://doi.org/10.1002/smll.201902393
547. Offeddu GS, Haase K, Gillrie MR et al (2019) An on-chip model of protein paracellular and transcellular permeability in the microcirculation. *Biomaterials* 212:115–125. https://doi.org/10.1016/j.biomaterials.2019.05.022
548. Liu KZ, Cao HH, Shashaty K et al (2024) Deep and dynamic metabolic and structural imaging in living tissues. *Sci Adv* 10(50):eadp2438. https://doi.org/10.1126/sciadv.adp2438
549. Wan ZP, Zhang S, Zhong AX et al (2024) Transmural flow upregulates PD-L1 expression in microvascular networks. *Adv Sci* 11(26):2400921. https://doi.org/10.1002/advs.202400921
550. Offeddu GS, Serrano JC, Chen SW et al (2021) Microheart: a microfluidic pump for functional vascular culture in microphysiological systems. *J Biomech* 119:110330. https://doi.org/10.1016/j.jbiomech.2021.110330
551. Blazeski A, Floryan MA, Zhang YZ et al (2024) Engineering microvascular networks using a KLF2 reporter to probe flow-dependent endothelial cell function. *Biomaterials* 311:122686. https://doi.org/10.1016/j.biomaterials.2024.122686
552. Haase K, Piatti F, Marcano M et al (2022) Physiologic

flow-conditioning limits vascular dysfunction in engineered human capillaries. *Biomaterials* 280:121248. https://doi.org/10.1016/j.biomaterials.2021.121248
553. Floryan M, Cambria E, Blazeski A et al (2025) Long-term physiological flow rescues regressed microvascular networks and increases their longevity. *npj Biol Phys Mech* 2:24. https://doi.org/10.1038/s44341-025-00028-0
554. Hirose S, Osaki T, Kamm RD et al (2025) Polyploidy of MDA-MB-231 cells drives increased extravasation with enhanced cell-matrix adhesion. *APL Bioeng* 9:016105. https://doi.org/10.1063/5.0233329
555. Angelidakis E, Chen S, Zhang S et al (2023) Impact of fibrinogen, fibrin thrombi, and thrombin on cancer cell extravasation using in vitro microvascular networks. *Adv Healthc Mater* 12(19):2202984. https://doi.org/10.1002/adhm.202202984
556. Offeddu GS, Hajal C, Foley CR et al (2021) The cancer glycocalyx mediates intravascular adhesion and extravasation during metastatic dissemination. *Commun Biol* 4:255. https://doi.org/10.1038/s42003-021-01774-2
557. Hajal C, Ibrahim L, Serrano JC et al (2021) The effects of luminal and trans-endothelial fluid flows on the extravasation and tissue invasion of tumor cells in a 3D *in vitro* microvascular platform. *Biomaterials* 265:120470. https://doi.org/10.1016/j.biomaterials.2020.120470
558. Song J, Miermont A, Lim CT et al (2018) A 3D microvascular network model to study the impact of hypoxia on the extravasation potential of breast cell lines. *Sci Rep* 8:17949. https://doi.org/10.1038/s41598-018-36381-5
559. Chen MB, Hajal C, Benjamin DC et al (2018) Inflamed neutrophils sequestered at entrapped tumor cells via chemotactic confinement promote tumor cell extravasation. *Proc Natl Acad Sci USA* 115(27):7022–7027. https://doi.org/10.1073/pnas.1715932115
560. Jeon JS, Bersini S, Gilardi M et al (2015) Human 3D vascularized organotypic microfluidic assays to study breast cancer cell extravasation. *Proc Natl Acad Sci USA* 112(1):214–219. https://doi.org/10.1073/pnas.1417115112
561. Offeddu GS, Cambria E, Shelton SE et al (2024) Personalized vascularized models of breast cancer desmoplasia reveal biomechanical determinants of drug delivery to the tumor. *Adv Sci* 11(38):2402757. https://doi.org/10.1002/advs.202402757
562. Nguyen HT, Kan EL, Humayun M et al (2025) Patient-specific vascularized tumor model: blocking monocyte recruitment with multispecific antibodies targeting CCR2 and CSF-1R. *Biomaterials* 312:122731. https://doi.org/10.1016/j.biomaterials.2024.122731
563. Shin Y, Choi SH, Kim E et al (2019) Blood–brain barrier dysfunction in a 3D in vitro model of Alzheimer's disease. *Adv Sci* 6(20):1900962. https://doi.org/10.1002/advs.201900962
564. Ko EC, Spitz S, Pramotton FM et al (2023) Accelerating the in vitro emulation of Alzheimer's disease-associated phenotypes using a novel 3D blood–brain barrier neurosphere co-culture model. *Front Bioeng Biotechnol* 11:1251195. https://doi.org/10.3389/fbioe.2023.1251195
565. Pavlou G, Spitz S, Pramotton FM et al (2025) Engineered 3D human neurovascular model of Alzheimer's disease to study vascular dysfunction. *Biomaterials* 314:122864. https://doi.org/10.1016/j.biomaterials.2024.122864
566. Wan ZP, Floryan MA, Coughlin MF et al (2023) New strategy for promoting vascularization in tumor spheroids in a microfluidic assay. *Adv Healthc Mater* 12(14):2201784. https://doi.org/10.1002/adhm.202201784
567. Greco Song HH, Rumma RT, Ozaki CK et al (2018) Vascular tissue engineering: progress, challenges, and clinical promise. *Cell Stem Cell* 22(3):340–354. https://doi.org/10.1016/j.stem.2018.02.009
568. Lee H, Cusick RA, Browne F et al (2002) Local delivery of basic fibroblast growth factor increases both angiogenesis and engraftment of hepatocytes in tissue-engineered polymer devices1. *Transplantation* 73(10):1589–1593. https://doi.org/10.1097/00007890-200205270-00011
569. Zisch AH, Lutolf MP, Ehrbar M et al (2003) Cell-demanded release of VEGF from synthetic, biointeractive cell-ingrowth matrices for vascularized tissue growth. *FASEB J* 17(15):2260–2262. https://doi.org/10.1096/fj.02-1041fje
570. Banfi A, von Degenfeld G, Gianni-Barrera R et al (2012) Therapeutic angiogenesis due to balanced single-vector delivery of VEGF and PDGF-BB. *FASEB J* 26(6):2486–2497. https://doi.org/10.1096/fj.11-197400
571. Schwarz ER, Speakman MT, Patterson M et al (2000) Evaluation of the effects of intramyocardial injection of DNA expressing vascular endothelial growth factor (VEGF) in a myocardial infarction model in the rat: angiogenesis and angioma formation. *J Am Coll Cardiol* 35(5):1323–1330. https://doi.org/10.1016/S0735-1097(00)00522-2
572. Koike N, Fukumura D, Gralla O et al (2004) Creation of long-lasting blood vessels. *Nature* 428(6979):138–139. https://doi.org/10.1038/428138a
573. Gupta R, Tongers J, Losordo DW (2009) Human studies of angiogenic gene therapy. *Circ Res* 105(8):724–736. https://doi.org/10.1161/circresaha.109.200386
574. Cooke JP, Losordo DW (2015) Modulating the vascular response to limb ischemia: angiogenic and cell therapies. *Circ Res* 116(9):1561–1578. https://doi.org/10.1161/circresaha.115.303565
575. Miller JS, Stevens KR, Yang MT et al (2012) Rapid casting of patterned vascular networks for perfusable engineered three-dimensional tissues. *Nat Mater* 11(9):768–774. https://doi.org/10.1038/nmat3357
576. Sundaram S, Lee JH, Bjørge IM et al (2024) Sacrificial capillary pumps to engineer multiscalar biological forms. *Nature* 636(8042):361–367. https://doi.org/10.1038/s41586-024-08175-5
577. Baranski JD, Chaturvedi RR, Stevens KR et al (2013) Geometric control of vascular networks to enhance engineered tissue integration and function. *Proc Natl Acad Sci USA* 110(19):7586–7591. https://doi.org/10.1073/pnas.1217796110
578. Mirabella T, MacArthur JW, Cheng D et al (2017) 3D-printed vascular networks direct therapeutic angiogenesis in ischaemia. *Nat Biomed Eng* 1:83. https://doi.org/10.1038/s41551-017-0083
579. Stevens KR, Scull MA, Ramanan V et al (2017) In situ expansion of engineered human liver tissue in a mouse model of chronic liver disease. *Sci Transl Med* 9(399):eaah5505. https://doi.org/10.1126/scitranslmed.aah5505
580. Qi DJ, Wu SH, Kuss MA et al (2018) Mechanically robust cryogels with injectability and bioprinting supportability for adipose tissue engineering. *Acta Biomater* 74:131–142. https://doi.org/10.1016/j.actbio.2018.05.044
581. Kuss M, Kim J, Qi DJ et al (2018) Effects of tunable, 3D-bioprinted hydrogels on human brown adipocyte behavior and metabolic function. *Acta Biomater* 71:486–495. https://doi.org/10.1016/j.actbio.2018.03.021
582. Xue W, Yu SY, Kuss M et al (2022) 3D bioprinted white adipose model for *in vitro* study of cancer-associated cachexia

induced adipose tissue remodeling. *Biofabrication* 14(3):034106. https://doi.org/10.1088/1758-5090/ac6c4b
583. Wang Y, Shi W, Kuss M et al (2018) 3D bioprinting of breast cancer models for drug resistance study. *ACS Biomater Sci Eng* 4(12):4401–4411. https://doi.org/10.1021/acsbiomaterials.8b01277
584. Wang Y, Mirza S, Wu SH et al (2018) 3D hydrogel breast cancer models for studying the effects of hypoxia on epithelial to mesenchymal transition. *Oncotarget* 9(63):32191–32203. https://doi.org/10.18632/oncotarget.25891
585. Helms HR, Oyama KA, Ware JP et al (2024) Multiplex single-cell bioprinting for engineering of heterogeneous tissue constructs with subcellular spatial resolution. bioRxiv. https://doi.org/10.1101/2024.02.01.578499
586. Helms HR, Bertassoni LE (2025) Protocol for single-cell spatial transcriptomic profiling of cultured cells and engineered tissues without embedding or sectioning. *STAR Protoc* 6(3):104074. https://doi.org/10.1016/j.xpro.2025.104074
587. Seo BR, Chen XY, Ling L et al (2020) Collagen microarchitecture mechanically controls myofibroblast differentiation. *Proc Natl Acad Sci USA* 117(21):11387–11398. https://doi.org/10.1073/pnas.1919394117
588. Sung KE, Su G, Pehlke C et al (2009) Control of 3-dimensional collagen matrix polymerization for reproducible human mammary fibroblast cell culture in microfluidic devices. *Biomaterials* 30(27):4833–4841. https://doi.org/10.1016/j.biomaterials.2009.05.043
589. Christiansen DL, Huang EK, Silver FH (2000) Assembly of type I collagen: fusion of fibril subunits and the influence of fibril diameter on mechanical properties. *Matrix Biol* 19(5):409–420. https://doi.org/10.1016/S0945-053X(00)00089-5
590. Wen Z, Orduno M, Liang ZX et al (2024) Optimization of vascularized intestinal organoid model. *Adv Healthc Mater* 13(31): 2400977. https://doi.org/10.1002/adhm.202400977
591. Liu C, Nguyen RY, Pizzurro GA et al (2023) Self-assembly of mesoscale collagen architectures and applications in 3D cell migration. *Acta Biomater* 155:167–181. https://doi.org/10.1016/j.actbio.2022.11.011
592. Khan ZM, Rossello-Martinez A, Mak M (2025) Impact of mechanical and architectural signals in the tumor microenvironment on melanoma. *Adv Healthc Mater* 14(28):e01759. https://doi.org/10.1002/adhm.202501759
593. Xiao H, Sylla K, Gong XY et al (2024) Proteolysis and contractility regulate tissue opening and wound healing by lung fibroblasts in 3D microenvironments. *Adv Healthc Mater* 13(30): 2400941. https://doi.org/10.1002/adhm.202400941
594. Dogan E, Salemizadehparizi F, Cecen B et al (2023) Recent advances in tumors-on-chips. In: Gonçalves G, Marques P, Mano J (Eds.), New Trends in Smart Nanostructured Biomaterials in Health Sciences (1st Ed.). Elsevier, p.79–117. https://doi.org/10.1016/b978-0-323-85671-3.00006-3
595. Cecen B, Karavasili C, Nazir M et al (2021) Multi-organs-on-chips for testing small-molecule drugs: challenges and perspectives. *Pharmaceutics* 13(10):1657. https://doi.org/10.3390/pharmaceutics13101657
596. Wolf KJ, Weiss JD, Uzel SGM et al (2022) Biomanufacturing human tissues via organ building blocks. *Cell Stem Cell* 29(5): 667–677. https://doi.org/10.1016/j.stem.2022.04.012
597. Liu JS, Gartner ZJ (2012) Directing the assembly of spatially organized multicomponent tissues from the bottom up. *Trends Cell Biol* 22(12):683–691. https://doi.org/10.1016/j.tcb.2012.09.004
598. Miri AK, Mirzaee I, Hassan S et al (2019) Effective bioprinting resolution in tissue model fabrication. *Lab Chip* 19(11):2019–2037. https://doi.org/10.1039/C8LC01037D
599. Bhusal A, Dogan E, Nguyen HA et al (2022) Multi-material digital light processing bioprinting of hydrogel-based microfluidic chips. *Biofabrication* 14(1):014103. https://doi.org/10.1088/1758-5090/ac2d78
600. Dogan E, Austin A, Pourmostafa A et al (2026) Design considerations for photoinitiator selection in cell-laden gelatin methacryloyl hydrogels. *Biomater Sci* 14(3):807–816. https://doi.org/10.1039/d5bm00550g
601. Dogan E, Holshue C, Bhusal A et al (2023) Cell encapsulation in gelatin methacryloyl bioinks impairs microscale diffusion properties. *Front Bioeng Biotechnol* 11:1193970. https://doi.org/10.3389/fbioe.2023.1193970
602. Dogan E, Galifi CA, Cecen B et al (2024) Extracellular matrix regulation of cell spheroid invasion in a 3D bioprinted solid tumor-on-a-chip. *Acta Biomater* 186:156–166. https://doi.org/10.1016/j.actbio.2024.07.040
603. Pourmostafa A, Uskach G, Jafari M et al (2026) Extracellular matrix physical properties regulate cancer cell morphological transitions in 3D hydrogel microtissues. *Acta Biomater* 210: 17–26. https://doi.org/10.1016/j.actbio.2025.12.008
604. Pourmostafa A, Bhusal A, Haridas Menon N et al (2024) Integrating conductive electrodes into hydrogel-based microfluidic chips for real-time monitoring of cell response. *Front Bioeng Biotechnol* 12:1421592. https://doi.org/10.3389/fbioe.2024.1421592
605. Bhusal A, Dogan E, Nieto D et al (2022) 3D bioprinted hydrogel microfluidic devices for parallel drug screening. *ACS Appl Bio Mater* 5(9):4480–4492. https://doi.org/10.1021/acsabm.2c00578
606. Wang XX, Li W, Kumar V (2006) A method for solvent-free fabrication of porous polymer using solid-state foaming and ultrasound for tissue engineering applications. *Biomaterials* 27(9): 1924–1929. https://doi.org/10.1016/j.biomaterials.2005.09.029
607. Wang H, Li W (2008) Selective ultrasonic foaming of polymer for biomedical applications. *J Manuf Sci Eng* 130(2):021004. https://doi.org/10.1115/1.2823078
608. Ma L, Zhou CC, Lin BY et al (2010) A porous 3D cell culture micro device for cell migration study. *Biomed Microdevices* 12(4):753–760. https://doi.org/10.1007/s10544-010-9429-y
609. Ma L, Barker J, Zhou CC et al (2012) Towards personalized medicine with a three-dimensional micro-scale perfusion-based two-chamber tissue model system. *Biomaterials* 33(17):4353–4361. https://doi.org/10.1016/j.biomaterials.2012.02.054
610. Zhu HY, Wang VY, Li W (2025) Fabricating biomimetic porous PEEK scaffolds for bone implants. *Int J Polym Mater Polym Biomater* 74(1):30–38. https://doi.org/10.1080/00914037.2024.2314606
611. Zhu H, Chang A, Valle N et al (2025) Modeling of phase separation and growth in immiscible polymer blends for fabrication of high-strength medical implants. In: Proceedings of the ASME 20th International Manufacturing Science and Engineering Conference, p.1–7. https://doi.org/10.1115/MSEC2025-155740
612. Zhu HY, Chang A, Valle N et al (2025) Phase-field modeling and simulation of high-strength porous polymer fabrication via immiscible polymer blending for bone implants. *J Manuf Sci Eng* 147(8):081002.

https://doi.org/10.1115/1.4068548
613. Zhu HY, Wang VY, Li W (2024) A 3D printing-based hybrid manufacturing method for high-strength polymeric medical implant fabrication. *Manuf Lett* 41:1064–1069. https://doi.org/10.1016/j.mfglet.2024.09.131
614. Zhu HY, Morquecho EV, Li W (2023) Solid-state foaming of poly(ether-ether-ketone)/hydroxyapatite composites. *J Cell Plast* 59(5–6):379–393. https://doi.org/10.1177/0021955x231215762
615. Li W, Wang H, Kumar V et al (2012) Method of selective foaming for porous polymeric material. US Patent 8247464
616. Lee SC, Gillispie G, Prim P et al (2020) Physical and chemical factors influencing the printability of hydrogel-based extrusion bioinks. *Chem Rev* 120(19):10834–10886. https://doi.org/10.1021/acs.chemrev.0c00015
617. Temple JP, Hutton DL, Hung BP et al (2014) Engineering anatomically shaped vascularized bone grafts with hASCs and 3D-printed PCL scaffolds. *J Biomed Mater Res Part A* 102(12): 4317–4325. https://doi.org/10.1002/jbm.a.35107
618. Kengla C, Renteria E, Wivell C et al (2017) Clinically relevant bioprinting workflow and imaging process for tissue construct design and validation. *3D Print Addit Manuf* 4(4):239–247. https://doi.org/10.1089/3dp.2017.0075
619. Lee H, Kengla C, Kim HS et al (2024) Enhancing craniofacial bone reconstruction with clinically applicable 3D bioprinted constructs. *Adv Healthc Mater* 13(4):2302508. https://doi.org/10.1002/adhm.202302508
620. Xu L, Varkey M, Jorgensen A et al (2020) Bioprinting small diameter blood vessel constructs with an endothelial and smooth muscle cell bilayer in a single step. *Biofabrication* 12(4):045012. https://doi.org/10.1088/1758-5090/aba2b6
621. Zhang KL, Fu Q, Yoo J et al (2017) 3D bioprinting of urethra with PCL/PLCL blend and dual autologous cells in fibrin hydrogel: an *in vitro* evaluation of biomimetic mechanical property and cell growth environment. *Acta Biomater* 50:154–164. https://doi.org/10.1016/j.actbio.2016.12.008
622. Ke DX, Yi HL, Est-Witte S et al (2020) Bioprinted trachea constructs with patient-matched design, mechanical and biological properties. *Biofabrication* 12(1):015022. https://doi.org/10.1088/1758-5090/ab5354
623. Park JH, Hong JM, Ju YM et al (2015) A novel tissue-engineered trachea with a mechanical behavior similar to native trachea. *Biomaterials* 62:106–115. https://doi.org/10.1016/j.biomaterials.2015.05.008
624. Kim JH, Seol YJ, Ko IK et al (2018) 3D bioprinted human skeletal muscle constructs for muscle function restoration. *Sci Rep* 8(1):12307. https://doi.org/10.1038/s41598-018-29968-5
625. Lee H, Kim W, Lee J et al (2021) Self-aligned myofibers in 3D bioprinted extracellular matrix-based construct accelerate skeletal muscle function restoration. *Appl Phys Rev* 8(2):021405. https://doi.org/10.1063/5.0039639
626. Kim JH, Kim I, Seol YJ et al (2020) Neural cell integration into 3D bioprinted skeletal muscle constructs accelerates restoration of muscle function. *Nat Commun* 11:1025. https://doi.org/10.1038/s41467-020-14930-9
627. Wang Z, Lee SJ, Cheng HJ et al (2018) 3D bioprinted functional and contractile cardiac tissue constructs. *Acta Biomater* 70:48–56. https://doi.org/10.1016/j.actbio.2018.02.007
628. Merceron TK, Burt M, Seol YJ et al (2015) A 3D bioprinted complex structure for engineering the muscle–tendon unit. *Biofabrication* 7(3):035003. https://doi.org/10.1088/1758-5090/7/3/035003
629. Ali M, Pr AK, Yoo JJ et al (2019) A photo-crosslinkable kidney ECM-derived bioink accelerates renal tissue formation. *Adv Healthc Mater* 8(7):1800992. https://doi.org/10.1002/adhm.201800992
630. Moon YW, Dobroski T, Willson K et al (2025) 3D bioprinted thick hepatic constructs with vascular network as a physiologically relevant *in vitro* organ model. *Mater Today Bio* 32:101786. https://doi.org/10.1016/j.mtbio.2025.101786
631. Gao T, Gillispie GJ, Copus JS et al (2018) Optimization of gelatin–alginate composite bioink printability using rheological parameters: a systematic approach. *Biofabrication* 10(3):034106. https://doi.org/10.1088/1758-5090/aacdc7
632. Gillispie GJ, Copus J, Uzun-Per M et al (2023) The correlation between rheological properties and extrusion-based printability in bioink artifact quantification. *Mater Des* 233:112237. https://doi.org/10.1016/j.matdes.2023.112237
633. Gillispie GJ, Han A, Uzun-Per M et al (2020) The influence of printing parameters and cell density on bioink printing outcomes. *Tissue Eng Part A* 26(23–24):1349–1358. https://doi.org/10.1089/ten.tea.2020.0210
634. Uzun-Per M, Gillispie GJ, Tavolara TE et al (2021) Automated image analysis methodologies to compute bioink printability. *Adv Eng Mater* 23(4):2000900. https://doi.org/10.1002/adem.202000900
635. Park JH, Gillispie GJ, Copus JS et al (2020) The effect of BMP-mimetic peptide tethering bioinks on the differentiation of dental pulp stem cells (DPSCs) in 3D bioprinted dental constructs. *Biofabrication* 12(3):035029. https://doi.org/10.1088/1758-5090/ab9492
636. Visscher DO, Lee H, van Zuijlen PPM et al (2021) A photo-crosslinkable cartilage-derived extracellular matrix bioink for auricular cartilage tissue engineering. *Acta Biomater* 121:193–203. https://doi.org/10.1016/j.actbio.2020.11.029
637. Lee SJ (2024) Personalized reconstruction with three-dimensional printed urological tissue constructs. *Eur Urol Focus* 10(2):259–262. https://doi.org/10.1016/j.euf.2024.01.006
638. Carreno-Galeano G, Ali M, Yoo JJ et al (2025) 3D bioprinted renal constructs using kidney-specific ECM bioink system on kidney regeneration. *Adv Healthc Mater* 14(24):2502576. https://doi.org/10.1002/adhm.202502576
639. Hung BP, Naved BA, Nyberg EL et al (2016) Three-dimensional printing of bone extracellular matrix for craniofacial regeneration. *ACS Biomater Sci Eng* 2(10):1806–1816. https://doi.org/10.1021/acsbiomaterials.6b00101
640. Nyberg E, Rindone A, Dorafshar A et al (2017) Comparison of 3D-printed poly-ε-caprolactone scaffolds functionalized with tricalcium phosphate, hydroxyapatite, bio-oss, or decellularized bone matrix. *Tissue Eng Part A* 23(11–12):503–514. https://doi.org/10.1089/ten.tea.2016.0418
641. Nyberg E, Farris A, O'Sullivan A et al (2019) Comparison of stromal vascular fraction and passaged adipose-derived stromal/stem cells as point-of-care agents for bone regeneration. *Tissue Eng Part A* 25(21–22):1459–1469. https://doi.org/10.1089/ten.tea.2018.0341
642. Singh S, Nyberg EL, O'Sullivan AN et al (2022) Point-of-care treatment of geometrically complex midfacial critical-sized bone defects with 3D-printed scaffolds and autologous stromal vascular fraction. *Biomaterials* 282:121392. https://doi.org/10.1016/j.biomaterials.2022.121392
643. Singh S, Zhou YX, Farris AL et al (2023) Geometric mismatch promotes anatomic repair in periorbital bony defects in skeletally mature Yucatan minipigs. *Adv Healthc Mater* 12(29):2301944. https://doi.org/10.1002/adhm.202301944
644. Sarkar N, Zhao JT, Zhang NY et al (2024) 3D printed O_2-generating

scaffolds enhance osteoprogenitor- and type H vessel recruitment during bone healing. *Acta Biomater* 185:126–143. https://doi.org/10.1016/j.actbio.2024.07.011
645. Rindone AN, Grayson WL (2022) Illuminating the regenerative microenvironment: emerging quantitative imaging technologies for craniofacial bone tissue engineering. *ACS Biomater Sci Eng* 8(11):4610–4612. https://doi.org/10.1021/acsbiomaterials.1c01373
646. Rindone AN, Liu XN, Farhat S et al (2021) Quantitative 3D imaging of the cranial microvascular environment at single-cell resolution. *Nat Commun* 12:6219. https://doi.org/10.1038/s41467-021-26455-w
647. Ren YK, Senarathna J, Grayson WL et al (2022) State-of-the-art techniques for imaging the vascular microenvironment in craniofacial bone tissue engineering applications. *Am J Physiol Cell Physiol* 323(5):C1524–C1538. https://doi.org/10.1152/ajpcell.00195.2022
648. Ren YK, Chu XY, Senarathna J et al (2024) Multimodality imaging reveals angiogenic evolution in vivo during calvarial bone defect healing. *Angiogenesis* 27(1):105–119. https://doi.org/10.1007/s10456-023-09899-0
649. Ren YK, Senarathna J, Chu XY et al (2023) Vascular-centric mapping of in vivo blood oxygen saturation in preclinical models. *Microvasc Res* 148:104518. https://doi.org/10.1016/j.mvr.2023.104518
650. Laurencin CT, Khan Y (2013) Regenerative Engineering (1st Ed.). CRC Press, Boca Raton, USA. https://doi.org/10.1201/b14925
651. Laurencin CT, Khan Y (2012) Regenerative engineering. *Sci Transl Med* 4(160):e3004467. https://doi.org/10.1126/scitranslmed.3004467
652. Cooper JA, Sahota JS, Gorum WJ et al (2007). Biomimetic tissue-engineered anterior cruciate ligament replacement. *Proc Natl Acad Sci USA* 104(9):3049–3054. https://doi.org/10.1073/pnas.0608837104
653. Cushnie EK, Ulery BD, Nelson SJ et al (2014) Simple signaling molecules for inductive bone regenerative engineering. *PLoS ONE* 9(7):e101627. https://doi.org/10.1371/journal.pone.0101627
654. Otsuka T, Phan AQ, Laurencin CT et al (2020) Identification of heparan-sulfate rich cells in the loose connective tissues of the axolotl (*Ambystoma mexicanum*) with the potential to mediate growth factor signaling during regeneration. *Regen Eng Transl Med* 6(1):7–17. https://doi.org/10.1007/s40883-019-00140-3
655. Esdaille CJ, Washington KS, Laurencin CT (2021) Regenerative engineering: a review of recent advances and future directions. *Regen Med* 16(5):495–512. https://doi.org/10.2217/rme-2021-0016
656. Barui S, Ghosh D, Laurencin CT (2022) Osteochondral regenerative engineering: challenges, state-of-the-art and translational perspectives. *Regen Biomater* 10:rbac109. https://doi.org/10.1093/rb/rbac109
657. Hosseini FS, Nair LS, Laurencin CT (2021) Inductive materials for regenerative engineering. *J Dent Res* 100(10):1011–1019. https://doi.org/10.1177/00220345211010436
658. Seyedsalehi A, Daneshmandi L, Barajaa M et al (2020) Fabrication and characterization of mechanically competent 3D printed polycaprolactone-reduced graphene oxide scaffolds. *Sci Rep* 10: 22210. https://doi.org/10.1038/s41598-020-78977-w
659. Daneshmandi L, Holt BD, Arnold AM et al (2022) Ultra-low binder content 3D printed calcium phosphate graphene scaffolds as resorbable, osteoinductive matrices that support bone formation *in vivo*. *Sci Rep* 12:6960. https://doi.org/10.1038/s41598-022-10603-3
660. Awale GM, Barajaa MA, Kan HM et al (2023) Regenerative engineering of long bones using the small molecule forskolin. *Proc Natl Acad Sci USA* 120(22):e2219756120. https://doi.org/10.1073/pnas.2219756120
661. Xu YY, Luong D, Walker JM et al (2017) Modification of poly(propylene fumarate)–bioglass composites with peptide conjugates to enhance bioactivity. *Biomacromolecules* 18(10): 3168–3177. https://doi.org/10.1021/acs.biomac.7b00828
662. Chávez-Madero C, de León-Derby MD, Samandari M et al (2020) Using chaotic advection for facile high-throughput fabrication of ordered multilayer micro- and nanostructures: continuous chaotic printing. *Biofabrication* 12(3):035023. https://doi.org/10.1088/1758-5090/ab84cc
663. Hooper R, Cummings C, Beck A et al (2024) Sheet-based extrusion bioprinting: a new multi-material paradigm providing mid-extrusion micropatterning control for microvascular applications. *Biofabrication* 16(2):025032. https://doi.org/10.1088/1758-5090/ad30c8
664. Vazquez-Armendariz J, Tejeda-Alejandre R, Bahhur A et al (2022) Meltelectrowriting of polycaprolactone thin membranes with high porosity. *Procedia CIRP* 110:282–286. https://doi.org/10.1016/j.procir.2022.06.051
665. U.S. National Science Foundation HAMMER Engineering Research Center (2025) 2025 Melt Electrowriting Workshop. https://hammer.osu.edu/events/2025/06/2025-melt-electrowriting-workshop [Accessed on 11 March 2026]
666. Chmielewska A, Dean D (2024) The role of stiffness-matching in avoiding stress shielding-induced bone loss and stress concentration-induced skeletal reconstruction device failure. *Acta Biomater* 173:51–65. https://doi.org/10.1016/j.actbio.2023.11.011
667. Olivas-Alanis LH, Sanguedolce M, Souza JM et al (2024) Finite element analysis for the virtual surgical planning of stiffness-matched personalized load-bearing percutaneous implants. *Procedia CIRP* 125:66–71. https://doi.org/10.1016/j.procir.2024.08.012
668. Khattab NR, Olivas-Alanis LH, Chmielewska-Wysocka A et al (2024) Evaluation of stiffness-matched, 3D-printed, NiTi mandibular graft fixation in an ovine model. *BioMedical Eng OnLine* 23(1):105. https://doi.org/10.1186/s12938-024-01289-x
669. Avey T, Cho D, Zhang JY et al (2024) Determining critical Zn/Ca atomic ratio and its role in mechanical and corrosion properties of biodegradable Mg-Ca-Zn-Mn alloys. *Materialia* 37:102203. https://doi.org/10.1016/j.mtla.2024.102203
670. Hoelzle DJ, Thurston B, Vazquez-Armendariz J et al (2024) Kinematic analysis of engagement and bending capabilities of a point-of-care, incremental skeletal fixation plate bending system. *Manuf Lett* 41:1585–1595. https://doi.org/10.1016/j.mfglet.2024.09.185
671. Thurston B, Vazquez-Armendariz J, Olivas-Alanis LH et al (2024) Robotic bending of craniomaxillofacial fixation plates. *Procedia CIRP* 125:213–218. https://doi.org/10.1016/j.procir.2024.08.037
672. Wu Y, Ravnic DJ, Ozbolat IT (2020) Intraoperative bioprinting: repairing tissues and organs in a surgical setting. *Trends Biotechnol* 38(6):594–605. https://doi.org/10.1016/j.tibtech.2020.01.004
673. Wang X, Zhang D, Singh YP et al (2024) Progress in organ bioprinting for regenerative medicine. *Engineering* 42:121–142. https://doi.org/10.1016/j.eng.2024.04.023
674. Moncal KK, Gudapati H, Godzik KP et al (2021)

Intra-operative bioprinting of hard, soft, and hard/soft composite tissues for craniomaxillofacial reconstruction. *Adv Funct Mater* 31(29):2010858. https://doi.org/10.1002/adfm.202010858
675. Moncal KK, Aydın RST, Godzik KP et al (2022) Controlled co-delivery of pPDGF-B and pBMP-2 from intraoperatively bioprinted bone constructs improves the repair of calvarial defects in rats. *Biomaterials* 281:121333. https://doi.org/10.1016/j.biomaterials.2021.121333
676. Moncal KK, Yeo M, Celik N et al (2023) Comparison of *in-situ* versus *ex-situ* delivery of polyethylenimine-BMP-2 polyplexes for rat calvarial defect repair *via* intraoperative bioprinting. *Biofabrication* 15(1):015011. https://doi.org/10.1088/1758-5090/ac9f70
677. Kang Y, Yeo M, Derman ID et al (2024) Intraoperative bioprinting of human adipose-derived stem cells and extra-cellular matrix induces hair follicle-like downgrowths and adipose tissue formation during full-thickness craniomaxillofacial skin reconstruction. *Bioact Mater* 33:114–128. https://doi.org/10.1016/j.bioactmat.2023.10.034
678. Yeo M, El-Mallah JC, Horchler SN et al (2026) Coupling intraoperative bioprinting and surgical micropuncture for synergistic scaffold vascularization. *Biomaterials* 326:123711. https://doi.org/10.1016/j.biomaterials.2025.123711
679. Fayyazbakhsh F, Khayat MJ, Sadler C et al (2023) 3D-printed hydrogels dressings with bioactive borate glass for continuous hydration and treatment of second-degree burns. *Int J Bioprinting* 9(6):118. https://doi.org/10.36922/ijb.0118
680. Fogg K, Tseng NH, Peyton SR et al (2023) Roadmap on biomaterials for women's health. *J Phys Mater* 6(1):012501. https://doi.org/10.1088/2515-7639/ac90ee
681. McLoughlin ST, McKenna AR, Fisher JP (2023) 4D bioprinting via molecular network contraction for membranous tissue fabrication. *Adv Healthc Mater* 12(27):e2300642. https://doi.org/10.1002/adhm.202300642
682. Van Belleghem S, Torres L Jr, Santoro M et al (2020) Hybrid 3D printing of synthetic and cell-laden bioinks for shape retaining soft tissue grafts. *Adv Funct Mater* 30(3):1907145. https://doi.org/10.1002/adfm.201907145
683. Kuo CY, Eranki A, Placone JK et al (2016) Development of a 3D printed, bioengineered placenta model to evaluate the role of trophoblast migration in preeclampsia. *ACS Biomater Sci Eng* 2(10):1817–1826. https://doi.org/10.1021/acsbiomaterials.6b00031
684. Melchiorri AJ, Hibino N, Best CA et al (2016) 3D-printed biodegradable polymeric vascular grafts. *Adv Healthc Mater* 5(3): 319–325. https://doi.org/10.1002/adhm.201500725
685. Wang MO, Vorwald CE, Dreher ML et al (2015) Evaluating 3D-printed biomaterials as scaffolds for vascularized bone tissue engineering. *Adv Mater* 27(1):138–144. https://doi.org/10.1002/adma.201403943
686. Arumugasaamy N, Rock KD, Kuo CY et al (2020) Microphysiological systems of the placental barrier. *Adv Drug Deliv Rev* 161:161–175. https://doi.org/10.1016/j.addr.2020.08.010
687. Choe R, Devoy E, Kuzemchak B et al (2022) Computational investigation of interface printing patterns within 3D printed multilayered scaffolds for osteochondral tissue engineering. *Biofabrication* 14(2):025015. https://doi.org/10.1088/1758-5090/ac5220
688. Bracaglia LG, Messina M, Winston S et al (2017) 3D printed pericardium hydrogels to promote wound healing in vascular applications. *Biomacromolecules* 18(11):3802–3811. https://doi.org/10.1021/acs.biomac.7b01165
689. Yeatts AB, Gordon CN, Fisher JP (2011) Formation of an aggregated alginate construct in a tubular perfusion system. *Tissue Eng Part C Meth* 17(12):1171–1178. https://doi.org/10.1089/ten.tec.2011.0263
690. Nguyen BB, Ko H, Moriarty RA et al (2016) Dynamic bioreactor culture of high volume engineered bone tissue. *Tissue Eng Part A* 22(3–4):263–271. https://doi.org/10.1089/ten.tea.2015.0395
691. Nguyen BB, Moriarty RA, Kamalitdinov T et al (2017) Collagen hydrogel scaffold promotes mesenchymal stem cell and endothelial cell coculture for bone tissue engineering. *J Biomed Mater Res* 105(4):1123–1131. https://doi.org/10.1002/jbm.a.36008
692. Sa MW, Nguyen BB, Moriarty RA et al (2018) Fabrication and evaluation of 3D printed BCP scaffolds reinforced with ZrO_2 for bone tissue applications. *Biotech Bioeng* 115(4):989–999. https://doi.org/10.1002/bit.26514
693. Yeatts AB, Both SK, Yang WX et al (2014) In vivo bone regeneration using tubular perfusion system bioreactor cultured nanofibrous scaffolds. *Tissue Eng Part A* 20(1–2):139–146. https://doi.org/10.1089/ten.TEA.2013.0168
694. Kronstadt SM, Patel DB, Born LJ et al (2023) Mesenchymal stem cell culture within perfusion bioreactors incorporating 3D-printed scaffolds enables improved extracellular vesicle yield with preserved bioactivity. *Adv Healthc Mater* 12(20):2300584. https://doi.org/10.1002/adhm.202300584
695. Lyu JJ, Liu Y, Gurm HS et al (2023) Electroplating a miniature diamond wheel for grinding of the calcified plaque inside arteries. *Med Eng Phys* 113:103969. https://doi.org/10.1016/j.medengphy.2023.103969
696. Shih AJ, Liu Y, Zheng YH (2016) Grinding wheel motion, force, temperature, and material removal in rotational atherectomy of calcified plaque. *CIRP Ann* 65(1):345–348. https://doi.org/10.1016/j.cirp.2016.04.012
697. Ramaraju H, Landry AM, Sashidharan S et al (2022) Clinical grade manufacture of 3D printed patient specific biodegradable devices for pediatric airway support. *Biomaterials* 289:121702. https://doi.org/10.1016/j.biomaterials.2022.121702
698. Akman R, Ramaraju H, Verga A et al (2022) Multimodal 3D printing of biodegradable shape memory elastomer resins for patient specific soft tissue repair. *Appl Mater Today* 29:101666. https://doi.org/10.1016/j.apmt.2022.101666
699. Hollister SJ, Flanagan CL, Morrison RJ et al (2016) Integrating image-based design and 3D biomaterial printing to create patient specific devices within a design control framework for clinical translation. *ACS Biomater Sci Eng* 2(10):1827–1836. https://doi.org/10.1021/acsbiomaterials.6b00332
700. Jakab K, Marga F, Kaesser R et al (2019) Non-medical applications of tissue engineering: biofabrication of a leather-like material. *Mater Today Sustain* 5:100018. https://doi.org/10.1016/j.mtsust.2019.100018
701. Zheng YH, Belmont B, Shih AJ (2016) Experimental investigation of the abrasive crown dynamics in orbital atherectomy. *Med Eng Phys* 38(7):639–647. https://doi.org/10.1016/j.medengphy.2016.04.006
702. Liu Y, Li BZ, Zheng YH et al (2017) Experiment and smooth particle hydrodynamics simulation of debris size in grinding of calcified plaque in atherectomy. *CIRP Ann* 66(1):325–328. https://doi.org/10.1016/j.cirp.2017.04.090
703. Zheng YH, Liu Y, Pitre JJ et al (2018) Computational fluid dynamics modeling of the burr orbital motion in rotational atherectomy with particle image velocimetry validation. *Ann Biomed Eng* 46(4):567–578. https://doi.org/10.1007/s10439-018-1984-z

704. Liu Y, Liu Y, Zheng YH et al (2019) Catheter thermal energy generation and temperature in rotational atherectomy. *Med Eng Phys* 70:29–38. https://doi.org/10.1016/j.medengphy.2019.06.014
705. Zheng YH, Liu Y, Liu Y et al (2019) Multigrain smoothed particle hydrodynamics and Hertzian contact modeling of the grinding force in atherectomy. *J Manuf Sci Eng* 141(4):041015. https://doi.org/10.1115/1.4042603
706. Liu Y, Zheng YH, Li AD et al (2019) Cutting of blood clots–experiment and smooth particle Galerkin modelling. *CIRP Ann* 68(1):97–100. https://doi.org/10.1016/j.cirp.2019.04.025
707. Liu Y, Reddy AS, Cockrum J et al (2020) Standardized fabrication method of human-derived emboli with histologic and mechanical quantification for stroke research. *J Stroke Cerebrovasc Dis* 29(11):105205. https://doi.org/10.1016/j.jstrokecerebrovasdis.2020.105205
708. Gebrezgiabhier D, Liu Y, Reddy AS et al (2021) A human brain test bed for research in large vessel occlusion stroke. *J Neurosurg* 135(4):1072–1080. https://doi.org/10.3171/2020.7.jns202278
709. Reddy AS, Liu Y, Cockrum J et al (2021) Construction of a comprehensive endovascular test bed for research and device development in mechanical thrombectomy in stroke. *J Neurosurg* 134(4):1190–1197. https://doi.org/10.3171/2020.1.jns192732
710. Liu Y, Zheng YH, Reddy AS et al (2021) Analysis of human emboli and thrombectomy forces in large-vessel occlusion stroke. *J Neurosurg* 134(3):893–901. https://doi.org/10.3171/2019.12.jns192187
711. Liu Y, Gebrezgiabhier D, Zheng Y et al (2022) Arterial collapse during thrombectomy for stroke: clinical evidence and experimental findings in human brains and in vivo models. *Am J Neuroradiol* 43(2):251–257. https://doi.org/10.3174/ajnr.a7389
712. Liu Y, Gebrezgiabhier D, Reddy AS et al (2022) Failure modes and effects analysis of mechanical thrombectomy for stroke discovered in human brains. *J Neurosurg* 136(1):197–204. https://doi.org/10.3171/2020.11.jns203684
713. Perkins SJ, Funes M, Cheah D et al (2024) Safety window for effective lesion crossing in patients with chronic thromboembolic pulmonary hypertension. *J Soc Cardiovasc Angiogr Interv* 3(8): 102142. https://doi.org/10.1016/j.jscai.2024.102142
714. Parchment NJ, Argenti C, Sharma SB et al (2025) Variation in compressive mechanical properties between subacute and chronic venous thrombosis in a novel unilateral iliac thrombosis model. *Vasc Med* 30(2):124–135. https://doi.org/10.1177/1358863x241308481
715. Chisena RS, Sengenberger J, Shih AJ et al (2021) Novel preclinical method for evaluating the efficacy of a percutaneous treatment in human ex vivo calcified plaque. *Med Biol Eng Comput* 59(4):799–811. https://doi.org/10.1007/s11517-021-02334-w
716. Brooks KA, Lai AY, Tucker SJ et al (2023) External airway splint placement for severe pediatric tracheobronchomalacia. *Int J Pediatr Otorhinolaryngol* 169:111559. https://doi.org/10.1016/j.ijporl.2023.111559
717. Hollister SJ, Flanagan CL, Zopf DA et al (2015) Design control for clinical translation of 3D printed modular scaffolds. *Ann Biomed Eng* 43(3):774–786. https://doi.org/10.1007/s10439-015-1270-2
718. Les AS, Ohye RG, Filbrun AG et al (2019) 3D-printed, externally-implanted, bioresorbable airway splints for severe tracheobronchomalacia. *Laryngoscope* 129(8):1763–1771. https://doi.org/10.1002/lary.27863
719. Morrison RJ, Hollister SJ, Niedner MF et al (2015) Mitigation of tracheobronchomalacia with 3D-printed personalized medical devices in pediatric patients. *Sci Transl Med* 7(285):e3010825. https://doi.org/10.1126/scitranslmed.3010825
720. Tsai AY, Moroi MK, Les AS et al (2021) Tracheal agenesis: esophageal airway support with a 3-dimensional–printed bioresorbable splint. *JTCVS Tech* 10:563–568. https://doi.org/10.1016/j.xjtc.2021.08.037
721. Zopf DA, Hollister SJ, Nelson ME et al (2013) Bioresorbable airway splint created with a three-dimensional printer. *N Engl J Med* 368(21):2043–2045. https://doi.org/10.1056/nejmc1206319
722. Ramaraju H, Verga AS, Steedley BJ et al (2025) Investigation of the biodegradation kinetics and associated mechanical properties of 3D-printed polycaprolactone during long-term preclinical testing. *Biomaterials* 321:123257. https://doi.org/10.1016/j.biomaterials.2025.123257
723. Baumberger T (2023) Hydrolytic embrittlement: a security breach in structural materials made of biodegradable polymers. *MRS Bull* 48(1):10–11. https://doi.org/10.1557/s43577-022-00421-3
724. Shi M, Jiao Q, Yin TH et al (2023) Hydrolysis embrittles poly(lactic acid). *MRS Bull* 48(1):45–55. https://doi.org/10.1557/s43577-022-00368-5
725. Park JH, Tucker SJ, Yoon JK et al (2024) 3D printing modality effect: distinct printing outcomes dependent on selective laser sintering (SLS) and melt extrusion. *J Biomed Mater Res Part A* 112(7):1015–1024. https://doi.org/10.1002/jbm.a.37682
726. Brazhkina O, Park JH, Brown M et al (2025) In vivo assessment of iPSC-cardiomyocyte loaded auxetic cardiac patches following chronic myocardial infarction. *Biomaterials* 323:123418. https://doi.org/10.1016/j.biomaterials.2025.123418
727. Brazhkina O, Park JH, Park HJ et al (2021) Designing a 3D printing based auxetic cardiac patch with hiPSC-CMs for heart repair. *J Cardiovasc Dev Dis* 8(12):172. https://doi.org/10.3390/jcdd8120172
728. Coelho PG, Hollister SJ, Flanagan CL et al (2015) Bioresorbable scaffolds for bone tissue engineering: optimal design, fabrication, mechanical testing and scale-size effects analysis. *Med Eng Phys* 37(3):287–296. https://doi.org/10.1016/j.medengphy.2015.01.004
729. Ho NC, Hollister SJ, Agrawal V et al (2023) Evaluation of topology optimization using 3D printing for bioresorbable fusion cages: a biomechanical study in a porcine model. *Spine* 48(4): E46–E53. https://doi.org/10.1097/brs.0000000000004491
730. Knutsen AR, Borkowski SL, Ebramzadeh E et al (2015) Static and dynamic fatigue behavior of topology designed and conventional 3D printed bioresorbable PCL cervical interbody fusion devices. *J Mech Behav Biomed Mater* 49:332–342. https://doi.org/10.1016/j.jmbbm.2015.05.015
731. Akman R, Ramaraju H, Hollister M et al (2025) Thermal post-processing of 3D-printed poly(glycerol dodecanedioate) controls mechanics and shape memory properties. *Polym Sci Technol* 1(2):132–143. https://doi.org/10.1021/polymscitech.5c00012
732. Akman R, Ramaraju H, Hollister SJ (2021) Development of photocrosslinked poly(glycerol dodecanedioate): a biodegradable shape memory polymer for 3D-printed tissue engineering applications. *Adv Eng Mater* 23(10):2100219. https://doi.org/10.1002/adem.202100219
733. Akman R, Ramaraju H, Moore S et al (2024) Manufacture dependent differential biodegradation of 3D printed shape memory

polymers. *Virtual Phys Prototyp* 19(1):e2371504. https://doi.org/10.1080/17452759.2024.2371504
734. Migneco F, Huang YC, Birla RK et al (2009) Poly(glycerol-dodecanoate), a biodegradable polyester for medical devices and tissue engineering scaffolds. *Biomaterials* 30(33):6479–6484. https://doi.org/10.1016/j.biomaterials.2009.08.021
735. Ramaraju H, Akman RE, Safranski DL et al (2020) Designing biodegradable shape memory polymers for tissue repair. *Adv Funct Mater* 30(44):2002014. https://doi.org/10.1002/adfm.202002014
736. Ramaraju H, Garcia-Gomez E, McAtee AM et al (2024) Shape memory cycle conditions impact human bone marrow stromal cell binding to RGD- and YIGSR-conjugated poly (glycerol dodecanedioate). *Acta Biomater* 186:246–259. https://doi.org/10.1016/j.actbio.2024.07.057
737. Ramaraju H, Massarella D, Wong C et al (2023) Percutaneous delivery and degradation of a shape memory elastomer poly(glycerol dodecanedioate) in porcine pulmonary arteries. *Biomaterials* 293:121950. https://doi.org/10.1016/j.biomaterials.2022.121950
738. Ramaraju H, Solorio LD, Bocks ML et al (2020) Degradation properties of a biodegradable shape memory elastomer, poly(glycerol dodecanoate), for soft tissue repair. *PLoS ONE* 15 (2):e0229112. https://doi.org/10.1371/journal.pone.0229112
739. Ramaraju H, Ul-Haque A, Verga AS et al (2020) Modulating nonlinear elastic behavior of biodegradable shape memory elastomer and small intestinal submucosa(SIS) composites for soft tissue repair. *J Mech Behav Biomed Mater* 110:103965. https://doi.org/10.1016/j.jmbbm.2020.103965
740. Harris JCL, Verga AS, Hollister SJ (2025) Matching polyjet 3D printed material properties to human left heart tissue mechanical behavior. *J Biomed Mater Res Part B Appl Biomater* 113(12):e70002. https://doi.org/10.1002/jbmb.70002
741. Verga AS, Tucker SJ, Gao YM et al (2022) Nonlinear viscoelastic properties of 3D-printed tissue mimicking materials and metrics to determine the best printed material match to tissue mechanical behavior. *Front Mech Eng* 8:862375. https://doi.org/10.3389/fmech.2022.862375
742. Huebsch N, Arany PR, Mao AS et al (2010) Harnessing traction-mediated manipulation of the cell/matrix interface to control stem-cell fate. *Nat Mater* 9(6):518–526. https://doi.org/10.1038/nmat2732
743. Hodi FS, Giobbie-Hurder A, Adu-Berchie K et al (2025) First-in-human clinical trial of vaccination with WDVAX, a dendritic cell–activating scaffold incorporating autologous tumor cell lysate, in patients with metastatic melanoma. *Cancer Immunol Res* 13(7):978–989. https://doi.org/10.1158/2326-6066.cir-24-0333
744. Ali OA, Emerich D, Dranoff G et al (2009) In situ regulation of DC subsets and T cells mediates tumor regression in mice. *Sci Transl Med* 1(8):e3000359. https://doi.org/10.1126/scitranslmed.3000359
745. Neagu A, Jakab K, Jamison R et al (2005) Role of physical mechanisms in biological self-organization. *Phys Rev Lett* 95(17):178104. https://doi.org/10.1103/physrevlett.95.178104
746. Organovo (2026) Organovo I. https://organovo.com/contact/ [Accessed on 19 April 2026]
747. Nguyen DG, Funk J, Robbins JB et al (2016) Bioprinted 3D primary liver tissues allow assessment of organ-level response to clinical drug induced toxicity *in vitro*. *PLoS ONE* 11(7):e0158674. https://doi.org/10.1371/journal.pone.0158674
748. Modern Meadow (2026) Modern Meadow: innovating materials with bio-design technologies. https://modernmeadow.com/ [Accessed on 19 April 2026]
749. Harvey C (2014) This Brooklyn startup wowed the science community with lab-made 'meat chips'. https://www.businessinsider.com/modern-meadow-grows-meat-in-a-lab-2014-9 [Accessed on 19 April 2026]
750. INNOVERA (2026) Biofabricated leather reinvented | sustainable & animal-free. https://innovera-world.com/ [Accessed on 2 March 2026]
751. Mercedes-AMG (2026) Mercedes-AMG CONCEPT AMG GT XX—A new dimension of performance. https://theshopmag.com/news/modern-meadow-development-partnership-mercedes-benz/ [Accessed on 19 April 2026]
752. Moroni L, Boland T, Burdick JA et al (2018) Biofabrication: a guide to technology and terminology. *Trends Biotechnol* 36(4): 384–402. https://doi.org/10.1016/j.tibtech.2017.10.015
753. Ning LQ, Gil CJ, Hwang B et al (2020) Biomechanical factors in three-dimensional tissue bioprinting. *Appl Phys Rev* 7(4): 041319. https://doi.org/10.1063/5.0023206
754. Chung J, Shen B, Kong ZJ (2024) Anomaly detection in additive manufacturing processes using supervised classification with imbalanced sensor data based on generative adversarial network. *J Intell Manuf* 35(5):2387–2406. https://doi.org/10.1007/s10845-023-02163-8
755. Qiu P (2013) Introduction to Statistical Process Control (1st Ed.). Chapman and Hall/CRC, New York, USA. https://doi.org/10.1201/b15016
756. Li YF, Wang LN, Lee D et al (2022) Monitoring runtime metrics of fog manufacturing via a qualitative and quantitative (QQ) control chart. *ACM Trans Internet Things* 3(2):1–19. https://doi.org/10.1145/3501262
757. Li YF, Mohan K, Sun HY et al (2017) Ensemble modeling of in situ features for printed electronics manufacturing with in situ process control potential. *IEEE Robot Autom Lett* 2(4):1864–1870. https://doi.org/10.1109/LRA.2017.2713242
758. Morrison RJ, Kashlan KN, Flanangan CL et al (2015) Regulatory considerations in the design and manufacturing of implantable 3D-printed medical devices. *Clin Transl Sci* 8(5):594–600. https://doi.org/10.1111/cts.12315
759. Karvinen J, Kellomäki M (2023) Design aspects and characterization of hydrogel-based bioinks for extrusion-based bioprinting. *Bioprinting* 32:e00274. https://doi.org/10.1016/j.bprint.2023.e00274
760. National Institutes of Health (2025) NIH to prioritize human-based research technologies. https://www.nih.gov/news-events/news-releases/nih-prioritize-human-based-research-technologies [Accessed on 6 June 2026]
761. Jung O, Song MJ, Ferrer M (2021) Operationalizing the use of biofabricated tissue models as preclinical screening platforms for drug discovery and development. *SLAS Discov* 26(9):1164–1176. https://doi.org/10.1177/24725552211030903
762. Hua WJ, Gaharwar AK (2026) 3D biofabricated in vitro models as new approach methodologies for animal alternatives. *npj Biomed Innov* 3:20. https://doi.org/10.1038/s44385-026-00073-x
763. Hyun I, Scharf-Deering JC, Sullivan S et al (2022) How collaboration between bioethicists and neuroscientists can advance research. *Nat Neurosci* 25(11):1399–1401. https://doi.org/10.1038/s41593-022-01187-2

Authors and Affiliations

Yunxia Chen[1] · Kyle R. Phillips[2] · Eben Alsberg[3,4,5] · Thomas E. Angelini[1,2,6,7] · Nasim Annabi[8,9] · Anthony Atala[10] · Amit Bandyopadhyay[11] · Leon M. Bellan[12,13] · Luiz E. Bertassoni[14,15,16,17,18] · Adriana Blazeski[19] · Thomas Boland[20] · Susmita Bose[11] · Jason A. Burdick[21,22] · Robert C. Chang[23] · Christopher S. Chen[24,25] · Roland K. Chen[11] · Douglas B. Chrisey[26,27] · Elizabeth Cosgriff-Hernandez[28] · Paul D. Dalton[29] · David Dean[30] · Aixiang Ding[3] · Bin Duan[31] · Marc Ferrer[32] · John P. Fisher[33,34] · Gabor Forgacs[35,36] · Debolina Ghosh[37] · Warren L. Grayson[38,39,40,41,42] · Murat Guvendiren[43,44] · MD Ahasan Habib[45] · Sarah C. Heilshorn[46] · Ashley Hicks[28] · Scott J. Hollister[47] · Congrui Jin[48] · Yifei Jin[49] · Roger D. Kamm[19,50] · Bashir Khoda[51] · Robert Langer[52,53] · Cato T. Laurencin[37,54,55,56,57] · Sang Jin Lee[10] · Kam W. Leong[58,59] · Ming C. Leu[60] · Wei Li[61] · Michael Mak[62] · Amir K. Miri[44] · Roger J. Narayan[63,64] · Liqun Ning[65] · Brenda M. Ogle[66,67] · Ibrahim T. Ozbolat[68,69,70,71,72,73] · Zhijian Pei[74] · Peihua Qiu[75] · Krishanu Saha[30,76] · Jayant Saksena[26,27] · Vahid Serpooshan[77,78] · Albert Shih[79] · Rohan A. Shirwaiker[80,81,82] · Pranav Soman[83] · Ali Tamayol[84] · Mark W. Tibbitt[85] · Changxue Xu[86] · Yunzhi Peter Yang[46,87,88] · Lijie Grace Zhang[89] · James J. Yoo[10] · Shaochen Chen[90,91] · Yu Shrike Zhang[92,93,94] · Yong Huang[1,2,7]

Yunxia Chen and Kyle R. Phillips have contributed equally to this work.

Except for the co-first authors and the corresponding authors, all authors are listed alphabetically.

✉ James J. Yoo
James.Yoo@wfusm.edu

✉ Shaochen Chen
shc064@ucsd.edu

✉ Yu Shrike Zhang
yszhang@bwh.harvard.edu

✉ Yong Huang
yongh@ufl.edu

1 Department of Mechanical and Aerospace Engineering, University of Florida, Gainesville, FL 32611, USA

2 J. Crayton Pruitt Family Department of Biomedical Engineering, University of Florida, Gainesville, FL 32611, USA

3 Richard and Loan Hill Department of Biomedical Engineering, University of Illinois Chicago, Chicago, IL 60612, USA

4 Jesse Brown Veterans Affairs Medical Center (JBVAMC), Chicago, IL 60612, USA

5 Departments of Mechanical & Industrial Engineering, Orthopaedic Surgery, and Pharmacology and Regenerative Medicine, University of Illinois Chicago, Chicago, IL 60612, USA

6 Department of Physics, University of Florida, Gainesville, FL 32611, USA

7 Department of Materials Science and Engineering, University of Florida, Gainesville, FL 32611, USA

8 Department of Chemical and Biomolecular Engineering, University of California Los Angeles, Los Angeles, CA 90095, USA

9 Department of Bioengineering, University of California Los Angeles, Los Angeles, CA 90095, USA

10 Wake Forest Institute for Regenerative Medicine, Wake Forest University School of Medicine, Winston-Salem, NC 27157, USA

11 School of Mechanical and Materials Engineering, Washington State University, Pullman, WA 99164, USA

12 Department of Mechanical Engineering, Vanderbilt University, Nashville, TN 37235, USA

13 Department of Biomedical Engineering, Vanderbilt University, Nashville, TN 37235, USA

14 Knight Cancer Precision Biofabrication Hub, Knight Cancer Institute (KCI), Oregon Health and Science University (OHSU), Portland, OR 97201, USA

15 Cancer Early Detection Advanced Research Center (CEDAR), KCI, OHSU, Portland, OR 97201, USA

16 Division of Oncological Sciences, School of Medicine, OHSU, Portland, OR 97201, USA

17 Department of Biomedical Engineering, School of Medicine, OHSU, Portland, OR 97201, USA

18 Department of Oral Rehabilitation Biosciences, School of Dentistry, OHSU, Portland, OR 97201, USA

19 Department of Biological Engineering, Massachusetts Institute of Technology, Cambridge, MA 02139, USA

20 Department of Metallurgical, Materials and Biomedical Engineering, University of Texas at El Paso, El Paso, TX 79965, USA

21 Department of Chemical and Biological Engineering, University of Colorado Boulder, Boulder, CO 80303, USA

22 BioFrontiers Institute, University of Colorado Boulder, Boulder, CO 80303, USA

23 Department of Mechanical Engineering, Stevens Institute of Technology, Hoboken, NJ 07030, USA

24 Biological Design Center and Department of Biomedical Engineering, Boston University, Boston, MA 02215, USA

25 Wyss Institute for Biologically Inspired Engineering, Harvard University, Boston, MA 02215, USA

26 Department of Physics and Engineering Physics, Tulane University, New Orleans, LA 70118, USA

27 Department of Biomedical Engineering, Tulane University, New

Orleans, LA 70118, USA

[28] Department of Biomedical Engineering, University of Texas at Austin, Austin, TX 78712, USA

[29] Department of Bioengineering, Phil and Penny Knight Campus for Accelerating Scientific Impact, University of Oregon, Eugene, OR 97403, USA

[30] Department of Biomedical Engineering, University of Wisconsin-Madison, Madison, WI 53706, USA

[31] Mary & Dick Holland Regenerative Medicine Program, University of Nebraska Medical Center, Omaha, NE 68198, USA

[32] Division of Preclinical Innovation, National Center for Advancing Translational Sciences (NCATS), The National Institutes of Health, Rockville, MD 20850, USA

[33] Fischell Department of Bioengineering, University of Maryland, College Park, MD 20742, USA

[34] Center for Engineering Complex Tissues, University of Maryland, College Park, MD 20742, USA

[35] Department of Physics, University of Missouri, Columbia, MO 65211, USA

[36] Fork & Good, Inc., Jersey City, NJ 07302, USA

[37] Cato T. Laurencin Institute for Regenerative Engineering, University of Connecticut, Farmington, CT 06030, USA

[38] Department of Biomedical Engineering, Johns Hopkins University School of Medicine, Baltimore, MD 21205, USA

[39] Translational Therapeutics & Regenerative Engineering Center, Johns Hopkins University School of Medicine, Baltimore, MD 21231, USA

[40] Institute for Nanobiotechnology, Johns Hopkins University, Baltimore, MD 21218, USA

[41] Department of Materials Science and Engineering, Johns Hopkins University, Baltimore, MD 21218, USA

[42] Department of Chemical and Biomolecular Engineering, Johns Hopkins University, Baltimore, MD 21218, USA

[43] Department of Chemical and Materials Engineering, New Jersey Institute of Technology, Newark, NJ 07102, USA

[44] Department of Biomedical Engineering, New Jersey Institute of Technology, Newark, NJ 07102, USA

[45] Department of Mechanical and Mechatronics Engineering Technology, Rochester Institute of Technology, Rochester, NY 14623, USA

[46] Department of Materials Science & Engineering, Stanford University, Stanford, CA 94305, USA

[47] Wallace H. Coulter Department of Biomedical Engineering, Georgia Institute of Technology, Atlanta, GA 30332, USA

[48] Department of Engineering Technology and Industrial Distribution, Texas A&M University, College Station, TX 77843, USA

[49] Department of Mechanical Engineering, University of Nevada Reno, Reno, NV 89557, USA

[50] Department of Mechanical Engineering, Massachusetts Institute of Technology, Cambridge, MA 02139, USA

[51] Department of Mechanical Engineering, University of Maine, Orono, ME 04469, USA

[52] Department of Chemical Engineering, Massachusetts Institute of Technology, Cambridge, MA 02139, USA

[53] David H. Koch Institute for Integrative Cancer Research, Massachusetts Institute of Technology, Cambridge, MA 02139, USA

[54] Department of Biomedical Engineering, University of Connecticut, Storrs, CT 06269, USA

[55] Department of Orthopaedic Surgery, University of Connecticut Health Center, Farmington, CT 06030, USA

[56] Department of Materials Science and Engineering, University of Connecticut, Storrs, CT 06269, USA

[57] Department of Chemical and Biomolecular Engineering, University of Connecticut, Storrs, CT 06269, USA

[58] Department of Biomedical Engineering, Columbia University, New York, NY 10025, USA

[59] Department of Systems Biology, Columbia University Medical Center, New York, NY 10032, USA

[60] Department of Mechanical and Aerospace Engineering, Missouri University of Science and Technology, Rolla, MO 65409, USA

[61] Walker Department of Mechanical Engineering, University of Texas at Austin, Austin, TX 78712, USA

[62] Department of Pharmacological Sciences, Stony Brook University, Stony Brook, NY, 11794, USA

[63] Joint Department of Biomedical Engineering, University of North Carolina and North Carolina State University, Raleigh, NC 27695, USA

[64] Department of Materials Science and Engineering, North Carolina State University, Raleigh, NC 27695, USA

[65] Department of Mechanical Engineering, Cleveland State University, Cleveland, OH 44115, USA

[66] Department of Biomedical Engineering, University of Minnesota, Minneapolis, MN 55455, USA

[67] Department of Pediatrics, University of Minnesota, Minneapolis, MN 55455, USA

[68] The Huck Institutes of Life Sciences, Penn State University, University Park, PA 16802, USA

[69] Engineering Science and Mechanics Department, Penn State University, University Park, PA 16802, USA

[70] Department of Biomedical Engineering, Penn State University, University Park, PA 16802, USA

[71] Materials Research Institute, Penn State University, University Park, PA 16802, USA

[72] Department of Neurosurgery, Penn State University, University Park, PA 16802, USA

[73] Cancer Institute, Penn State University, Hershey, PA 17033, USA

[74] Department of Industrial and Systems Engineering, Texas A&M University, College Station, TX 77843, USA

[75] Department of Biostatistics, University of Florida, Gainesville, FL 32610, USA

[76] Wisconsin Institute for Discovery, University of Wisconsin-Madison, Madison, WI 53715, USA

[77] Children's Heart Institute, McGovern Medical School, UTHealth, Houston, TX 77030, USA

[78] Center for Innovation in Congenital Heart Disease, UTHealth, Houston, TX 77030, USA

[79] Department of Mechanical Engineering, University of Michigan, Ann Arbor, MI 48109, USA

[80] Edward F. Pitts Department of Industrial & Systems Engineering, North Carolina State University, Raleigh, NC 27695, USA

[81] Bezos Center for Sustainable Protein, North Carolina State University, Raleigh, NC 27695, USA

[82] Comparative Medicine Institute, North Carolina State University, Raleigh, NC 27695, USA

[83] Department of Biomedical and Chemical Engineering, Syracuse University, Syracuse, NY 13244, USA

[84] Department of Biomedical Engineering, University of Connecticut Health Center, Farmington, CT 06030, USA

[85] Macromolecular Engineering Laboratory, Department of Mechanical and Process Engineering, ETH Zurich, Zurich 8092, Switzerland

[86] Department of Industrial, Manufacturing, and Systems Engineering, Texas Tech University, Lubbock, TX 79409, USA

[87] Department of Orthopedic Surgery, Stanford University, Stanford, CA 94305, USA

[88] Department of Bioengineering, Stanford University, Stanford, CA 94305, USA

[89] Department of Mechanical and Aerospace Engineering, George Washington University, Washington, DC 20052, USA

[90] Aiiso Yufeng Li Family Department of Chemical and Nano Engineering, University of California San Diego, La Jolla, CA 92093, USA

[91] Department of Bioengineering, University of California San Diego, La Jolla, CA 92093, USA

[92] Division of Engineering in Medicine, Department of Medicine, Brigham and Women's Hospital, Harvard Medical School, Cambridge, MA 02139, USA

[93] Harvard Stem Cell Institute, Harvard University, Cambridge, MA 02138, USA

[94] Broad Institute of MIT and Harvard, Cambridge, MA 02142, USA